



Joint Institute for Nuclear Research



## REPORT

**on preliminary results of the implementation of the Agreement  
between the Government of the Russian Federation  
and the international intergovernmental research organization Joint  
Institute for Nuclear Research  
on the construction and operation of a complex  
of superconducting rings on colliding beams of heavy ions NICA  
(NICA complex)**

as of 01/01/2020



Dubna, 2020.

## **Content:**

### Introduction

1. The basic configuration scheme, the main characteristics and working documents of the “NICA Complex” project
2. Status of implementation of the basic configuration of the complex
  - 2.1 Accelerator block of the NICA complex
    - 2.1.1 Injection complex
    - 2.1.2 Ion sources
      - 2.1.2.1 Laser source and light ion source
      - 2.1.2.2 Source of polarized ions (SPI)
      - 2.1.2.3 Heavy ion source «KRION»
      - 2.1.2.4 Linac LU-20M
      - 2.1.2.5 Heavy ion linear accelerator HILAc
      - 2.1.2.6 Light ion linear accelerator LILAc
    - 2.1.3 Booster synchrotron
      - 2.1.3.1 Cryo-magnetic system
      - 2.1.3.2 Electron cooling system
      - 2.1.3.3 Systems of the beam injection and extraction, beam transport lines
      - 2.1.3.4 Power supply and quench protection systems of the Booster
      - 2.1.3.5 Radio frequency system
      - 2.1.3.6 Diagnostic and control system
      - 2.1.3.7 Vacuum system
    - 2.1.4 Ion Synchrotron Nuclotron
      - 2.1.4.1 Nuclotron operation modes
      - 2.1.4.2 Main systems of the Nuclotron
    - 2.1.5 Collider
      - 2.1.5.1 The Collider optical structure and its elements
        - 2.1.5.1.1 The magnetic field correction system
        - 2.1.5.1.2 A cryostat system of SC magnets
      - 2.1.5.2 The beam cooling systems
        - 2.1.5.2.1 Stochastic cooling system
        - 2.1.5.2.2 Electron cooling system
      - 2.1.5.3 Power supply system and its switching
      - 2.1.5.4 Beam transfer channel from the Nuclotron to the Collider (Channel NC)

- 2.1.5.5 RF stations of the NICA Collider
- 2.1.5.6 Collider diagnostic control and monitoring system
- 2.1.5.7 Vacuum system
- 2.2 Experimental setups
  - 2.2.1 Multi Purpose Detector (MPD)
    - 2.2.1.1 Conceptual design of the MPD detector
    - 2.2.1.2 Superconducting magnet
      - 2.2.1.2.1 Solenoid
      - 2.2.1.2.2 Magnet yoke
    - 2.2.1.3 Time Projection Chamber – TPC
      - 2.2.1.3.1 A TPC design
      - 2.2.1.3.2 Readout Chamber (ROC)
      - 2.2.1.3.3 Gas system
      - 2.2.1.3.4 TPC laser calibration system
      - 2.2.1.3.5 Cooling system
      - 2.2.1.3.6 Front-End Electronics (FEE) and data readout system
      - 2.2.1.3.7 Detector control system (DCS)
      - 2.2.1.3.8 HV and LV systems
      - 2.2.1.3.9 TPC assembly and infrastructure
    - 2.2.1.4 TOF identification system
      - 2.2.1.4.1 Multigap resistive plate chambers
      - 2.2.1.4.2 Front-end electronics
      - 2.2.1.4.3 Readout and data acquisition electronics
      - 2.2.1.4.4 Closed loop gas supply system
      - 2.2.1.4.5 HV & LV power supply
      - 2.2.1.4.6 Slow control system
      - 2.2.1.4.7 Cooling system
      - 2.2.1.4.8 Integration in MPD
    - 2.2.1.5 Detector FFD
      - 2.2.1.5.1 FFD sub-detectors
      - 2.2.1.5.2 Sub-detector electronics
      - 2.2.1.5.3 Vertex electronics
      - 2.2.1.5.4 Readout electronics
      - 2.2.1.5.5 Calibration system
      - 2.2.1.5.6 HV power supply
      - 2.2.1.5.7 Detector control system
      - 2.2.1.5.8 Cable system
      - 2.2.1.5.9 Cooling system

- 2.2.1.5.10 Integration in MPD
- 2.2.1.6 Forward Hadron Calorimeter (FHCAL)
  - 2.2.1.6.1 FHCAL module design
  - 2.2.1.6.2 Readout of the FHCAL modules
  - 2.2.1.6.3 FHCAL energy calibration
- 2.2.1.7 Ecal Detector
  - 2.2.1.7.1 Ecal design
  - 2.2.1.7.2 FE electronics
  - 2.2.1.7.3 Ecal integration
  - 2.2.1.7.4 Test infrastructure for mass production
- 2.2.1.8 The Inner Tracking System ITS
- 2.2.1.9 The MPD thin-wall beampipe
- 2.2.1.10 MPD Data Acquisition (DAQ) system and computer cluster
  - 2.2.1.10.1 DAQ Electronics
  - 2.2.1.10.2 MPD DAQ network
  - 2.2.1.10.3 MPD Mini Data Center (MCD) and Control Room
  - 2.2.1.10.4 MPD DAQ software
- 2.2.1.11 Engineering Support
  - 2.2.1.11.1 Architecture of mechanical structure
  - 2.2.1.11.2 Technical description and equipment
  - 2.2.1.11.3 Management
- 2.2.1.12 Integration in MPD
- 2.2.2 Detector for study of Baryonic Matter at Nuclotron (BM@N)
  - 2.2.2.1 Wide aperture Silicon Tracking System – STS
    - 2.2.2.1.1 STS module
    - 2.2.2.1.2 Ladder assembly
    - 2.2.2.1.3 DAQ system
    - 2.2.2.1.4 System integration
  - 2.2.2.2 Forward Silicon Detectors
  - 2.2.2.3 GEM central tracking system
  - 2.2.2.4 Outer tracker based on DCH chambers
  - 2.2.2.5 Gas system for central and outer trackers
  - 2.2.2.6 Outer tracking system based on CSC chambers
  - 2.2.2.7 Time of Flight System TOF-700
    - 2.2.2.7.1 Design of the ToF-700 wall
    - 2.2.2.7.2 mRPC's design and assembling
    - 2.2.2.7.3 Heating and thermal stability of “warm” mRPC
    - 2.2.2.7.4 Front-end electronics (FEE) of mRPC

- 2.2.2.7.5 The support of ToF-700 wall
  - 2.2.2.7.6 TOF-700 data analysis
  - 2.2.2.8 Time-of-Flight system ToF-400
    - 2.2.2.8.1 Construction of mRPC, assembling and testing of ToF modules
    - 2.2.2.8.2 Electronics for ToF
    - 2.2.2.8.3 Gas system
    - 2.2.2.8.4 HV & LV power supply and Slow control system
  - 2.2.2.9 Detector T0 and Trigger System
    - 2.2.2.9.1 Detector for BM@N heavy ion program
    - 2.2.2.9.2 Detector for SRC experiments
  - 2.2.2.10 Zero degree calorimeter ZDC
    - 2.2.2.10.1 Moving platform
    - 2.2.2.10.2 Readout electronic and ZDC calibration
  - 2.2.2.11 Forward Hadron Calorimeter FHCAL
  - 2.2.2.12 Electromagnetic calorimeter Ecal
  - 2.2.2.13 BM@N DAQ system and computing
    - 2.2.2.13.1 Electronics modules
    - 2.2.2.13.2 Network infrastructure
    - 2.2.2.13.3 DAQ software
  - 2.2.2.14 The experimental hall of BM@N setup
  - 2.2.2.15 First experimental runs and BM@N status
- 2.2.3 Spin Physics Detector (SPD) for study of nucleon spin structure
- 2.3 Scientific and engineering infrastructure
- 2.3.1 Buildings of the Collider complex (Building No. 17)
  - 2.3.2 Cryogenic compressor station
  - 2.3.3 A building of the NICA Center
  - 2.3.4 Other building and experimental pavilions
  - 2.3.5 Auxiliary and technological equipment
  - 2.3.6 Cryogenic complex
    - 2.3.6.1 Helium compressors and helium facilities
    - 2.3.6.2 Nitrogen compressors and nitrogen facilities
  - 2.3.7 Infrastructure of energy-supplying and energy-saving engineering systems
    - 2.3.7.1 Energy supply systems
    - 2.3.7.2 The power supply system of the beam output channel from the Nuclotron to the Measuring pavilion

- 2.3.7.3 The power supply system for the transport of a beam of charged particles in the building 205
    - 2.3.8 Facility for assembly and testing of sc-magnets
  - 2.4 Computer unit and computer networks of the distributed information and computing cluster of the NICA project
    - 2.4.1 General structure of the computer unit and network
    - 2.4.2 Distributed computing network
    - 2.4.3 On-line cluster
    - 2.4.4 The NICA off-line cluster
      - 2.4.4.1 LHEP NICA off-line cluster
      - 2.4.4.2 LIT NICA off-line cluster
    - 2.4.5 File systems of the distributed cluster
    - 2.4.6 Software of the NICA Complex
    - 2.4.7 Engineering infrastructure of the computer unit
  - 2.5 NICA innovation block
    - 2.5.1 New nuclotron applied beamlines
    - 2.5.2 Stations for chip irradiation and radiobiological researchers
    - 2.5.3 Station for investigation in the field of nuclear energetic and transmutation SINET
    - 2.5.4 Chip irradiation by low energy ions in SOCIT
- 3. Personnel issues, mobility and activity of project participants
- 4. International cooperation
- Conclusion

## **Introduction**

The mega-science “NICA Complex” project is being implemented at the Joint Institute for Nuclear Research (JINR) in accordance with the Institute’s development plans and the Agreement between the Government of the Russian Federation (RF) and the International Intergovernmental Research Organization Joint Institute for Nuclear Research (JINR) on the construction and operation of a complex of superconducting rings on colliding beams of heavy ions NICA – NICA Complex (hereinafter – the Agreement). Works on the construction of the basic configuration of the NICA Complex project is carried out in all its facilities in accordance with the Agreement using the approved JINR budget funds, target funds of the RF received by JINR in 2016 – 2019 in accordance with the Agreement and its expansion as part of the national project Russian Federation “Science”, as well as the contributions of other project participants.

The presented report describes the progress in the creation of the NICA Complex achieved in 2019 (reports for 2017 and 2018 are located on the website at: <http://nica.jinr.ru>).

## 1. The basic configuration scheme, the main characteristics and working documents of the “NICA Complex” project

The basic configuration of the “NICA Complex” project is shown in Fig. 1.1. The complex will make it possible to accelerate and collide heavy ions, up to gold ions, in the optimal energy range, from the minimum – in the zone of extracted beams, to the most achievable  $\sqrt{s_{NN}} = 11$  GeV (for  $\text{Au}^{+79}$ , in the nucleon-nucleon center of mass system) at the collider, with an average luminosity of  $L = 10^{27} \text{ cm}^{-2}\text{s}^{-1}$ , which will allow to study nuclear matter in a state of maximum baryonic density, inaccessible to research in other laboratories of the world.

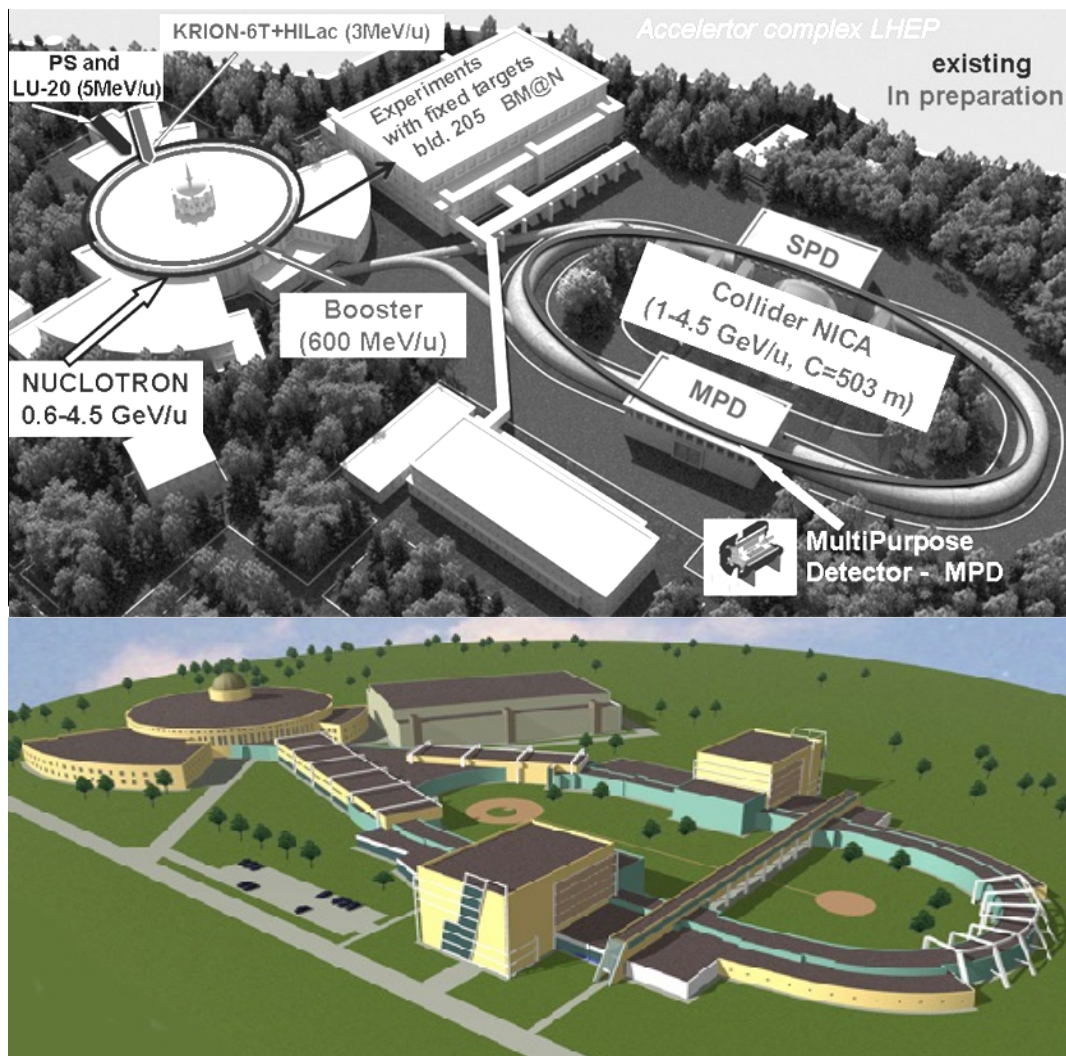


*Fig. 1.1. Scheme of the basic configuration of the “NICA Complex” project: at the top – the main elements of the complex and basic parameters; bottom – the architectural complex of existing buildings (the Nuclotron and the pavilion for experiments on extracted beams) and the building under construction #17, which will house a collider and two MPD and SPD set-ups.*

In addition, protons and deuterons with longitudinal and transverse polarization in the energy range up to  $\sqrt{s_{NN}} = 27$  GeV and  $\sqrt{s_{NN}} = 12.6$  GeV, respectively, with luminosities up to  $10^{32}$  cm<sup>-2</sup>s<sup>-1</sup>, will accelerate and collide at the Collider. These conditions will provide priority in the field of studies of the nucleon spin structure and clarification of the most important questions of the spin nature.

An updated passport of the “NICA Complex” project is available at [http://nica.jinr.ru/docs/TDR\\_spec\\_Fin0\\_for\\_site\\_short.pdf](http://nica.jinr.ru/docs/TDR_spec_Fin0_for_site_short.pdf). A more detailed technical description of the accelerator part of the NICA complex is available at <http://nucloweb.jinr.ru/nica/TDR.html>. The following are links to the scientific program of the project (“White Book”) – <http://nica.jinr.ru/files/WhitePaper.pdf>., BM@N detector project – [http://nica.jinr.ru/files/BM@N/BMN\\_CDR.pdf](http://nica.jinr.ru/files/BM@N/BMN_CDR.pdf), MPD detector project – [http://nica.jinr.ru/files/CDR\\_MPD/MPD\\_CDR\\_en.pdf](http://nica.jinr.ru/files/CDR_MPD/MPD_CDR_en.pdf) and SPD detector proposal – <http://indico.jinr.ru/getFile.py/access?resId=11&materialId=3&confId=718>.

## **2. Status of the implementation of the basic configuration of the complex**

The creation of the basic configuration of the NICA Complex project began at the end of 2013 at the stage of preparing the Agreement for signing. After its signing in June 2016, the JINR budget funds allocated from the Russian Federation and other countries (Germany, South Africa) are used in the implementation of the project. Among the largest contracts, partially or fully funded in 2019, are the contract for the construction of building 17, the creation of coils and the entire cold mass of the magnet, the control system and its engineering infrastructure, the contract for the production of iron yoke and magnet supports, and a contract for creation of the first high-frequency system VCH-1, for the development of satellite helium refrigerators with the company NPO Geliymash, for the transportation of the beam from the Nuclotron to the Collider, a contract for the construction of a cryogenic compressor station, a contract for the manufacture of collider beam lens elements, a contract for the manufacture of precision collider current sources, a contract for the manufacture of modules of the electromagnetic calorimeter of the MPD installation and a contract for the manufacture of lead plates of the electromagnetic calorimeter of this installation, a contract for the purchase of equipment to increase the computing power of the DAQ experiment BM @ N, as well as a contract for the manufacture of switching cabinets for the power supply system of the magnetic elements of the channel for transporting a beam of charged particles in the housing 205.

In parallel with the creation of objects of the basic configuration of the NICA Complex project, its scientific program is being implemented.

Below is the status of work completed in 2019.

### **2.1. Accelerator block of the NICA complex**

The NICA accelerator complex (Fig. 1.1) provides accelerated beams of ions from p to U including polarized beams of light nuclei at energies from 3.2 MeV/u up to 4.5 GeV/u for fixed target, external target and colliding beam experiments.

The accelerator complex includes:

- the injection complex, consisting of two independent parts – for light and for heavy ions;
- the booster synchrotron (Booster) at magnetic rigidity of 25 T·m dedicated to acceleration of heavy ions;
- the upgraded Nuclotron, main accelerator of the NICA facility at magnetic rigidity of 38.5 T·m;

- the NICA collider (two storage rings with two interaction points) (IP) at magnetic rigidity of 45 T·m, average luminosity  $L = 10^{27} \text{ cm}^{-2}\text{s}^{-1}$  for gold ion collisions at  $\sqrt{s_{NN}}$  up to 11 GeV/u;
- the Nuclotron internal target station;
- the experimental areas for applied research;
- required beam transport lines.

The facility construction is provided in accordance with the “Passport of the NICA accelerator complex”, Dubna, 2015, and “Technical project of the NICA acceleration complex”, Dubna, 2015.

Light ion injection chain was modernized and commissioned in 2016. Accelerator part of the heavy ion injection chain was commissioned in 2016.

Modernized Nuclotron starts operation for the NICA experimental program (BM@N and radiobiology programs) in 2018.

To the end of 2019 the completion of the following works are expected:

- commissioning of the transport line from heavy ion linear accelerator to the Booster,
- the Booster assembly and commissioning of its cryogenic magnetic structure, vacuum and power supply systems.

### **2.1.1. Injection complex**

Injection complex (Fig. 2.1.1.1) consists of two independent parts:

- injector of light ions into the Nuclotron;
- injector of heavy ions into the Booster.

Injector of light ions into the Nuclotron includes:

- light ion source (Duoplasmatron);
- source of polarized ions (SPI);
- laser ion source (LIS);
- linear accelerator, consisting of Radio Frequency Quadrupole section (RFQ) and Alvarez type drift tube linac LU-20M;
- required beam transport lines.

In the full configuration of the NICA facility the linear accelerator will be replaced by new Light Ion Linear Accelerator (LILAc), which is under construction now.

Injector of heavy ions into the Booster includes:

- heavy ion source «KRION»;
- Heavy Ion Linear Accelerator (HILAc), consisting of Radio Frequency Quadrupole section (RFQ) and two sections of drift tube linac (IH DTL),
- required beam transport lines.

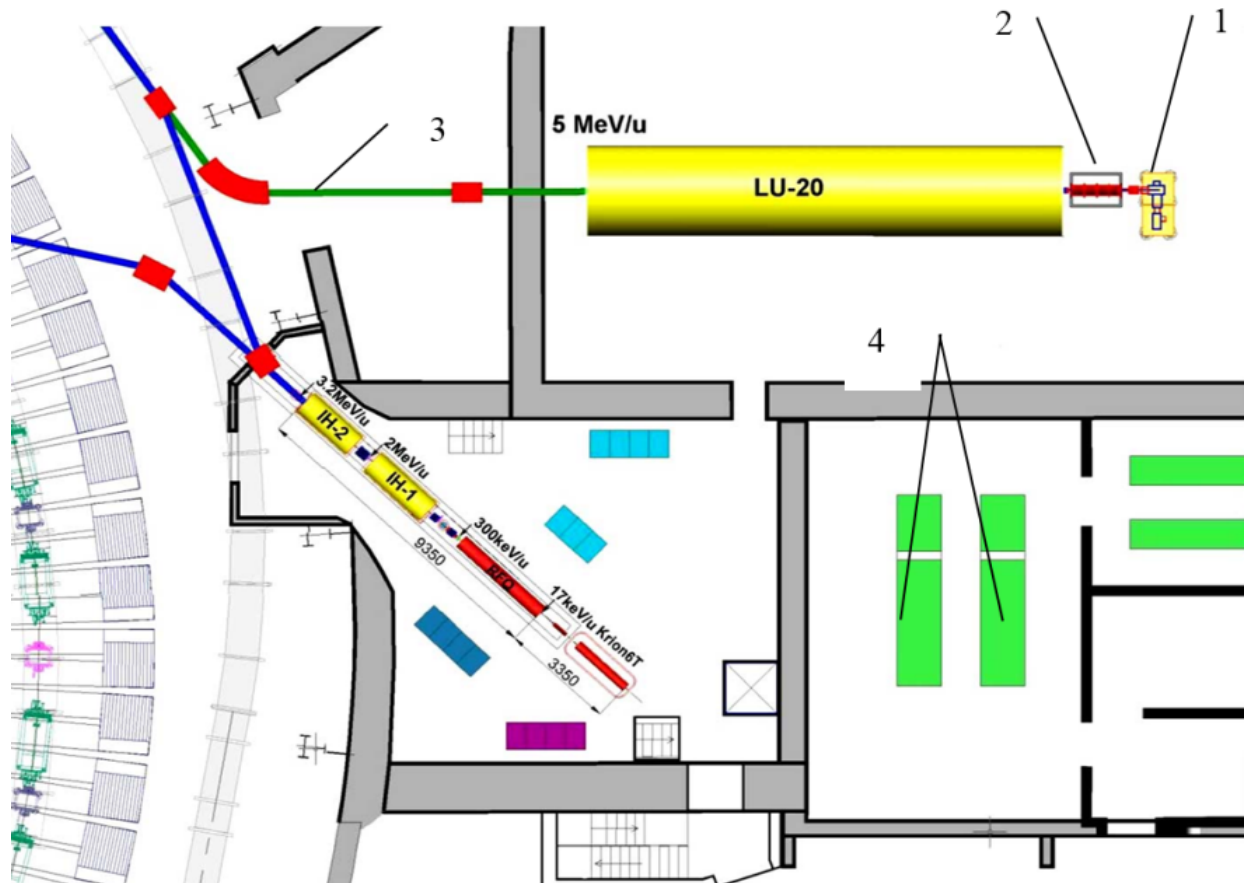


Fig. 2.1.1.1. Location of the injector complex elements: 1 – High Voltage platform for light ion source, LIS and SPI; 2 – RFQ fore injector; 3 – beam transport line from LU-20M to Nuclotron; 4 – LU-20M RF amplifier.

## 2.1.2. Ion sources

### 2.1.2.1. Laser source and light ion source

The light ion laser source, developed at the JINR Laboratory of High energy physics in 1983, is based on a CO<sub>2</sub> laser. The principle of its operation is based on the extraction of ions from the laser plasma formed as a result of the action of a focused laser pulse on the target. The radiation flux density at the target was  $\sim 10^{10}$  W/cm. and the spectrum of accelerated ions was  ${}^6\text{Li}^{3+}$ ,  ${}^7\text{Li}^{3+}$ ,  $\text{B}^{4+}$ ,  $\text{C}^{4+}$ ,  $\text{N}^{5+}$ ,  $\text{O}^{6+}$ ,  $\text{F}^{7+}$ ,  $\text{Mg}^{8+}$ ,  $\text{Si}^{11+}$ . To obtain ions with a higher charge state, an Nd-YAG two lasers were purchased in UK and included into the laser source and test bench for the source parameter optimization. The laser radiation flux density at the target is estimated to be  $\sim 10^{13}$  W/cm. The tests of the laser on the stand confirmed the presence of six charge states of ions in the carbon plasma. Thus, the new laser source can be configured to produce both light ions of high charge states and ions with a low Z/A ratio for testing both new accelerators – the HILAc and LILAc.

Duaplasmotron source is intended for generation of intensive beams of light ions including  $\text{He}^{+2}$ .

### 2.1.2.2. Source of polarized ions (SPI)

The main purpose of the SPI is to provide the intensity of the accelerated polarized beams at the JINR Accelerator Complex up to  $5 \cdot 10^{10}$  particles/pulse. The polarized beams are generated in the following elements of the source:

- Thermal hydrogen (deuterium) atoms are produced in RF discharge dissociator.
- The atoms are polarized by passage through inhomogeneous magnetic field of sextupole magnets.
- Nuclear polarization is increased with RF transitions.
- Polarized atoms are converted into polarized ions in the plasma ionizer.

Main systems of the source (gas feeling, vacuum, electronic and RF racks, High-current power supply – Fig. 2.1.2) are located at High Voltage platform. For the source operation the remote-control system was created.

The SPI is based in substantial part on the equipment from IUCF (Bloomington, USA). The SPI is created in cooperation with INR of RAS (Moscow), commissioning at LU-20M was provided in 2016.

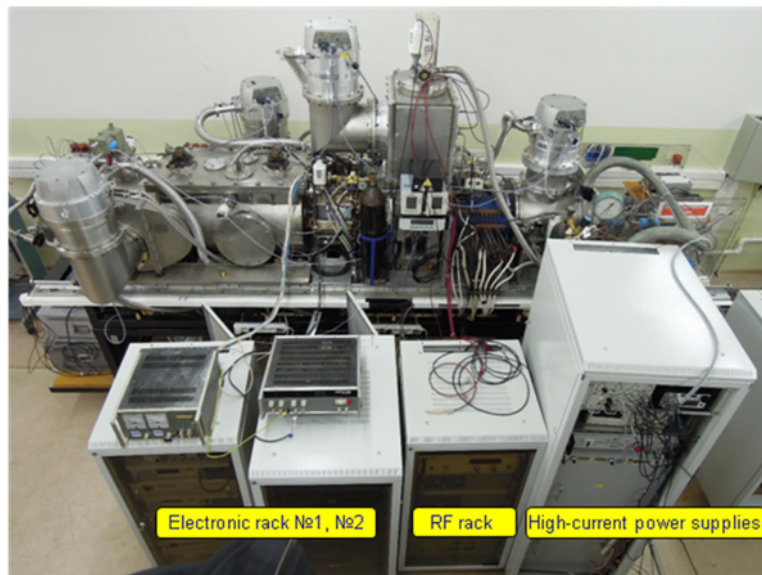


*Fig. 2.1.2.1. SPI in assembly at test bench.*

### 2.1.2.3. Heavy ion source «KRION»

Beams of the heavy ions with a high charge states will be produced by the electron-string source (ESIS) “KRION”. This source was developed in JINR and based on the phenomenon discovered during the study of operating modes of the electron-beam

source EBIS, operating in the reflective mode. It was found that under certain conditions, the “cloud” of repeatedly reflected electrons enclosed in a strong solenoid magnetic field exhibits property similar to the phase transition. This leads to a gradual increase in the electron plasma density and the transition to a new stationary state called the electron string. In the frame development of basic version of the NICA facility the “stand” version of the source KRION-6T was constructed. In the accelerating run of the Nuclotron in 2018, the beams  $C^{6+}$ ,  $Ar^{16+}$  и  $Kr^{26+}$  were used, and the operating modes of the source were also investigated (Fig 2.1.2.2).



*Fig 2.1.2.2. KRION-6T at injector facility during the Nuclotron run in March 2018.*

The construction of the source for total NICA configuration – the source “KRION – 6N” is progressing.

The source «KRION-N» (Fig. 2.1.2.3) – cryogenic ultra-high vacuum ionizer with 6 T superconducting solenoid, having three temperature terminals (4.2 °K, 40 °K and 300 °K) consists of:

- electron-ion-optic system;
- cryo-magnetic system;
- cryogenic vacuum system;
- system for injection of a working substances into the electron string;
- electric power and control systems.

The source length is 1460 mm. Additionally one presumes construction and installation diagnostic devices for measurement of emittance and for analysis of charge state composition of the extracted beam.

Parameters of the NICA ion sources are summarized in the Table 2.1.2.1.

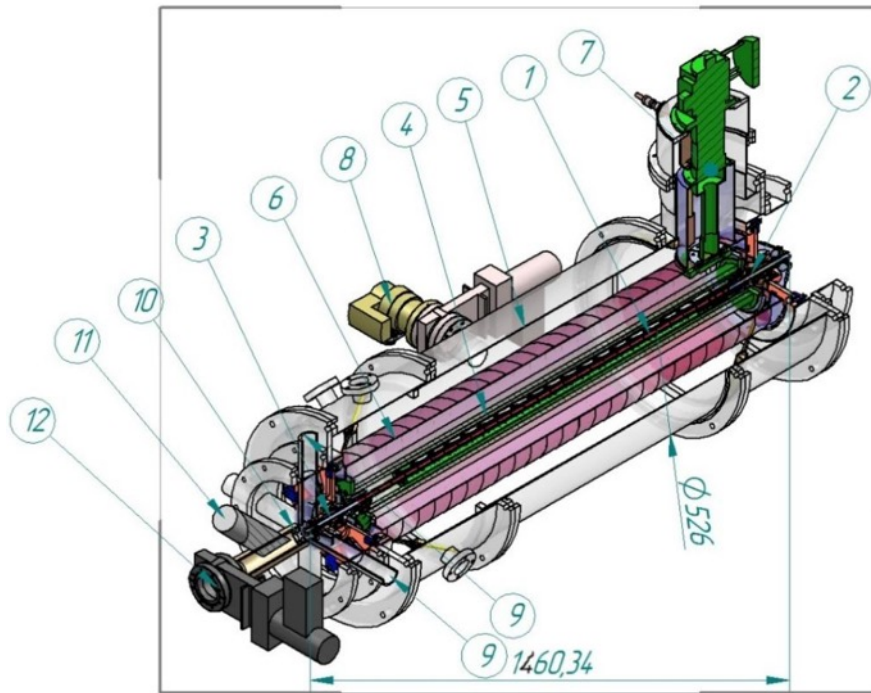


Fig. 2.1.2.3. Ion source «KRION-N», 1 — elements of the electron-ion-optic system located along the solenoid axis, 2 — electron gun and 3 — electron reflector, located outside the solenoid in the residual magnetic fields of  $B_{max}/20$ , 4 — 1200 mm superconducting solenoid, 5 — external vacuum vessel, 6 — copper thermal shield, 7 — head of cryo-cooler, 8 — vacuum valve, 9 — chamber for movable detectors, 10 — electrostatic lens for control of extracted ion beam, 11 — entrance of time-of-flight 15exed15et, 12 — vacuum valve at the entrance into accelerating section.

Table 2.1.2.1.

### Parameters of Particle Sources of NICA Injection Facility

Source	KRION-6N	Laser source	Duoplasmatron	SPI
Particles	$Au^{31+}$	Light ions up to $Mg^{10+}$	$H^+$ , $D^+$ , $He^{2+}$	$\uparrow H^+$ , $\uparrow D^+$
Particles per cycle	$\sim 2.5 \cdot 10^9$	$\sim 10^{11}$	$H^+$ , $D^+ \sim 5 \cdot 10^{12}$ $He^{2+} \sim 10^{11}$	$5 \cdot 10^{11}$
Repetition, Hz	10 (3 pulses for 5 sec)	0.5	1	0.2

#### 2.1.2.4. Linac LU-20M

The injector of light ion into Nuclotron is based on modernized LU-20M accelerator and consists of:

- fore-injector on the basis of RFQ accelerator;
- Alvarez type accelerator LU-20M;
- beam transport line from LU-20M to Nuclotron with debuncher.

It includes the following main systems and subsystems:

- vacuum system;

- low level Radio Frequency system (LLRF);
- LU-20M powerful RF amplifier “Radonit”;
- RFQ powerful RF amplifier;
- power supply system for axial and quadrupole lenses, dipole magnets;
- beam diagnostic system;
- Control system.

The fore-injector (Fig. 2.1.2.4, Fig.2.1.2.5) includes the Low energy beam transport line (LEBT), 3 sections of 4-road RFQ accelerator and the Medium energy beam transport line (MEBT). Main parameters of the fore injector are listed in the Table 2.1.2.2.

LEBT consisting of accelerating tube, two magnetic axial lenses, buncher and beam diagnostic box was created in cooperation with INR RAS and commissioned in 2016. RFQ accelerator was designed and constructed in the frames of agreement between JINR, ITEP and MEPhI. LLRF and RFQ powerful amplifier was constructed by ITEP. LEBT and RFQ were commissioned in 2016. MEBT consisting of two triplets of quadrupole lenses and buncher was designed by ITEP, the buncher was constructed at Chernogolovka. The MEBT was commissioned in 2017.

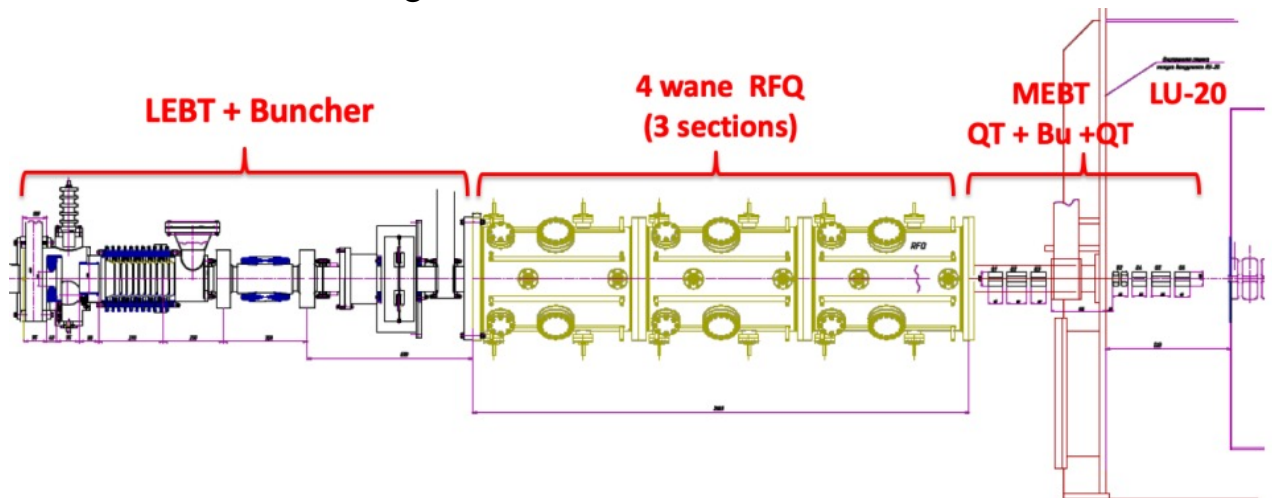
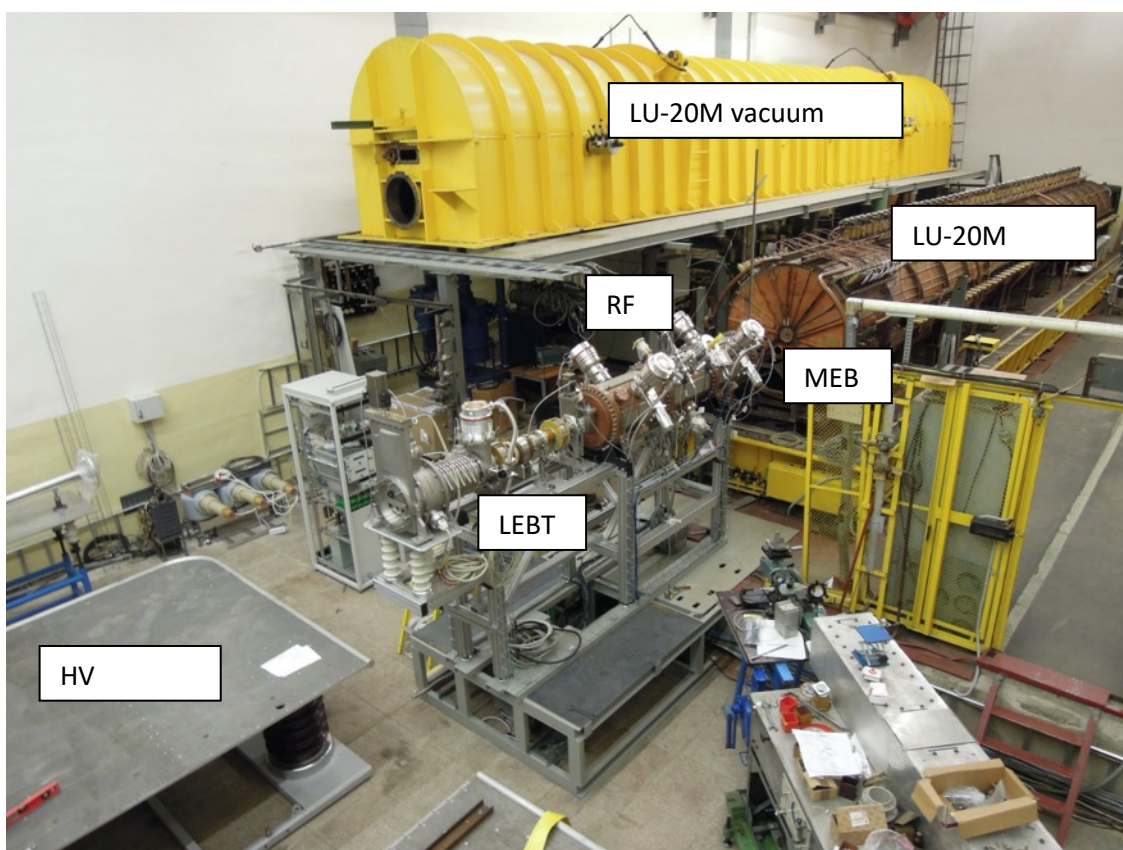


Fig. 2.1.2.4. Structure of LU-20M fore injector.

Table 2.1.2.2.

Main parameters of the LU-20M fore injector

Ion charge to mass ratio $q/A$	1.0	0.5	$\geq 0.3$
Injection energy, [keV]	31	61.8	103
Max current, [mA]	10	20	10
Output energy [MeV/u]	0.156		
Norm emittance (output) [ $\pi \cdot \text{cm} \cdot \text{mrad}$ ]	$\leq 0.5$		
RFQ length, [m]	2.2		
Transmission, %	$> 85\%$	$> 89\%$	$> 93\%$
In LU-20 acceptance	70 %	71 %	80 %



*Fig. 2.1.2.5. LU-20M fore injector during assembly.*

The LU-20 accelerator was put into operation in 1972 as proton injector for Synchrotron. For its operation in the frame of NICA facility at parameters corresponding to the “Technical project of the NICA acceleration complex” the modernization was provided in 2013 – 2018 including the following works:

- creation of new fore injector;
- partial modernization of RF generator “Rodonit”;
- creation of modern vacuum system;
- creation of new power supply system of LU-20 quadrupole lenses;
- modernization of power supply system for magnetic elements of the LU-20 – Nuclotron beam transport line;
- creation of new debuncher;
- development of the beam diagnostic system;
- modernization of control and timing systems.

At the “Rodonit” generator new solid state switches were installed at modulators, control and supply systems were modernized.

Structure of the new vacuum system of the fore injector, LU-20M and beam transport line are shown on the Fig. 2.1.2.6 – Fig. 2.1.2.7. Vacuum control system was created.

The debuncher in the beam transport line to the Nuclotron was created in cooperation with INR RAS.

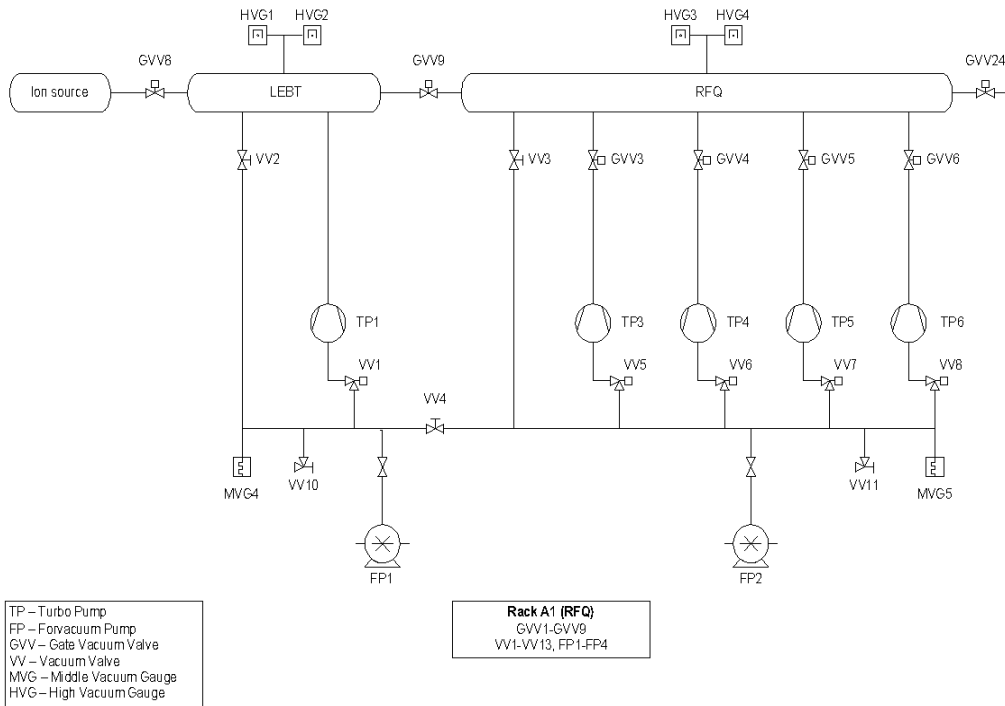


Fig. 2.1.2.6. Structure of the LU-20M fore injector vacuum system.

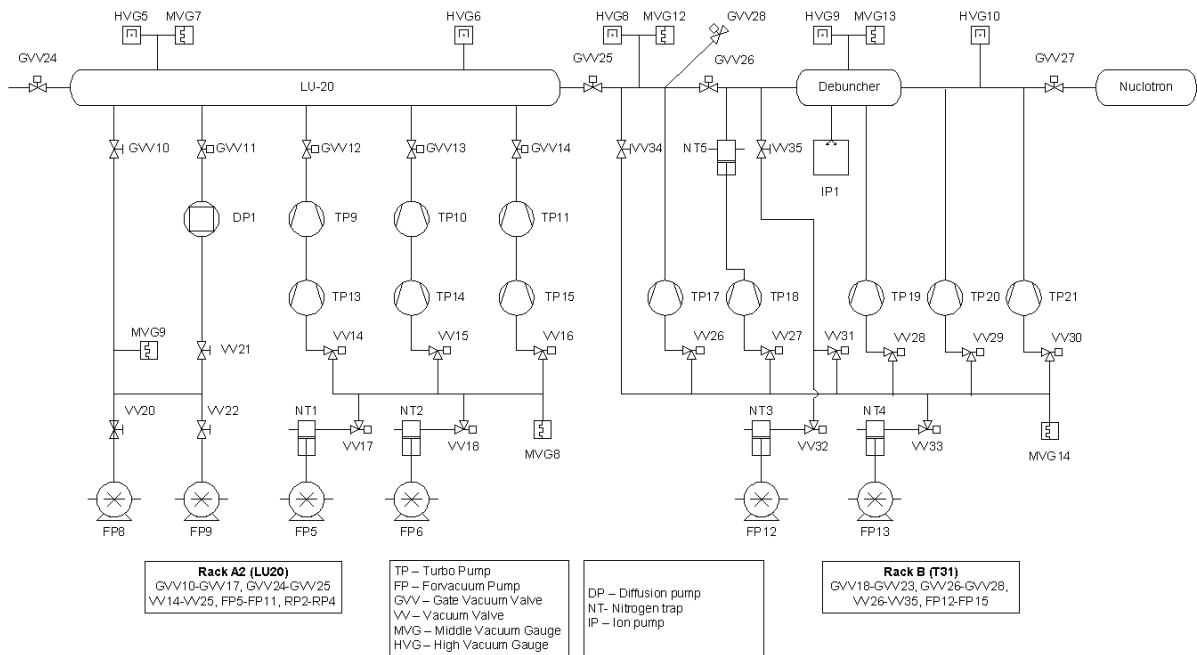


Fig. 2.1.2.7. Structure of the vacuum system of LU-20M and beam transport line to the Nuclotron.

LU-20M was put into operation in 2018 with about half-year delay in comparison with initial plan. The delay is related mainly to long term of works to find contractors in RF. Main parameters of LU-20M are listed in the Table 2.1.2.3.

Main parameters of LU-20M

Harmonics number	$2\beta\lambda$
Injection energy	156 keV/u
Output energy	5 MeV/u
Working frequency	145 MHz
Diameter of the cavity	1,4 m
Cavity I	14,4 m
Drift tube number	57 + 2 half-tubes
Quality factor	40000
Synchronous phase	31,5°
Focusing structure	FODO
Field gradient of quadrupole lenses	(58,4 ÷ 7,4) T/m
Acceptance	220 $\pi$ ·mm·mrad

### 2.1.2.5. Heavy ion linear accelerator HILAc

The HILAc (Fig. 2.1.2.8) provides heavy ion (up to U) at charge to mass ratio  $\geq 0.16$  for

- further injection into Booster;
- for area-3 of applied researches, which will be developed for investigations of radiation damages in microelectronics; heavy ions with the energy of 3.2 MeV/u will be used for irradiation of decapsulation microchips.

The injector of heavy ions into the Booster based on HILAc includes:

- low energy beam transport line (LEBT), consisting of accelerating tube, two magnetic axial lenses and beam diagnostic box;
- RFQ section, accelerating ions up to 300 keV/u;
- medium energy beam transport line, including two doublets of quadrupole lenses and buncher;
- two IH DTL sections, with quadrupole doublet in between, providing 3.2 MeV/u of the output energy;
- beam transport line from HILAc to Booster, including debuncher.

The HILAc includes the following main systems:

- low level RF system,
- powerful RF system on the basis of solid state amplifiers at 100.6 MHz and total pulsed power of about 1 MW,
- vacuum system,
- power supply system for quadrupole lenses,
- water cooling system.

In 2015 the HILAC was installed in the workplace in the hall of the injection complex – about one year later than in initial contract. The delay was determined mainly by delay in the repairmen of the building for the accelerator location. In 2016 first beam acceleration was demonstrated. In 2018, a series of tests on HILAc commissioning had been carried out to measure the energy and estimate transmission coefficient of accelerated beams from laser ion source.



*Fig. 2.1.2.8. The HILAc at the accelerator complex.*

### **2.1.2.6. Light ion linear accelerator LILAc**

In the total version of the NICA complex as an injector into the Nuclotron the Light Ion Linear accelerator (LILAc) will be used. The LILAc, like the HILAc, designed by Bevatech GmbH, is intended for acceleration of polarized deuterons and protons, as well as light ions with a charge to mass ratio of  $Z / A \geq 0.33$  up to 13 MeV/u.

The injector of light ion into the Nuclotron on the basis of LILAc (Fig. 2.1.2.9) consists of:

- Low energy beam transport line (LEBT)
- Accelerating section with radio-frequency quadrupole (RFQ),
- Medium energy beam transport line (MEBT) with rebuncher (REB)
- Three accelerating sections with drift tubes structure (IH1, IH2, IH3);

- Beam transport line from LILAc to the Nuclotron with debuncher.
- It includes the following main systems and subsystems:
- RF system including the powerful RF amplifiers and Low level Radio Frequency system (LLRF),
  - Vacuum system;
  - Power supply system for axial and quadrupole lenses, dipole magnets,
  - Beam diagnostic system,
  - Control system.

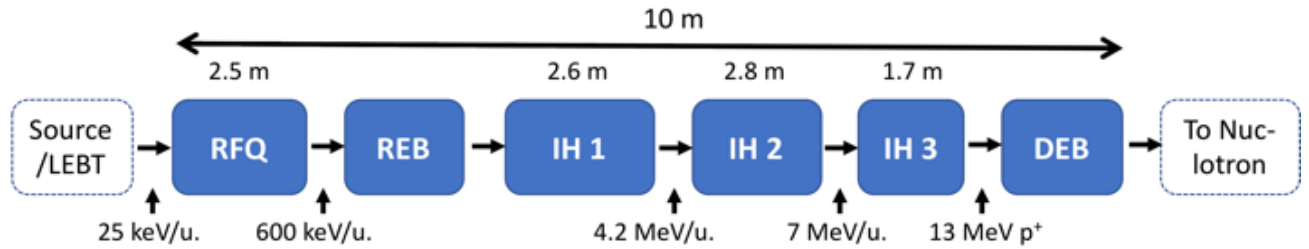


Fig. 2.1.2.9. Lilac cavity scheme.

The Linac will be located in LU-20 hall at JINR (Fig. 2.1.2.10). The main parameters of the LILAc are summarised in the Table 2.1.2.4.



Fig. 2.1.2.10. Location of the LILAc elements in LU-20 hall.

Table 2.1.2.4.

LILAc Main Parameters

Parameter	Protons	C <sup>4+</sup>
A/Q	1	3
Injection Energy	25 keV	300 keV

Exit Energy	13 MeV	84 MeV
Beam current	5 mA	15 mA
Rep. Rate Limit	$\leq 5$ Hz	
Current Pulse Duration	30 $\mu$ s	
RF Pulse Length	200 $\mu$ s	
RF Frequency	162.5 MHz	
Transmission	$\geq 80\%$	
Length of the Linac	$\leq 10$ m	

### *LEBT, RFQ, MEBT*

For the LILAC two different ion sources, a laser ion source (LIS) and a source of polarized ions (SPI), will be used. From the LIS it is planned to receive light ions, while the SPI will generate polarised and non-polarised protons and deuterons. The ion sources are placed on a high voltage terminal (up to 150 kV).

The LEBT channel with a length of about 1.8 m consists of 2 parts:

- The first part is an electrostatic section with ion optics and an electrostatic tube,
- The second part uses two magnetic solenoids with a maximum magnetic field of 1.2 T.

The LEBT channel is currently under redesign.

A 4-rod type RFQ is the first RF accelerating structure of the Linac of a length of 2.5 m. It accelerates, focuses and bunches the 30 keV/u DC beam from the LEBT to 600 keV/u. The cavity will be made of copper plated stainless steel, while the inner structure - the electrodes (rods), the stems and tuning plates - will be machined from solid copper. To ensure a stable operation in terms of field and frequency the RFQ will be equipped with one passive and one active piston tuner.

The MEBT section provides a proper beam matching from the RFQ into the first IH-DTL structure. A standard concept was applied, consisting of two short quadrupole doublet magnets for the transverse beam matching with 2 magnetic steerers attached and a two gap Re-buncher cavity in the centre. It resulted in a rather compact layout - only about 0.8 m in total - but with enough space reserved for on-line beam diagnostic elements. For the latter a beam position monitor, BPM, as well as an ACCT are foreseen to determine the beam position, bunch signal and beam current.

### *IH-DTL*

A compact DTL section of the LILac has been designed by using the beam dynamics simulation codes LORASR and validation in Tracewin. A beam energy gain from 0.6 MeV/u to 7.0 MeV/u for the design particle with a mass over charge ratio  $A/q = 3$  is obtained within a Linac length of about 7 m. A post accelerator for protons with an energy of 13 MeV adds up to a total Linac length of 10 m.

Beam dynamics design uses KONUS beam dynamics, which allows for multi gap cavities and a small number of transverse focusing elements. These are powerful magnetic quadrupole lenses (doublets or triplets), which can be integrated into the cavities or placed as external elements in between the resonators.

The DTL consists of three IH cavities:

- The first IH tank (IH1) has two internal quadrupole triplet lenses and achieves an energy gain from 0.6 to 4.2 MeV/u.
- The second one (IH2) has one quadrupole triplet and provides an end energy of 7.0 MeV/u.
- The third IH Tank is a post accelerator for protons only with an end energy of 13 MeV and no internal lens.

As beam diagnostic elements each structure will be followed by a BPM and where applicable an additional current transformer to measure transmission.

### *RF and LLRF*

Each cavity will be fed by a dedicated high power amplifier to provide the corresponding power for the accelerating fields in the cavities. The LLRF control soft- and hardware is realized in the MicroTCA.4 standard will be developed together with Bevatech and the MicroTCA Technology Lab at DESY based on the LLRF system from XFEL.

It was decided to use solid state high power amplifier for the 6 cavities due to modularity, reliability and decreasing costs, also underpinned by the experience with the HILAC project. The power budget was planned considering the cavity RF losses, beam loading and a 30 % power margin. It was estimated to use 10 kW amplifier for the buncher cavities, 300 kW and 600 kW for the RFQ and the IH cavities 1 and 2, and approximately 300 kW for IH cavity 3. These values may still vary in the future since final RF calculations are still in progress.

The Low Level Radio Frequency (LLRF) system, to control the RF fields of the accelerating cavities, is based on MicroTCA.4 standard. The electronic cards for all 6 cavities fit into one crate with 9 units height.

The system is generator driven, thus, the RF reference adjusted in amplitude and phase and with a baseband vector modulator provides the input signal to the high power solid state amplifier (SSAM). For accelerator operation, the cavity field gradients and phases can be user defined where the stability of the fields is ensured through digital real-time fast feedbacks programmed in Field Programmable Gate Arrays (FPGAs). The cavities frequency is measured and readjusted on demand through motor tuners with a LLRF system for each cavity.

For the beam transport from LILAc to the Nuclotron the existing beam transport line will be used. The LILAc control and timing systems will be based on existing ones of the LU-20M.

The LEBT, RFQ, REB1, IH1, IH2 sections are under construction by German firm BEVATECH. These sections will be delivered in JINR in 2021. The IH3 section is under design, it will be delivered in JINR in 2022.

### 2.1.3. Booster synchrotron

Superconducting booster synchrotron (Booster) is the heavy ion injector of the Nuclotron. Main goals of the Booster operation are the following:

- beam storage at injection energy ( $2 \cdot 10^9$  ions of  $^{197}\text{Au}^{31+}$ );
- acceleration at minimum loss by achievement of ultra-high vacuum conditions in the beam pipe,
- formation of the required beam phase volume by electron cooling application;
- acceleration of heavy ions to the energy required for effective stripping;
- fast extraction of the beam for injection into the Nuclotron.

For the beam transfer into the Nuclotron the Booster is equipped with corresponding beam transport line.

The Booster with a perimeter of 211 m and a structure of four periods is placed inside the yoke of the Synchrophasotron magnet (Fig. 2.1.3.1). The maximum field of the Booster dipole magnets is 1.8 T (magnetic rigidity is 25 T·m), which corresponds to the  $^{197}\text{Au}^{31+}$  ion energy of 578 MeV/u.

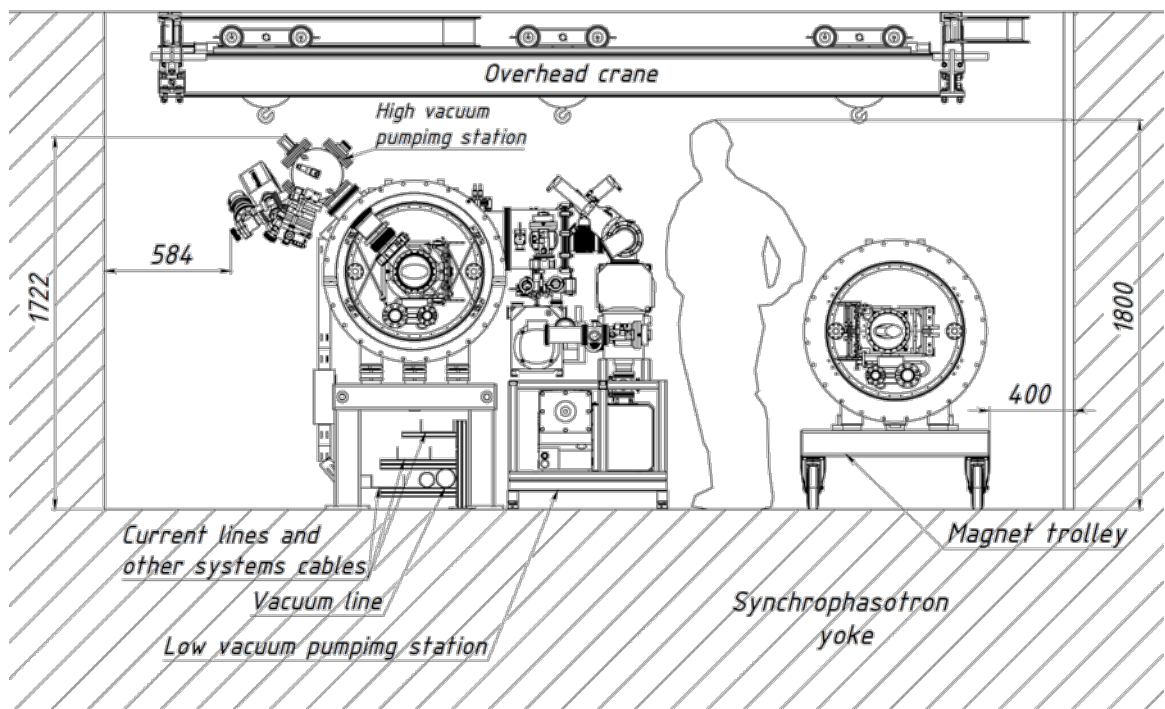


Fig. 2.1.3.1. Location of the Booster magnets inside the yoke of the Synchrophasotron magnet.

The Booster (Fig. 2.1.3.2) includes the systems listed below.

*Cryo-magnetic system*, including dipole magnets, quadrupole lenses, correctors, vacuum chambers, cryostat system. The magnetic structure of the Booster consists of 4 superperiods, each of them includes 5 regular periods and one period that does not contain dipole magnets. The regular period includes focusing and defocusing

quadrupole lenses, 2 dipole magnets, and 4 small free straight sections designed to locate multipole correctors, collimators, and diagnostic equipment. The listed elements of the magnetic system belong to the structural elements of the Booster. Periods that do not contain dipole magnets are designed to locate inserted elements. The inserted elements are: the beam injection and extraction systems, the accelerating RF system and the electron cooling system.

*The electron cooling system (ECS)* of the Booster, designed to form the required value of the phase volume of the beam, has maximum electron energy of 60 keV. The electron cooling system is designed and manufactured in the Budker Institute of nuclear physics (BINP, Novosibirsk). ECS includes the following systems: main magnetic structure of ECS, electron gun and collector, magnetic optics, vacuum system and diagnostics of ECS, automated control system of ECS, power supply systems, engineering systems.

*Injection and extraction systems, transfer of the beam, beam transport lines*, including the following systems: injection System, fast extraction system, beam transport line from the Booster to the Nuclotron, slow extraction system, test benches for injection and extraction systems.

*Power supply system of booster magnets*, including the main and two additional power supplies, power supplies for correctors, energy evacuation system, quench detection system.

*Radio-frequency system (RF)*, including accelerating stations and control system. The Booster acceleration stations were designed and manufactured at Budker INP (Novosibirsk), delivered to JINR and tested on a testbench with a magnetic field cycle imitator in 2014.

*Diagnostic and control system* including the following subsystems and devices: magnetic field ramp dB/dt measurement system, cycle control system, pickups, diagnostics, orbit correction system, thermometry system, Booster ACS, orbit measurement system, ionization monitor. Additionally, the system includes test benches for the diagnostic and ACS elements.

*Vacuum system*, including a pumping system of the beam pipe, the pumping system of the insulation vacuum volume and control system of the vacuum equipment. The system also includes high-vacuum stands.

*The beam transport line from the Booster to the Nuclotron* also belongs to the Booster systems and is functionally combined with the beam injection and extraction systems.

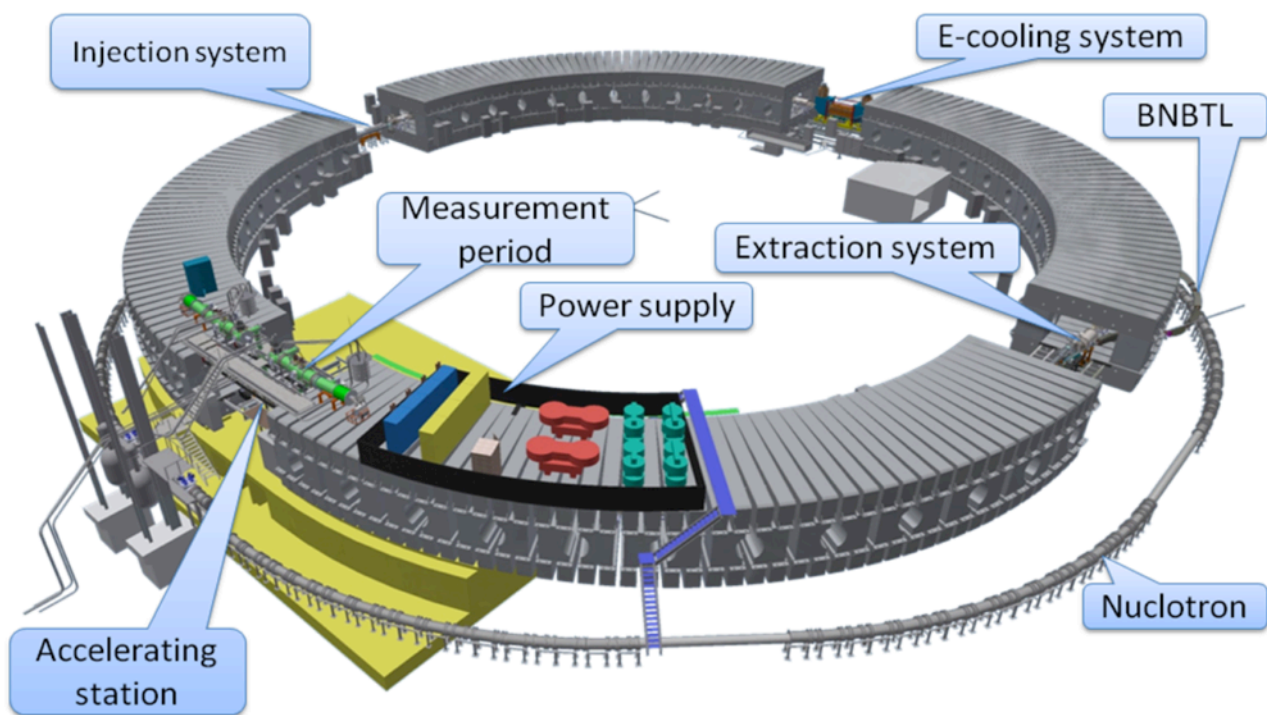


Fig. 2.1.3.2. Location of the main Booster systems.

The structure of the Booster, the working cycle and the parameters of the radio-frequency accelerating system were presented and approved by the experts at the NICA MAC meeting on June 07, 2011. The main parameters of the Booster are listed in the Table 2.1.3.1.

Table 2.1.3.1.

#### Main parameters of the Booster

1. Общие данные	
Ions	$^{197}\text{Au}^{31+}$
Injection energy	3.2 MeV/u
Maximum energy	600 MeV/u
Magnetic rigidity at injection	1.6 T·m
Maximum magnetic rigidity	25 T·m
Circumference	210.96 m
Transition energy	3.25 GeV/u
2. Optic structure and magnetic elements	
Number of super-periods	4
Number of DFO periods	24
Number of dipole magnets	40
Number of quadrupole lenses	48
Effective length:	
Dipole magnets	2.2 m
Quadrupole lenses	0.47 m
Magnetic field of the bending magnets:	
At injection	0.11 T
Maximum	1.8 T
Gradient of the F lenses: at injection,	1.28 T/m

maximum	21.01 T/m
Gradient of the D lenses: at injection,	-1.31 T/m
maximum	-21.48 T/m
Bending radius in the dipole magnets	14.09 m
Number of long straight sections	4
Length of the long straight section	7 m
Lengths of the small straight sections	0.7/0.85/0.95 m
3. Lattice and beam parameters	
Betatron tunes:	
$Q_x$	4.8
$Q_z$	4.85
Chromaticity:	
$\Delta Q_x/(\Delta p/p)$	-5.1
$\Delta Q_z/(\Delta p/p)$	-5.5
Orbit compaction factor	0.05
Amplitude of corrected orbit	4 mm
Acceptance:	
Horizontal	$150 \pi \text{ mm} \cdot \text{mrad}$
Vertical	$57 \pi \text{ mm} \cdot \text{mrad}$
Beam emittance at injection $\varepsilon_{x,z}$	$15 \pi \text{ mm} \cdot \text{mrad}$
Horizontal emittance after acceleration $\varepsilon_x$	$< 11 \pi \text{ mm} \cdot \text{mrad}$
Vertical emittance after acceleration $\varepsilon_z$	$< 1.5 \pi \text{ mm} \cdot \text{mrad}$
Relative momentum spread at injection	$\pm 10^{-3}$
Maximum momentum spread	$\pm 2.3 \cdot 10^{-3}$
Momentum spread after acceleration	$\pm 2.2 \cdot 10^{-4}$
Revolution period at injection	8.5 $\mu\text{s}$
After acceleration	0.89 $\mu\text{s}$

Assembly of the Booster has been started in 2016 with the installation of the electron cooling system in its nominal position. Work on ECS tuning to design parameters is currently in the final stage. The first elements of the booster magnetic system were delivered to the accelerator hall in September 2018.

In accordance with the initial plan the completion of the assembly and the beginning of the Booster system commissioning was scheduled for the end of 2018. The delay of about a year is due to three main reasons:

- delay in the manufacture of beam position monitors by the manufacturer for more than six months;
- delay in the assembly of doublets of lens caused by unforeseen work on adjustment of the beam position monitors with a violation of the purity of the ultra-high vacuum volume of the beam chamber and its subsequent restoration;
- the need for repair and retesting of several coils of quadrupole lenses, caused by violations of the technological process during their manufacture.

Completion of the Booster assembly is scheduled for the end of 2019. The first run of the Nuclotron with a new heavy ion injection chain is scheduled for the end of 2020.

### 2.1.3.1. Cryo-magnetic system

The Booster magnetic system is designed by analogy with the magnetic system of the operating fast-cycling superconducting accelerator Nuclotron. The technology of the magnet manufacturing of the Nuclotron has been proposed and developed in the Laboratory of High Energies of JINR. It is highly efficient and reliable with relative simplicity and low cost. The presence of technological sites for the production and testing of the magnets in the Laboratory, as well as trained personnel makes it even more reasonable to choose magnets of the “window frame” type with a winding of hollow superconductor for the NICA Booster.

*The dipole magnets.* The main parameters of the Booster dipole magnets are given in the Table 2.1.3.2. The design of the dipole magnet is a sector magnet of the “window frame” type with a “cold” yoke of laminated transformer steel.

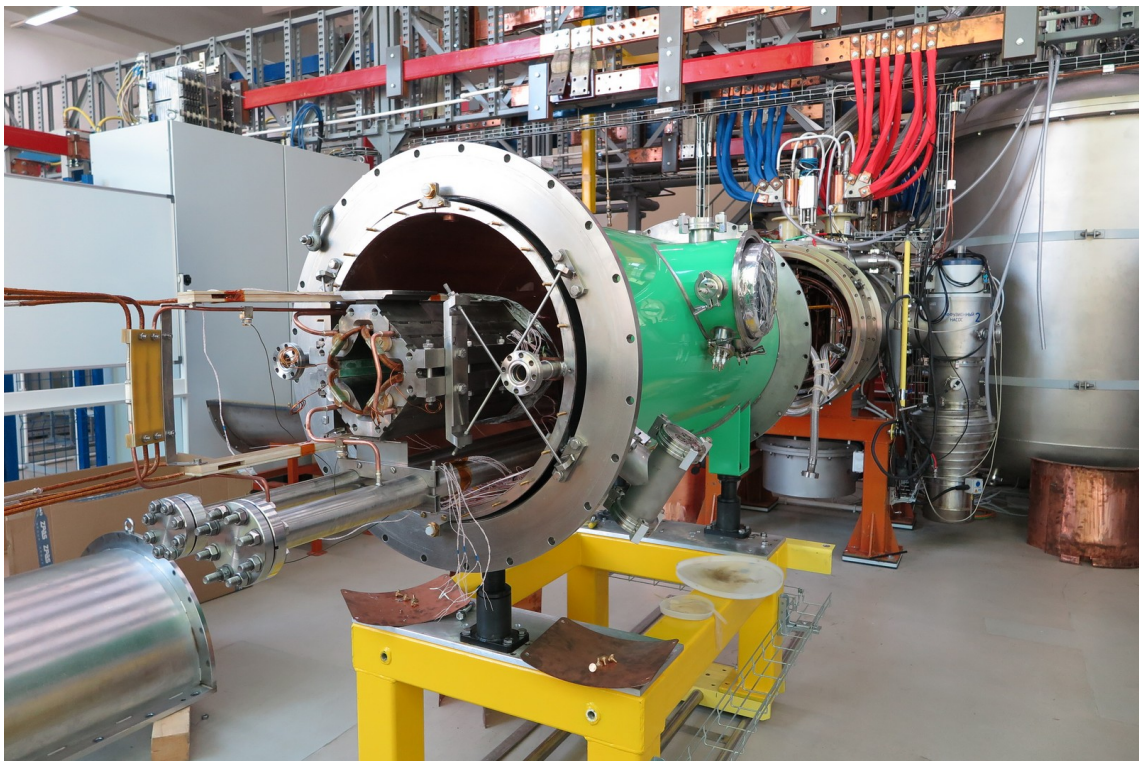
The booster dipole magnet inside the cryostat is presented on Fig. 2.1.3.3. The magnet is fixed in the cryostat with the help of 8 rods in such a way that after its cooling down from room to helium temperature, the position in space of the optical axis of the magnet remains unchanged. The diameter of the vacuum vessel of the cryostat is 640 mm. The thermal shield cooled by a stream of liquid nitrogen is located between the vacuum vessel and the magnet. The direct and return helium headers collectors are attached to the bottom of the magnet. The single-layer curved magnet winding is made of a hollow superconducting cable developed at the JINR LHE for the Nuclotron magnets. The cooling channel with forced two-phase (boiling) helium flow is inside the cable. The winding is placed in the gap of the iron yoke of the magnet, which compensate ponderomotive forces acting on the coil. The yoke is made of sheets of electrical steel 0.65 mm thick, bonded together by welding to steel corners and plates. The yoke is cooled by helium flow after winding.

Table 2.1.3.2.

The main parameters of the NICA Booster dipole magnets

Number of the magnets in the ring	Unit	40 + 1 reference magnet
Magnetic rigidity, $B\rho$	T·m	25
Maximum magnetic field in aperture, $B_{\max}$	T	1.8
Minimum magnetic field in aperture, $B_{\min}$	T	0.11
The magnet effective length, $L$	m	2.2
Magnetic field ramp rate, $dB/dt$	T/s	1.2
Magnetic field imperfection, $\Delta B/B$ at radius of 30 mm		$\pm 6 \cdot 10^{-4}$

Vacuum chamber aperture, hor./vert.	mm/mm	128/65
Bending angle	grad	9
Bending radius	m	14.09
Gap between poles (hor/vert)	mm/mm	150/67
Length of the iron yoke	m	2.14
Width of the yoke	m	0.31
Height of the yoke	m	0.228
Geometry length of the magnet	m	2.36
Weight of the magnet	kg	850
Current at maximum field	kA	9.68
Number of turns in the coil (per pole)		10(5)
Inductance	$\mu\text{H}$	630
Total cycle duration	s	4.02
Dynamical heat releases	W	8.4
Static heat flow (without current)	W	4.4
Total heat releases	W	12.8
The cooling channel diameter inside the cable	mm	3.0
Length of the cable in the coil	m	54
Length of the bus bars	m	12
Pressure difference between direct and return headers	kPa	$\leq 27$
Maximum temperature of the helium in the coil	K	4.65



*Fig. 2.1.3.3. The Booster dipole magnet inside the cryostat.*

Presently all the Booster dipole magnets are manufactured, tested and installed in the nominal positions inside the yoke of the Synchrohasatron magnet (Fig. 2.1.3.4).



*Puc. 2.1.3.4. Sections of the dipole magnets inside the tunnel.*

*The Booster quadrupole magnet is similar to the Nuclotron one and is a magnet with a superconducting winding and a laminated “cold” iron yoke with hyperbolic poles. Quadrupole magnets are installed in the vacuum vessel in pairs. The doublet of the Booster lenses is presented on the fig. 2.1.3.5 during the assembly of the half-yokes. The main parameters of the Booster quadrupole magnets are given in the table 2.1.3.3.*

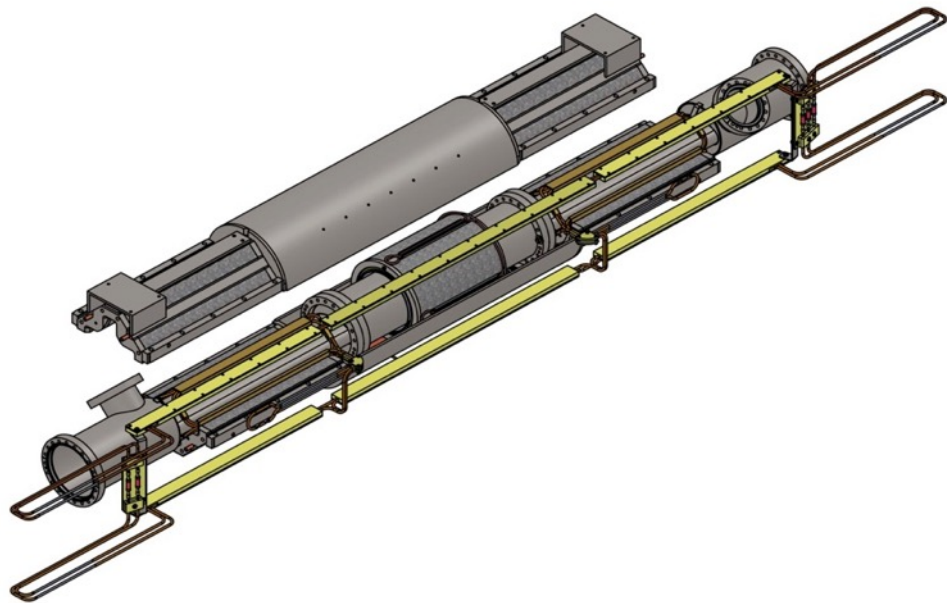


*Fig. 2.1.3.5. The doublet of the Booster lenses during the assembly of the half-yokes, the multi-pole corrector is located in the gap between the lenses.*

Table 2.1.3.3.

## The main parameters of the Booster quadrupole magnets

Number of the magnets in the ring	Unit	48 + 2 reference magnets
Maximum field gradient, $G_{\max}$	T/m	21.5
Minimum field gradient, $G_{\min}$	T/m	1.3
Effective length, $L$	m	0.47
Gradient ramp rate, $dG/dt$	(T/m)/s	14.3
Imperfection of the field gradient, $\Delta G/G$ at radius 30 mm		$\pm 6 \cdot 10^{-4}$
Distance from the pole to axis	m	0.0475
Vacuum chamber aperture, hor./vert.	mm/mm	128/65
Geometry length	m	0.66
Width of the yoke	m	0.226
Height of the yoke	m	0.226
Magnet weight	kg	110
Current at maximum gradient	kA	9.68
Number of turns in the coil (per pole)		8(2)
Inductance	$\mu\text{H}$	96
Total cycle duration	s	4.02
Dynamical heat releases	W	0.84
Static heat flow (without current)	W	3.0
Total heat releases	W	4.8
The cooling channel diameter inside the cable	mm	3.0
Length of the cable in the coil	m	19
Length of the connecting cables (bus bars)	m	12
Pressure difference between direct and return headers	kPa	$\leq 25$
Maximum temperature of the helium in the coil	K	4.65

*Cryostats, vacuum chambers.*

Cryostat system includes the following components (subsystem):

- cryogenic helium system;
- nitrogen system;
- monitoring system.

*The cryogenic helium system* is aimed for cooling the magnetic elements of the accelerator with liquid helium. The system includes:

- cryostats for input and output of helium from the accelerator ring;
- cryostats for current leads;
- subcoolers;
- helium headers;
- helium cooling channels of the magnetic elements;
- cooling channels of current leads;
- “cold” shut-off and control valves.

*The nitrogen system* is aimed for cooling of the thermal shields and HTS current leads. The system includes:

- nitrogen shields;

- siphons for input and output of nitrogen from the accelerator;
- “cold” shut-off and control valves.

*The monitoring system* is aimed to monitor the cooling process of the magnets according to the following parameters: temperatures of magnetic elements, current leads, thermal shields; pressures in helium communications.

The system includes:

- temperature sensor;
- pressure sensors.

An independent role in the monitoring of cooling is played by the *system of detecting the quench of superconducting windings*.

The insulating vacuum volume of the cryostat is divided into two half-rings. In each half-ring, a chain of 20 dipole magnets and 12 doublets of lenses are connected in parallel to the supply and return helium headers. The hydraulic resistances of lattice magnets and non-structural elements are chosen so that at the outlet of each of the parallel cooling channels the mass content of helium is about 90 % at operating cycle.

The connection of ultra high vacuum beam pipe between the magnetic system modules is carried out in the mobile clean zone (Fig. 2.1.3.6).

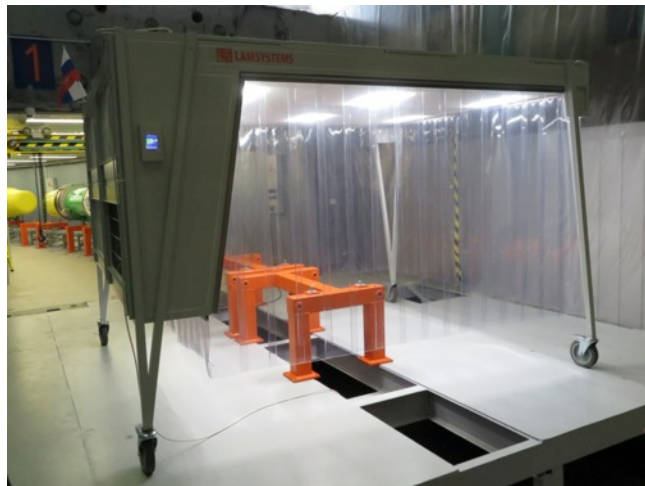


*Fig. 2.1.3.6. The mobile clean zone.*

Completion of the magnetic system assembly is scheduled for the end of 2019.

### **2.1.3.2. Electron cooling system**

The electron cooling system (ECA), designed to form the necessary parameters of the ion beam, both on the ion injection energy of 3.2 MeV/u and on the intermediate energy of 60 MeV/u, is located in the 4<sup>th</sup> long straight section of the Booster cryo-magnetic system (Fig. 2.1.3.7).

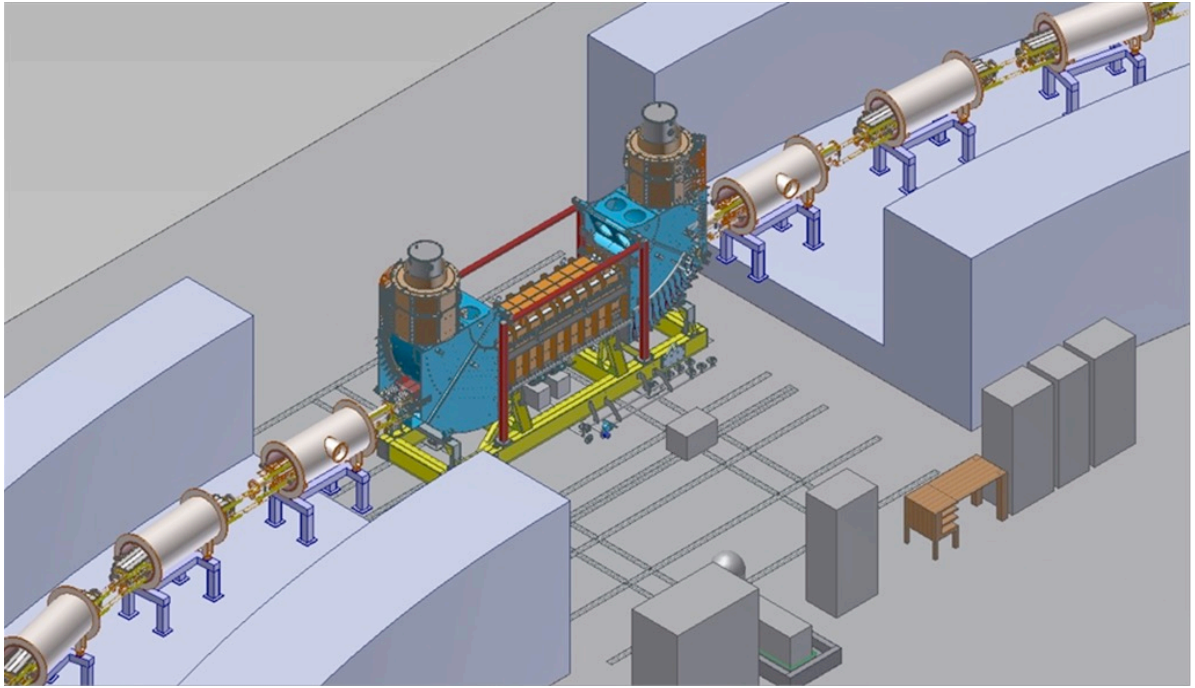


*Fig. 2.1.3.7. The forth long straight section of the Booster with the electron cooling system.*

The Booster ECS (Fig. 2.1.3.8) is an electron accelerator operating in a 34exed34et3434 mode. The electron gun forms an electron beam with the necessary parameters, which is transported to the electron collector by a system of straight and toroidal solenoids. In the straight section the trajectory of the electron and ion beam are coincide, which leads to the effect of interaction between them.

The electron cooling system includes the following elements:

- electron gun, working in a continuous mode;
- coils of the transverse magnetic field and electrostatic plates for correction of electron drift in toroids;
- toroidal solenoids to align the electron trajectory with the ion beam orbit;
- straight solenoid of the straight section where the process of ion cooling by electrons takes place;
- magnetic screen to create the required uniformity of the field in the straight section;
- electron collector, which is under the potential closed to the cathode one of the electron gun, which allows the cooling system to operate in the mode of energy recoperation;
- dipole magnets for ion beam orbit correction, which compensate the influence of toroids on the ion trajectory;
- ion channel of the Booster, passing through the bending toroids;
- two pickup stations at the entrance and exit of the straight solenoid for electron beam diagnostics.

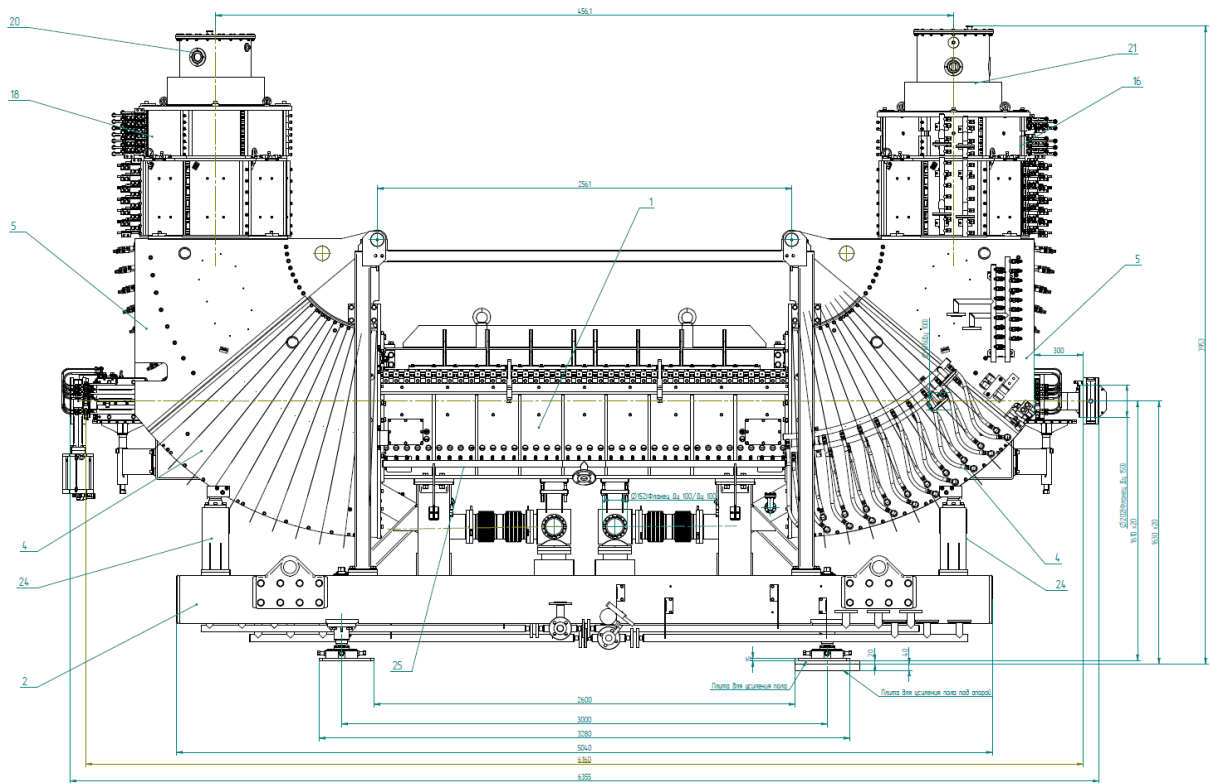


*Fig.2.1.3.8. The Booster electron cooling system. 1-cooling section with the straight solenoid surrounded by the magnetic screen, 2 – support, 4-toroidal coils, 5-toroidal section casing, 16 – section of the gun solenoid, 18 – section of the collector solenoid, 20-electron collector, 21-electron gun, 24-support for the magnetic corrector.*

The electron cooling system includes the following elements:

- electron gun, working in a continuous mode;
- coils of the transverse magnetic field and electrostatic plates for correction of electron drift in toroids;
- toroidal solenoids to align the electron trajectory with the ion beam orbit;
- straight solenoid of the straight section where the process of ion cooling by electrons takes place;
- magnetic screen to create the required uniformity of the field in the straight section;
- electron collector, which is under the potential closed to the cathode one of the electron gun, which allows the cooling system to operate in the mode of energy recuperation;
- dipole magnets for ion beam orbit correction, which compensate the influence of toroids on the ion trajectory;
- ion channel of the Booster, passing through the bending toroids;
- two pickup stations at the entrance and exit of the straight solenoid for electron beam diagnostics.

Main parameters of ECS are listed in the Table 2.1.3.4.

Table 2.1.3.4.

Main parameters of the Booster electron cooling system

Electron energy, keV	1.5 ÷ 60
Accuracy of the energy tuning and energy stability, $\Delta E/E$	$\leq 1 \cdot 10^{-5}$
Collector potential relative to the cathode, kV	0.5 ÷ 2,0
Electron beam current, A	0.2 ÷ 1,0
Beam current stability, $\Delta I/I$	$\leq 1 \cdot 10^{-4}$
Loss current of the electron, $\delta I/I$	$\leq 3 \cdot 10^{-5}$
Power consumption at cathode, W	100
Maximum power consumption at collector, W	2 000
Length of the straight solenoid, mm	2522
Cooling system length, mm	5715
<b>Total length including vacuum valves, mm</b>	<b>6355</b>
Cathode diameter in the electron gun, cm	3.0 ÷ 5.0
Longitudinal magnetic field, kG	1.0 ÷ 2.0
Magnetic field imperfection at the cathode, $\Delta B/B$	$< 10^{-3}$
Magnetic field imperfection in the straight solenoid, $\Delta B/B$	$< 10^{-4}$
Residual gas pressure at the cathode, Torr	$< 10^{-9}$
Residual gas pressure in the cooling section, Torr	$< 10^{-10}$
<b>Total power consumption at 2 kG field, kW</b>	<b>500</b>

**2.1.3.3. Systems of the beam injection and extraction, beam transport lines**

*Beam injection system* is aimed for realization of one from three alternative injection modes:

- single turn,
- single multy-turn,
- repeated multy- turn.

The system includes себя (Fig. 2.1.3.9):

- electrostatic septum (ESS) with high Voltage power supply;
- three pairs of the inflector plates IP1 – IP3 (kickers) with pulsed power supplies;

additional current sources for structural dipole magnets (blue rectangles) for formation of controlled bump of the orbit.

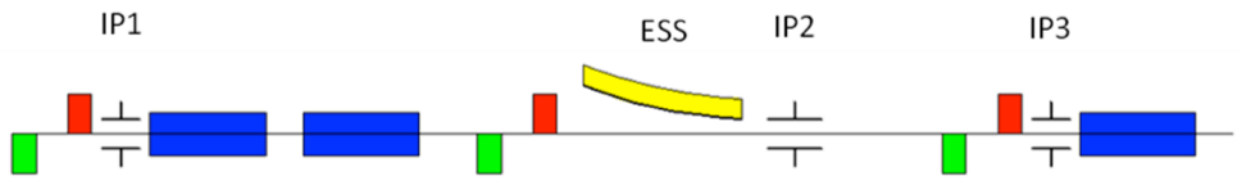


*Fig. 2.1.3.9. Schematics of the injection system.*

Main elements of the injection system are located in the first straight section of the Booster (Fig. 2.1.3.10).

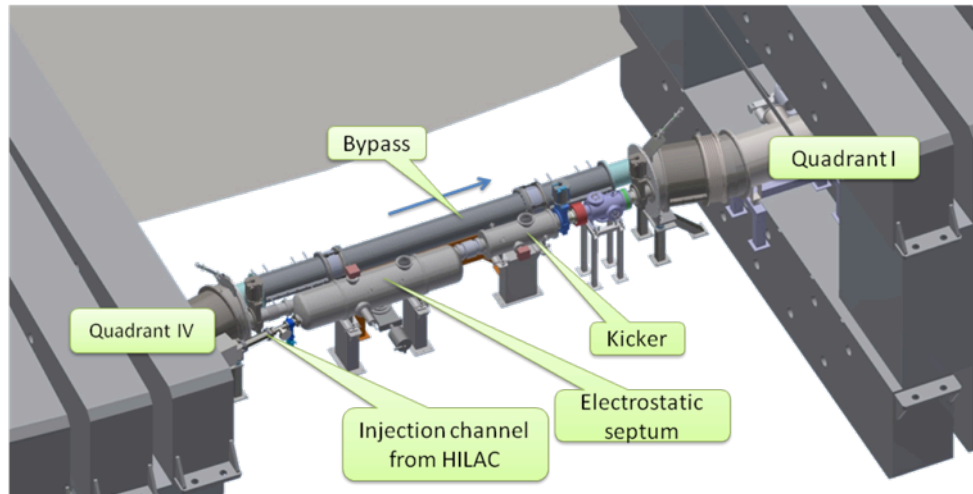


*Fig. 2.1.3.10. Location of the injection system elements.*

In the Booster basic configuration ESS и IP2 will be installed (Fig. 2.1.3.11), manufactured by Cryosystems/HiVac and BEVATECH/PINK companies correspondingly.



*Fig. 2.1.3.11. Electrostatic septum during manufacturing (left) and inflector plates IP2 (right).*

Assembly of the system will be completed in 2019, the commissioning is scheduled for the beginning of 2020.

*Beam extraction system* is aimed to stripping of the gold ions accelerated in the Booster and the beam transfer into beam transport line to the Nuclotron. Its main elements (kicker and two sections of the septum) are located in the third Booster

straight section (Fig. 2.1.3.12).

The extraction system and beam transport line to the Nuclotron are under manufacturing in BINP (Novosibirsk). Term of delivery to JINR is March 2010. Assembly and commissioning of the extraction system and beam transport line are scheduled for 2020.

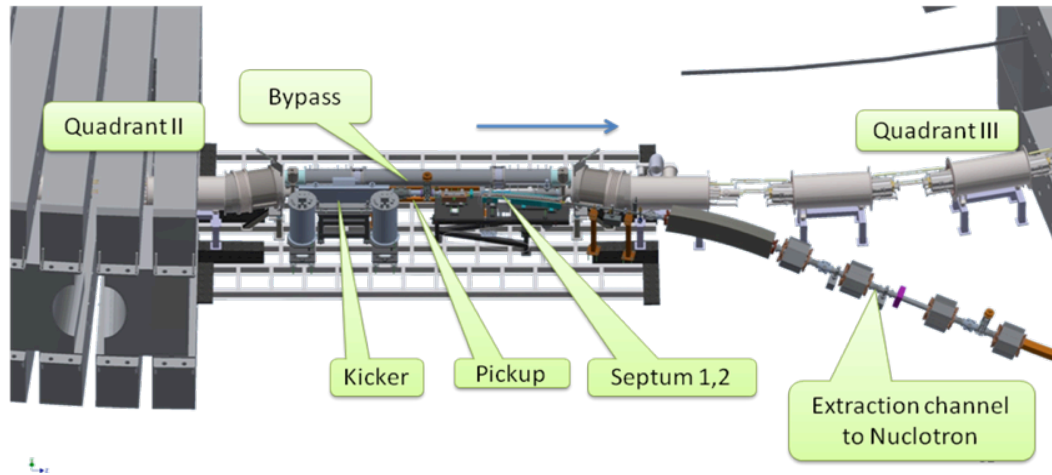


*Fig. 2.1.3.12. Location of the beam extraction system elements.*

Beam transport line from HILAc to Bycrep includes 7 quadrupole and 2 dipole magnets, debuncher, beam diagnostic devices (Fig 2.1.3.13), vacuum and power supply systems.

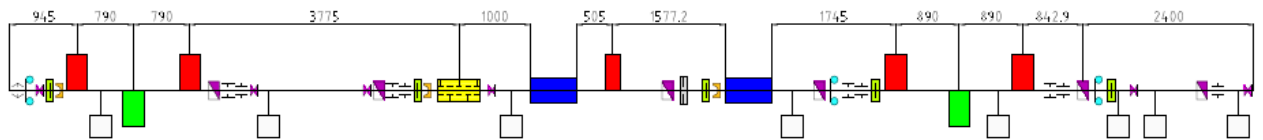


*Fig 2.1.3.13. Schematics of the beam transport line from HILAc to Booster.*



*Fig. 2.1.3.14. Elements of the transport line from HILAc to Booster during the assembly.*

The *Booster-Nuclotron beam transport line* (Fig. 2.1.3.15) passes through the magnet yoke of the former Synchrophasotron accelerator, then the channel route descends down to The Nuclotron ring through an opening in the concrete floor above The Nuclotron tunnel. The beam line has a complex three-dimensional geometry, and beam transportation in it is performed horizontally and vertically at the same time. The transport line consists of the main path of ion transfer to the Nuclotron and a branch for the dump of the ions in non-target charge state. The optical system of the line consists of 5 dipole magnets, 8 quadrupole lenses, a septum magnet for the dump of ions of non-target charge state and 3 two-coordinate dipole correctors. The total length of the line is 25.5 m. the Azimuthal size of the channel is approximately  $45^\circ$ , which corresponds to the injection of a beam through one superperiod (octant) of the Nuclotron from the extraction point of the Booster.

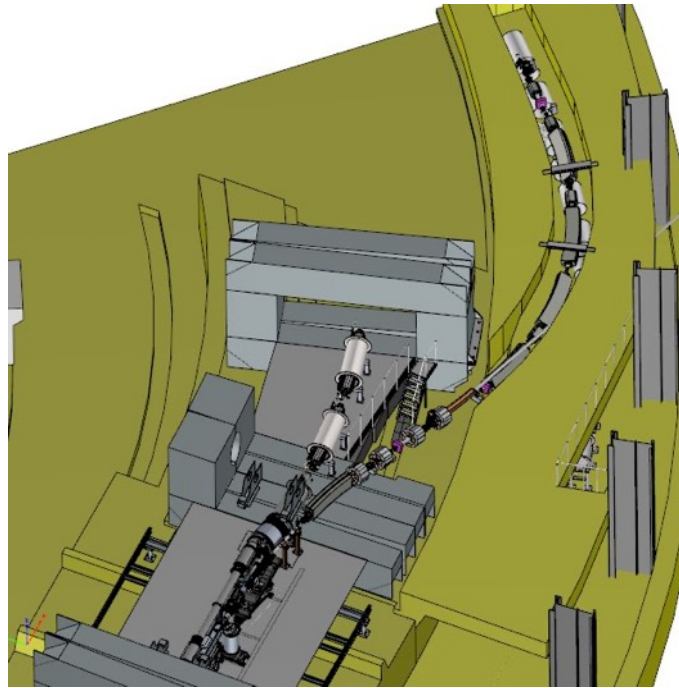


*Fig. 2.1.3.15. View of the region containing the fast beam extraction from the Booster and Booster-Nuclotron transport line*

The vacuum system of the Booster-Nuclotron transport line ensures the achievement of an operating vacuum of the order of  $10^{-9}$  Torr along the ion beam pipe of the line, except for the initial section of the line with differential pumping, in which the residual gas pressure is reached at the vacuum level of the Booster ring of  $10^{-11}$  Torr. The line is under manufacturing at BINP. In accordance with the contract, the term of delivery is March 2020. Assembly and commissioning of the line is scheduled for 2020.

### 2.1.3.4. Power supply and quench protection systems of the Booster

The system is based on a series connection of structural dipole magnets, quadrupole focusing and defocusing Booster lenses (Fig. 2.1.3.16, left) The main powerful source IP1 of the power supply system generates the required current with a given rate of growth of the field in the General circuit. For flexible adjustment of the working point of the accelerator two additional power supply IP2 and IP3 of significantly lower power are used. And P2 allows you to simultaneously change the field gradient in focusing and defocusing lenses, and P 3° only in defocusing ones. IP2 and IP3 permit both – to add current to the load and to take some of the current from the load. The equivalent load (its circuit is shown in Fig. 2.1.3.16, right) is aimed for testing of the power supply system.

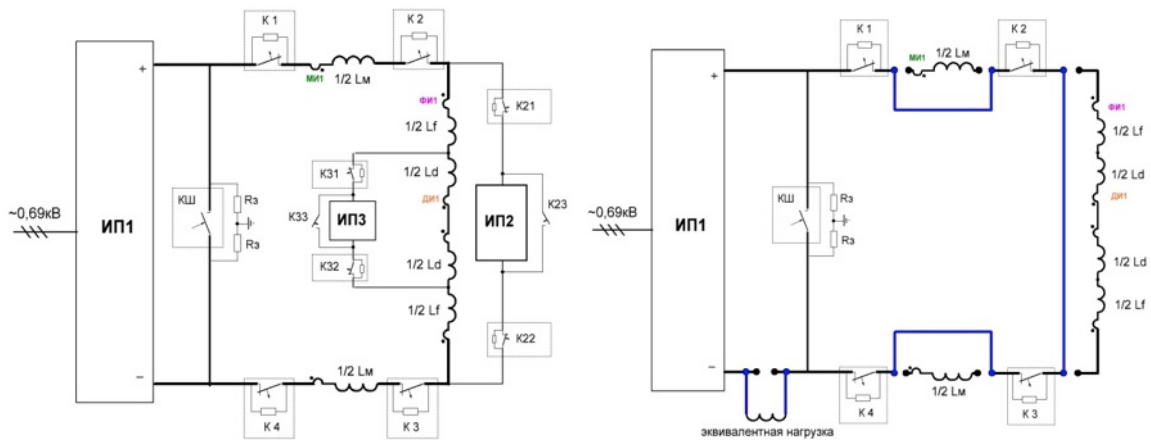


*Fig.2.1.2.16. Scheme of the Booster power supply system;  
left – commutation for supply of the Booster superconducting magnets,  
right – commutation on the equivalent load.*

Dipole magnets connected in series (2 chains of  $\frac{1}{2} L_m$ ) and quadrupole magnets ( $\frac{1}{2} L_f$  и  $\frac{1}{2} L_d$  two chains each) are connected to power supply through the energy evacuation switches symmetrically in respect to the supply Voltage. Inductance of the magnet groups and value of the dissipative resistors are chosen from the following condition: the potential at current leads relatively to the ground has to be not larger than 500 V as at nominal condition as in the case of malfunction of one of the switches. During energy evacuation the switch K12 is switched on simultaneously with switch off K1 – K4. Energy evacuation characteristic time is 160 ms.

The additional source IP2 aimed for current correction in the focusing and defocusing lenses is connected to the circuit of series-connected lenses through the energy evacuation switches K21 and K22. These switches are switching off at the quench, detected by the external quench detection system, and switch on the resistors for energy dissipation into the circuit. Simultaneously the switch K23 is switching on and switches off IP2 from magnets. Similarly, the source IP3 for the current

correction in defocusing lenses is connected to the defocusing lens circuit through the switches K31, K32 and K33. In the measuring magnets MI1, lenses F1 and D1 (Fig. 2.1.2.16) the induction magnetic field sensors are installed, the signal from which enters the diagnostic and control devices.

The location of the equipment is presented on the principle scheme of the Booster power supply system (Fig. 2.1.3.17). The numbering of the equipment is given in a continuous order.

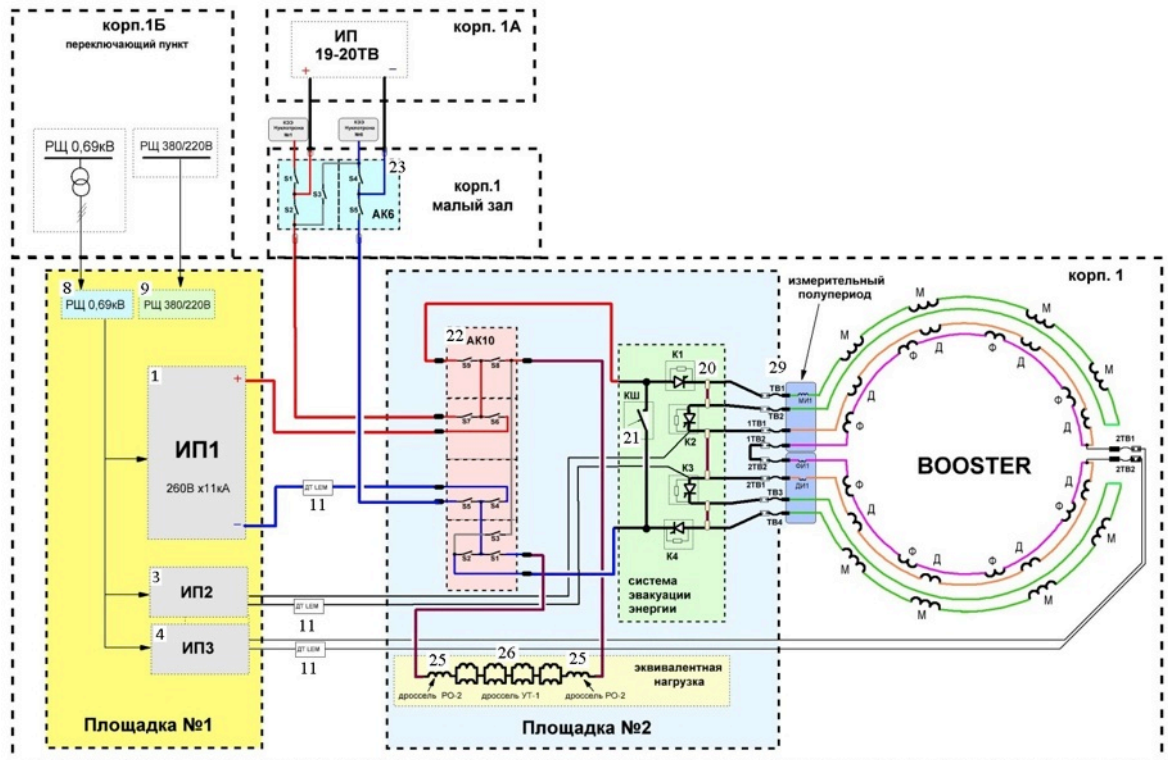
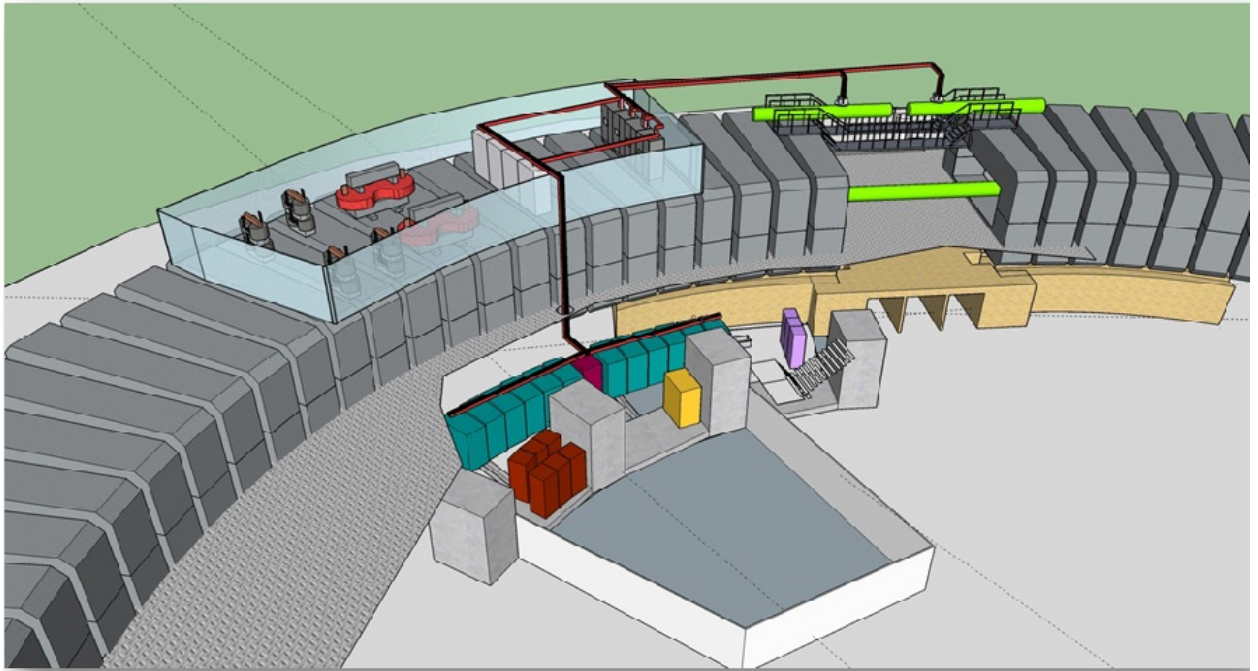


Fig.2.1.3.17. Scheme of the Booster power supply powerful circuit.

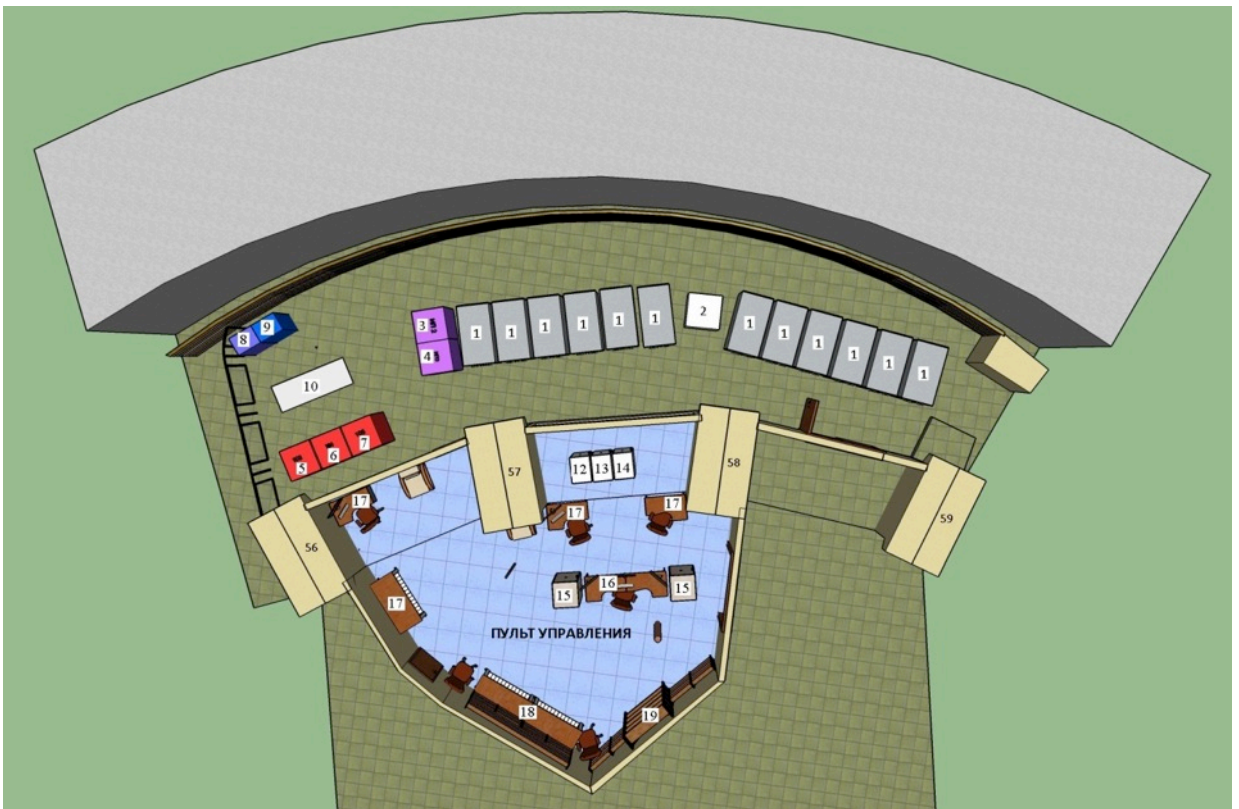
Equipment of the Booster power supply system (Fig. 2.1.3.18) is located:

- at the site No. 1 in the basement of the building No. 1, where power supplies IP1, IP2, IP3, control panel equipment, power boards RSCH0,69 and RSCH0,4 are installed;
- at the site No. 2 on the top of the Synchrophasotron magnet, where the high-current equipment of the AK 10 switches, the K1-4 energy evacuation switches, the RO2 and UT1 chokes of the equivalent load is located;
- in a small hall of the building No. 1 – the high-current equipment of the AK6 switchboard.

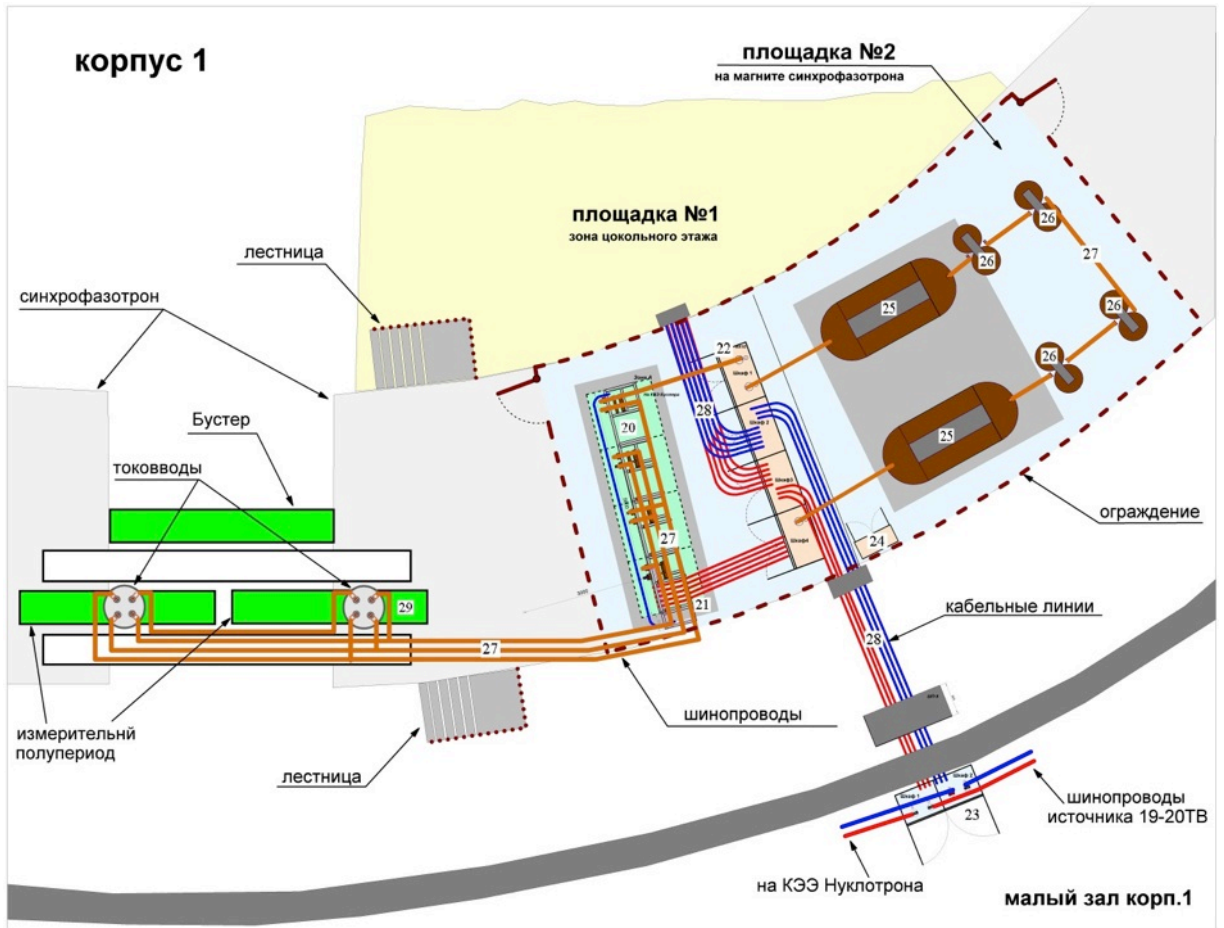
Presently the installation of the main equipment of the power supply and protection system has been completed (Fig. 2.1.3.19), the completion of the commissioning of the system is scheduled for the end of 2019.



a) general view



б) site No. 1 in the basement of the building No. 1.



c) site No. 2 on the top of the Synchrofasotron magnet

Fig.2.1.3.18. View of the location of the Booster power supply system equipment.



Fig.2.1.3.19. The Booster power supply units.

### 2.1.3.5. Radio frequency system

The radio-frequency accelerating system of the Booster is aimed to accelerate the ions up to gold ( $^{197}\text{Au}^{31+}$  is the reference ion) from 3.2 MeV/u to 578 MeV/u. The Booster can be used as the first synchrotron of the NICA collider injection chain, or as an independent accelerator with its own physical program. The main parameters of the RF system are given in the Table 2.1.3.5.

Two identical accelerator stations are installed in the Booster ring (Fig. 2.1.3.20) are consisting of a resonator module, a generator module, an air cooling system and a control rack. The mass of the accelerating station is 1760 kg, including the mass of the resonator – 860 kg, generator – 900 kg, dimensions of the accelerator station in assembly – 1400×1020×1705, separately: the dimensions of the resonator -□ 1400×550×605, generator – 1275×1020×1100 mm.

Table 2.1.3.5.

Parameters of the radio-frequency accelerating system of the Booster

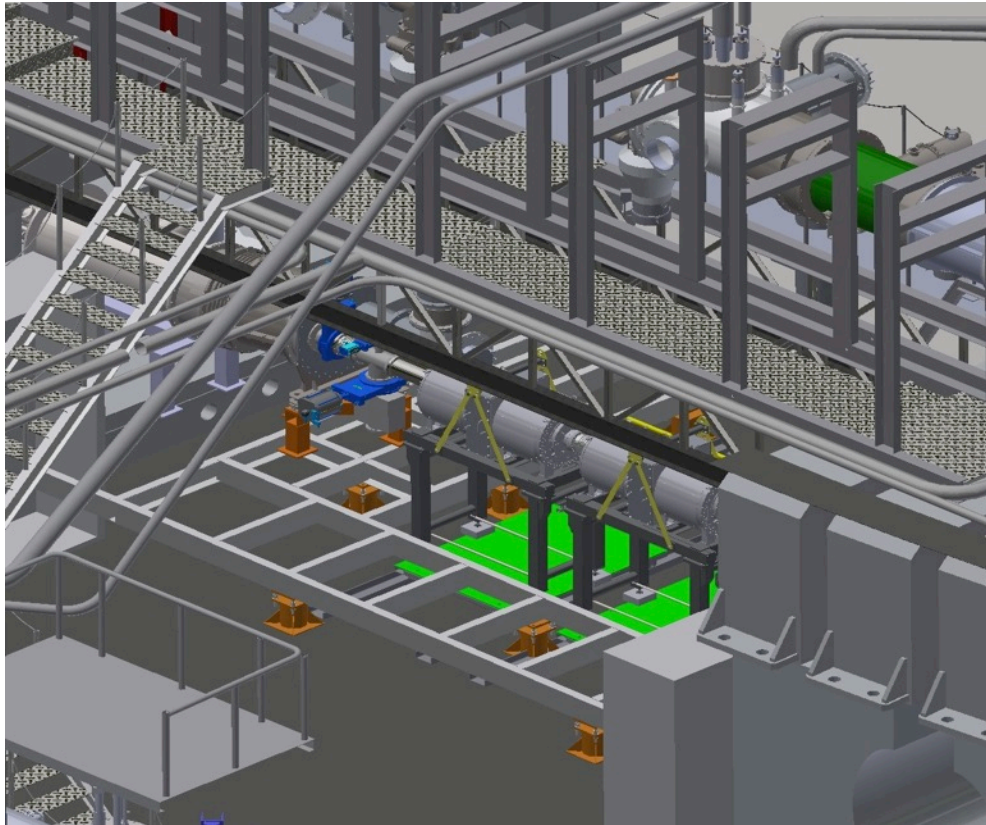
№	Parameter	
1	Frequency variation range, MHz	0.5 ÷ 5.5
2	Minimum/maximum amplitude of the frequency modulation, kV	0.1/10
3	Inner diameter of the resonator, m	< 1.2
4	Diameter of the vacuum chamber, mm	160
5	The resonator length, m	1.2
6	Number of resonators	2
7	Maximum field ramp, T/s	1.2



Fig. 2.1.3.20. The Booster accelerating stations at JINR test bench

Accelerating stations are located one after the other in the 2<sup>nd</sup> straight section of the

Booster (Fig. 2.1.3.21). Resonators and RF generators are located directly on the ring. The control racks are located in the vicinity in a protected area.



*Fig.2.1.3.21. Location of the RF system in the second straight section of the Booster.*

At the entrance and exit of the gap there are transitions from the vacuum chamber of RF stations, located at room temperature, to the "cold" beam chamber of the Booster. During the backing procedure, the vacuum chamber of the RF stations is separated from the beam chamber of the Booster by high-vacuum gates 10848-CE44 DN160. Pumping stations in the process of their heating is carried out by a turbomolecular pump with a "dry" forevacuum pump.

Commissioning of the system is scheduled for 2020.

#### **2.1.3.6. Diagnostic and control system**

Diagnostic and control system is a set of equipment and software consisting of a few independent subsystems. In addition, the system provides the computing, networking, and software infrastructure to develop and safely fail-safe CS tasks and interactions between its various components.

The Booster beam diagnostic systems provides:

- measurement of the average beam current and intensity;
- measurement of the longitudinal beam profiles;

- measurement of the beam closed orbit;
- measurement of the beam betatron oscillation frequencies.

At the present time the booster thermometry subsystem (250 channels) was mounted and adjusted. The cycle control subsystem was put into trial operation. Forty-eight power supplies for dipole correctors and 24 power supplies for multipole correctors were mounted. The alignment stand for beam position monitors was created and 24 monitors are aligned.

The automated control system includes:

- measurement of the cryogenic temperatures in the magnets and lenses of the Booster;
- control of the magnetic field correctors;
- magnetic field cycle setting system;
- power management system of inflector plates of the Booster injection system.

Infrastructure the ACS includes:

- ACS computer cluster;
- network infrastructure;
- software services;
- TANGO services;
- data archiving-data acquisition for various Booster systems;
- monitoring of hardware and software services;
- logbook of the ACS operations;
- the Booster control room software.

The infrastructure of the automated control system consists of a distributed network of computers connected by Ethernet network. The system is implemented in the form of three levels:

- the access level to the equipment (front-end level);
- the service level;
- and the client level.

The components of all three layers are interconnected using a transport Protocol that operates over TCP / IP. NICA ACS uses the TANGO controls system as a software binder.

Splitting the ACS components into several levels allows to remove most of the computational tasks, data processing and storage tasks from computers directly connected to the equipment and sensors, and locate them in another place, because

these tasks are no longer dependent on interaction with specific equipment. The most efficient way to organize a service level is virtualization.

Virtual servers have a number of advantages over physical servers:

- easy operation-create, clone, backup;
- efficient division of tasks with guaranteed allocation of resources;
- high security of tasks;
- fine adjustment of allocated resources;
- high availability implementation – the tasks are removed to other physical servers in case of problems.

For the tasks of the ACS Booster, a cluster of several physical Supermicro servers is used under the control by the Proxmox virtualization system, which is a full-fledged open server platform for creating and managing virtual infrastructure, including virtual machines, storage, virtual networks and high availability clusters. The physical servers of the cluster are combined using a fast 10 Gbit redundant network. Servers are both nodes of distributed network storage CEPH and nodes for running virtual machines ACS. Highly reliable SSD drives with a reliability of 5 DWPD (drive write per day) are used as the basis for building highly reliable distributed CEPH storage, which is used to store and execute disk images of virtual servers.

Completion of installation and testing of diagnostic and control system elements and their commissioning is scheduled for the 2021.

#### **2.1.3.7. Vacuum system**

The Booster vacuum system consists of 4 superconducting arcs operating at cryogenic temperatures and 4 straight sections located at room temperature (Fig. 2.1.3.22). The Booster circumference is 210 meters, the average length of the straight sections of the Booster is 7 meters. Presently the vacuum volumes of two straight sections have been delivered to JINR: RF stations and electron cooling systems. Both volumes are manufactured in the BINP. During the installation and testing of the electron cooling system, the necessary vacuum conditions at the level of  $2 \times 10^{-9}$  Pa were achieved.

The straight section of the injection system is under the manufacturing stage and should be delivered to JINR in 2019. The straight section of the beam extraction system together with the transport line to the Nuclotron is under manufacturing in the BINP. In all "warm" areas, titanium sublimating pumps in combination with ion pumps are used as the final vacuum pumping stage. As an additional means of pumping are used non-evaporated getters.

The design of “cold” vacuum chambers of arches is completed, and various chambers operating at cryogenic temperatures are fabricated. The thin-walled, bent beam pipes for the dipole magnets as well as beam pipes for quadrupole magnets were developed at JINR and manufactured by FRAKOTERM (Poland). Vacuum tests of the beam pipes are currently being performed. It is assumed that the main components of the residual gas in arches will be hydrogen molecules and atoms, so the Booster vacuum stations include pumps based on non-evaporated getters.

In the basic configuration of the Booster vacuum system 8 pumping stations (two for each arc) based on turbomolecular pumps will be installed only, that will permit to achieve a pressure of  $10^{-8}$  Pa. In the future, the use of 24 pumping stations located in arches through each 9 meters will improve vacuum conditions by several times. Achieving the necessary vacuum conditions at the level of  $10^{-9}$  Pa is assumed after installing the additional sublimation pumps between all the booster magnets.

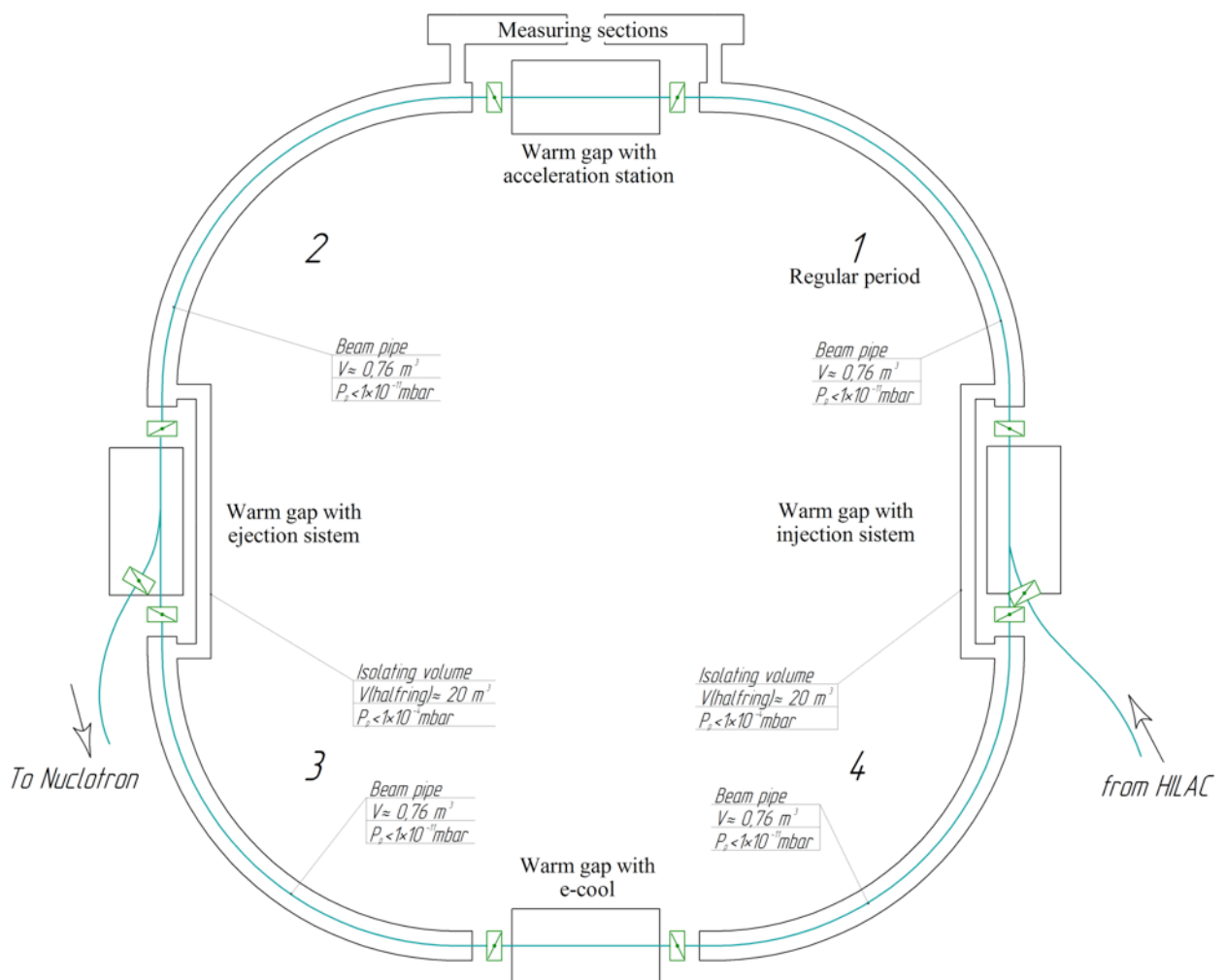


Fig. 2.1.3.22. Vacuum volumes of the Booster beam pipe and cryostats.

## 2.1.4. Ion Synchrotron Nuclotron

The Nuclotron (Table 2.1.4.1) is a superconducting (SC) synchrotron used as the main accelerator of the complex, which provides experimental set-ups of the NICA complex with ion beams from protons to gold nuclei and polarized beams of light nuclei. The maximum dipole magnet field at stable long-term operation is 1.8 T (magnetic rigidity 38.5 T × m). This corresponds to the proton kinetic energy of 10.65 GeV, the same for deuterons and light ions (the charge to mass ratio  $Z/A = 1/2$ ) is 4.91 GeV/u, and for  $^{197}\text{Au}^{79+}$  3.79 GeV/u.

Table 2.1.4.1

The main parameters of the Nuclotron

Parameter	Characteristics
Accelerator type	SC synchrotron
Accelerated particles	$p\uparrow$ , $d\uparrow$ , nuclei
Injection energy, MeV/u	5 ( $p\uparrow$ , $d\uparrow$ ), 578 ( $^{197}\text{Au}^{79+}$ )
Magnetic rigidity corresponding to stable long-term operation, T·m	38.5
Circumference, m	251,52
Number of superperiods	8
Periodicity of quadrupole magnets	32
Betatron tunes, $Q_x/Q_y$	6/8
Duration of the injection cycle into collider, s	1.5 ÷ 4.2 (active <sup>1</sup> ); 5 (total)
Dipole magnet field, T	0.03 ÷ 1.8 ( $p\uparrow$ , $d\uparrow$ ) 0.46 ÷ 1.8 (nuclei)
Bending radius, m	21.68 ÷ 21.31 (depending on dipole field)
Magnetic field ramp, T/s	1.0
Injection type	Single-turn
Extraction methods	Single-turn, slow
Vacuum pressure in beam chamber, Torr	$10^{-9}$
Intensity of the $^{197}\text{Au}^{79+}$ beam, ions per injection cycle	$1 \cdot 10^9$
Critical energy, GeV/u	7.0
Acceleration frequency range, MHz	0.6 ÷ 6.9 ( $p\uparrow$ , $d\uparrow$ ) 0.947 ÷ 1.147 (nuclei)
RF harmonic number	5 ( $p\uparrow$ , $d\uparrow$ ) 1 (nuclei)
Chromaticity of betatron tunes, horiz./vert.	-7.8/-10.0
Duration of the slow extraction, s	≤ 10

<sup>1</sup> Active part of the cycle

To provide all the necessary operation modes, the Nuclotron is equipped with two injection chains:

1. Laser source and source of polarized protons and deuterons + linear accelerator LU-20.
2. Heavy ion source + heavy ion linear accelerator HILAc + the Booster.

To transfer the beams to experimental set-ups with fixed targets and transfer the beams to the collider rings, the Nuclotron is equipped with slow and fast single-turn beam extraction systems.

The main Nuclotron systems were created as part of the project “Modernization of the Synchrotron Magnet System”. The Nuclotron was commissioned in 1993. In the process of construction of the NICA complex, a number of existing systems of the Nuclotron are being modernized and new ones needed to work as part of the new accelerator complex are being developed.

#### **2.1.4.1. Nuclotron operation modes**

The NICA project assumes the use of 6 modes of the accelerator complex operation and, correspondingly, 6 different operating modes of the Nuclotron.

*Mode 1.* The acceleration of heavy ions in the Nuclotron for fixed target experiments is performed after they are accelerated in the Booster up to an energy of 578 MeV/u followed by complete stripping at the exit to the Booster-Nuclotron channel, transportation and injection into Nuclotron. Particles are accelerated at the first RF harmonics to the experiment energy, the beam is adiabatically debunched and the slow extraction system is transferred to the beam transfer channel to the 50exed 205. The slow extraction time duration is of 5-10 s. The total duration of the Nuclotron cycle in mode 1 is 15 – 20 s.

*Mode 2.* The acceleration of heavy ions for accumulation in the Collider is performed in the same way until ions reach the desired energy. Then the ion bunch of the required length is formed by the adiabatic increasing the RF voltage and extracted by the single-turn extraction system synchronized with the single-turn injection system of the collider coming to it through the beam transfer channel from the Nuclotron to the Collider. The total cycle duration is 4.02 s.

*Mode 3.* The acceleration in Nuclotron of polarized protons and deuterons for fixed target experiments is carried out after transportation of the particles from the LU-20 accelerator and injection them into the Nuclotron at the energy of 5 MeV/u (the magnetic field of the dipole magnets is approximately 0.03 T for deuterons and 0.015 for protons). The acceleration and extraction procedure is the same as for heavy ions in fixed target experiment (Mode 1).

Mode 4. The polarized proton or deuteron acceleration procedure for accumulation in the Collider differs from Mode 3 only in the scheme. In this case, fast (single-turn) extraction is to be used according to the Mode 2.

Mode 5. Acceleration of various types of ions for carrying out experiments on an internal target is performed according the Modes of items 1 or 2, depending of the type of accelerated ions. The extraction of the beam is not carried out. The experiments are performed on a plateau of the ion energy (and the Nuclotron magnetic fields). The plateau duration is up to 300 s.

Mode 6 is the mode of so-called asymmetric collider, whose ions in each of two rings differ in mass and/or charge. Acceleration in the Nuclotron ions to be stored in the Collider during its operation in the asymmetric mode are performed for each of the two types of the particles in Modes 2 or 4 with subsequent extraction and accumulation in different rings.

#### **2.1.4.2. Main systems of the Nuclotron**

The Nuclotron facility includes the following main subsystem and elements:

1. Beam transfer channel from linear accelerator LU-20 and its injection system into Nuclotron;
2. SC magnetic system;
3. Vacuum system of the Nuclotron;
4. Power supplies of the Nuclotron SC magnets, the system of quench control and evacuation of energy stored in SC magnets;
5. Beam injection system from the Booster to the Nuclotron;
6. Acceleration RF station;
7. Diagnostics and control system of the Nuclotron, stochastic cooling system;
8. Slow extraction system of the Nuclotron;
9. Beam transfer channel to the experimental set-ups in the building 205 and Measurement Pavilion;
10. Single-turn extraction system for the beam transfer to the Collider;
11. Systems of diagnostics and control of particle polarization.

Description of beam transfer channel from the Booster to the Nuclotron is done in the section “Booster synchrotron”.

3. Beam transfer channel from linear accelerator LU-20<sup>2</sup> and its injection system into Nuclotron were designed and constructed in the beginning of 1990<sup>th</sup> when the Nuclotron was being mounted and prepared for operation. The channel structure functions at injection point were matched to the Nuclotron ones, the particle momentum spread and the injected bunch length were decreased.

---

<sup>2</sup> LU-20 abbreviation is from Russian “Linear Uskoritel’ (Accelerator)” for protons of 20 MeV energy

The channel has the magnetic system consisting of 10 quadrupole lenses and two dipole bending magnets, the vacuum pumping system based on turbomolecular pumps, the pulsed deflector (kicker), debunching device (debuncher) with the RF power supply, the beam diagnostics system including 4 wire profilometers, fast current transformer for the beam current measurement, the Faraday cup, and the channel control system.

The channel has a magnetic system of 10 quadrupole lenses and two dipole magnets, a vacuum pumping system based on turbomolecular pumps, a pulse deflector, a debuncher with an RF power system, a beam diagnostics system including 4 wire beam profilometers, a fast current transformer and beam current monitor based on Faraday cylinder.

Modernization of the channel has been fulfilled in 2014 – 2016: the 1<sup>st</sup> quadrupole lens triplet has been changed, power supplies of the channel magnets and the vacuum pumping system have been completely reconstructed. Presently the channel is used for proton and light ion transfer to the Nuclotron.

#### 4. SC magnetic system of the Nuclotron.

The magnetic system consists of the dipole, quadrupole and correction SC magnets. The Nuclotron was commissioned in 1993 and since this time was upgraded several times. The magnetic structure (Table 2.1.4.2) has 8 superperiods, each of which includes 3 regular periods of the FODO type and one period that does not contain dipole magnets (large straight section). The magnetic structure consists of 96 dipole and 64 quadrupole SC magnets.

Table 2.1.4.2

The main parameters of the structure SC magnets of the Nuclotron

Parameter	Dipole magnet	Quadrupole magnet
Weight, kg	500	200
Yoke type	Window frame	Hyperbolic poles
Length of iron yoke , mm	1370	450
Overall length, mm	1462	450
Aperture (hor. × ver.), mm	110 x 55	120 x 63
Number of turns in winding	2 x 8	4 x 5
Length of the SC cable in winding, m	62	24
Induction at excitation current of 6.4 kA, T	2.11	-
Gradient of the magnetic field at excitation current of 5.6 kA, T/m	-	33.4
Inductance, mH	1.1	0.44
Stored energy, kJ	19.8	6.9

## 5. Vacuum system of the Nuclotron.

The Nuclotron vacuum system consists of two subsystems: the insulation volume and the high vacuum beam chamber. The pressure in the insulation vacuum volume is to be below  $10^{-3}$  Pa.

The Nuclotron beam chamber is made of stainless steel with a thickness of 0.5 mm according to the technology prescribed for high-vacuum products. Eight sections of the chamber with a length of 1.5 m each have an operation temperature of 4.5 K – 5 K, they act like cryogenic pumps. Six “warm” sections of 3 m each have a temperature of 80 K to 300 K, they are used as acceleration cavities. In the remaining sections of a total length about 200 m, the temperature of the chamber wall varies from 10 K to 30 K, depending on the parameters of the magnetic field cycle in the Nuclotron. In these regions, the chamber is cooled due to the thermal contact of its walls with the iron yoke of dipoles and lenses of the magnet structure of the accelerator. The cross section of the chamber is elliptical with axes 110 mm and 55 mm.

The high-vacuum system of the beam chamber created during the implementation of the Nuclotron upgrading project provides a ring circumference-averaged residual gas pressure of  $10^{-7}$  Pa.

“Warm” straight sections of the high-vacuum chamber are located outside the cryostats and have room temperature. They are separated from the other elements of the Nuclotron by sections of the “warm-cold” transition. In the “warm” straight sections are located:

- station of internal targets,
- current transformers of the beam diagnostic system,
- ionization beam profile and intensity monitor,
- kicker of the Nuclotron stochastic cooling system.

During the implementation of the Nuclotron modernization project, the “warm” straight sections was completely reconstructed.

## 6. Power supplies of Nuclotron SC magnets, the system of quench control and evacuation of the energy stored in SC magnets.

The power supply system of the Nuclotron magnets provides precise reproduction of the reference function (current versus time) in three fundamentally different modes:

- stabilization of direct current when the voltage at the load is close to zero (SC magnets!),
- increase or decrease in time the current with constant first and second time derivatives and at a voltage in the range from zero to several hundred volts.

The system for the formation of the growth and drop functions of the magnetic field in the structural magnets of the Nuclotron is based on the power supply circuit of the series-connected the structural magnets. Operation and maintenance of currents should be provided in the range from 50 A to 6000 A in a superconducting highly inductive load. This task is unique in global practice.

The power supply system of the Nuclotron has been substantially modernized. As result, a new quality and stability of the current supply of the magnetic system were achieved. The accuracy of maintaining and reproducibility current values reaches  $1 \cdot 10^{-4}$  in a wide range of parameter variation, which is today close to the practical limit for accelerator systems in the world.

*The system of energy evacuation* from structural magnets provides a safe extraction of the energy stored in the magnets when an SC magnet transition to a normally conducting state occurs. The system is based on a ballast resistor, installed outside a cryostat together with a switching device that closes the circuit of a group of magnets to this resistor in case of superconductivity failure.

During Nuclotron upgrade, the schemes and approaches to detecting the normal phase in the magnet windings were changed, all cable lines and transition sensors were replaced with new ones. The design was based on operational experience of the NIICA team and modern solutions.

#### 7. *Beam injection system from the Booster to the Nuclotron.*

The single-turn beam injection system allows to place a bunch transported from the Booster into equilibrium orbit of the Nuclotron. The system consists of a Lambertson magnet and a pulsed ironless dipole magnet – the kicker.

The Lambertson magnet is a dipole magnet with two apertures: the separated areas for the injected and circulating beams. In the first area, a horizontal magnetic field of up to 1.1 T is initiated by superconducting windings that deflects vertically the injected beam. Both areas are separated by steel wall of special form to minimize the scattered magnetic field in the circulation region. Even more, to decrease the level of this scattered field, a superconducting coil compensating this field is placed. The Lambertson magnet and the compensating coil are operated from individual power supplies.

The walls of the vacuum chamber somewhat reduce the acceptance of the Nuclotron. To restore it to the initial value during beam injection, the exit of the Lambertson magnet can be shifted by 15 mm.

The kicker of 2 m length consists of two pairs of conductors installed inside the vacuum box. The conductors are switched so that they form a magnetic field

perpendicular to the plane of the beam orbit. The kicker power supply is pulsed, based on the pulse-forming line. Its repetition frequency is 0.25 Hz, the maximum amplitude of the current pulse is 25 kA. The durations of the leading and trailing edges are no more than 500 ns. The duration of the pulse plateau is 500 ÷ 700 ns.

The design of the main elements of the injection system has been completed. The production of prototypes and electrical models is near completion. Then fabrication of the system will be ordered.

#### 8. Acceleration RF station.

The Nuclotron acceleration RF system is designed to accelerate particles and form beam bunches before being transferred to the Collider, as well as to spread the bunches around the ring circumference on a magnetic field plateau for performing slow extraction or producing experiments on an internal target. The RF system allows also the rebunching of the beam on the intermediate plateau of the magnetic field with a change in the harmonics of the RF voltage for transferring the bunches from the Nuclotron to the Collider.

The main parameters of the acceleration RF system of the Nuclotron are shown in Table 2.1.4.3.

Table 2.1.4.3

The main parameters of the acceleration RF system of the Nuclotron

Parameter	Value
Accelerating harmonic number	5
Frequency of the RF voltage, MHz: a) minimum b) maximum	0,615 6
Maximum rate of the RF voltage, MHz/s	30
Maximum gain of the particle energy per one turn, keV	8,25
Number of accelerating electrodes	4
Length of accelerating electrode, m	2,7
Gap between electrode pair, m	1,2
Efficiency: a) pair of accelerating electrodes b) one accelerating electrode	0,65 0,34
Number of the accelerating stations	2
Amplitude of the RF voltage on electrode, kV a) minimum b) maximum	0,55 9
Interval between successive starts of acceleration stations, mcs	600

### 7. Diagnostics and control system of Nuclotron, the stochastic cooling system.

The Nuclotron automated control system (ACS) is based on Tango Controls technology and includes subsystems corresponding to the main systems of the accelerator.

Since 2013, the radical update of the ACS of Nuclotron is in progress. Most of the electronic equipment is replaced. Particularly, the control systems for beam injection, for slow beam extraction (see p. 7) to improve the beam spreading characteristics, and others were significantly modernized. Some other subsystems, like controlling of RF variation, automated tuning of Nuclotron operation modes, Nuclotron synchronization system to be operated within the global timing of the entire NICA complex based on “White Rabbit technology” are under development.

An independent control system is used to monitor the vacuum equipment.

To provide the safe operation of the complex, an Automatic Radiation Safety Monitoring System (ARSMS) is used.

The Nuclotron *diagnostic system* includes subsystems of thermometry of SC magnets, diagnostics of beam parameters, measurement and correction of a closed orbit (“Orbit” system).

The circulating beam diagnostic system is designed to measure

- the beam position and profile in the plane transverse to beam orbit axis and (beam position monitors – so-called pick-up stations and beam profilometer – ionization profilometer based on microchannel plates),
- longitudinal structure of particle bunch (pick-up monitors and fast current transformers),
- beam current with current transformers,
- particle transverse oscillation frequency (Q-meter) and particle momentum dispersion,
- particle loss monitors.

The Nuclotron *stochastic cooling system* (SCS) is designed to test the elements of the NICA collider stochastic cooling system and to cool the longitudinal degree of freedom of the beam circulating in the Nuclotron. (Nuclotron SCS single channel).

The main parameters of the stochastic cooling system of the Nuclotron are shown in Table 2.1.4.4.

The pickup and kicker designed and fabricated at the Julich Research Center have sixteen rings each of which has 8 loops for signal recording. They are assembled in a single design. Signals from loops located on the same azimuth are summed using

connection boards. The signals from each of the boards with high-frequency cables are output through the flange of the vacuum chamber, in which the entire assembly is located. The kicker vacuum chamber is located in the “warm” straight section, whereas the pickup vacuum chamber is located inside the cryostat in the straight section diametrically opposite to the “warm” one.

Table 2.1.4.4.

The main parameters of the stochastic cooling system of the Nuclotron

Energy range of operation, GeV/u	2.5 ÷ 3
Frequency bandwidth, GHz	2 ÷ 4
Impedance of the kicker and pick-up, Ohm	144
Average power of the kicker, W	≤ 100
Overall gain (without losses), dB	110

SCS underwent some upgrade, mainly in diagnostic equipment.

#### 8. Slow extraction system of the Nuclotron.

The slow extraction system outputs the beam accelerated in Nuclotron to the entrance of the beam transfer channel (BTC) to the experimental facilities in 57exed 205 and the small experiment pavilion. The particles of the beam circulating in the Nuclotron on the magnetic field plateau are extracted using a controlled increase in the amplitude of transverse particle oscillation due to a shift of the betatron frequencies to the nonlinear resonance region  $Q_x = 22/3$  and noise effect on to the circulating beam using a diagnostic kicker. Slow beam extraction is performed by a two-step scheme, the calculated efficiency of which is at least 95%: the first step is deflecting particles in a horizontal plane by an electrostatic septum, at the second step, a Lambertson magnet (LM) is used, which leads the beam in the vertical plane to the level of the BTC.

Main characteristics of a slow extraction system is extraction cycle duration and homogeneity of the extracted particles flux  $J$ . For the Nuclotron the first is up to 20 sec., the second is better than  $\Delta J/J \leq 0.1$ .

#### 9. Beam transfer channel to the experimental set-ups in the 57exed. 205 and Measurement Pavilion.

The beam transfer channel (BTC) is used for transportation the beam from the Nuclotron to the BM@N and the Short Range Correlation (SRC) experimental set-ups in 57exed. 205 and set-ups for applied research in Measurement Pavilion (Fig. 2.1.4.1). The length of the BTC from the Nuclotron exit to BM@N is about 170 m, of which more than 40 m are the air gaps. In the evacuated part of the channel, the

pressure is 0.1 Pa. The existing channel does not meet the experiments' requirements to extracted beams (Table 2.1.4.5) and has to be modernized over a length of 110 m. Its vacuum chamber diameter is 196 mm. The channel beam diagnostics is to be modernized and developed as well.

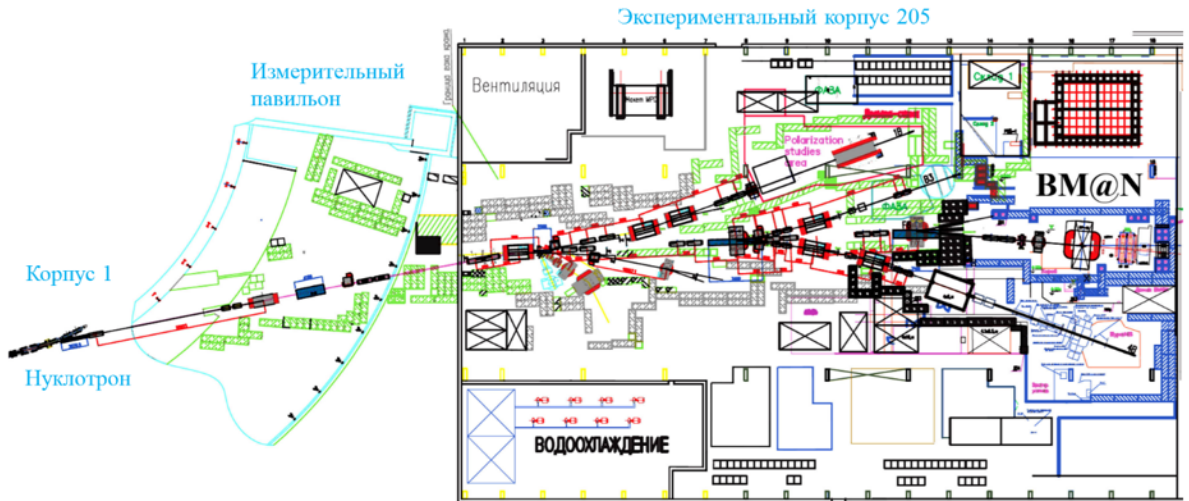


Fig. 2.1.4.1. Scheme of location of the BTL and experimental set-ups in Building 205

Table 2.1.4.5

#### General parameters of the Nuclotron extracted beams

Parameter	Value
Ions	$C^{6+}$ , $Kr^{36+}$ , $Au^{79+}$
Beam intensity, ion/cycle	$10^4 \div 10^8$
Ion energy, GeV/u	$1 \div 4$
On magnetic rigidity, T×m	$14 \div 40$
Transfer efficiency, %	95
Transverse 95 % emittances, hor/ver, $\pi \cdot \text{мм} \cdot \text{мрад}$	3.0/8.0
Longitudinal root-mean-square momentum spread	$2 \cdot 10^{-4}$

The channel contains quadrupole lenses, bending and correcting magnets. The vacuum chamber of the channel and the beam diagnostic system are manufactured by Belgorod State University. The mounting of vacuum and diagnostic equipment is planned for 2020.

The power supplies for the channel magnets are designed for currents from 600 to 4000 A at relatively low voltage of 75 – 230 V.

The central system of electric power supply undergoes an essential modernization since 2018. It is performed by Russian firms “Research and Production Enterprist LM Invertor”, “EPP-T”, “DCC engineering” and Polish firm “Frako Term”.

Commissioning of the upgraded channel and all the power supply systems is planned for October 2020.

10. Single-turn extraction system for the beam transfer to the Collider.

The system of single-turn beam extraction from the Nuclotron (Table 2.1.4.6) is designed for transfer of an ion beam through the channel Nuclotron-Collider to the Collider. Its scheme is to similar a single-turn injection scheme (see item 5 above).

Table 2.1.4.6.

Parameters of the kicker magnet of the Nuclotron fast beam extraction system

Parameter	Value
Nominal magnetic field, T	0.13
Effective length, mm	3000
Bending angle (at $B\rho = 45 \text{ T}\cdot\text{m}$ ), mrad	8
Diameter of conductors, mm	8
Field integral quality, $\Delta\int Bdl/\int Bdl$ , %	$\pm 1$
Current amplitude in the pair of conductors, kA	20
Pulse duration, ns	1500
Inductance of the one pair of conductors, $\mu\text{H}$	0.45

The Lambertson magnet (Table 2.1.4.7) of the fast beam extraction system consists of two sections, which have the following apertures:

LM1: beam exit region cross section is  $35 \times 130 \text{ mm}^2$ , trapezoidal beam circulation region is  $85 \times 70 \text{ mm}^2$ ;

LM2: exit area cross section is  $276 \times 44 \text{ mm}^2$ , the beam circulation area of a trapezoidal cross section is  $134 \times 70 \text{ mm}^2$ .

Table 2.1.4.7.

Parameters of the Lambertson magnet of the fast beam extraction system

Parameter	LM1	LM2
Maximum magnetic field, T	1.0	1.5
Effective length, mm	1500	1500
Bending angle (at $B\rho = 45 \text{ T}\cdot\text{m}$ ), mrad	33	50
Magnet gap, mm	35	44
Septum thickness, mm	3	15
Field integral quality, $\Delta\int Bdl/\int Bdl$ , %	$\pm 5$	$\pm 5$
Maximum current in the main coil, kA	6.0	6.0

## 11. Systems of diagnostics and control of particle polarization

The systems are used presently in fixed target experiments with polarized protons and deuterons in the Nuclotron. According to the NICA project main mode of Nuclotron operation with polarized particle beams will be the particle acceleration up to 12 GeV protons and 6 GeV/u deuterons for transfer to the Collider and performing experiments with colliding polarized beams there. For protons it will need to resolve the problem of spin resonance crossing at the energy of 6 GeV. Such experiments are in progress presently.

For polarization diagnostics the following devices are used:

- devices for measuring the beam polarization degree, installed in the beam transfer channel from LU-20 to the Nuclotron (item 1 above), in the “warm” straight section of the Nuclotron and in the beam transfer channel bringing the beam into the 60exed 205;

- a spin orientation control system, which is a magnetic optics element located in the beam transfer channel from LU-20 and directly on the Nuclotron ring.

## 2.1.5 Collider

The superconducting synchrotron – Collider of the NICA complex – is aimed

- to provide the most achievable  $\sqrt{s_{NN}} = 11$  GeV (for  $\text{Au}^{+79}$ , in the nucleon-nucleon center of mass system) with an average luminosity of  $L = 10^{27} \text{ cm}^{-2}\text{s}^{-1}$ ,
- to provide interactions of protons (deuterons) with longitudinal and transverse polarization in the energy range up to  $\sqrt{s_{NN}} = 27$  GeV ( $\sqrt{s_{NN}} = 12.6$  GeV), with luminosity up to  $10^{32} \text{ cm}^{-2}\text{s}^{-1}$ .

The NICA project assumes the use of 3 modes of the accelerator complex operation and, correspondingly, 3 different operating modes of the Collider.

Mode 1. The accumulation of heavy ions in the Collider, their acceleration and formation of a bunched ion beams, and performing experiments on colliding beams.

Mode 2. The mode of asymmetric collider: accumulation of various types of ions, preparation of colliding beams like in Mode 1 and performing experiments on colliding beams of heavy and light ions.

Mode 3. The mode of polarized beams: accumulation of polarized protons and/or deuterons acceleration, the same procedure of beams formation and performing experiments on spin physics with colliding beams of polarized particles.

### 2.1.5.1. The Collider optical structure and its elements

The optical structure is a sequence of dipole, quadrupole and correction magnets, placed along the collider circumference. This forms magnetic optics for both circulating beams. The main task of magnetic optics is the following:

- provide the design peak luminosity of the Collider:  $10^{26} - 10^{27} \text{ cm}^{-2}\cdot\text{s}^{-1}$ ;
- maintain the luminosity lifetime not less 1 hour that is much longer the beam preparation time at injection and storage (10 min).

The maximum luminosity of the Collider requires:

- compact circumference;
- large dynamic acceptance (both transverse and longitudinal);
- a sufficiently small value of the beta function  $\beta^*$  at the interaction point (IP) of the beams;
- an optimum ratio of the bunch length  $\sigma_s$  to the  $\beta^*$ ;
- the maximum possible number of bunches in orbit.

The optical structure of the Collider complies the above requirements when using Nuclotron-type superconducting (SC) magnet technology for dipole and quadrupole magnets (Table 2.1.5.1), for the magnets correcting natural chromaticity and other nonlinearities of the magnetic field of the rings and for the dipole magnets of the

vertical beam deflection that provides superposition of counterpropagating colliding beams at the IP.

Table 2.1.5.1

General parameters of the NICA Collider

Parameter	
Accelerating particles	p <sup>+</sup> , d <sup>+</sup> , Au <sup>79+</sup>
Total energy of ion (per nucleon) $\sqrt{s_{NN}}$ in IP, GeV/u	4 ÷ 11
<sup>197</sup> Au <sup>79+</sup> ion kinetic energy in each ring, GeV/u	1 ÷ 4.5
Circumference of the ring, m	503.04
Injection energy, GeV/u	1 ÷ 3.8
Maximum magnetic rigidity, T·m	44.5
Maximum dipole field, T	1.8
Maximum quadrupole gradient, T/m	23
Magnetic field growth rate, T/s	0.1
Beta-function in IP, m	0.6 <sup>3</sup>
Betatron tunes, $Q_x / Q_y$	9.44/9.44 <sup>4</sup>
Beam injection scheme	One-turn,
Beam extraction (dump) scheme	One-turn
Vacuum pressure in beam pipe, Pa	10 <sup>-9</sup>

In Fig. 2.1.5.1 (from left to right) are shown dipole magnet, quadrupole lenses, criostats and vacuum beam pipe of the Collider.



*Fig. 2.1.5.1. From left to right: dipole magnet, quadrupole lenses, cryostats and vacuum beam pipe of the Collider.*

Collider rings have the form of a racetrack with a circumference of 503.04 m (double Nuclotron circumference) and are placed one above the other with a distance between beam axes of 0.32 m. The magnetic system of the Collider (Table 2.1.5.2) is designed of two-aperture dipole and quadrupole magnets of the Nuclotron type, except quadrupole magnets of the final (near IP) beam focusing and dipole magnets of the vertical beam deflection mentioned above, which have one aperture design.

<sup>3</sup> Reducing beta-function at IP is possible and will be tested at commissioning of the Collider.

<sup>4</sup> Working point  $Q_x/Q_y = 9.1/9.1$  is foreseen as well.

A cell of the FODO type (focus-gap-defocus-gap) is selected as the basis of magnetic optics. The phase shift of betatron oscillations in horizontal and vertical positions on one cell is  $90^\circ$ .

On the length of the FODO cell, the beta functions do not exceed 20 m. In the free spaces between the dipoles (M) and quadrupoles (L) the multipole correctors (MPC), beam position monitors (BPM), as well as a vacuum equipment connection module are positioned. The MPC includes several types of windings. The BPM (pick-up stations) are located near each quadrupole lens and measure either the horizontal position of the beam axis (in the focusing quadrupole magnet), or vertical one (in the defocusing quadrupole magnet). The maximum displacement of the beam axis from the center line of the dipole magnet aperture due to the curvature of the trajectory (sagitta) is of 10 mm.

Both Collider rings have two long straight sections, which have common central parts with IP in their centers. In the straight section the following elements are placed:

- MPD and SPD detectors;
- elements of the beam injection system (septum and kicker);
- emergency beam dumping tools;
- RF accelerating systems;
- electron cooling system;
- elements of stochastic cooling system (pick-up stations and kickers);
- feedback system elements;
- beam halo collimation system.

For tuning the magnetic optics of each ring, 52 additional power supplies of low power are used. They can independently adjust each of the quadrupole magnets in the short straight sections, the final focusing lenses and the magnets of the vertical beam deflection.

Table 2.1.5.2

General parameters of the collider dipole and quadrupole magnets

Parameter	Value
Twin-aperture dipole magnets in arcs	
Number of elements	80
Maximum magnetic field, $B_{\max}$ , T	1.8
Minimum magnetic field, $B_{\min}$ , T	0.57
Relative magnetic field inhomogeneity, $\Delta B/B$ at radius $r=30$ mm	$\leq 2 \cdot 10^{-4}$
Ramp rate of the magnetic field $dB/dt$ , T/s,	$\leq 0.1$
Effective length, m	1.94

Beam pipe aperture (horizontal/vertical), mm	120 /70
Bending angle, grad	4.5
Yoke length, width, height, mm	1912 x 364 x 550
Distance between beam axes, mm	320
Overall weight, kg	1670
Operating current at maximum magnetic field, kA	10.4
Number of turns in the coil (per pole)	10(5)
Inductance of each of two coils, $\mu\text{H}$	450
Twin-aperture quadrupole magnets	
Number of elements	70
Maximum magnetic field gradient, $G_{\text{max}}$ , T/m	23.1
Minimum magnetic field gradient, $G_{\text{max}}$ , T/m	7.3
Relative magnetic field gradient inhomogeneity, $\Delta G/G$ at radius $r=30$ mm	$\leq 2 \cdot 10^{-4}$
Ramp rate of the magnetic field gradient, $dG/dt$ , T/(m·s)	$\leq 1.3$
Effective length, m	0.47
Beam pipe aperture (horizontal/vertical), mm	120 /70
Pole radius, mm	47.5
Yoke length, width, height, mm	474 x 302 x 605
Distance between beam axes, mm	320
Overall weight, kg	350
Operating current at maximum magnetic field, kA	10.4
Number of turns in the coil (per pole)	8(2)
Inductance of each of two coil, $\mu\text{H}$	48
Number of twin-aperture dipole magnets for vertical beam deflection	4
Number of one-aperture dipole magnets for vertical beam deflection	4
Number of one-aperture quadrupole magnets for final focusing	12
Number of one-aperture corrector magnets	128
General parameters of the collider magnetic system	
Length of periodic FODO-cell, m	11.96
Betatron phase advance in FODO-cell <sup>5</sup> , grad	90
Number of FODO-cells in arc	12
Length of the bending arc, m	141.72
Length of the long straight section, m	109.80
Circumference of the ring, m	503.04

<sup>5</sup> Except the cells with “missing” dipole magnets (for nulling the horizontal dispersion)

General parameters of the magnet cryogenic system	
Diameter of the LHe cooling tube, mm	3.0
Overall heat release, W	12.8
Maximum helium temperature in the coil, K	4.65
Pressure difference between inlet and outlet helium collectors, kPa	< 27

### ***2.1.5.1.1. The magnetic field correction system***

The magnetic field correction system consists of 62 combined multipole correction magnets for each of two rings and 4 correctors – common for both Collider rings (128 correction magnets in total). The longitudinal length of the multipole corrector is 0.3 m. Each corrector contains up to 5 superconducting windings of the “cosine  $\theta$ ” type. Multipole correctors are located near quadrupole magnets in the ring.

The coupling suppression system consists of skew quadrupoles whose winding is a part of multipole correction magnets located in the straight sections. The beta functions  $\beta_y$ ,  $\beta_x$  do not exceed 5 m along the entire ring circumference at all beam energies.

The chromaticity correction system consists of sextupole windings, which include multipole correction magnets located near the corresponding quadrupole magnets in the western (W) and eastern I arcs. The system includes 4 sextupole families.

The dynamic aperture correction system consists of 3 families of octupole windings as part of multipole correctors located symmetrically in the W and E halves of the rings in the northern (N) and southern (S) straight sections.

### ***2.1.5.1.2. The cryostat system of SC magnets***

The cryostat system of SC magnets has design based on engineering solutions developed at creation at the LHEP, JINR of the SC magnets of the synchrotron Nuclotron, which obtained in time well-known name “SC magnets of the Nuclotron type”. They are magnets with a forced cooling system, when liquid helium does not “bathe” the SC winding, but flowing in specially provided cooling channels. The SC winding is made of a hollow superconductor, inside of which two-phase (65exed65-liquid) helium flows. The yoke is made of sheets of electrical steel fastened together by welding. It is cooled by a two-phase helium flow coming from the winding exit.

The ultra high-vacuum beam chamber (UHVBC) is tightly inserted into the iron yoke and has a stable thermal contact with it for cooling.

Dipole magnets are placed in cryostats, which consist of a vacuum shell, a heat shield, a helium cooling channels, a magnet suspension system and a stand. The

cryostat provides the achievement of superconductivity temperature in the magnet and its long-term maintenance.

In the vacuum shell, an insulating vacuum of  $10^{-5}$  Pa is maintained. Inside the vacuum shell is a heat shield, cooled by liquid nitrogen at a temperature of 77 K. The surface of the shield is covered with vacuum multilayer thermal insulation. The magnet is fastened (suspended) in the cryostat on 8 spokes-rods, ensuring its fixed position at cooling. The magnet is supplied with liquid helium from the direct header. From the magnet, helium enters the return header. All SC magnets of the collider magnetic system are connected in parallel to direct and return helium headers. Bus bars of SC cables pass through each module of the magnets providing electrical connection of magnets of each type.

Quadrupole (focusing) magnet module consist of 2 aperture magnet, two (for each of the circulating beams) multipole correction magnets (MCM), two BPM, two UHVBC with pumping tubes and a magnet cryostat. The latter consists of a vacuum shell, a thermal shield, a helium direct and return headers, a suspension system of the magnet and a stand.

The collider vacuum volumes are divided into insulating vacuum space of the cryostat described above and beam chamber volumes, which, in turn, are divided into “warm” at room temperature and “cold”, whose walls under operating conditions are in the range temperatures from 4.2 K to 300 K. The pressure in the beam chamber is not higher than  $2 \times 10^{-9}$  Pa. With a collider circumference of 503.04 m, the largest its part is occupied by “cold” sections. They contain superconducting magnets, elements of a beam diagnostics and control system, tools of injection, and sections of warm-to-cold transitions. In warm sections, the RF stations, electron cooling system and elements of stochastic cooling system, detectors and beam diagnostic devices are situated.

The SC focusing system is an essential part of the basic configuration of the collider and the NICA project on the whole. Its fabrication is in active phase: the prototypes of dipole and quadrupole magnets are made and tested; their serial production was started in the fall of 2018. At the end of 2019, all vacuum shells for dipole magnets and lenses in arches were manufactured, 77 yokes of dipole magnets and 40 yokes of lenses in arches, 36 and 16 sets of windings of dipole and quadrupole magnets, respectively, bellows expansion joints for connecting vacuum shells were completely manufactured. Manufacturing of other elements is in progress.

#### **2.1.5.2. The beam cooling systems**

The beam cooling systems are designed to achieve design luminosities in

experiments with colliding ion beams in the NICA Collider. It is necessary to form short bunches of high intensity at a small six-dimensional phase volumes and maintain this phase volume of the bunches during operation in the collision mode to preserve luminosity. As a result, the question of cooling ion beams directly on the energy of the experiment becomes very urgent, and therefore the collider uses electron and stochastic cooling systems.

### ***2.1.5.2.1. Stochastic cooling system***

The Stochastic Cooling System (SCS) of the NICA Collider is designed to achieve and maintain design luminosity of  $10^{27} \text{ cm}^{-2}\cdot\text{s}^{-1}$  in the ion energy range from 3 to 4.5 GeV / u. Main parameters of the collider stochastic cooling system are shown in the Table 2.1.5.3.

Table 2.1.5.3

Parameters of the collider stochastic cooling system

Parameter	Value
Energy range, GeV/u	3.0 ÷ 4.5
Bandwidth, GHz	2.0 ÷ 4.0
Gain range, dB	84 ÷ 122 ± 0,5
Range of the delay, ps	537 816 ÷ 544 453 ± 1
Average power of one stochastic cooling channel, W	500

To cool the ion longitudinal degree of freedom, the filter method of the SCS is chosen. In the basic configuration, the SCS consists of longitudinal cooling channels only. As the basis for measuring the noise of the beam (pickups) and correction of the particles momentum spread (kickers) the slot ring coupler system was chosen. The unit cell of this structure is a ring with eight azimuth sensor loops. Several rings are connected by microstrip boards summing the signal in each of the azimuth directions. The possibility of combining signals from different directions together with high impedance makes possible application of this structure for both longitudinal and transverse cooling. To meet the requirements for achieving ultra-high vacuum, the original design of the structure was made changed: the vacuum chamber was moved inside the pickup rings and fabricated of ceramic. To prevent electrical breakdowns due to the accumulation of charge from the beam, the inner surface of the chamber is metallized with titanium of a thickness of 100 nm. The camera wall has electrical contact with an external grounding loop. For assembly, the pickup rings are cut along the longitudinal generatrix. The kicker design is identical to the pickup design. Both pickup and kicker consist of sections of 16 cells. Collider ring has 2 pickup sections and 4 kicker ones. At the beam entrance in kicker and exit

are ferrite TT2-111R absorbers of special design to suppress the propagation of high order RF modes through the beam chamber.

Currently, a number of SCS components have been manufactured: a test bench for pickups and kickers, 4 powerful amplifiers (30 W) for kickers, a ceramic tube with flanges, some equipment necessary for SCS development has been purchased: a vector and scalar 68exed68et, digital delays, an optical platform and other.

#### ***2.1.5.2.2. Electron cooling system***

The cooling of ions in the Collider by an electron beam is necessary to completely suppress the effects of beam heating by intra-beam scattering (IBS) and nonlinear resonances when the frequency of betatron oscillations is shifted under the influence of the beam space charge (BSC). To cool the ions in the NICA Collider at an experimental energy of  $1 \div 4.5$  GeV/u, a high-voltage electron cooling system (HV E-Cooler) with an electron energy of up to 2.5 MeV is created. (Table 2.1.5.4).

In the energy range from 3 to 4.5 GeV/u, the time of electron cooling is somewhat less than the characteristic time of IBS heating and is comparable with the time of stochastic cooling. However, in the energy range below 3 MeV/u, the electron cooling time is much shorter than the IBS time (approximately 20 times at 1 GeV/u). Electron cooling reduces the transverse emittance and the bunch longitudinal size, thereby increasing the luminosity of the Collider. At an ion energy of 4.5 GeV/u, the cooling time is 250 seconds. The steady-state bunch length is  $\sigma_s = 0.6$  m, and the longitudinal momentum spread of the particles is about  $1.2 \cdot 10^{-3}$ .

The main problem that arises when applying electron cooling is the recombination of ions with cooling electrons in the electron cooling section that leads to ion loss. The recombination can be suppressed by two methods: increasing the electron temperature by excitation their Larmor rotation and/or formation of a hollow electron beam.

The magnitude of the maximum magnetic field in the cooling section up to 0.2 T is required to provide the adiabaticity of electron motion at crossing the sections of an inhomogeneous solenoidal magnetic field at the joints of solenoids and strong “magnetization” of electrons in the solenoid of the cooling section. The latter allows efficient cooling at high transverse electron temperatures, which is necessary to suppress recombination, as mentioned above. The cooling rate when using a magnetized electron beam is determined mainly by the temperature of the longitudinal degree of freedom of electrons.

Table 2.1.5.4

## Parameters of the Collider electron cooling system

Parameter	Value
Energy range, MeV	0.2÷2.5 MeV
High voltage stability ( $\Delta U/U$ )	$\leq 10^{-4}$
Electron current, A	0.1÷1
Diameter of the electron beam in the cooling section, mm	5÷20
Length of the cooling section, m	6
Bending radius of electrons in transport channels, m	1÷1.3
Magnetic field in the cooling section, kGs	0.5÷2
Vacuum pressure in the cooling section, mbar	$10^{-11}$
Beta-function in cooler (horizontal/vertical), m	(11 ÷ 13)/(13 ÷ 14)
Transversal temperature of electrons, eV	50
Longitudinal temperature of electrons, meV	5,0
Life time of electrons due to recombination, hours	1
Distance of the lower beam axis from the floor, mm	1500
Distance of the upper beam axis from the floor, mm	1820
Energy consumption of electron cooling system, kW	650

The HV E-Cooler of NICA has two independent “coolers”. Each of them has two electron cooling systems that consists of

- solenoid magnetic system;
- electrostatic accelerator of a maximum electron energy of 2.5 MeV that includes:
  - electron gun for currents up to 1 A,
  - electron collector with the beam current recovery efficiency of  $\Delta I/I \leq 10^{-4}$  and potential of 5 kV relatively to the gun cathode,
  - Wien filter,
  - accelerator column with two acceleration tubes having the electric field gradient of 10 kV / cm,
  - sections with high voltage and magnetic field power supplies, both are powered by a cascade transformer;
- vacuum system providing a pressure of 10 pPa;
- system for measurement of magnetic field lines straightness in the cooling section with angular deviation accuracy  $\leq 10^{-5}$  rad.;
- distilled water cooling system;
- oil cooling system;
- SF6 gas insulation systems.

The accelerating and decelerating tubes of each cooler are in one tank with SF<sub>6</sub> gas at a pressure of 8 atm. An electron beam is generated in an electron gun, accelerated in an electrostatic tube and sent through the transport channel to the cooling section, where it interacts with ions. After passing the cooling section, the electrons come into the tube with a decelerating electric field and are absorbed in the collector. For the most efficient use of the site allocated for the HV E-Cooler, the cooling sections of both coolers are placed one above the other and have the same length. The electron beams in them, move in opposite directions according to direction of the ion beams to be cooled. The distance between the centers of the vacuum chambers of the two coolers in the cooling sections is 32 mm.

The transport channels of the electron cooling system consist of individual elements: 90-degree toroidal solenoids and straight sections. To minimize violation of electron motion at crossing the joints of solenoids with different values of the longitudinal magnetic field, short matching sections are set between them. The solenoids of the cooling section of each of two coolers consist of 92 coils. At a field of 2 kG the current in each coil is 219.4 A. The power consumption of the two solenoids is 130 kW.

The cooling section solenoid is the most important element of the magnetic system. The quality of the magnetic field, just the linearity of the magnetic field lines at the level of 10 microrad, defines the efficiency of electron cooling and is achieved by alignment with a precision of not worse than 10 μm. The total power consumption of the HV E-Cooler magnetic system is about 450 kW.

In HV E-Cooler, electron guns with a variable electron beam profile are used, which is achieved by using a segmented control electrode located near the cathode. The gun is placed in a solenoid (its cathode is immersed in the solenoid field) that “magnetizes” the motion of electrons. This design allows to control both the beam current and its profile.

An electron collector is needed to absorb the beam after electron is decelerated down in an electrostatic tube. It is a Faraday cylinder with additional electrodes, which create a confining potential for secondary electrons emitted from collector walls by primary electron bombardment. The confinement is supplemented by a magnetic “cork” reflecting the secondary electrons inside the collector. Collector power supply provides voltage up to 5 kV at the current up to 3 A.

To increase the efficiency of electron capture, we supplement the collector with a special insert, so called Wien filter, which suppresses the flow of electrons reflected from the collector. Application of the Wien filter reduces the level of beam current loss to  $\Delta I / I \approx 10^{-6}$  at a beam current of  $\approx 1$  A.

The electrostatic accelerator of each of the NICA Collider electron cooling systems has 2 accelerator tubes, sections with high voltage and magnetic field sources and a cascade transformer that feeds them. The accelerator column consists of 42 sections of 64 mm length. At the top of the column a high-voltage terminal with a gun, a collector and a Wine filter, as well as control electronics are placed. The gun and the collector are inserted in a longitudinal magnetic field created by two solenoids in the high-voltage terminal. All equipment in the terminal is powered by a cascade transformer.

The entire electrostatic accelerator is placed in a high-voltage tank filled with SF6 gas under pressure up to 8 atm. Electric fields that arise in accelerators are stable up to a electric field strength of 370 kV/cm.

The cascade transformer (Fig. 2.1.5.2) design meets the requirements of minimizing power losses and obtaining the maximum possible coupling coefficient between cascades.

Autonomous cascade transformers, two in each tank, will be used in HV E-Cooler. The first transformer transfers distributed power to sections which contain high-voltage modules of the main rectifier and power supplies for solenoids, which create a magnetic field.

The second cascade transformer feeds a powerful rectifier-recuperator that provides potential difference between gun cathode and electron collector and a crate with control electronics. Both are suspended at potential up to 2.5 MV. The total power transmitted by the transformer to the loads is 19 kW that divides between the rectifier-recuperator (15 kW) the control electronic crate and the solenoid (4 kW).

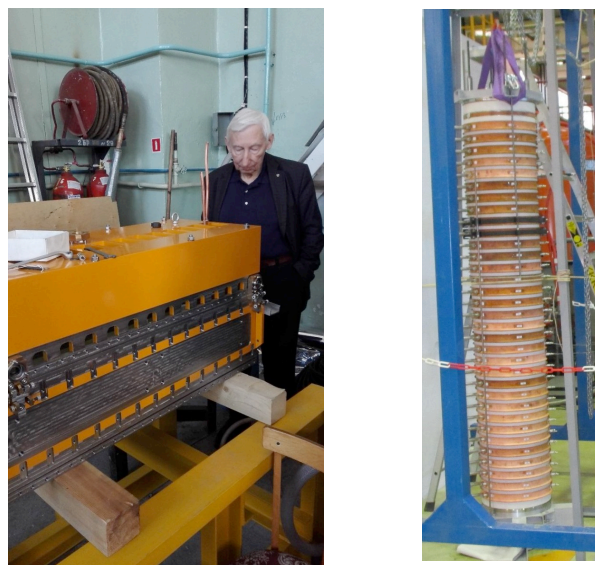


*Fig. 2.1.4.2. Solenoid of electron cooling section (right) and cascade transformer(left).*

Each of the vacuum systems is divided, in turn, into three segments separated from each other and from the Collider vacuum chambers by valves. All parts of the vacuum system, including numerous electrical feedthroughs and ceramic insulators, sustain heating up to 250 ° C.

Construction of the electron cooling system was started in BINP SB RAS in 2016. The commissioning of cooling system in JINR is planned for the end of 2021 (two year earlier than planned). A number of key elements have been manufactured at present: solenoid of electron cooling section, coils of toroidal sections, electron collector, tank bodies, cascade transformers, and other elements.

The HV E-Cooler belongs to extended configuration of the Collider.

### 2.1.5.3. Power supply system and its switching

Each of the rings of the Collider has a separate power supply (PS) system, consisting of 3 main and 52 additional PS (Tables 2.1.5.5, 2.1.5.6). The maximum current in Collider magnets is 10.4 kA that corresponds to the energy of gold ions 4.5 GeV/u. This current is provided by the main PS. The first main PS is used in Collider for all dipole magnets and quadrupole lenses, both focusing and defocusing, connected in series. Two other main PSs, having power less by one order of magnitude than the first PS, provide balance between currents in focusing and defocusing lenses. Besides, the second main PS feeds all lenses connected in series, whereas the third PS feeds the defocusing lenses only. Such a communication scheme allows to have significant flexibility for tuning magnetic structure. Particularly, at transition from working point 9.44 to 9.1 the current in all quadrupole lenses is to be decreased by 300 A (except lenses of final focuses) and by 9A additionally in defocusing lenses.

The length of each pair of quadrupole lenses of the straight sections was optimized to the section length. Each pair of lenses in straight sections and each final focus lens have individual PS with correction current up to 300 A. The total number of individual power supplies is 52.

All Collider PSs were constructed by Russian firm “LM Inverter”. These PSs belong to base Collider configuration. The construction was started in 2019, the installation is planned in 2020.

Table 2.1.5.5

Structure and main parameters of the collider power supply system

Power supply unit	Maximum current, A	PS Number
Main power supply for structural magnets	11000	2
Subsidiary PS for all quadrupoles in bending arcs	1000	52

Table 2.1.5.6

## Electrical parameters of the structural collider magnets

Overall inductance of the dipole magnets, mH	36
Overall inductance of the focusing quadrupole magnets, mH	4.6
Overall inductance of the defocusing quadrupole magnets, mH	4.6
Dipole magnet current at maximum field (1,8 T), kA	10.4
Stability of the maximum dipole magnet current, $\Delta I / I$	$2 \cdot 10^{-5}$
Focusing quadrupole magnet current at maximum field gradient, kA	10.4
The variation range of the focusing quadrupole current, %	10
Stability of the focusing quadrupole current, $\Delta I / I$	$2 \cdot 10^{-4}$
Defocusing quadrupole magnet current at maximum field gradient, kA	10.4
The variation range of the defocusing quadrupole current, %	8
Stability of the defocusing quadrupole current, $\Delta I / I$	$2 \cdot 10^{-4}$
Maximum voltage applied to the circuit of all structural magnets connected in series at the ramp rate of the magnetic field of 0,1 T/s, V	26

#### 2.1.5.4. Beam transfer channel from the Nuclotron to the Collider (Channel NC)

The channel is located both in the existing and in the anew constructed buildings of LHEP. The channel passes from the Nuclotron tunnel (building No. 1), through an extension to building No. 1 and then through the tunnel, which after 23 m is divided into southern (164 m) and northern (153.5 m) branches through which the beam enters the upper and lower rings of the Collider.

The Channel NC has an *optical system* that matches the ion bunch emittance with the Collider acceptance. Matching was implemented for all structural functions, except vertical dispersion and its derivative. The calculated parameters of NC channel (Table 2.1.5.7) met the requirements of the project.

Table 2.1.5.7.

## General parameters of the beam in the NC channel

Ions	Au <sup>79+</sup>
Intensity of the beam per injection pulse	$\leq 1 \cdot 10^9$
Ion energy range, GeV/u	1.0 ÷ 4.0
Ion magnetic rigidity, T·m	14 ÷ 40
Efficiency of the beam transfer, %	95
The beam transverse emittance (95 %), $\pi \cdot \text{mm} \cdot \text{mrad}$	< 3.0 (horiz.) / < 1.5 (vert.)
R.m.s. momentum spread	$< 2 \cdot 10^{-4}$

The magnetic elements of the NC channel are “warm” and operate in a pulsed mode with a repetition rate of 0.25 Hz in the common part of the channel and 0.125 Hz in

its branches. In the channel the sector dipole magnets are used (Table 2.1.5.8). The magnets are water-cooled.

Table 2.1.5.8.

General parameters of the dipole magnets in the NC transport channel

Parameter	Value	
	Long magnet	Short magnet
Magnetic field, T	1.5	
Magnet aperture, mm	60	
Effective length, mm	2000	1200
Bending angle ( $B\rho = 45 \text{ T}\cdot\text{m}$ )	0,0667	0.04
Field integral along trajectory, $\text{T}\cdot\text{m}$	3	1.8
Field integral quality $\Delta Bdl / Bdl $	$\leq \pm 5 \cdot 10^{-3}$	
<i>Electrical parameters</i>		
Current amplitude, A	530	
Winding resistance at 20°C, Ohm	0.738	0.46
Inductance of magnet, mH	173	103
Pulse duration, s	0.18	0.096
Pulse repetition, Hz	0.25	
Voltage amplitude, kV	1400	
Power average consumption at $I_{\text{max}}$ , kW	3.24	1.13
Water cooling pressure, bar	6.0	
Temperature drop at $I_{\text{max}}$ , °C	13.3	3.7
Cooling water consumption, l/min	3,1	3.9

Quadrupole magnets are of two types: long 0.5 m and short 0.33 m long. The maximum field gradient is 30 T / m, the maximum current is 230 A. Magnets are air cooled. Correction magnets of horizontal and vertical deflection produce a magnetic field of up to 114 mT at the current of 89 A. The magnets are air-cooled.

PS of the channel magnets generate half-sine current pulses at repetition rate of 0.25 Hz. Average total power consumption of the NC channel magnetic system does not exceed 150 kW.

The NC channel has a beam diagnostic system. It measures the beam intensity, position, profile, and losses of transported ions. The system includes 4 current transformers, 21 pickup electrode modules, 12 luminophore profilometers, 8 ion loss monitors and the signal processing units. The diagnostic equipment of the Channel is designed for a range of intensities above  $10^7$  deuterons and light ions and from  $10^6$  to  $2 \cdot 10^9$  heavy ions up to  $\text{Au}^{79+}$ .

Vacuum equipment provides a pressure below  $10^{-7}$  Pa except the final sections of the channel branches, where the maximum pressure is permissible not lower than  $5 \cdot 10^{-9}$  Pa.

Both collider rings have *the systems of beam injection and dumping*.

*The injection system* is made by a single-turn scheme. Its main elements are septum and kicker magnets, as well as subsystem of the closed-orbit bump. It includes the collider structural dipoles with additional current leads. Septum magnets are used to bring the beam into the vacuum chambers of the Collider rings, where the kicker magnets put it in the closed orbit. The application of local bumps of a closed orbit at the injection area reduces the requirements to the parameters of the kicker magnets.

*The dumping system* transfers the beam circulating in the Collider to the absorbers when degradation of the beams (and the luminosity) is significant and new ion accumulation cycle is to be made, either in emergency situations when a SC magnet suffers a quench, or beam losses critically increase.

Elements of two dumping systems are placed inside cryostats in the straight sections of the half-ring E.

The beams are extracted from the Collider by a set of kicker and septum magnets mounted symmetrically to the tools of the beam injection system in both rings so that the extracted beams are sent in opposite directions of the beam injection. Kicker magnets (Table 2.1.5.9) send circulating beams into septum magnets, which complete the extraction of the beams to the absorbers. The beam from the upper ring is extracted horizontally using kicker and pulsed septum magnets. The beam from the lower ring is two steps: first horizontally by the kicker, and then vertically by the Lambertson magnet and an inclined pulsed septum magnet.

After the beams are removed from the Collider cryostat, they are transported to the absorbers by air. Absorbers are an iron core and concrete environment, which also provide biological protection.

Injection magnets operate alternately in a pulsed mode with a periodicity of 8 s. (period of ions injection in the Collider ring). The operation mode of the closed-orbit bump subsystem is cyclic. At the end of the accumulation, its power sources are turned off.

Table 2.1.5.9

General parameters of the kicker magnets for injection and beam dump systems

Parameter	injection	dumping
Maximum magnetic field, T	0,05	0,11
Effective length, m	4.0	4.0

Bending angle ( $B\rho = 40 \text{ T}\cdot\text{m}$ ), mrad	5	10
Wire diameter, mm	8.0	8.0
Horizontal aperture, mm	40	50
Vertical aperture, mm	30	40
Field integral quality $\Delta Bdl / Bdl $ , %	$\pm 1.0$	$\pm 5.0$
Current maximum amplitude, kA	8.0	16.0
Pulse duration, ns	$\leq 600$	$> 1700$
Inductance of one pair of conductors, $\mu\text{H}$	0,4	0,4

The beam-dump devices have the average pulse repetition periodicity during the Collider routine operation about 1000 s. The Lambertson magnet of the beam dumping system is switched in series in the PS circuit of the Collider structural magnets and operates in a cyclic mode according to the cycle of the Collider magnetic field.

The NC channel belongs to basic configuration of the Collider. The construction of the channel is carried out by the French company SigmaPhi since 2017. The equipment delivery is scheduled for the end 2019, mounting will be started in summer 2020.

#### 2.1.5.5. RF stations of the NICA Collider

The ion storage and formation of an ion beam in the Collider is carried out using three different RF systems. Their first type is the so called “barrier” RF voltage station (RF-1) (Fig. 2.1.5.3) which is used to accumulate and accelerate particles in the energy range from 1 to 4.5 GeV/u. This station creates a succession of accelerating and decelerating rectangular voltage pulses with an amplitude of up to 5 kV (Table 2.1.5.10).



*Fig. 2.1.5.3. RF-1 voltage station.*

Table 2.1.5.10

## Parameters of RF1 station and accumulated beams

Parameter	Value	
	Energy, GeV/u	1.0
Longitudinal size of RF1 station	1405	
Number of stations per ring	1	
Voltage pulse amplitude, kV	5.0	
Maximum duration of voltage flat-top, ns	80.0	
Minimum duration of voltage flat-top, ns	10.0	
Duration of pulse leading and trailing edges, ns	10.0	
Maximum power, kW	21.0	
Pulse number during ion revolution period	4	
Plateau of injection kicker, ns	200.0	
Injection kicker leading edge, ns	200.0	
Injection kicker trailing edge, ns	200.0	
Injection repetition rate into each collider ring, Hz	0.125	
Maximum accelerating voltage, V	$\pm (300 \pm 30)$	
Fronts of accelerating voltage pulses, ns.	10	
Number of injection cycles during accumulation	5	55
Ion number injected per cycle from Nuclotron	$10^9$	$10^9$
Ions accumulated in the collider	$4.4 \times 10^9$	$5.3 \times 10^{10}$
Accumulation efficiency without cooling	0,7	0.7
Accumulation efficiency with cooling	0.93	0.94
RF separatrix barrier, $(dp/p)_h$	$7.3 \times 10^{-4}$	$1.1 \times 10^{-3}$
Longitudinal emittance of the accumulated bunch, eV·s	59	202

The RF-2 station of harmonic RF voltage (Fig.2.1.5.4, Table 2.1.5.11) operates at the frequency of the 22<sup>nd</sup> harmonic of the particle revolution frequency in the Collider rings. It is built on the basis of a shortened capacitance vacuum coaxial resonator. The maximum voltage amplitude is 25 kV. Each ring of the collider contains four RF-2 stations, i.e. their total accelerating voltage is 100 kV. The resonant frequency of the resonator is tuned (depending of the experiment energy of 1–4.5 GeV/u) within 11–13 MHz.

Stations of the third type RF-3 (Fig. 2.1.5.4, Table 2.1.5.11) are based also on a shortened capacitance vacuum coaxial resonator. They generate a harmonic voltage at the 66<sup>th</sup> harmonic of the particle revolution frequency in the rings with a maximum amplitude of 125 kV. Eight RF-3 stations per each ring provide total accelerating voltage 1 MV. The resonant frequency of the resonator is tuned (depending on the experiment energy of 1–4.5 GeV/u) within 34–39 MHz.



*Puc. 2.1.5.4. RF-2 (left) and RF-3 (right) of the Collider.*

Table 2.1.5.11

Parameters of RF2 and RF3 resonators

Station	RF-2	RF-3
Length (without bellows), mm	1660	1626
Accelerating voltage, kV	25	125
Number of resonators per the ring	4	8
Total accelerating voltage, kV/ring	100	1000
Minimum voltage at ion adiabatic capture, kV	1.5	22
Ion revolution frequency, MHz	0.522-0.587	
Harmonic number	22	66
RF-frequency, MHz	11.484÷12.914	34.452÷38.742
Frequency tuning, MHz	1.5	4.3
Characteristic impedance, Ohm	75÷87	50
Proper quality factor, Q	3400÷3700	6700÷7200
Frequency ramp rate, kHz/s	14.7	25.7
Shunt impedance, kOhm	260÷320	335÷425
Current of the ion beam, A	2.8 A at 3 GeV/u	
RF power loss per one resonator , kW	4.8÷3.9	23.4÷18.4
Power of RF amplifier, kW	7	40
Instability of voltage phase, grad.	±0,2	
Resource of short-connector, cycles	10 <sup>5</sup>	
Aperture of vacuum chamber, mm	100	
Vacuum pressure in resonator, Torr	≤3×10 <sup>-11</sup>	
Weight, t	1.5	1.5
Overall sizes (length×width×height), mm	1951×1753×2540	1832×1423×2540

Resonators of RF-2 and RF-3 stations are tuned by capacitive tuners. All stations have mechanical short circuits (SC) of accelerating gaps. When the SC of a station is closed (shorted), the beam “sees” a smooth chamber, not a resonant cavity.

After successive  $^{192}\text{Au}^{79+}$  injection cycles from the Nuclotron and the accumulating with RF-1 the required number of particles, the RF-1 system is turned off and closed. The beam expands occupying the entire perimeter of the Collider, and the RF-2 system slowly turns on adiabatically forming 22 bunches. The process is accompanied by cooling – electron and/or stochastic. The amplitude of the RF-2 increases until the bunch longitudinal size fits in the separatrix of the 66<sup>th</sup> harmonic (RF-3). At this moment in time, the RF-3 turns on adiabatically slowly when the RF-2 station is operating and the bunch is intercepted from RF-2 to RF-3.

The bunching of the beam at the 66<sup>th</sup> harmonic of the revolution frequency in the presence of an RF-2 with an amplitude of 100 kV with an adiabatic increase in the total voltage of the RF-3 from 21.87 kV to 0.8 MV and cooling with a time of 100 sec provides the formation of bunches with mean square design length of 0.6 m and the mean square design ion momentum spread of  $10^{-3}$ . These parameter values are required for the collision mode and design luminosity of colliding bunches.

The RF-3 system, along with the formation of short ion bunches, can be used to accelerate them when the ring magnetic field and the frequency of the RF-3 station rise concordantly. The rate of change of frequency of 25.7 kHz/s determines the rate of ion acceleration. For RF-2, it is equal to 150 (MeV/u)/s. The acceleration of ions with RF3 stations occurs 2.5 times faster than is done using RF-1 stations.

Excitation of the RF-2 and RF-3 resonators is implemented by transistor amplifiers (Fig.2.1.5.5) produced by Limited Liability Company Research & Production Enterprise (LLC RPE) Triada TV, Novosibirsk.



*Fig.2.1.5.5 RF3 amplifier of the Collider.*

Two RF-1 and four RF-2 stations belong to basic configuration of the Collider equipment. Four additional RF-2 and sixteen RF-3 stations will complete Collider extended configuration. The construction of three RF systems was started in 2016-2017 in BINP SB RAS. Presently the BINP team constructed and tested two RF-1 stations, which will be delivered to JINR in spring 2020. Mounting of these stations in the Collider building will be started in summer 2020. Fabrication of four RF-2 station is in progress, one working prototype is fabricated and tested (Fig. 2.1.5.6).



*Fig.2.1.5.6 Test of working RF-2 prototype station.*

Mounting of these four stations is scheduled for August-September 2020. Fabrication of four other RF-2 stations and sixteen RF-3 stations is in progress. Working RF3 prototype is also fabricated and tested (Fig. 2.1.5.7). According to the project schedule all they delivery and mounting will be in 2021, i.e. two years earlier than the initial NICA project plan assumed.



*Fig. 2.1.5.7. Working RF-3prototype station of Collider.*

### **2.1.5.6. Collider diagnostic control and monitoring system**

The Collider Control and Diagnostic System (CDS) is a set of hardware and software, consisting of several independent subsystems, like computing, network and software infrastructure for the development and execution of tasks of other control systems. The Collider CDS is based on common principles with the Booster CDS and consists of the following subsystems:

- beam diagnostics in the collider rings;
- CDS of parameters of the magnetic system;
- infrastructure of automatic control system (ACS).

The Collider beam diagnostic system provides a measurement of

- average beam current;
- longitudinal profiles of bunches of a bunched beam;
- parameters of the equilibrium beam orbit;
- position in space and time of individual short bunches;
- frequencies of ion betatron oscillations.

CDS of the magnetic system parameters provides:

- temperature control of the elements of the magnetic system;
- control of magnetic field correctors;
- diagnostics and control of the magnetic field variation in the elements of the Collider magnetic system.

The ACS infrastructure consists of a distributed network of computers interconnected by an Ethernet network. The system is made in the form of three levels – the level of access to equipment, service level and client level. The components of all three levels are interconnected using a transport protocol that works via TCP/IP. NICA ACS uses the TANGO control system as middleware. For the tasks of the ACS of Collider, Booster and Nuclotron, a cluster of several Supermicro physical servers is used under the control of the Proxmox virtualization system, which is a completely open server platform for creating and managing a virtual infrastructure, including virtual machines, storage, virtual networks and high availability clusters. Cluster physical servers are combined using a fast 10 Gbps duplicated network. Servers are both nodes of the distributed network storage Ceph and nodes for execution ACS virtual machines. Highly reliable solid-state drives (SSDs) with reliability of 5 DWPD (drive writes per day) are used as the basis for building highly reliable Ceph distributed storage that is used to store and execute virtual server disk images.

Operational control and management points are part of the overall CDS and are located in rooms No. 137 (local control panel No. 1) and No. 187 (local control panel No. 2) connected by cable routes with an annular cable channel of the tunnel 500x500 mm<sup>2</sup>.

CDS equipment belongs to basic configuration of the project. Presently, significant part of CDS components has been purchased, including hardware for data acquisition and processing produced by the Libera Hadron and Instrumentation Technology firms, network server equipment from PXI National Instruments firm, high frequency current amplifiers from FEMTO Messtechnik GmbH company, current transformers from Bergotz Instrumentation firm, microchannel plates for beam profilometers, etc. At present time the Bergotz parametric transformer is undergoing bench tests. The design of Collider arches pickup electrodes was developed, and the construction of monitors for straight sections was started. The design of the stripline beam position monitors for SPD and MPD straight sections has been developed. Mounting of diagnostic equipment is planned in fall 2020.

### 2.1.5.7. Vacuum system

Vacuum volumes of the Collider are divided into insulating vacuum space of the cryostat, as described in section 2.1.5.1 – 2.1.5.2, and the volumes of the beam chamber. The latter, in turn, are divided into “warm” ones at room temperature and “cold”, whose walls under operating conditions are in the temperature range from 4.2 K to 300 K. The pressure in the beam chamber is not higher than  $2 \times 10^{-9}$  Pa.

With a total collider length of about 500 m, the largest part is occupied by “cold” straight sections and arches. They contain SC magnets, elements of a beam diagnostic and control system, injection systems, and sections of heat-cold transitions. In warm sections, there are RF stations, the HV E-Cooler, SCS, detectors and beam diagnostic devices.

Operation and control of vacuum equipment is carried out by the automated CDS of the NICA Collider (section 2.1.5.6).

The equipment of the vacuum system belongs to the basic configuration.

Beam vacuum chambers and pickup electrodes and connection bellows are manufactured by the Polish company FRAKOTERM since beginning of 2019. Vacuum chambers to be installed in the “empty” sections parallel to 26 RF stations are manufactured by Budker INP. Currently, a significant amount of standard vacuum equipment, including high-vacuum valves, leak detectors, diffusion pumps for providing insulating vacuum of the cryostat system of SC magnets, high vacuum pumps, etc., has been purchased. The mounting of vacuum equipment of the straight sections and arches of the Collider is scheduled for summer 2020.

## 2.2. Experimental setups

Three experimental set-ups belong to the basic configuration of the NICA Complex: MPD – Multi Purpose Detector, for study hot and dense baryonic matter at the NICA Collider, BM@N – Baryonic Matter at Nuclotron, for the same investigations in fixed target experiments at Nuclotron, and SPD – Spin Physics Detector, for study of hadron spin structure at Collider. Two first of them should be ready for investigation till the end of construction of the basic configuration of the NICA Complex, works on the last ones should be started.

### 2.2.1. Multi Purpose Detector (MPD)

A scientific program on heavy-ion physics launched recently at JINR is devoted to a detailed exploration of the QCD phase diagram and search for the signals of deconfinement phase transition and the critical endpoint. Comprehensive investigations in the unexplored region of the phase diagram of strongly interacting matter will be performed by a careful energy and system-size scan with ion species ranging from protons to Au<sup>79+</sup> over the energy range  $4 < \sqrt{s_{NN}} < 11$  GeV. So, a goal is to design and build a multifunctional detector to measure heavy-ion collisions and investigate the basic Quantum Chromo Dynamics structure of matter.

The main advantages of the MPD project is that the NICA accelerator facility will provide a vast choice of beams (from protons to gold ions) in the energy range which brackets onset of deconfinement (centre-of-mass energy from 4 to 11 GeV). A high luminosity of NICA ( $L = 10^{27} \text{cm}^{-2}\text{s}^{-1}$ ) allows small enough energy steps and provide high interaction rate. The key feature of the proposed MPD detector design that allows studying of nuclear collisions with high precision are:

- high event rate (up to 6 kHz) allows very subtle measurements of the energy and centrality dependence of any phenomenon under interest;
- MPD has full azimuthal coverage and will measure most of the momentum range in the pseudo-rapidity interval  $-2 < \eta < 2$ ;
- tracking and particle identification system including TPC for energy loss and TOF for time-of-flight measurements complemented by an electromagnetic calorimeter for photons and electrons with good time and energy resolution.

#### 2.2.1.1. Conceptual design of the MPD detector

The MPD set-up has been designed as a  $4\pi$  spectrometer capable of detecting of charged hadrons, electrons and photons in heavy-ion collisions at high luminosity in the energy range of the NICA collider. To reach this goal, the detector will comprise a precise 3-D tracking system and a high-performance particle identification (PID) system based on the time-of-flight measurements and calorimetry. The basic design

parameters have been determined by physics processes in nuclear collisions at NICA and by several technical constrains guided by a trade-of of efficient tracking and PID against a reasonable material budget. At the design luminosity, the event rate in the MPD interaction region is about 6 kHz; the total charged particle multiplicity exceeds 1000 in the most central Au+Au collisions at  $\sqrt{s_{NN}} = 11$  GeV. As the average transverse momentum of the particles produced in a collision at NICA energies is below 500 MeV/c, the detector design requires a very low material budget.

The aim of this Project is to build a first stage of the MPD setup, which consists of the superconducting solenoid, Time-Projection Chamber (TPC), barrel Time-Of-Flight system (TOF), Electromagnetic Calorimeter (Ecal), Forward Hadron Calorimeter (FHCAL) and Fast Forward Detector (FFD).

The whole Central Detector (CD) will be a 9 m long cylinder of about 6,6 m in diameter. The cross-sectional view of the MPD Central Detector is shown in Fig. 2.2.1.1.

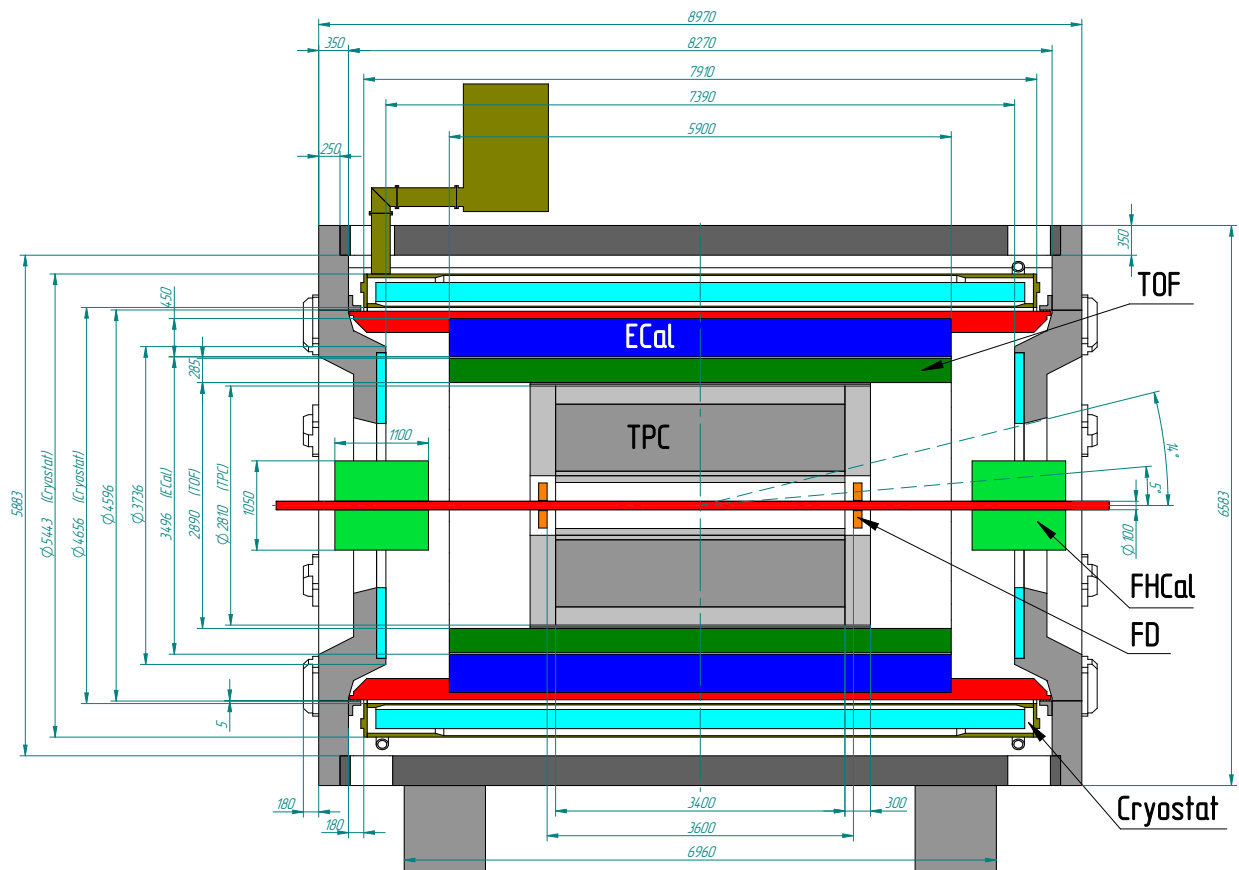


*Fig. 2.2.1.1. Cutaway side view of a basic configuration of the MPD Central Detector.*

### 2.2.1.2. Superconducting magnet

A constituent part of the MPD is a superconducting solenoid magnet with a superconducting NbTi coil and a steel flux return yoke. The superconducting magnet of MPD is intended for providing a highly homogeneous magnetic field of 0.57 T in an aperture 4596 mm in diameter to ensure the transverse momentum resolution within the range of 0.1–3 GeV/c at NICA.

The MPD magnet consists of (Fig. 2.2.1.2):

- a cryostat with a superconducting coil and a control Dewar;
- a flux return yoke with two support rings, 28 bars, and two poles with trim coils;
- magnet support cradles;
- auxiliary platforms for moving the poles;
- roller skates for movement of the magnet and its poles.

In addition, there are power supplies for the superconducting coil and for the trim coils in the poles, a SC coil quenching protection system, a cryogenic system with the cryogenic pipeline, a vacuum system, helium refrigerator and a magnet control system.

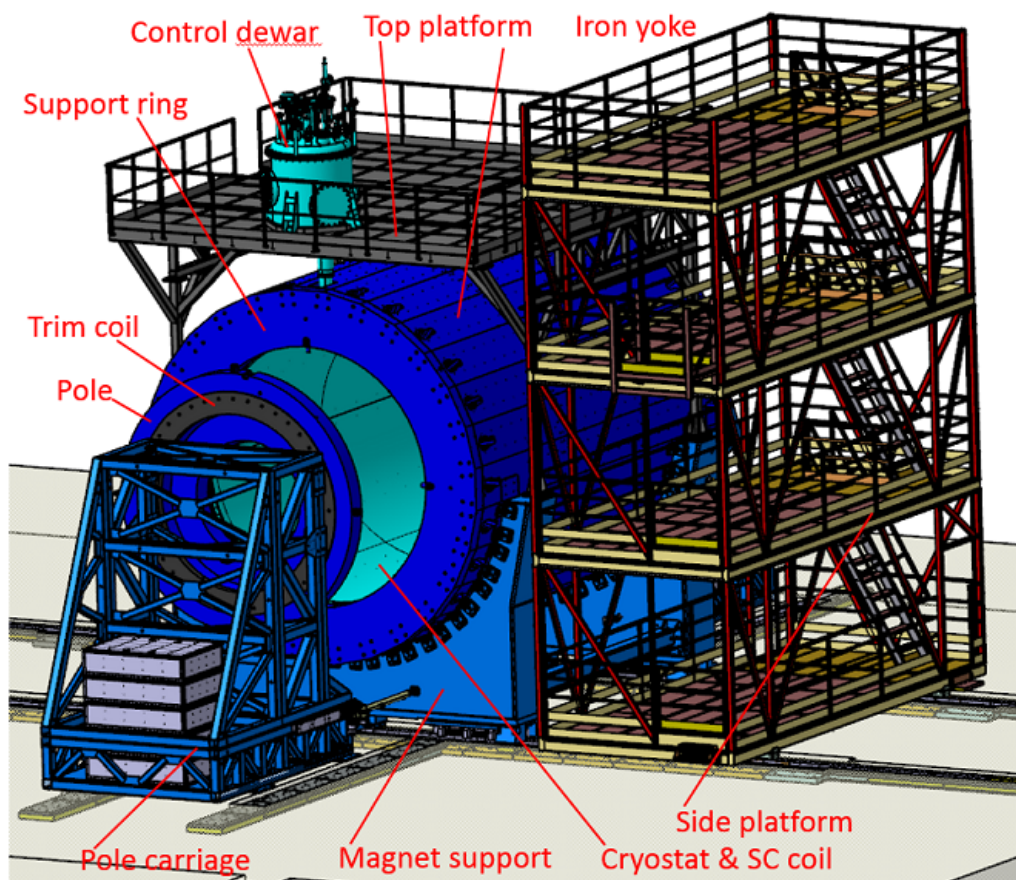


*Fig. 2.2.1.2. Overall view of the magnet.*

### ***2.2.1.2.1. Solenoid***

Rated current of the magnet is 1790 A (it corresponds to a field in the aperture of 0.5 T). The maximum magnet field at which the specified value of the integral of the radial component of the induction in the area of TPC Int  $\leq 1.5$  mm is maintained, and which can be achieved with a maximum level of technological deviations from the optimized geometry of the magnetic system, is 0.57 T.

In 2014 the Technical Project of the magnet has been developed by company “Neva-Magnet” in St. Petersburg (Russia) according to JINR’s request.

In 2015 the manufacturer company has been defined for production of the Solenoid and its auxiliary equipment such as power supplies, control and protection system, vacuum system etc. Then, in the end of 2015 related contract has been signed with ASG Superconductors s.p.a (Italy).

First stage of production was the developing of the working documentation of equipment including drawings, assembly procedures, quality control plans and calculations. Once it was finished, the superconducting cable with total length of about 28 km (Fig. 2.2.1.3) has been purchased for the magnet by ASG in Japanese company Furukawa Electric in the beginning of 2017. Such a big length of cable has been supplied divided into 10 equal pieces which has been connected to each other by welding during the winding of the SC coil.



*Fig. 2.2.1.3. Batch of the SC cable.*

A conductor with a bare cross section of 4.1x20 mm is used for winding the superconducting coil (the insulated conductor cross section is 4.5x20.4 mm<sup>2</sup>). The

conductor is manufactured by co-extrusion of stabilizing high-purity aluminium (purity 99.999%, RRR>1000) and a superconducting NbTi wire 1.75 mm in diameter (Cu/SC ratio =0.9/1). Highly pure aluminium ensures high stability of the coil due to the low matrix resistance at the helium temperature, which allows the premature propagation of the normal zone to be avoided when local heat emissions occur in the coil due to mechanical disturbances during the energizing and de-energizing of the magnet.

In parallel the production of 3 modules of the aluminium support cylinder for the superconducting coil has been finished (Fig. 2.2.1.4). The cable has been tested additionally by request of JINR to ensure in its good quality.



*Fig. 2.2.1.4. One of the support cylinder modules.*

To correct the magnetic field in the TPC region, there are trim coils fixed in the pole recesses. They are wound using a hollow copper conductor  $42 \times 42 \text{ mm}^2$  in cross. The trim coils will be cooled by demineralized return water circulating in a closed loop. The maximum possible temperature of the cooling water is taken to be  $T = 25 \text{ K}$  at the entrance to the trim coil and  $T = 55 \text{ K}$  at the exit (temperature difference  $T = 30 \text{ K}$ ). Copper trim coils for the magnet has been produced by April 2018 (Fig. 2.2.1.5).



*Fig. 2.2.1.5. Trim coil.*

Once the support cylinder modules and SC cable was ready, the winding of the SC coils started in March 2017 with custom winding machine and “impregnation” oven specially built for this magnet (Fig. 2.2.1.6). Winding and “impregnation” of the superconducting coil modules was finished in the end of 2018 while the production of the vacuum vessel for the magnet was done in parallel



*Fig. 2.2.1.6. Winding machine (left) and “impregnation” oven (right).*

The vacuum vessel (Fig.2.2.1.7). is the main part of the thermal insulation of the magnet. It is made of stainless steel. It consists of an inner and an outer shell 16 mm and 25 mm thick respectively. At the ends of the shells there are beads 45 mm thick, to which the cryostat flanges are attached. Two collars of the radial suspension are connected to the outer shell thickenings. The weight of the vacuum cryostat vessel is 49.1 t. Under all loads, the change in the outer cryostat dimensions (diametric or axial) must not exceed 2 mm.



*Fig 2.2.1.7. Vacuum vessel.*

Production of the vacuum vessel has been done by ASG’s subcontractor company Simic which has a big experience in production of the main hardware parts for the ITER project being constructed in France. After the production, all the necessary tests including the vacuum pumping have been positively done and reported. Testing was finished in the middle of 2018, and then the transportation of the vacuum vessel from Simic premises located in Venice (Italy) to ASG premises located in La Spezia (Italy) has been successfully finalized.

Once the winding of all 3 SC coil modules was finished, the assembly of the “cold” mass started in the beginning of 2019 (Fig 2.2.1.8.). The “cold” mass could be defined as 3 coil modules assembled into single coil including the cryogenic circuit piping, SC cable joints, radial and axial tie-rods for suspension etc. Its assembly has been successfully done in the middle of 2019.



*Fig. 2.2.1.8. Assembly of the “cold” mass.*

In parallel with cold mass assembly the procurement of all the auxiliary equipment such as power supplies, control system etc. for the magnet has been finalized by ASG. In particular, power supplies have been purchased in company SigmaPhi. The power supply system consists of a power supply for the superconducting coil, two switches in the coil power supply circuit (for increasing the reliability of the quench protection system operation), two power supplies for the trim coils and of dump resistors for de-energizing the SC coil. The switches allow the discharge resistance to be varied for varying the coil de-energizing rate.

Once the assembly of the cold mass is finished and the vacuum vessel is delivered to ASG premises, the complete assembly of the solenoid is started (Fig. 2.2.1.9).

Complete assembly could be described as insertion of the cold mass into the vacuum vessel, suspension of the cold mass by using the axial and radial tie-rods, installation of the nitrogen heat-shield and multi-layer 91 exed 91 e-insulation etc. Such complicated operation has been performed under the strict quality control by checking of the position of the cold mass relative to vacuum vessel and by control of the tension in the tie-rods.



*Fig. 2.2.1.9. Assembly of the solenoid in progress.*

The complete assembly of the solenoid has been finished by September 2019 (Fig. 2.2.1.10). Since that moment the solenoid is ready for transportation to JINR's premises.



*Fig. 2.2.1.10. Completely built solenoid.*

#### **2.2.1.2.2. Magnet Yoke**

In 2012, the geometry of the MPD detector was adopted in the final version (Fig. 2.2.1.11). The length of the magnetic circuit was 8970 mm, the outer diameter – 6.63 m. The total weight of the magnetic circuit, consisting of 2 support rings, 2

poles and 24 beams, is 630 tons. The weight of the MPD detector in the design configuration is 980 tons.

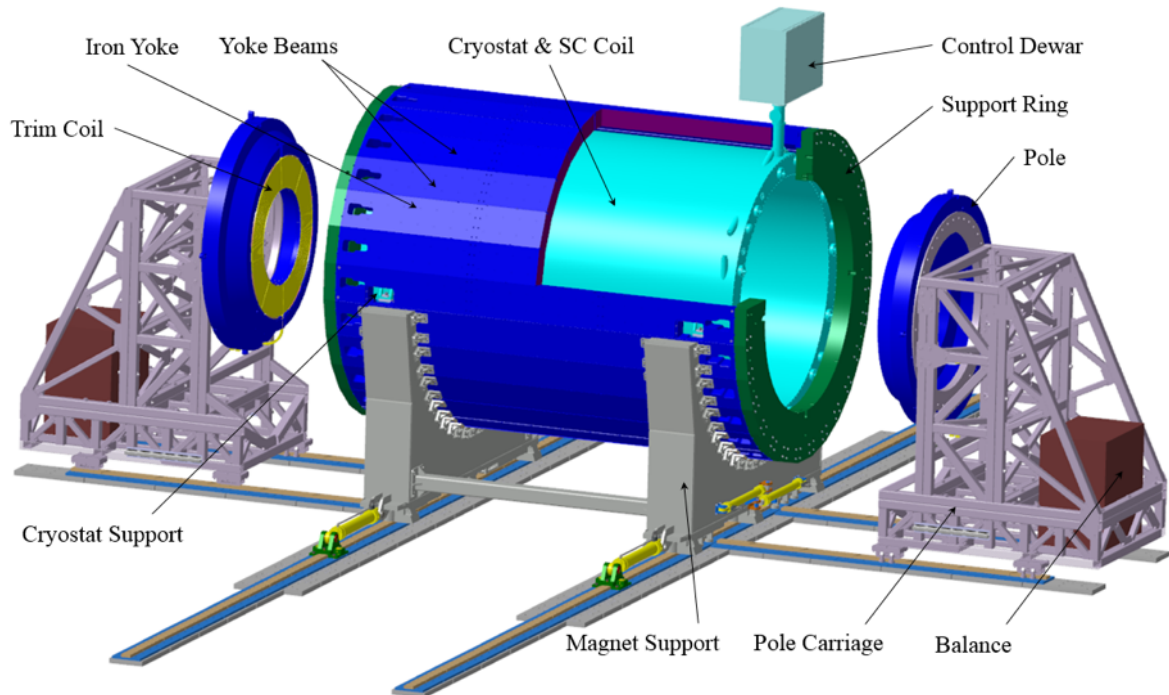


*Fig. 2.2.1.11. MPD magnetic circuit with poles on transport supports.*

In 2012-2016 by the staff of the LHEP Design Department (DD), working documentation (WD) was issued for the manufacture of a magnetic circuit in the configuration of 24 beams that make up the longitudinal part of the magnetic circuit, and then, for technological reasons, the WD was converted to a modern version with 28 beams. In the corresponding manner, the taxiway was released on the support rings, poles, lodgement, transport supports for the poles. Along the way, DD developed a technology for assembling a magnetic circuit, and also released a taxiway for the technological devices necessary for assembling a magnetic circuit. One of the most important technological devices is a manipulator (Fig. 2.2.1.12) for lifting 16-ton beams with a length of 8470 mm and turning them to the angle required during installation. It was brought free of charge from CERN, where it was used to assemble three cylinders of the hadron tile calorimeter of the ATLAS set-up at the LHC.

At the end of 2015, two fundamental contracts for the manufacture of the magnetic circuit were concluded:

- with «PP Specmash» (St. Petersburg, Russia), for the manufacture of forgings for 28 beams, 2 support rings and 2 poles;
- with VHM, Vitkovice (Ostrava, Czech Republic) for the manufacture of magnetic circuit parts (from our tolling raw materials), tool tray, pole transport

supports and all necessary technological equipment with the control assembly of the magnetic circuit in the factory.



*Fig. 2.2.1.12. The manipulator.*

In fact, the beams of the magnetic circuit were manufactured at NKMZ, Kramatorsk (Ukraine) (Fig. 2.2.1.13).

All physic-chemical parameters were performed in strict accordance with the WD. By chemical composition: carbon content in the range 0.08 – 0.10% (GOST 1050-88 regulates the carbon composition in the range of 0.07 – 0.14%), the remaining elements are in accordance with the same GOST.

Mechanical strength (yield strength): above 210 N/mm<sup>2</sup> specified in the WD for each casting, average value 241 N/mm<sup>2</sup>, minimum 225 N/mm<sup>2</sup>. Ultrasonic testing is normal. The magnetization curve B/N is normal.



*Fig. 2.2.1.13. Forgings of beams at NKMZ before shipment.*

Forgings for the support rings and the poles of the magnetic circuit were made in Italy at the “Forgiatura Morandini” enterprise (Fig. 2.2.1.14).

All physic-chemical parameters were also performed in strict accordance with the WD. By chemical composition: carbon content in the range 0.08 – 0.09%, other elements in accordance with GOST 1050-88.

Mechanical strength (yield strength): above  $210 \text{ N/mm}^2$  specified in the RD for each casting, average value  $231 \text{ N/mm}^2$ , minimum  $255 \text{ N/mm}^2$ . Ultrasonic testing is normal. The magnetization curve  $B / N$  is normal.

All forgings for beams and rings were delivered to VHM by July 2016 by the transport company AET Trans, St. Petersburg. The manufacture of all components of the magnetic circuit took more than 2 years from mid-2016 to December 2018.



*Fig. 2.2.1.14. Forgings of support rings and poles after preliminary processing with an allowance of 5 mm per contour (June 2016).*

All important dimensions of the parts of the magnetic circuit and the lodgement were made with higher accuracy than indicated in the WD. So, the covering size along the parallel landing faces of the 28-gon of the support ring is made with a tolerance of  $-0.03 \dots -0.06 \text{ mm}$  with a nominal size of  $5883 \text{ mm}$  and a tolerance of  $-0.1 \text{ mm}$ , and the asymmetry of the position of the faces relative to the common centre was  $0.02 \text{ mm}$  instead of the assigned  $0.2 \text{ mm}$ .

In June-July 2018, at the VHM plant, with the participation of engineers and technicians from JINR, a control assembly of the magnetic circuit was performed (Fig. 2.2.1.15). The overall dimensions of the magnetic circuit correspond to the nominal dimensions according to the drawing with a measurement accuracy of  $0.2 \text{ mm}$ . The alignment of the support rings was  $0.1 \text{ mm}$ , the non-perpendicularity of the support rings was  $0.5 \text{ mm}$  with a deviation to the outside at both ends (theoretically possible envelopes are  $20 \text{ mm}$  per side).

In February-March 2019, the main oversized parts of the magnetic circuit, the support rings with an outer diameter of  $6.7 \text{ m}$  and the poles with  $4.7 \text{ m}$ , were taken out by the transport company AET Trans (St. Petersburg), to the LHEP. To carry out customs procedures with oversized cargo, a temporary customs control zone was created on the territory of the LHEP (Fig. 2.2.1.16), which was closed on July 30, 2019 upon completion of the export of all equipment manufactured under a contract with VHM on schedule. For this transportation company AET Trans needed 37 vans, 7 of which were carrying oversized cargo.

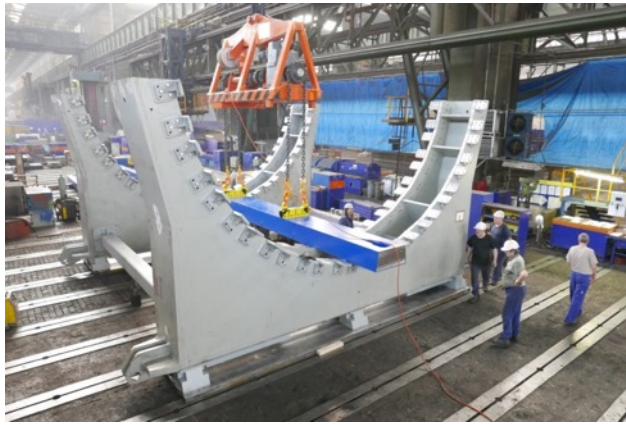


*Fig. 2.2.1.15. Installing the first bottom plate of the magnetic circuit (left). The magnetic circuit is assembled. June 2018.*

The next important step is the construction of a moving system (MS) of the assembled MPD (with a full nominal weight of 980 tons) and poles (weighing up to 100 tons with detectors installed on them). Under the current contract with SPP SPETSMASH LLC (St. Petersburg) all components of this system are manufactured, delivered to JINR and stored at the JINR warehouse. Installation and commissioning of the joint venture is scheduled for 2020.



*Fig. 2.2.1.16. Support rings and poles in the temporary customs control zone (March 2019).*

To enable safe movement of the MPD detector, into the construction drawings of the foundation of the pit of MPD pavilion, at the initiative of JINR, steel 100 mm thick foundation plates were introduced to distribute the weight load from the detector.

Under a contract with NPP SPETSMASH LLC in 2017, 2 sets of foundation slabs were manufactured for both the MPD and SPD pavilions. In April 2018, they also

delivered a set of rail slabs for the MPD pavilion. Rails and roller carriages for moving the detector and its poles were purchased in 2016 from Boerkey GmbH, Germany.

In November 2018, the construction company STRABAG installed foundation slabs in the pit of the MPD pavilion. The non-flatness of the upper surface of the plates (pre-machined at the factory) was 0.4 mm over a length of 30 m, which will subsequently allow the installation of the rail with similar accuracy, and this in turn will eliminate the high local loads from the roller trolleys and ensure uniform load on the rail tracks and foundation.

In August 2019, “Pelkom Dubna Machine-Building Plant” installed the rail plates and the rails themselves (Fig. 2.2.1.17).

The non-flatness of the upper surface of the rail was 0.4 mm over a working length of 7 m, which is several times less than the assigned non-flatness in the taxiway. The indirectness of the lateral surface of the base rail was 0.17 mm over a length of 30 m.



*Fig. 2.2.1.17. Rail tracks in the pit of the MPD pavilion. Working surfaces are closed by casings.*

### **2.2.1.3. Time Projection Chamber – TPC**

The Time-Projection Chamber (TPC) is the main tracking detector of the MPD central barrel. It is a well-known detector for 3-dimensional tracking and particle identification for high multiplicity events. The TPC/MPD will provide:

- the overall acceptance of  $\eta < 1.2$ ;
- the momentum resolution for charge particles under 3% in the transverse momentum range  $0.1 < p_t < 1$  GeV/c;
- resolution of two tracks of about 1 cm;

- hadron and lepton identification by  $dE/dx$  measurements with a resolution better than 8%.

These requirements must be satisfied at the NICA design luminosity with event rate about 7 kHz. Max charged particle multiplicity – up to 1000 tracks in central Au-Au collisions.

### 2.2.1.3.1. A TPC design

TPC consists of four cylinders (C1-C4) manufactured by the Russian industry from composite materials. This approach provides sufficient cylinders strength along (in the worst case, the deformation at load of  $F = 80$  kG in the middle is less than  $100 \mu\text{m}$ ) and a small radiation thickness ( $0.4 \text{ g/cm}^2$ ). All four cylinders are interconnected by two aluminum flanges. The gap between C1–C2 and C3–C4 is blow through by nitrogen  $\text{N}_2$  for protection against a high-voltage discharges and prevention of  $\text{H}_2\text{O}$  and  $\text{O}_2$  diffusion into the drift volume of the TPC.

The central high-voltage electrode-membrane divides the drift volume into two parts and creates the electric field strength which is necessary for the drift of the generated electron-ion clusters to the TPC end-caps (see Fig. 2.2.1.18, pos. 2). The membrane is produced with the  $110 \mu\text{m}$  Mylar film. The non-uniformity of magnetic field has to be not worse than  $B_r/B_z \sim 10^{-4}$ . The Field cage (see Fig. 2.2.1.18, pos. 3) has a symmetrical design, each part of which is located on both sides of the high-voltage electrode and consists from 112 pairs (outer and inner structures) of  $13 \text{ mm}$  wide mylar strips stretched on special rods with the same pitch and accuracy of  $50 \mu\text{m}$ . The high-voltage electrode is connected to the nearest mylar strip by a resistor and each subsequent strip is connected by a resistor to the next one. This chain forms a HV divider from  $-24 \text{ kV}$  (high voltage electrode) to zero (TPC end-caps).

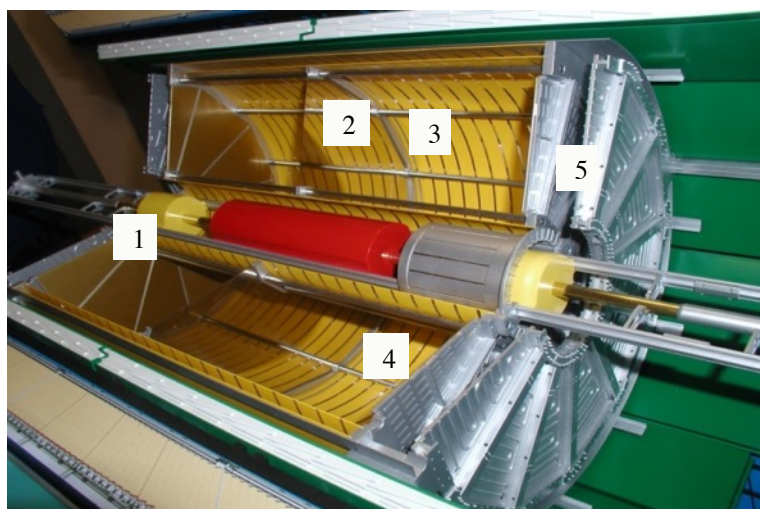


*Fig. 2.2.1.18. Central part of the MPD (mock up). 1- MWPC; 2 – HV electrode; 3 – field cage; 4 – flange with MWPCs and FEE electronics; 5 – end cap thermal screen.*

The main subsystems of TPC include:

- Readout Chambers (ROC)
- Gas System
- Laser Calibration System
- Cooling System
- FEE, Readout and DAQ
- DCS
- HV and LV systems

The basic design parameters of the TPC are summarized in Table 2.2.1.1.

Table 2.2.1.1

The basic parameters of the TPC

Item	Dimension
Length of the TPC	340 cm
Outer radius of vessel	140 cm
Inner radius of vessel	27 cm
Outer radius of the drift volume	133 cm
Inner radius of the drift volume	34 cm
Length of the drift volume	163 cm (of each half)
HV electrode	Membrane at the center of the TPC
Electric field strength	140 V/cm
Magnetic field strength	0.5 Tesla
Drift gas	90% Ar+10% Methane
Gas amplification factor	$10^4$
Drift velocity	5.45 cm/ $\mu$ s
Drift time	< 30 $\mu$ s
Temperature stability	< 0.5°C
Number of readout chambers	24 (12 per each end-plate)
Segmentation in $\phi$	30°
Pad size	5x12 mm <sup>2</sup> and 5x18 mm <sup>2</sup>
Number of pads	95232
Pad raw numbers	53
Zero suppression	up to 90%
Maximal event rate	< 7 kHz ( Lum. $10^{27}$ )
Electronics shaping time	180-190 ns
Signal-to-noise ratio	30:1
Signal dynamical range	10 bit
Sampling rate	10 MHz
Sampling depth	310 time buckets
Resolution of two tracks	1 cm

### **2.2.1.3.2. Readout Chamber (ROC)**

For the startup period of operation a ROC based on Multi-Wire Proportional Chambers (MWPC) with cathode pad readout and gate grid was chosen (see Fig. 2.2.1.18, pos.1). The gap between the anode wire plane and the cathode pad plane is the same as the gap between the anode wire and the cathode wire planes and is 3.0 mm. The anode wire pitch is set equal to  $S=3$  mm and it is multiple to the pad length. Cathode wire pitch is 1.5 mm. The gate grid is placed 3 mm above the cathode wires and its wire pitch is 1.25 mm. Gate grid is used to stop the flow of ions from MWPC to TPC drift volume. To ensure the gas gain at the level of  $G = 10^4$  with moderate anode wire potential, the 20- $\mu\text{m}$  diameter gold-plated tungsten-rhenium anode wire with tension 50 gram is used. The 75- $\mu\text{m}$  diameter copper-beryllium wire wound under an 80-g force is used for the cathode plane. The pad geometry is selected based on the pad response function calculation and measurements to provide the required spatial resolution, and the number of pad rows is determined by the momentum resolution requirement. There are 27 rows of  $5 \times 12$  mm pads in the inner area of the pad plane and 26 rows of pads with dimensions  $5 \times 18$  mm in the outer area. The total number of registration channels of the TPC is 95232. Pad plane is produced by multilayer printed circuit board technology. It has 4 layers: a layer with pads, a layer with a ground plane, a layer with signal routing and a layer with connectors that are 1 mm apart from each other for a parasitic capacity minimization, which together give a total board thickness of 3 mm.

### **2.2.1.3.3. Gas system**

The design of TPC gas system is based on the experience of the gas systems construction for STAR and PHENIX experiments at Brookhaven National Laboratory, USA. The system consists of two recirculation loops: inner and outer. It operates nominally as a closed circuit with the majority of mixture recirculation through the TPC in the inner loop. During normal operation a small amount of fresh mixture is added and an equivalent quantity (including TPC leakage) of the existing mixture is vented with the outer recirculation loop. The gas system can operate in an open configuration for purging the detector.

Gas mixture for the TPC at the correct pressure, temperature and composition are  $(10 \pm 0.1\%)$   $\text{CH}_4$  in Ar at internal TPC pressure  $2 \pm 0.01$  mbar with fresh gas flow 200 – 3 000 l/h.

Structurally, the gas system can operate as in the closed version for a long term experiment as in the opened one for purging of the TPC. Since the distance between the TPC and the gas system location is about 70 meters, the gas scheme contains two

circulating loops: outer – with the compressors and inner – with the blowers. These loops are assembled into two racks as shown in Fig. 2.2.1.19.

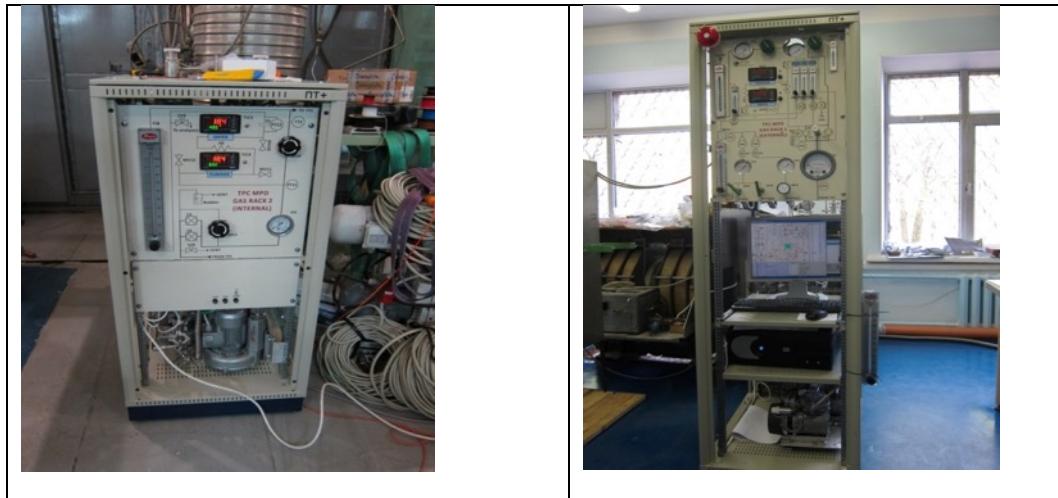


*Fig. 2.2.1.19. Assembled rack 1 and rack 2 for gas system*

#### **2.2.1.3.4. TPC laser calibration system**

Laser calibration system needed to minimize the error in the absolute measurement by the TPC. It takes into account both static and time-depend distortions in the electron drift path and determines drift velocity. The system is based on the two UV 266 nm wavelength lasers with short pulse (5 ns) and pulse power up to 130 mJ. Laser beam splitter provides 224 straight rays to simulate 1 mm diameter tracks – enough to have information about whole TPC volume.

Schematic view of laser beam and technical drawing of 28 “tracks” of 1 mm in diameter calibration system which is under realization presented in Fig. 2.2.1.20 and Fig. 2.2.1.21.

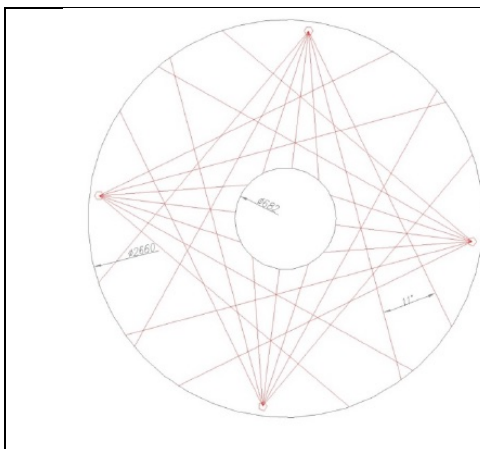


*Fig. 2.2.1.20. Schematic view of laser beam*

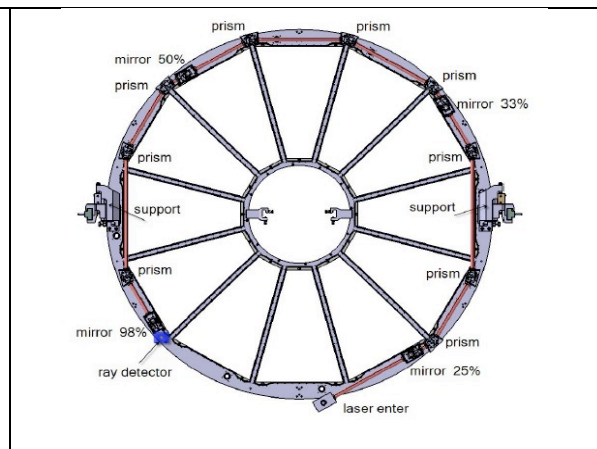


*Fig. 2.2.1.21. Technical drawing into 28 “tracks” of 1 mm in diameter*

### 2.2.1.3.5. Cooling system

Temperature stabilization will include a thermometric system using 180 Pt100 sensors placed on the detector body providing temperature measurements with an accuracy of  $0.1^{\circ}\text{C}$  and a thermal stabilization system (see Fig. 2.2.1.18, pos. 5) using distilled water as a thermal agent. The goal of design is a stability of the gas temperature inside the TPC volume within  $0.5^{\circ}\text{C}$ . TPC barrel thermal screen and the samples of cooling panels are shown in Fig. 2.2.1.22.

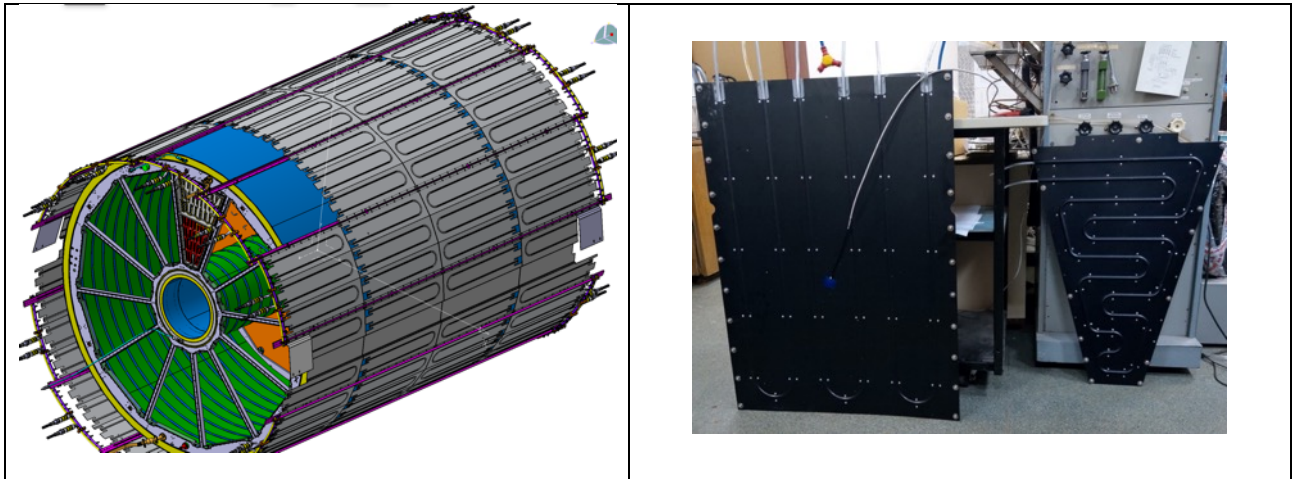


Fig. 2.2.1.22. TPC barrel thermal screen and cooling panels samples

### 2.2.1.3.6. Front-End Electronics (FEE) and data readout system

The TPC FEE is based on ASIC[3], FPGAs and high-speed serial links (see Fig. 2.2.1.23). To protect the FPGA firmware from SEU, standard proprietary methods are suggested.

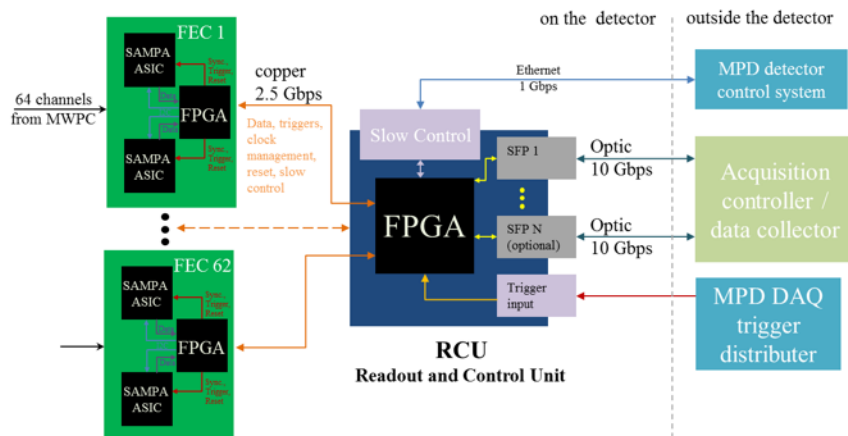
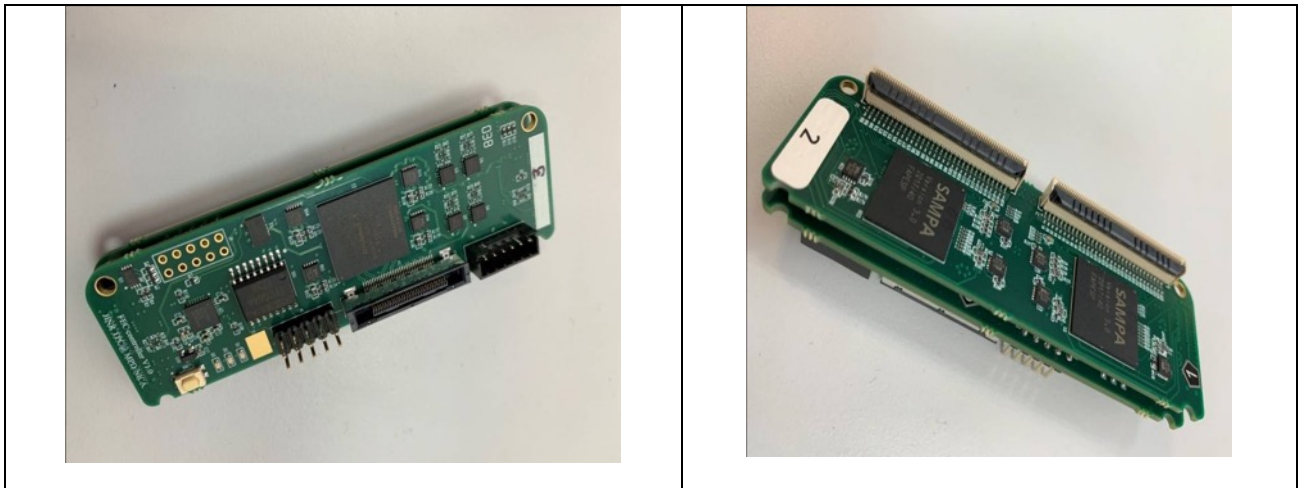


Fig. 2.2.1.23. Block diagram of data readout for one from 24 ROC chamber.

Each of 62 Front-End Cards (FECs), which are the basic elements of the data acquisition system from each ROC are controlled by common Readout and Control Unit (RCU). Each FEC has a separate bidirectional communication interface with the controller (cooper link, up to 2.5 Gbps), which is used for card management, data

receiving, FEC condition monitoring and providing of synchronization, triggering and reset signals (Fig. 2.2.1.24). Each of the 62 FECs operate in parallel and independently of each other, which provide overall system throughput at this level. The base functions of the RCU are the following: FECs management, data receiving from FECs, FECs synchronization, slow control, transfer of data to data collector via the optical interface, communication with the general MPD detector control system via an Ethernet port.



*Fig. 2.2.1.24. FEC for TPC: top view (service side), left and bottom view (to padplane connected side), right.*

Each of the 1488 FECs includes two ASICs called SAMPA which was developed by USP Brazil electronics group mainly for upgrade ALICE experiment at CERN. The SAMPA usage on cards made it possible to significantly reduce FEC size and due to it the radiation length of cards is about 3%  $X/X_0$  (+ about 3% new cooling system). Another significant advantage of the new FEC is their ability to work with both positive and negative polarity of input signals. This feature will be useful in the future with a planned upgrade of ROCs from MWPC to GEM detectors.

Necessity not only to reduce the amount of material at the TPC end-caps, but also to distribute it evenly, has been forced to develop a new card from two boards (Fig. 2.2.1.24). The first board (Fig. 2.2.1.24, right) contains two SAMPA chips giving in total of 64 independent registration channels. The SAMPA amplifies the analog signal from the TPC pads, digitizes it with a 10-bit sampling ADC with a frequency of 10 MHz, processes it when the signal processor is enabled and transmits via serial links.

The second board (see Fig. 2.2.1.24, left) is a FEC controller. It is based on CYCLONE V GX FPGA. The FPGA performs the following main functions: high-speed bidirectional serial interface with the controller (up to 2.5 Gbps), SAMPAs

management and configuration, data receiving from SAMPAs, FEC slow control features.

The first tests of the FECs showed their suitability for usage as TPC electronics. FPGA utilization in the data acquisition system provides us with great opportunities to further improvement of the system. The implementation of the FEC in the form of a double-desk board also gives us additional flexibility in the future upgrade of the system. If necessary, the controller part of the FEC can be replaced with another card, for example, with a flash-based FPGA (if it will be necessary due to radiation hard conditions of electronics operation).

### 2.2.1.3.7. Detector control system (DCS)

The control system of the TPC provides the control and monitoring of the HV power supplies for readout chambers ROC and HV electrode, the LV power supplies for front-end electronics, parameters of gas and cooling systems, laser calibration system operation. CAEN HV and LV equipment control by GECO 2020 software.

### 2.2.1.3.8. HV and LV systems

Block-diagram of TPC LV system based on the CAEN EASY3000 crates and A3100 PS modules (I=100A each) is shown in Fig. 2.2.1.25 (left). Additional custom made LV stabilization and distribution board LVN9 for FE cards designed and manufactured by INP BSU (Minsk) is shown in Fig. 2.2.1.25 (right).

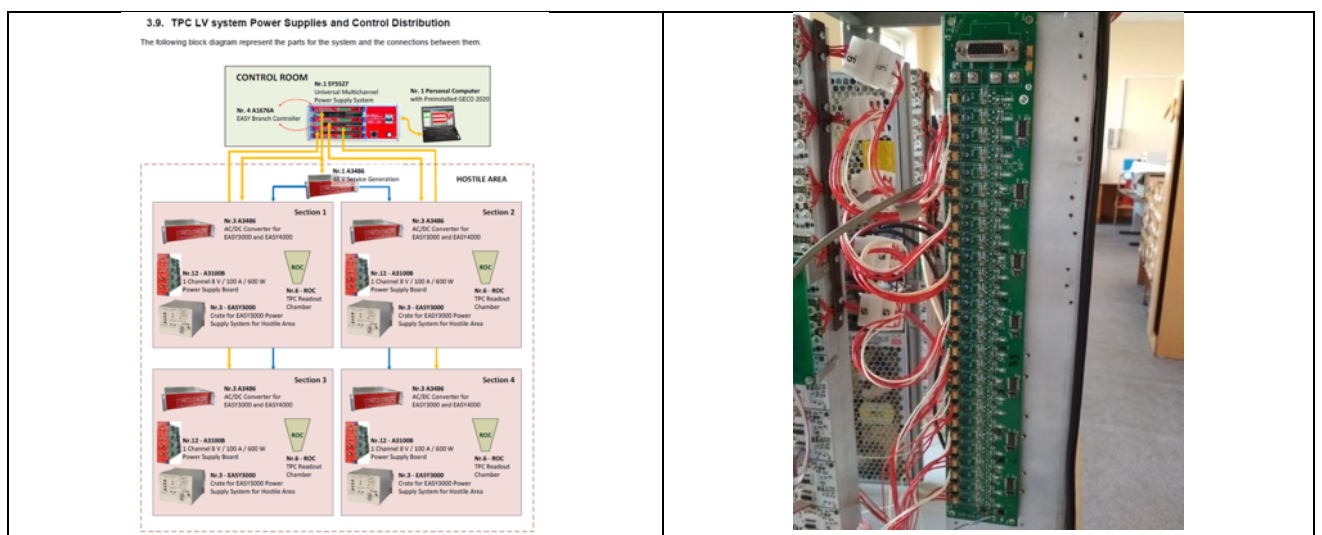


Fig. 2.2.1.25. Scheme of TPC LV system power supplies (left). Stabilization and distribution board LVN9 and control distribution based on CAEN (right).

TPC HV system based on standard CAEN hardware crate SY4527 with modules A7236DN, A7236DP, A1542HDN and software GECO 2020.

### 2.2.1.3.9. TPC assembly and infrastructure

Since the TPC field cage containment cylinders are not differ significantly each form other in size the TPC assembling will be done at horizontal position of each elements. The arrangement for TPC assembling is shown schematically in Fig. 2.2.1.26. The pair of precisely positioned rails placed on at surface, the strong “arm” I-beam with adjustable module, a system of three mobile and a special mobile platform create mechanical structure for step-by-step assembling of the TPC field cage elements.

The special assembly tooling was manufactured at Mechanical and Instrument Engineering Corporation (Bryansk, Russia) and was delivered to LHEP (see Fig. 2.2.1.27).

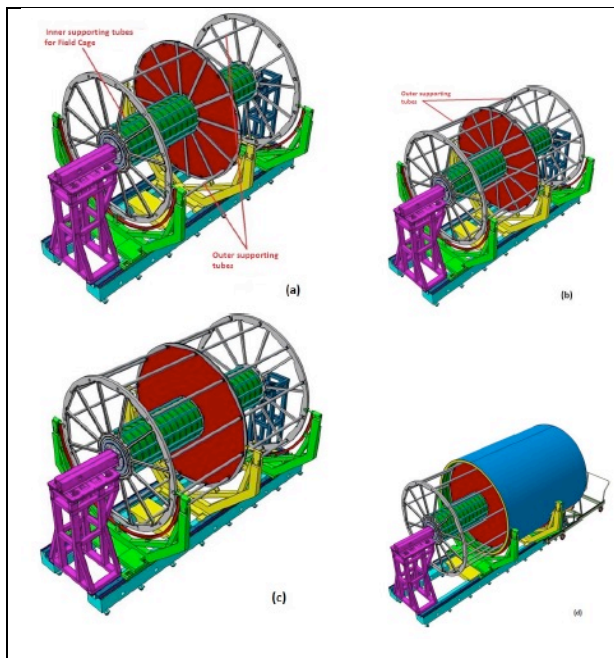


Fig. 2.2.1.26. TPC assembly steps



Fig. 2.2.1.27. Manufactured TPC assembly tooling

TPC assembly hall has been built for TPC assembly and testing. The common view of Bld.217 and general layout of the TPC assembly hall are shown in Fig. 2.2.1.28.



*Fig. 2.2.1.28. Building 217 common view and TPC gas supply system*

The hall has the clean area for the TPC assembling and two rooms for experimental equipment such as gas supply and regeneration system, cooling system, high voltage and the LV power supplies and so on. The clean room has square about 7 m x 12 m = 84 m<sup>2</sup> and air purity class 1000/ISO6 (see Fig. 2.2.1.29).



*Fig. 2.2.1.29. Clean room*

One of the TPC assembly step such as of C3 – C4 cylinders assembly is shown in Fig. 2.2.1.30.

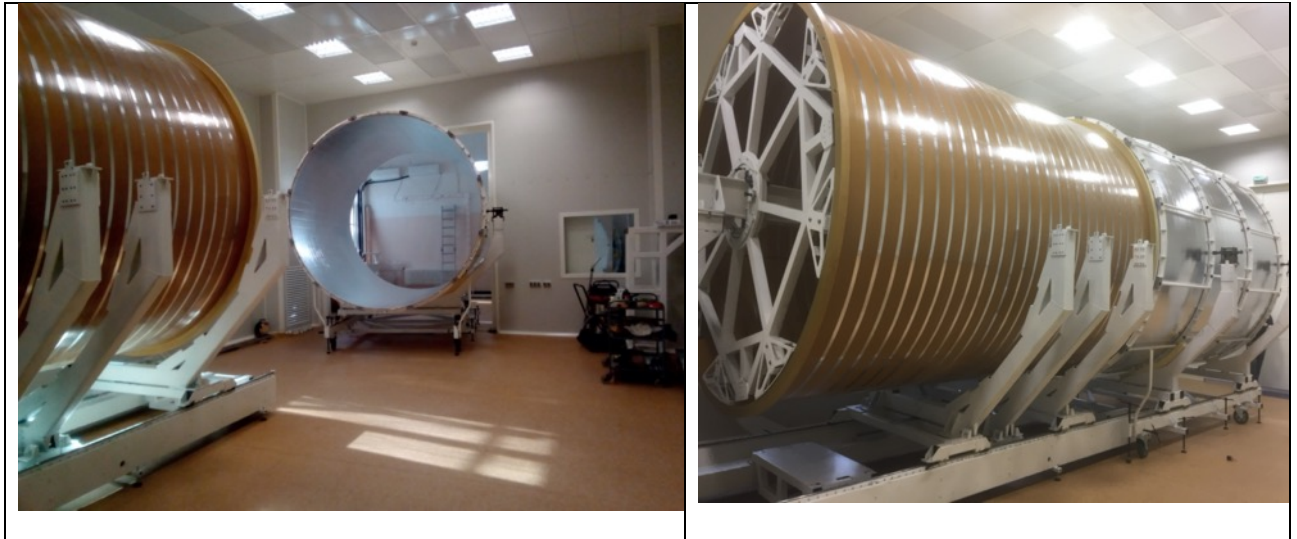


*Fig. 2.2.1.30. TPC C3-C4 cylinders assembly*

The TPC commissioning is planned on the end of 2020 and 2021 years.

#### **2.2.1.4. TOF identification system**

The Time-of-Flight detector is basic charged hadrons identification system of multipurpose detector. In base configuration, the TOF will be represented as a barrel – cylinder length of about 6 meters and diameter of 3 meters assembled of 28 modules (Fig. 2.2.1.32). Each module contains 10 MRPC sub-detectors (Fig. 2.2.1.33). The TOF detector system is organized in a modular way in order to minimize the number of components and cost. In addition to the TOF modules, the system includes the following service subsystems: low and high voltage power supplies, gas system, data acquisition electronics, cooling and slow control. Start configuration of the TOF system should be commissioned in 2020.

##### ***2.2.1.4.1. Multigap resistive plate chambers***

Each TOF module consists of 10 identical multigap resistive plate chambers with 24 readout channels each. Development and testing of MRPC prototypes were performed in period of 2013 – 2017. We tested several different versions of MRPCs with cosmic rays and deuteron beam of Nuclotron. The final version of MRPC made of commercial float glass with a thickness of 280  $\mu\text{m}$ . It has 15 gas gaps and provides time resolution around 50 ps.

During 2017-2018, all materials for the production of such MRPCs were purchased. Before mass production began, we had more than 90% of all necessary materials. Mass production of detector and modules started at the beginning of 2019. At the end of 2019, the production of 120 detectors and 10 modules will be completed. All modules production should be completed in 2020.

From the beginning of 2020, all TOF modules will be tested on cosmic rays stand, which was designed and commissioned especially for this goal in 2019.

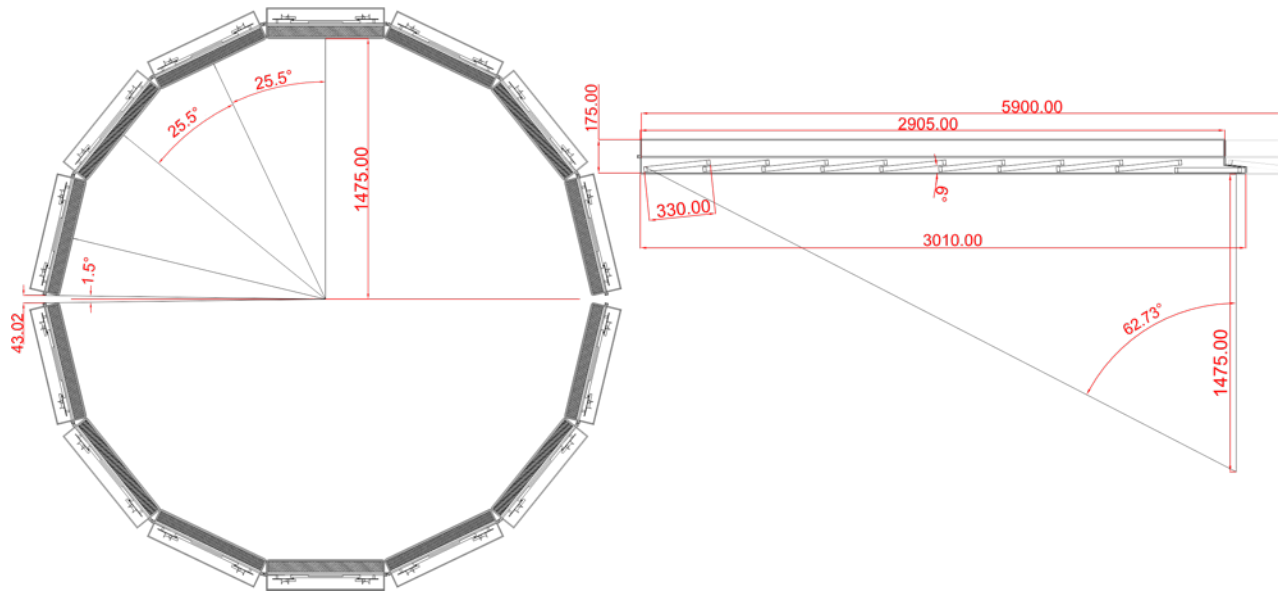


*Fig. 2.2.1.32. Scheme of the TOF system barrel with overall dimensions.*

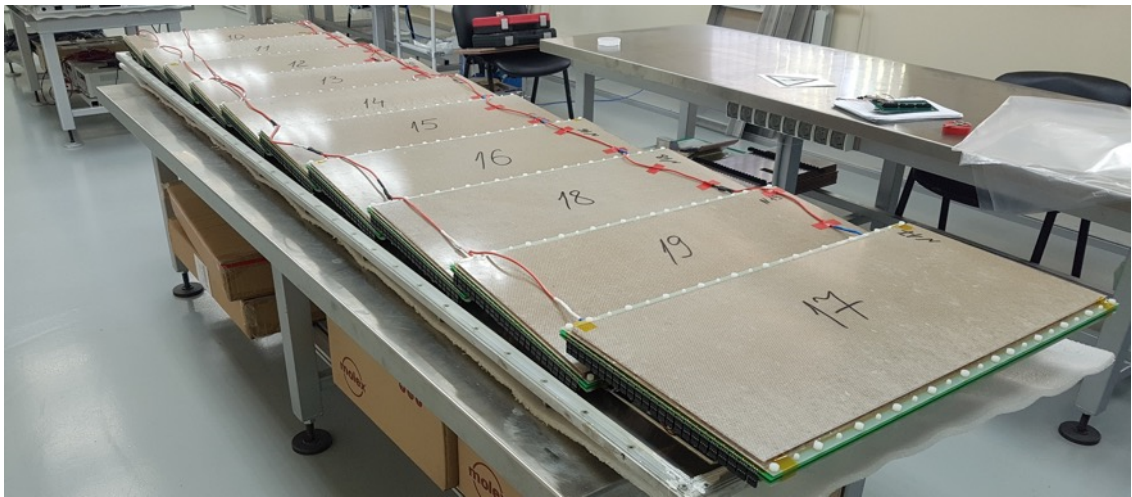


*Fig. 2.2.1.33. Arrangement of MRPC detectors in the TOF module.*

#### **2.2.1.4.2. Front-end electronics**

For the TOF MPD the 24-channel NINO based preamplifier board was developed [3] during 2015 – 2017. This preamplifier board is especially adapted for the two-side strip readout in MRPC at the MPD experiment. Overall dimensions of the preamplifier are 196.5 x 89 mm<sup>2</sup> (Fig. 2.2.1.34). Distinctive features of the MPD TOF preamplifier board are stabilized voltage supply of the NINO, the input

impedance matched to impedance of the MRPC, capacitors at the inputs for two-side strip readout, the threshold remote monitoring and control, and the board and the gas space thermal monitoring.

The production and testing of all necessary (560 pcs) preamplifiers is completed at the end of 2019.

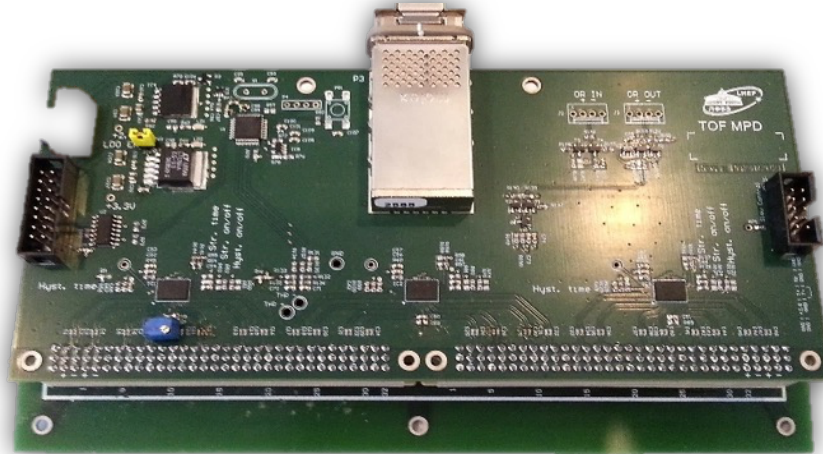


*Fig. 2.2.1.34. 24-channel NINO based preamplifier board with the CXP output connector.*

#### ***2.2.1.4.3. Readout and data acquisition electronics***

New VME64x VXS time-to-digital converter TDC72VHLv4 based on HPTDC chip was designed for MPD TOF and FFD readout. It is used for digitizing LVDS signals coming from the output of the NINO amplifier using cables Molex P/N 11102512xx with connectors Molex 76105-0585. Time sampling of the TDC72VHLv4 is 24.4 ps per bin. The TDC72VHLv4 provides the ability of the precise “White Rabbit” synchronization with other timing devices. The total necessary amount of the TDC for the TOF MPD is 196 (14 modules per each of 14 VME crates).

All VME crates was purchased and delivered in 2017-2019. The TDC72VHLv4 boards are in production from the beginning of 2019. Currently, 51 TDC boards are available and tested. Production, calibration and testing of readout electronics is planned to be completed by mid-2020. Signal cables are delivered un full in 2018.

#### ***2.2.1.4.4. Closed loop gas supply system***

The TOF detectors will be operated with a non-flammable Freon rich gas mixture containing 90% C<sub>2</sub>H<sub>2</sub>F<sub>4</sub> + 5% i-C<sub>4</sub>H<sub>10</sub> + 5% SF<sub>6</sub>. The total gas volume of the barrel is approximately 3000 liters taking into account the volume occupied by detectors. It

was decided to use a closed-circuit gas supply system (Fig. 2.2.1.35), due to large gas volume.

Design and production of the gas system lasted from 2017 to 2019. At the moment, the system is in operation and is used for the TOF test stand on cosmic rays. After checking all the modules by the end of summer 2020, it is planned to transfer the system to building 17 and make minor changes to its design.

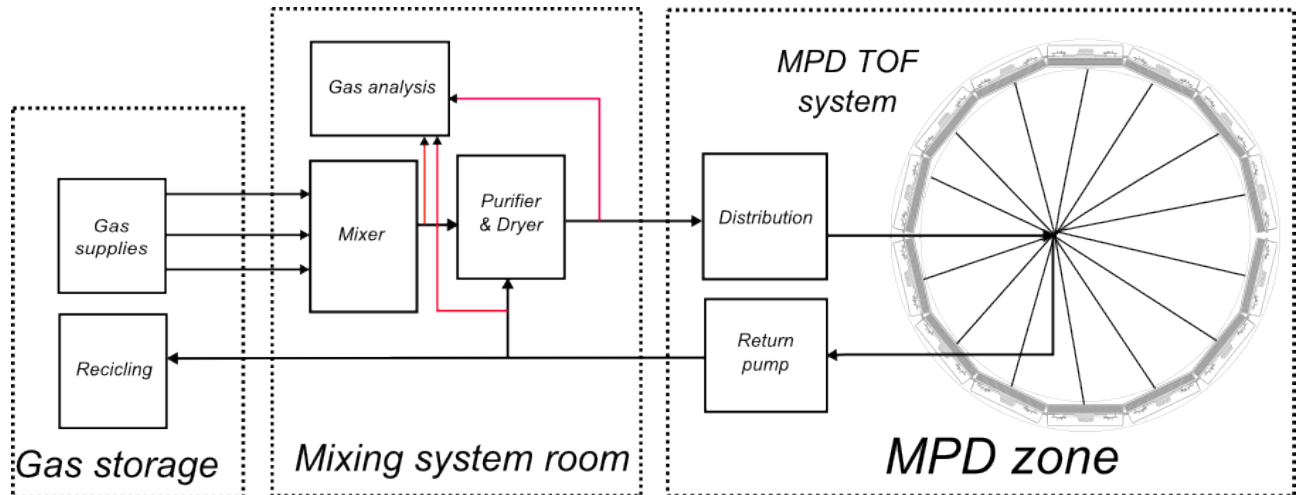


Fig. 2.2.1.35. Schematic view of the proposed TOF closed loop gas distribution system.

#### 2.2.1.4.5. HV & LV power supply

To provide high voltage power to the TOF modules, a high voltage system produced by ISEG and WIENER companies (Germany) is used. It consists of 28 4-channel power supplies iSeg EHS4080p(n) (up to 8 kV and 1 mA) housed in four MPOD crates from WIENER.

8 low voltage supply modules iSeg MPV 8016I are enough to power all preamps of the TOF system. Each iSeg MPV 8016I low voltage module has 8 channels with a maximum power of 50W per channel in different voltage ranges.

The HV and LV system devices was purchased and delivered in 2017 – 2019 in full.

#### 2.2.1.4.6. Slow control system

The Time-of-Flight system of the MPD is necessary to monitor several parameters of different subsystems such as temperature monitoring, voltage and current monitoring, gas flow monitoring, etc. At present, most of the slow control system has been developed and continues to develop. Some of the slow control equipment will be acquired already during the assembly of the TOF in MPD.

The development of the SCS of the TOF is planned to be done in the period 2018 – 2021.

#### **2.2.1.4.7. Cooling system**

Proper cooling of front-end and readout electronics is needed to prevent damages/fire and to satisfy the temperature requirements of the MPD central region (detector surface below 25°C).

The most optimal way of cooling for such heat dissipation is the use of a system based only on radiators and using closed loop of air. In this case, the active substance causes the temperature changes is only air. This option is more acceptable due to the low cost and less possibility of damage to electronics. However, this method does not let to control temperature with good accuracy.

Purchase and production of cooling system have to be done in 2020.

#### **2.2.1.4.8. Integration in MPD**

The installation of the TOF will begin after the finishing of the Ecal installation. Each module will be inserted in their position on both sides of the yoke of magnet. This will be done by means of a mobile support structure. The structure is equipped with adjustable rails of the same kind used inside the MPD barrel. To insert a module into the barrel it is enough to suspend the support structure with the hall crane in front of the chosen services sector and connect the rails together to form a unique sliding line that will allow pushing the module into the right position.

The design of part of integration equipment is finished. The production and assembling of integration devices in the MPD hall should be finished in summer 2020.

#### **2.2.1.5. Detector FFD**

The Fast Forward Detector (FFD) is important part of the MPD facility at the NICA collider [1] and its aim is to provide fast trigger of nucleus – nucleus collisions in center of the MPD setup and T0 pulse for TOF detector. The concept and technical details of the FFD are described in FFD TDR.

The FFD system, shown in Fig. 2.2.1.36, consists of two identical sub-detectors FFD<sub>E</sub> and FFD<sub>W</sub> based on 20 Cherenkov modules each, two units of sub-detector electronics (SDU) processing detector pulses, a trigger vertex electronics unit (VU), readout electronics, a picosecond laser calibration system, HV power supply, a detector control system (DCS), a cable system, a cooling system.

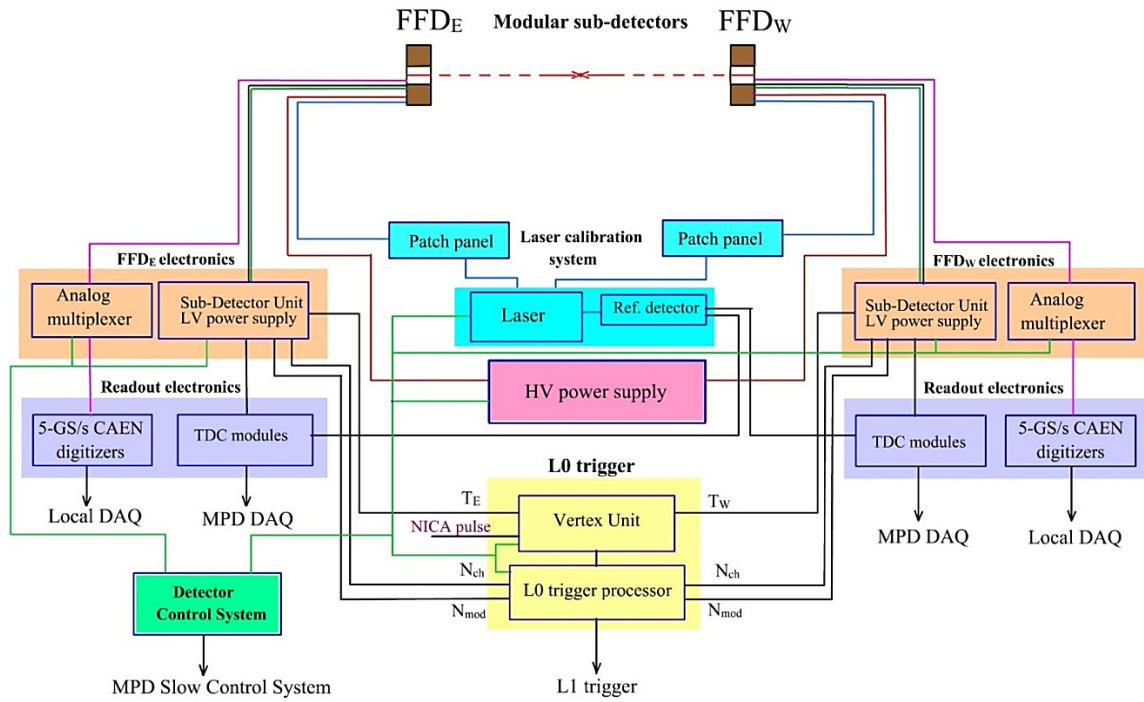


*Fig. 2.2.1.36. A block-diagram scheme of the FFD system.*

### **2.2.1.5.1. FFD sub-detectors**

Each FFD sub-detector consists of 20 identical Cherenkov modules with 100-channel granularity. Each module consists of a 10- mm lead plate converter, four quartz bars of radiator, a photodetector MCP-PMT XP85012/A1, front-end electronics board, HV divider, module housing with connectors and cables.

In period of 2013 – 2017 several different versions of prototypes of FFD modules were developed and tested with LED, cosmic rays, deuteron beam of Nuclotron and in magnetic field up to 0.9 T. As a result of these studies, we define a final choice of quartz radiator dimensions, front-end electronics scheme, a regime of MCP-PMT operation, type and length of cables, and a housing design. A view of the module is shown in Fig. 2.2.1.37.

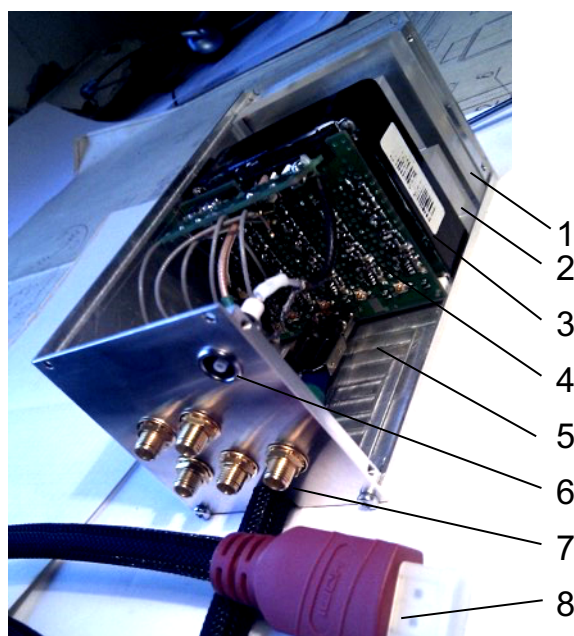


*Fig. 2.2.1.37. A view of FFD module: 1 – the lead plate, 2 – the quartz bars, 3 – MCP-PMT XP85012/A1, 4 – the FEE board, 5 – the module housing, 6 – the HV connector, 7 – the SMA outputs of analog signals, 8 – the HDMI cable.*

The obtained time resolution of individual channel of FFD module with cables and electronics used in MPD is  $\sigma_{\text{FFD}} \approx 44$  ps and it is better than 50 ps required for TOF system. Some results of the test measurements have been reported and published.

All main elements of the modules were purchased and produced including MCP-PMT XP85012/A1 (41 units), quartz radiators (160 units), and lead converters (40 units).

2018 – 2019 is a period of module production. It includes design, production and tests of front-end electronics boards, HV dividers, module housings and cables. Some special mechanical elements of the modules are produced with 3D printer in our group.

A view of sub-detector design is shown in Fig. 2.2.1.38.

2020 is period of assembly of FFD sub-detectors and test measurements with a stand created in 2019 for final tests with cosmic rays. The stand consists of four scintillation planes  $50 \times 50$  cm<sup>2</sup> with silicon photomultiplier readout, lead absorber, trigger electronics and readout electronics. The process of the plane production is shown in Fig. 2.2.1.39.

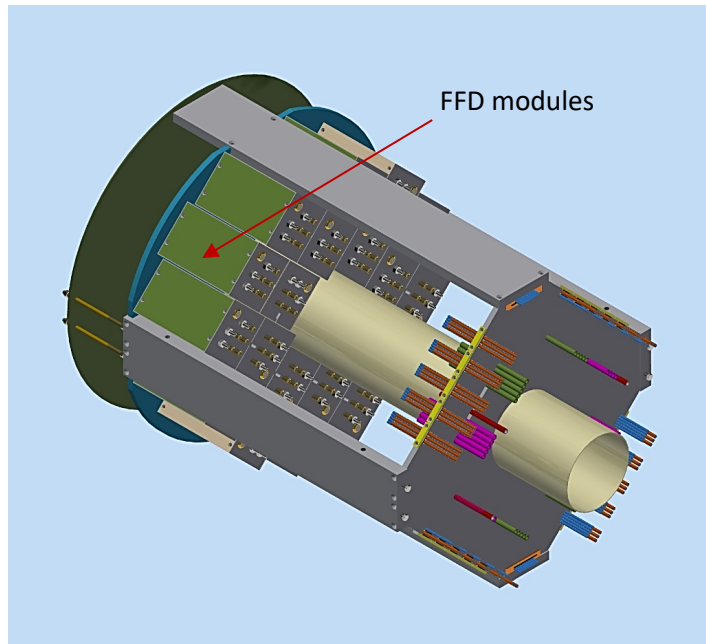


*Fig. 2.2.1.38. Design of the FFD sub-detector*



*Fig. 2.2.1.39. Production of the scintillation planes.*

### **2.2.1.5.2. Sub-detector electronics**

The SDU has a modular structure; it contains a set of modules placed in a VME crate having a custom back-plane. The set of modules includes a LV power supply Module (LVM), a Signal Processing Module (SPM), a Central Processing Module (CPM) and an Interface Module (IM). To provide fast FPGA configuration file downloading each module containing FPGA is equipped with the FPGA Configuration Loading Module (CLM) connected directly to a serial link interface. The backplane contains a parallel bus to control all modules located in the SDU crate using full-duplex multi-drop RS485 serial line and inter-module connections for fast signals and LV power lines between LVM and SPM.

Analog Multiplexer Modules (AMMs) are used for monitoring FFD channel operation. The inputs are connected to individual analog channels and output pulses are fed to digitizers.

Final project of the SDU was developed in 2016 – 2018. This year is period of module prototyping and tests. Also, two VME crate with power supplies were purchased. 2020 is period of module production and final tests.

#### ***2.2.1.5.3. Vertex electronics***

The Vertex Unit (VU) uses preprocessed data coming from the both SDUs (SDUE, SDUW). The VU consists of a Vertex Unit Module (VUM) and an Interface Module located in a VME crate with a custom backplane. Concept of this unit was developed in 2016 – 2018. Production and tests will be made in 2020 – 2021.

#### ***2.2.1.5.4. Readout electronics***

The main readout electronics of FFD is based on TDC72VHL sitting in VME crates of TOF detector. The LVDS pulses are fed from SDUs to TDC inputs using cables Molex P/N 11102512xx with connectors Molex 76105-0585.

The FFD local DAQ, used for FFD regime adjustment and monitoring, is based on 5-GS/s 16-inputs digitizers, CAEN mod. N6742. It consists of 2 NIM crates with 4 digitizer modules in each; optical cables AY2730 and PC optical link CAEN A3818C. All this equipment was purchased and delivered in 2017. Tests of readout electronics with FFD sub-detectors will be done in 2020.

#### ***2.2.1.5.5. Calibration system***

A special system based on PiLas laser with 30-ps pulse width and 405- nm wavelength is used for precision time calibration of FFD channels and monitoring the detector operation. Main parts of the system are a PiLas control unit, a box with laser head and optical system, quartz fiber bundles, patch boxes and optical cables, a reference photodetector with MCP-PMT PP0365G. A view of the elements (besides the optical fiber bundles) is shown in Fig. 2.2.1.40.

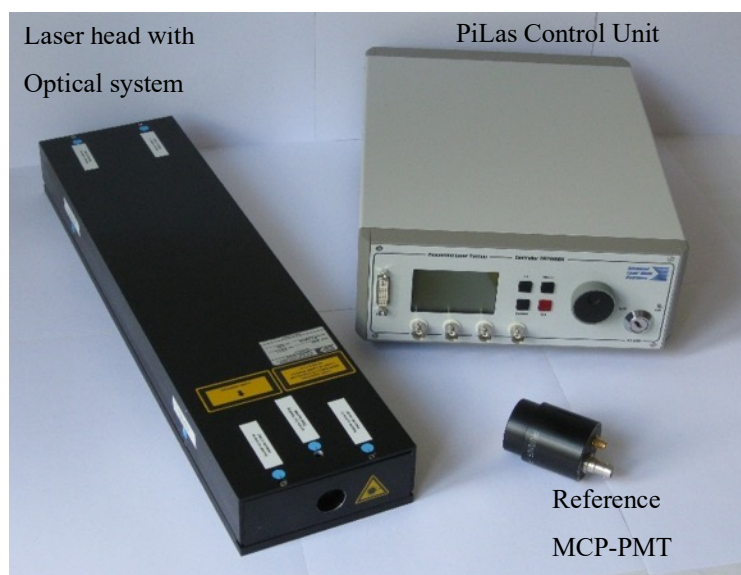


*Fig. 2.2.1.40. A view of the PiLas control unit, the box with laser head and optical system, and the photodetector MCP-PMT PP0365G.*

In period 2013 -2019 all elements of the system were purchased and produced. In 2019 we began test measurements with the laser system and final tests will be done in 2020 with FFD sub-detectors.

#### ***2.2.1.5.6. HV power supply***

To provide HV power to the MCP-PMTs of FFD modules, a high voltage system produced by ISEG and WIENER companies (Germany) is used. It consists of three 16-channel modules with multiple floating grounds and controller module from ISEG which are fixed in Mpod mini crate from WIENER. The HV system was purchased and delivered in 2017. Control software with interface is developed in 2019.

#### ***2.2.1.5.7. Detector control system***

The Detector Control System (DCS) provides the control and monitoring of the HV power supplies for MPC-PMTs, the LV power supplies for frond-end electronics, the FFD module operation, the SDUs and VU logic operation, the laser system operation, the local DAQ for calibration and monitoring of the FFD. Each subsystem has its own low-level server handling communication between a control PC and a subsystem. The server also provides GUIs for subsystem state presentation and for the expert level control and monitoring of subsystem. Development of the DCS will be made in a period 2018 – 2021.

#### ***2.2.1.5.8. Cable system***

Each FFD module is connected by a HDMI cable with the sub-detector electronics unit (SDU), by a HV cable with the HV power supply, by a 50-Ohm coaxial cable with analog multiplexer modules, and by a quartz fiber with fiber bundle of the laser calibration system. Additional cables are needed for connection between the SDUs of both FFD sub-detectors and the main and local readout electronics and the vertex electronics VU. The Detector Control System (DCS) also uses some cables for realization of its functions. The data from the local readout electronics, CAEN mod. N6742 modules, are transferred via optical link to a computer. In period 2013 – 2018 various cables were tested to make a final choice. Since 2019 we start purchase and production of the cables. Also, the test of all the cables is continued.

#### ***2.2.1.5.9. Cooling system***

A special cooling system is required for stabilization of temperature inside FFD modules with a value below  $+30^{\circ}\text{C}$ . The test showed, that a flow of 5 l/min of dry air or nitrogen is enough for this purpose. In 2019 a project of the cooling system is developed with tests of prototypes. Purchase and production of equipment and components have to be done in 2020.

#### ***2.2.1.5.10. Integration in MPD***

The installation of the FFD sub-detectors is made together with silicon detectors of ITS and vacuum tube using a special support cylinder for mechanical hardness. The design is in progress. The location of crates with SDU electronics and optical patch boxes must be close to cable outlets of MPD magnet and to TOF crates. Other FFD crates and equipment are located in a rack on the second floor of MPD overpass. The deadline of production of FFD sub-detectors and all sub-systems is the end of 2020 and 2021 is the period of final tests and installation.

#### **2.2.1.6. Forward Hadron Calorimeter (FHCAL)**

The Forward Hadron Calorimeter (FHCAL) is constructed in the frame of the collaboration between JINR and INR RAS (Moscow). This detector is one of the basic elements of MPD setup and is intended for the measurements of the geometry of heavy ion collisions. The main purpose of the FHCAL is to provide an experimental measurement of a heavy-ion collision centrality (impact parameter) and orientation of its reaction plane. Precise event by-event estimate of these basic observables is crucial for many physics phenomena studies to be performed with the MPD experiment.

FHCAL consists of two identical arms placed upstream and downstream the beam collision point. The modular structure of one FHCAL arm is presented in Fig. 2.2.1.41. Since the heavy fragments escape into beam holes, it is not possible to

discriminate the central and peripheral collisions using only the deposited energies in FHCAL. The subdivision of the calorimeter into two, inner and outer parts (see Fig. 2.2.1.1.), and the calculation of the energy depositions  $E_{in}$  and  $E_{out}$  separately in these calorimeter parts allows the construction of new observable, energy asymmetry:  $A_E = (E_{in} - E_{out}) / (E_{in} + E_{out})$ . Taking the two-dimensional correlation between the energy asymmetry,  $A_E$  and full energy deposition in calorimeter, it is possible to resolve the ambiguity in the centrality determination. The negative and positive parts of  $A_E$  correspond to central and peripheral events, respectively.

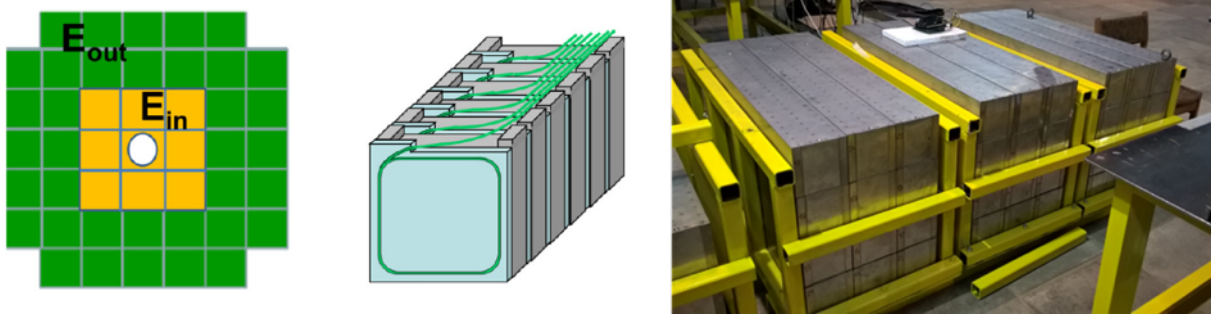


*Fig. 2.2.1.41. Left— Front view of FHCAL structure. It is subdivided into two (inner/outer) parts for the measurements of centrality. Center — structure of the individual module. Right – stack of produced modules ready for delivery to JINR.*

#### **2.2.1.6.1. FHCAL module design**

The FHCAL module transverse sizes of  $15 \times 15 \text{ cm}^2$  were chosen to match the size of the hadron showers. Each FHCAL module includes 42 lead-scintillator sandwiches with a sampling ratio 4:1 (the thickness of lead plates and scintillator tiles is 16 mm and 4 mm, respectively).

Light readout is provided by WLS-fibers embedded in the grooves in the scintillator tiles, this ensures high efficiency and uniformity of the light collection over the scintillator tiles within a few percent. WLS fibers Y-11(200) with double cladding and a 1 mm diameter produced by Kuraray Co. were used for the FHCAL assembling. To avoid the loss of light the bending radius of the WLS fiber must be larger than 5 cm. Spiral grooves in the scintillator tiles provide slightly better parameters than the circular ones, that is why they were selected to design the FHCAL modules. One end of the WLS-fiber inside the scintillator groove is mirrored by silver paint, this improves the light collection by about 30%.

Each scintillator tile is covered with a white reflector (TYVEK paper) to improve light collection. WLS-fibers from each of 6 consecutive scintillator tiles are collected together in the optical connector at the end of the module and polished to improve the optical contact with the photodetector. The longitudinal segmentation in 7 sections requires the same number of optical connectors and compensates the

nonuniformity of the light collection along the module caused by different lengths of the WLS-fibers.

All 42 layers of lead/scintillator sandwiches of the FHCAL module are loaded into the box made of 0.5 mm stainless steel sheet and tied together in one block with a length of about 90 cm (4 nuclear interaction lengths) by a 0.5 mm stainless steel tape. After assemblage the module is covered by another similar stainless steel box and these two up and down boxes are spot-welded providing a mechanically stable construction. The weight of each module is about 200 kg.

Each module of hadron calorimeter consists of 42 lead–scintillator tile sandwiches with the sampling ratio 4 : 1 (thickness of the lead plates and scintillator tiles are 16 and 4 mm, respectively) that satisfies the compensation condition. According to simulation, the sampling fluctuations provide the energy resolution of calorimeter as:  $\sigma_E/E \sim \sqrt{55\%/E}$  (GeV) The beam tests of the calorimeter with the same sampling confirm the results of simulation.

To optimize the light collection efficiency from the scintillators some R&Ds on the groove shapes were performed. Namely, a few types of the scintillator tiles were produced with circular and spiral grooves. The tests of all tiles were performed with  $^{90}\text{Sr}$   $\beta$ -source and trigger counter below the scintillator tile to detect electrons passed through the scintillator. The outer end of WLS fiber was glued into special optical connector that was viewed by Hamamatsu MPPC. The measurements of the light amplitude were done with the step of 2 cm along the diagonal of the scintillator. The results of measurements are shown in Fig. 2.2.1.42. One can see that both circular and spiral grooves give similar results with the light yield of about 20 photoelectrons with 5% average space nonuniformity in the light collection. The spiral groove provides slightly better parameters and have been selected for the design of FHCAL modules. The tiles are wrapped in reflector TYVEC.

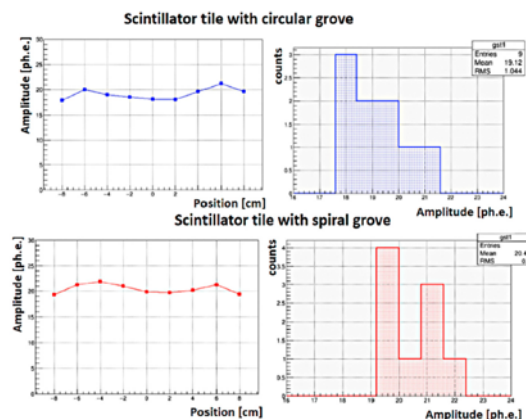


*Fig. 2.2.1.42. The light yield along the diagonal of scintillators with different types of the groves. TYVEC reflector was used for the measurements.*

### **2.2.1.6.2. Readout of the FHCAL modules**

The longitudinal segmentation of the calorimeter modules requires 7 compact photodetectors coupled to the optical connectors at the rear side of the module. The use of silicon photo- multipliers, SiPMs, is an optimum choice due to their remarkable properties such as high internal gain, compactness, low cost and immunity to magnetic fields. SiPMs have no nuclear counter effect due to their pixel structure. Hamamatsu MPPC S12572-010C/P with a pixel size of  $10 \times 10 \text{ mm}^2$  were selected to ensure a high dynamic range of detected energies. The Front-End-Electronics (FEE) used for the MPPC readout includes an amplifier and a shaper with differential output signals. Due to the shaper, the signal length is about  $0.2 \mu\text{s}$  which is a few times longer than the original signal width after the photodetectors. The necessity of a longer signal is related to the relatively low sampling frequency of the pipe-line ADC that digitizes the signal waveform. At present, a 64-channel 62.5 MS/s ADC64s2 board manufactured by the Dubna company AFI Electronics is used. The described readout scheme was used in beam tests of the FHCAL modules at low proton energies.

### **2.2.1.6.3. FHCAL energy calibration**

The individual calibration of longitudinal sections is essential for the monitoring of the light yield behavior. After module assembling, the light yield of all longitudinal sections was measured by using cosmic muons crossing all 7 sections in a module (Fig. 2.2.1.43 (a)). Unfortunately, the statistics of such horizontal muons is very pure that requires a few days of data acquisition. Therefore, other types of muons tracks passed through two or three neighbor sections were considered. The double or triple signal coincidences allow the reliable identification of muon tracks in the presence of electronic noises compared with the muon signal in a single section.

Fig. 2.2.1.43 (b) shows the light outputs for all sections of one of the modules. One can see a higher light yield for the last section, where the length of the WLS-fibers is the shortest. The observed dependence is a simple reflection of the light attenuation during the transportation in WLS-fibers. As seen, muons deposit about 40 photoelectrons/section making it possible to calibrate the energy scale of FHCAL modules during calorimeter operation in MPD setup.

At present, all 90 FHCAL modules are assembled at INR (Moscow) and are ready for the delivery to JINR, see Fig. 2.2.1.41. right. A few spare modules are in production now.

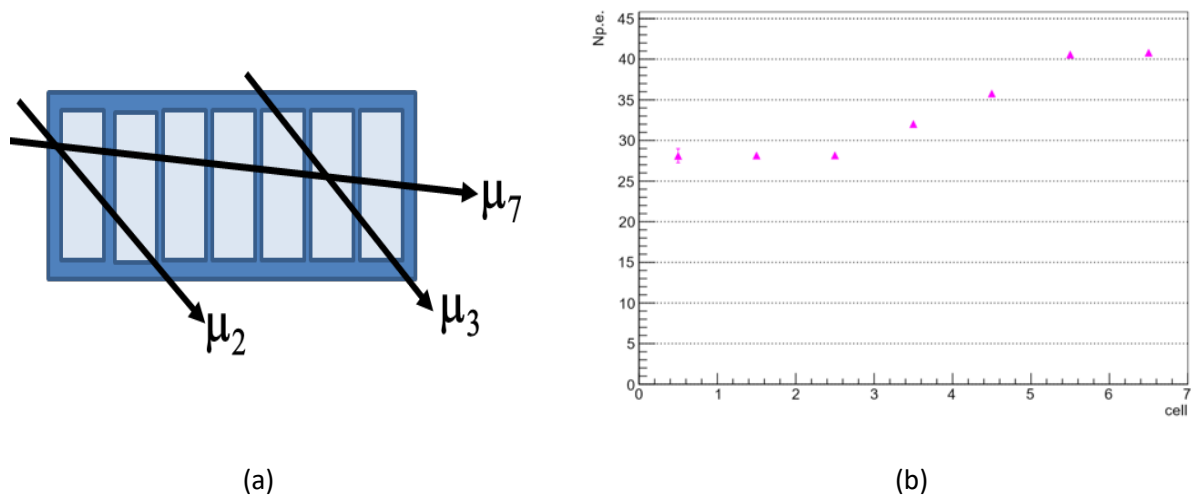


Fig. 2.2.1.43. (a) – scheme muon tracks selected for the tests. Lower index denotes the number of sections passed by muons. (b)–light output in each of longitudinal section for one of modules.

### 2.2.1.7. Ecal detector

The main goals of the calorimeter are the participation in particles identification (namely – final cleaning of the selected e<sup>+</sup>- sample) and measurements of the photons flux as well as reconstruction of some decays with participation of the photons. The final result depends on performances of other MPD detectors like TPC and TOF.

#### 2.2.1.7.1. Ecal design

Large-sized (6-meters-long and 4.5-meters in diameter) electromagnetic barrel calorimeter (Ecal) is an important part of the Multy-Purpose Detector (MPD) at heavy-ion NICA collider that covers the central pseudorapidity region of  $|\eta| < 1.2$  (Fig. 2.2.1.44). Ecal is optimized to provide precise spatial and energy measurements for photons and electrons in the energy range from about 40 MeV to 2-3 GeV. To deal with a high multiplicity of secondary particles from Au-Au reaction, Ecal has a fine segmentation and consists of 38 400 cells –“towers”, (Fig. 2.2.1.45). Taking all requirements (high energy resolution, large enough distance to the vertex, small Moliere radius, ability to work in the high magnetic field, high time resolution, resistance to radiation, and reasonable price) into consideration, a “121exed121et”-type electromagnetic calorimeter was selected. Each “tower” has a sandwich structure of 210 polystyrene scintillator and 210 lead plates with 16 Wave Length Shifting (WLS) fibers that penetrate the plates to collect the scintillation light; the thickness of each scintillator plate is 1.5 mm, and the thickness of lead plate is 0.3 mm (Fig. 2.2.1.45).

Design of the Ecal was done on the basis of many MC studies that were performed during last years. As the result of MC studies, a decision was taken to build the calorimeter with the projective geometry (Fig. 2.2.1.46) which is more complicated to construct than the simple structure that was planned in the beginning of Ecal project (in the 2014). The main advantage of the new design is reduction of dead zones, increase of detector efficiency, improvement of linearity and energy resolution of the calorimeter measurements in conditions of high multiplicity of secondary particles from collisions of heavy ions. In the same time, the new design of the calorimeter is more complicated and demands more engineering efforts. Calorimeter modules production become more complex and time-consuming, and requires more manpower. The above-mentioned problems resulted in some delay in the preparation of the mass production of the calorimeter modules.

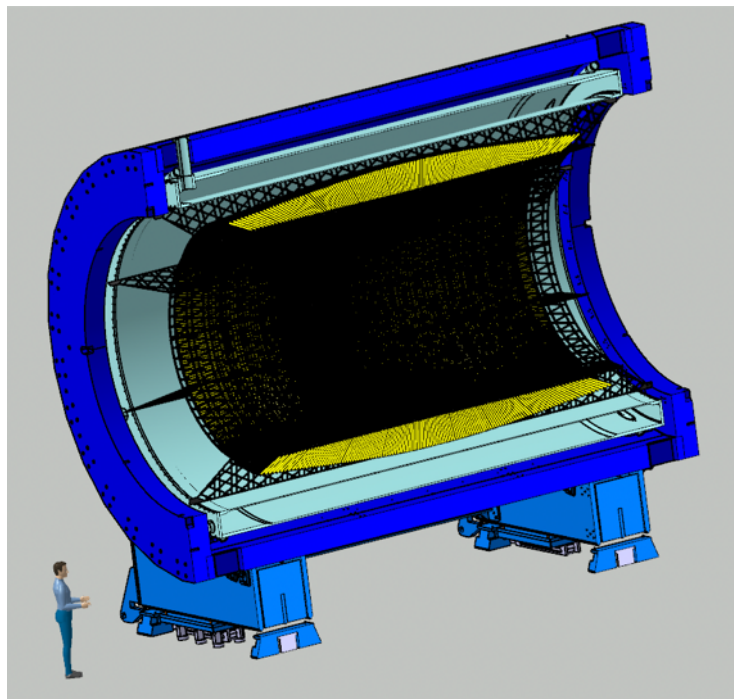


*Fig. 2.2.1.44. View of the Ecal inside of the Solenoid*

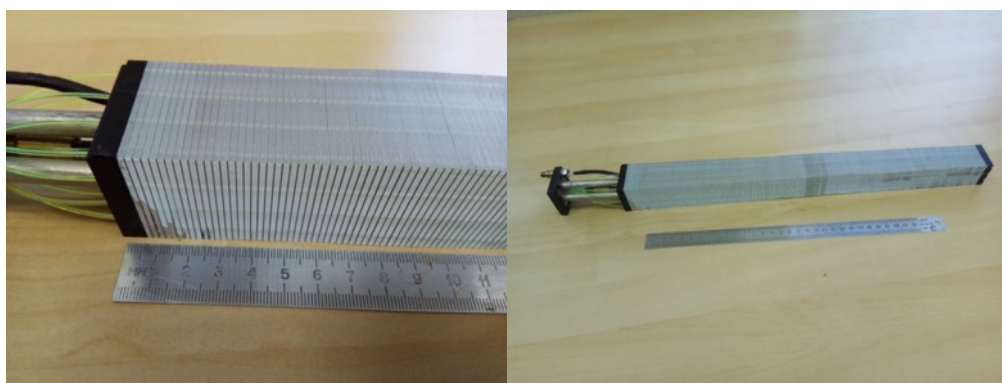


*Fig. 2.2.1.45. Photo of the tower for Ecal*



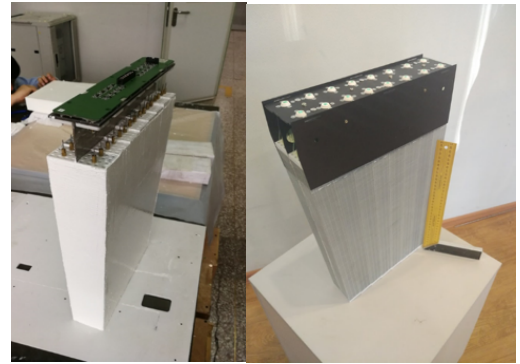


Fig. 2.2.1.47. Prototype modules. On the bottom-left panel, the readout electronics board is shown.

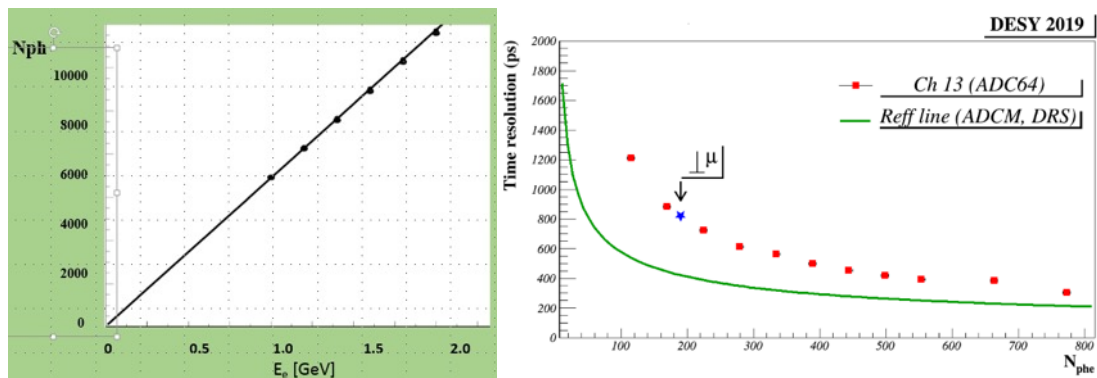


Fig. 2.2.1.48. Linearity of the light output (left panel) and the time resolution (right panel) of the Ecal module prototype. Results from the prototype modules tests with electron beam and cosmics.

Now, all engineering documentation for the mass production of the eight types of the calorimeter modules is completed and sent to the manufacturers of Ecal modules. Two companies (Polypak in Dubna and Uniplast in Vladimir) produced 10 million scintillation plates that is 100% of the total Ecal need. Polypak produced a complete set of tightening covers for module towers and crowns (to form output windows of WLS fibers) to cover the total Ecal need. WLS fibers to cover Russian quota of the modules production were purchased from Kuraray company. A glue-paint for gluing the towers into the modules was developed, and its production is managed. A technology for reflective coating application on lead plates was developed and adopted by two companies.

Russian quota of modules production (25%) should be completed in one year (viz., in the middle of 2020). The production of remaining modules in China cannot be finished before the end of 2020.

Geometrically, Ecal is organized into 25 sectors or 50 half-sectors. Each half-sector (Fig. 2.2.1.49) contains 48 modules (of 8 different types) that are glued into a fiberglass container (basket) as well as correspondent readout and slow-control electronics with total mass of about 1.5 ton. Model calculations demonstrate that the

cell structure of the basket with 2-mm-thick walls provides enough strength and rigidity to keep all possible deformations of the half-sector under its own weight under 0.5 mm for all possible orientations of half-sector in space. At the moment, a contract of production of 52 baskets is in the stage of final signing; we expect that 16 baskets will be delivered to JINR by October 2020, and whole number of baskets is expected to be delivered by Summer 2021.

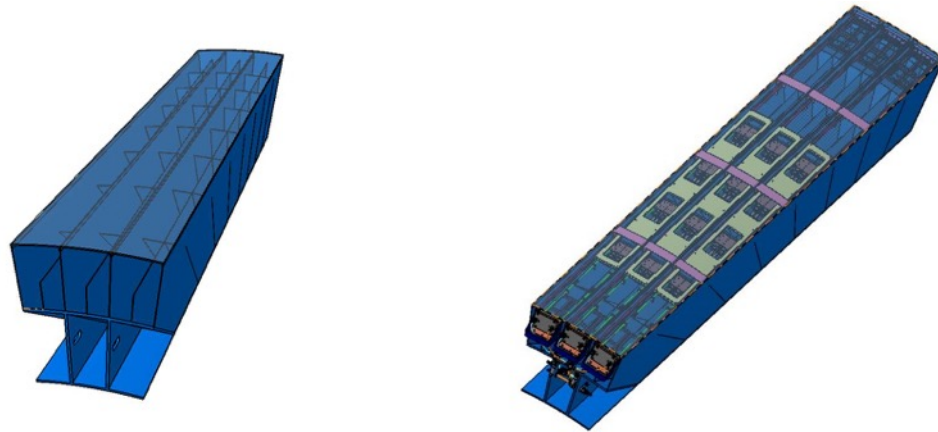


*Fig. 2.2.1.49. Ecal basket (left panel). Right panel shows the basket with installed readout electronics.*

#### **2.2.1.7.2. FE electronics**

Front-End (FE) electronics will be located directly on the calorimeter. This solution is chosen due to the listed bellow advantages:

- small path of analog signal to FE means less signal distortion and pickup noises;
- much simpler transport of digital signal from the calorimeter to the event building electronics; number of connectors between FE boards and electronics outside detector falls from 1536 (number of channels per sectors) in case of analog signal transport falls to 24 (number of channels per sector / number of channels in ADC board (64)) in case of digital signal transport. In the latter case we use very thin optical cable;
- very high event read out rate can be reached by using zero suppression and even signal processing directly on the FE board;
- one disadvantage of this solution is the need to extract the heat from the FE electronics out of MPD detector.

As a FE electronics unit we have designed and constructed ADC 64 channel board (Fig. 2.2.1.50).

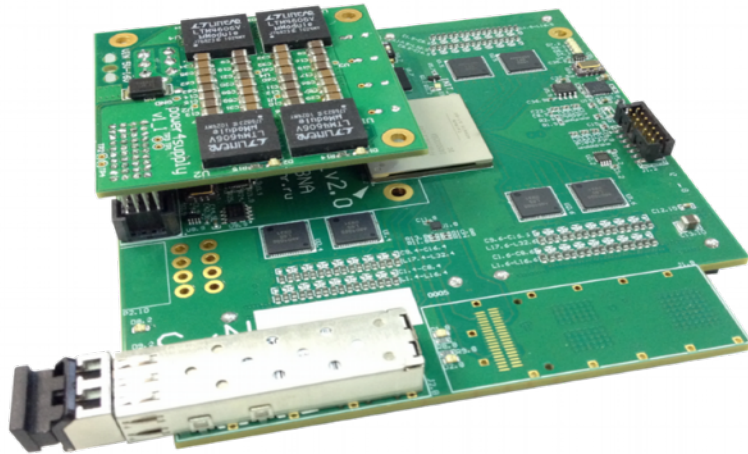


*Fig. 2.2.1.50. ADC64s2 – Front-End board with ADCs amplifiers and Ethernet communicator.*

ADC board is a waveform digitizer. It quantizes analogue input signal and samples it at fixed time intervals. Zero suppression logic is based on baseline estimation and threshold value. Signal shaping is performed in digital form with FIR filters. It allows to reduce the number of waveform points required for digital signal representation with minimum loss of accuracy. The ring type memory allows the read back of last 30  $\mu$ s of waveforms. It sets the limit on trigger latency to this value.

ADC board allows to be integrated to the White Rabbit system. White Rabbit provides sub- nanosecond accuracy and picoseconds precision of synchronization for large distributed systems.

### **2.2.1.7.3. Ecal integration**

Originally, the electromagnetic calorimeter was planned as a self-supporting structure, where each sector contributes as a power element to the whole structure. But after splitting of the Ecal modules production between Russian and Chinese sites (with different time schedules), ability to install and re-install calorimeter sectors (half-sectors) without whole calorimeter and MPD dismantle was requested. To meet this demand, we plan to use special support frame (about 8-meters-long and about 4.5-meters in diameter) made of carbon-fiber composite material that can hold whole load from MPD detectors without support from Ecal sectors (Fig. 2.2.1.51). This frame will consist of inner (20-mm-thick) and outer (15-mm-thick) cylindrical shells with 25 bulkheads (10-mm-thick) in between them to form 25 cells for calorimeter sectors installation. Rigidity calculations for the simplified frame model were performed and demonstrates that the planned total load of 120 tons will cause maximum frame deformations of about 2-3 mm that meets our demand to have deformations below 5 mm to keep ability of installation and re-installation of Ecal half-sectors. Strength calculations assures the frame ability to hold the load about 10

times higher than our maximal expectations, and durability calculations and tests assures 15-year frame operation. At the moment, a contract of the frame design and production is in the stage of final signing; we expect the frame delivery to JINR by the November 2020.

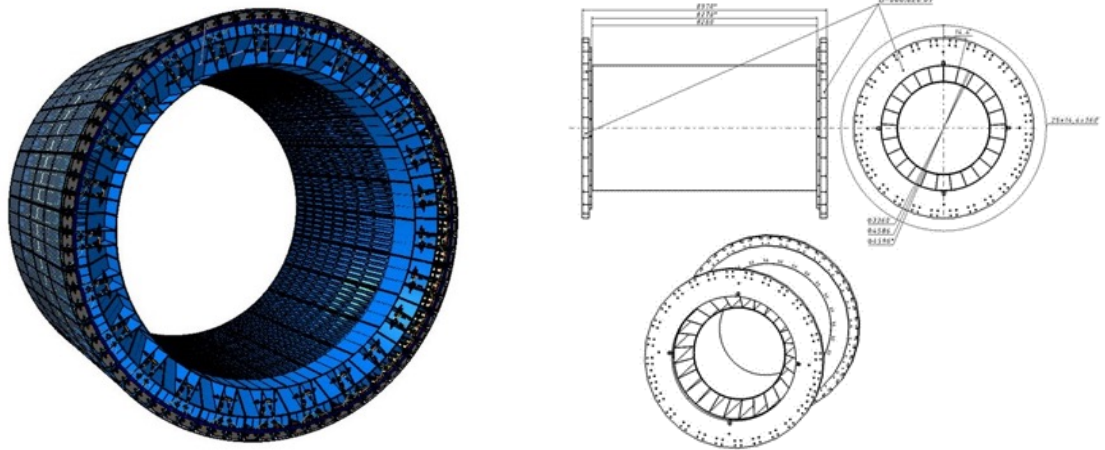


*Fig. 2.2.1.51. The power frame of MPD. On the left panel, installed half-sectors are shown. The drawing on the right panel shows the frame fastening on the magnet support rings.*

Readout and slow-control electronics have been developed at JINR. Prototype modules were produced and tested. Mass production of electronics will start in following months to be completed to the time of the calorimeter assembling in the second half of 2020. Production is distributed among Russian (readout electronics) and Chinese (slow control and preamplifiers) companies. Now, big efforts of the Ecal group are concentrated on the development of an innovative system for installation and replacements of the calorimeter electronics without the calorimeter dismantle. In this system, all heating parts of electronics are located inside the cooling boxes with ventilation, preamplifier boards with SiPMs outside the boxes use them as support structures, and these three-meters-long boxes are mounted on the rails in the half-sectors and can be moved in and out the calorimeter. Most complicated engineering problem in this design is to match reliably and with high precision (better than 0.5 mm) output windows of WLS bundles on the calorimeter modules with correspondent SiPMs on the preamplifier boards. Prototype of moving box with precise positioning for electronics is under test now at JINR. Water cooling system for the Ecal electronics is designed and under expertise of the MPD electronics group.

#### 2.2.1.7.4. *Test infrastructure for mass production*

In order to make a quality assurance of the produced modules and to perform a first-order calibration of the detectors, special stand (Fig. 2.2.1.52) has been developed to test simultaneously 12 Ecal modules in one load with cosmic muons. By the end of Winter 2020, we plan to have 8 such stands (for 8 different types of modules) in operation with total productivity of 96 modules (or 2 half-sectors) per every 2 weeks; that will allow us to test all Ecal modules throughout one year.



*Fig. 2.2.1.52. Prototype stand to test simultaneously 12 Ecal modules in one load with cosmic muons.*

MC study of the calorimeter is going on to find a possible influence of detector-dependent effects on the physics under study. Effect from the not-completely-projective geometry of the calorimeter is discovered and method of its correction is proposed.

#### 2.2.1.8. **The Inner Tracking System ITS**

The Inner Tracking System (*the ITS*) had been always considered as an important subsystem of the MPD which, however, due to its technical complexity and large cost could not have been included in the list the MPD sub-systems of the basic configuration. Such shaky status of the MPD ITS lasted until the moment the Protocol # 134 between CERN and JINR stating the legal terms for transaction of CERN developed novel technology and the know-how for building the MPD-ITS on the basis of Monolithic Active Sensors (*the MAPS*) ALPIDE was signed in 2018. This document laid a clear road towards the MPD ITS, probably, to be the most technologically sophisticated among all the detector systems being built at JINR.

The Multi-Purpose Detector (*the MPD*) is being constructed to study the properties of extremely dense nuclear matter formed in relativistic nucleus-nucleus collisions at NICA energies. The yields of strange and charmed particles are the important observables sensitive to critical phenomena in phase transitions of the QGP-matter at high net-baryon density. Highly efficient registration of such short-lived products of nuclear interactions using a vertex silicon detector will play a key role in the analysis of the possible onset of deconfinement enforced by fluctuations of dense nuclear matter under critical conditions. Without the MPD ITS studies of processes within the charmed sector are impossible.

The conceptional layout of the MPD ITS (Fig. 2.2.1.53) repeats the one used by the ALICE ITS2 but with number of layers of the ALIDE sensors reduced from seven (ALICE ITS2) to five (MPD ITS) due to much smaller diameter of the bore of the MPD TPC (500 mm). The MPD ITS will consist of two barrels with layers of different thickness and quite different construction of the support/cooling structure of the Outer (OB) and the Inner (IB) barrels.

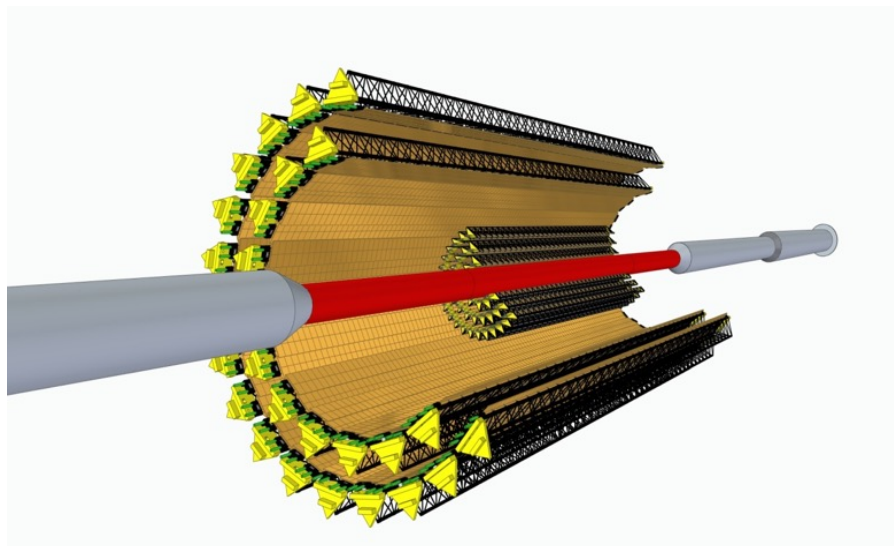


*Fig. 2.2.1.53. The conceptional layout of the ITS around a thin-wall MPD beam pipe*

The IB barrel comprises three most thin layers of MAPS. The design of the IB is proposed to be a subject of CERN and JINR joint R@D effort scheduled for 2020 - 2023. The expected thickness of these layers is 50  $\mu\text{m}$  of Si equivalent.

It is well known that two basic parameters i.e. the distance from the interaction point to the first layer and the thicknesses of the first three layers of tracker determine the ability of tracker to resolve secondary vertices of the decaying charmed particles. The smaller these parameters are the higher the resolution of the decay vertex from the primary one.

The requirement for reduction of the beampipe diameter contradicts the collider designers' natural wish to operate during the commissioning of the NICA with beampipes of increased diameter. This allows them more easily to tune a new machine. After a long series of debates a compromise was found between the MPD ITS and NICA accelerator contradictory work plans. The joint plan put forward was as follows for the MPD ITS:

- installation of the OB only with the beampipe of 64 mm diameter in 2022-2023;
- exchange of the beampipe to smaller diameter after the collider tuning time will be over (2024-2025);
- adding of the IB to the existing configuration with the beampipe of reduced diameter start of the experiments with charmed probes in 2025.

#### **2.2.1.9. The MPD thin-wall beampipe**

One of the most critical elements of the NICA MPD project is nine meters long thin-wall UHV compatible beampipe depicted in Fig. 2.2.1.54. This is more a sketch drawing and not something negotiated to the final product with industries. Manufacturing of the MPD beampipe is a very complex and very risky task for the MPD which can easily turn out to be a stopper of the whole project since RF industry had never produced similar objects before.

The LHC experiments gained enough experience in design and production of similar unique pipes the outer rare parts of which are made of aluminum while the central part of beryllium. The typical minimal wall thickness reached so far is 800 um both for beryllium and aluminum parts.

There is only one company at the moment which produces such unique products. This is the Materion situated in the USA. Due to policy of sanctions NICA is not able to order such beampipes from Materion and is currently developing technology for production of such beampipes elsewhere. Russian industry is capable of production of beryllium part of the beam pipe but meets technological challenge for production of the aluminum parts of required thickness and, especially, in assembly of all parts together UHV tight. German industry heavily involved in the EXFEL project at DESY has built thin wall aluminum beam pipes of relatively small dimensions. We are proposing our German partners to develop jointly in Germany and Russia technology further and build a beam pipe for the MPD. An item to develop jointly such beampipe with Germany is included in the list of GSI-NICA in-kind cooperation plan which is now being considered.

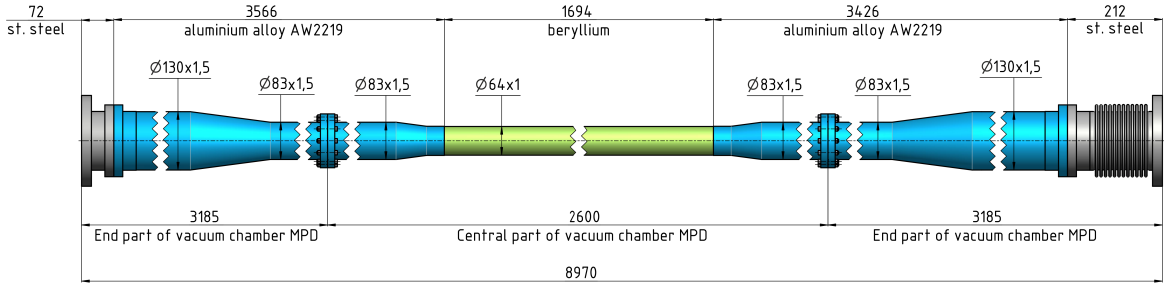


*Fig. 2.2.1.54. A tentative design of the MPD beam pipe. Absent is any indication of the vacuum equipment at the rare ends of the beampipe. According to the integration scenario the beampipe is baked at the vacuum stand and filled in with dry Neon and only then is shipped to the assembly stand c/o the MPD ITS team.*

### **2.2.1.10. MPD Data Acquisition (DAQ) system and computer cluster**

The core function of the DAQ system is realization of data transfer from the detector to the storage system. It includes the data flow from readout electronics to the First Level Processor (FLP) fabric, to the Event Building (EB), High Level Trigger (HLT) and to the Storage System. Main DAQ components are data transfer networks, data processing servers, online storage system, software packages, network communication protocols and data formats. Readout electronics interface, Clock and time synchronization (Timing) System, Trigger System are also included in MPD DAQ system.

#### **2.2.1.10.1. DAQ Electronics**

TDC Based Readout used for TOF and FFD subdetectors of MPD. Both subdetectors use similar DAQ architecture – CRU16 as Local Trigger Units (LTU) for trigger distribution and VXS crates for installing Detector Readout Electronics (DRE) – TTVXS and TDC72VHL modules (Fig. 2.2.1.55). In each VXS crate will be installed one TTVXS module.

There are total of 14 VXS Crates planned for TOF DAQ. In each crate will be installed 1 TTVXS module and 14 TDC72VHL modules. TTVXS module is a Time and Trigger Unit (TTU). It receives trigger information from its LTU, synchronization from Clock and Timing Network (White Rabbit Network) and controlled via Front-End Control Network. Inside VXS crate TTU distribute trigger and synchronous clock to DREs (TDC72VHL). DREs sends busy signals in reply to trigger back to TTU. Also, TTU monitors status of every DRE (voltages, temperature and etc). TTU and DRE sends data via 1Gb Ethernet, 1 link per module.

FFD DAQ is similar to TOF DAQ, but it uses 2 VXS crates and 5 DREs (TDC72VHL) per crate.

TTVXS is a Time and Trigger Unit (TTU) for VXS crate. It distributes trigger information and system synchronous clock to installed payload modules. Also, TTVXS module collects busy information from all payload modules. Connection topology is star. TTVXS and each payload module connects with 1 serial bidirectional link with speed up to 2.5 Gb/s, 1 bidirectional LVDS link, 1 LVDS link for transmitting and 1 LVDS link for receiving. All LVDS links speed is up to 125 Mb/s.

TTVXS has SMBus link to all payload modules for monitoring its status. TTVXS can transmit this information via Ethernet 10/100M.

TTVXS has 4 SFP+ connections for receiving synchronization and receiving trigger information from corresponding networks and send event data to data readout network. Connections speed can be up to 10 Gb/s. This module has 6 programmable input-output LVTTTL coaxial connectors. Functions of this connection is not fully defined yet and it is subject to discuss.

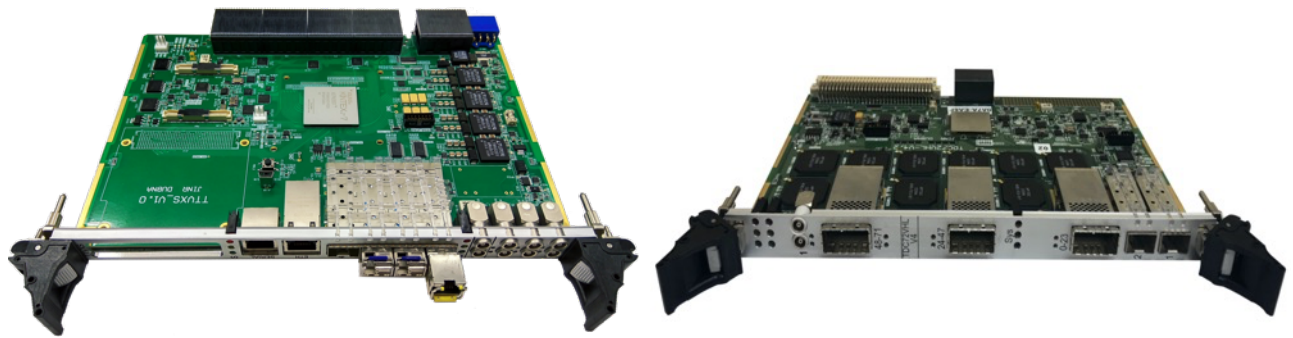


*Fig 2.2.1.55. TTVXS (left) and TDC72VHL (right) modules*

TDC DRE board performs time-stamping of discrete signals (hits) with typical accuracy of 20 ps. It is based on HPTDC chip. Hit timestamps are kept for 104  $\mu$ s in ring type memory. The total trigger latency should not exceed this value.

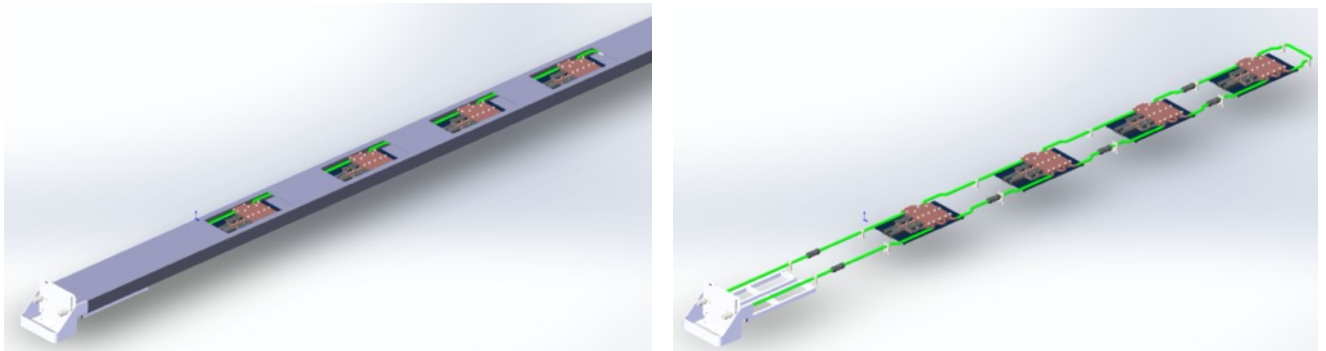
120 TDC72VHL modules and 4 TTVXS modules will be produced and tested till the end of 2019 year for MPD TOF testing stand. 80 TDC72VHL modules and 16 TTVXS modules will be produced in 2020.

ADC DRE board is a waveform digitizer. It quantizes analogue input signal and samples it at fixed time intervals. Zero suppression logic is based on baseline estimation and threshold value. Signal shaping is performed in digital form with FIR filters. It allows to reduce the number of waveform points required for digital signal representation with minimum loss of accuracy. The ring type memory allows the read back of last 30  $\mu$ s of waveforms. It sets the limit on trigger latency to this value.

ADC64Ecal electronic module designed for digitizing signal from Ecal and FHCAL detectors. It's a 64-channels 14bit 62.5 Msps waveform digitizer with Digital Signal

Processing core. Every module has 2 optical links (primary and reserve) for time synchronization, trigger distribution and readout data. The board is made in the form factor, which allows to locate the module into the special box for electronics inside the magnet. Electromagnetic tolerant and radiation hard components are applied in the ADC64Ecal. 15 modules are produced and tested. 20 modules will be produced till the end of 2019 year and 100 modules in 2020.

4 modules will be placed inside the one box and custom Liquid Cooling System (LCS) is under design for cooling electronics (Fig. 2.2.1.56). LCS for 12 electronic



modules will be produced and ready for the testing in the second quarter of 2020 year.

*Fig. 2.2.1.56. Box for electronics with LCS (left) and ADC64Ecal with LCS in the box (right).*

At the final configuration of MPD 600 modules ADC64Ecal (Fig. 2.2.1.57, left) will be used at Ecal and 12 modules at FHCAL. All these electronics must be synchronized and have the same trigger signal. Therefore CRU-16 is designed (Fig. 2.2.1.57, right). It's a common readout unit with White Rabbit support. It's capable to synchronize up to 16 modules, provide a trigger signals and collect the data form them. All collected data are transmitting to the switch, using 40 Gbps optical interface. 2 board are produced and tested and 10 modules will be produced in 2020.

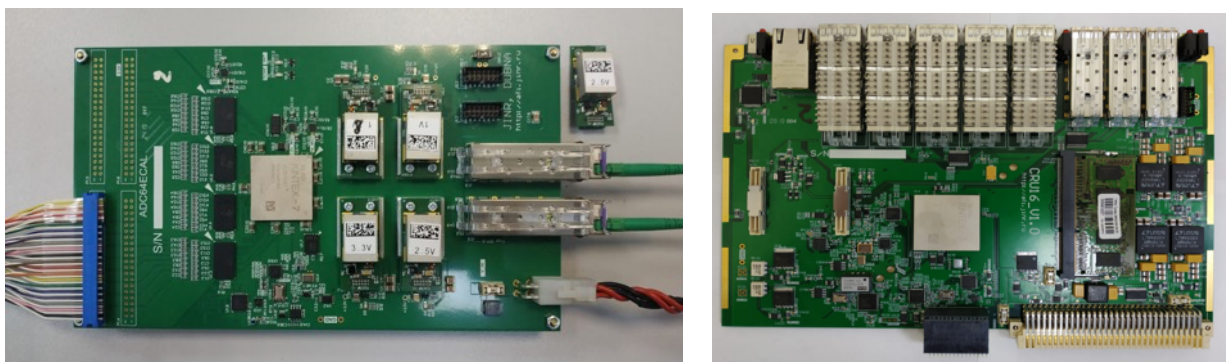


*Fig. 2.2.1.57. ADC64Ecal (left) and CRU-16 (right) electronic modules.*

### 2.2.1.10.2. MPD DAQ network

On the present time a network equipment has bought for the MPD DAQ network (see network structure in Fig. 2.2.1.58). It is covering the test run needs, partially.

In 2020 will be planned to purchase:

- computing equipment FLP (480 cores) 10 servers;
- interim data storage TDS (must be required 500 TB of useable data volume) 10 servers;
- network equipment for a data acceptance from electronics and for a infrastructure needs in quantity 12 switches;
- servers 134exed134e MPD DAQ Network processes monitoring and logging in quantity 10 pieces.

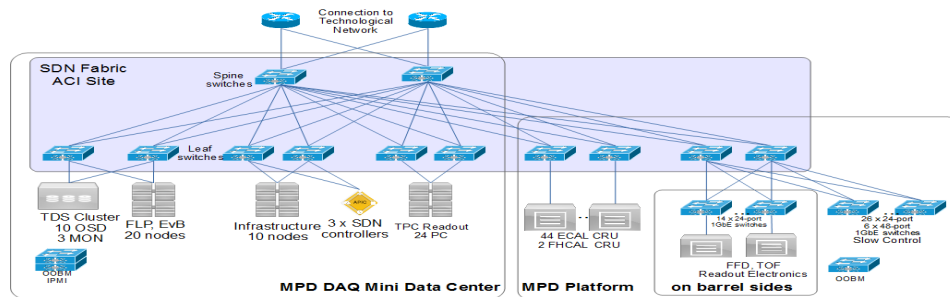


Fig. 2.2.1.58. MPD DAQ network structure.

Networking devices and DAQ electronics will be placed on and into the Barrel, at MPD platform and inside the MDC (see Fig. 2.2.1.59). At TPC, Ecal and FHCAL readout electronics will be placed into the Barrel. The data from these detectors will be transmitted to the network devices for TPC and to the CRU-16 modules for Ecal and FHCAL by optical links. Network devices and CRU-16 modules will be placed at the MPD platform. All aggregated by CRU-16 modules data will be transmitted to the MDC. Network devices and DRE at TOF and FFD detectors will be placed on the Barrel, around it. The data path is: from the DRE to the Network switches at platform, and from the Network switches to the MCD.

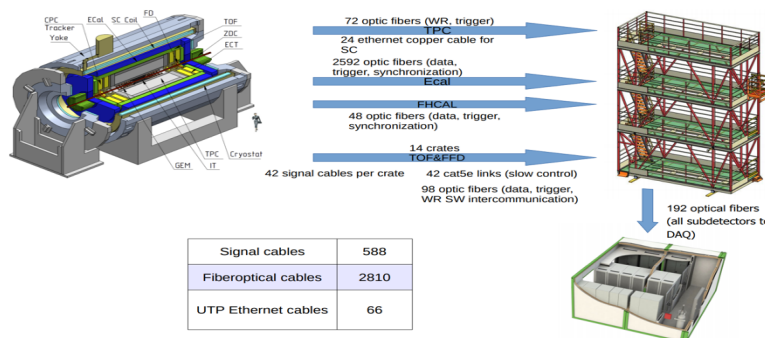


Fig. 2.2.1.59. MPD DAQ Network and DAQ Electronics location.

### **2.2.1.10.3. MPD Mini Data Center (MCD) and Control Room**

The contract for MCD and Control Room (see Fig. 2.2.1.60) production was concluded in 2019. Commissioning the Control Room set with the MCD for a test usage are planned in may 2020.

MDC specifications:

- input power consumption – 160 kW;
- IT power consumption – 50 kW (N+1)/70 kWmax;
- rack count – 7 racks;
- redundancy – N+1 (UPS, HVAC);
- battery backup time – 15 minutes;
- rack size – 600 x 1200 x 42U.
- Control Room specifications:
  - number of operator places – 20;
  - redundancy – N+1 (UPS);
  - battery backup time – 15 minutes.

Ventilation, air conditioning, fire extinguishing, access control and video surveillance systems will be present.

White Rabbit provides sub-nanosecond accuracy and picoseconds precision of synchronization for large distributed systems. It also allows for deterministic and reliable data delivery. DRE boards digitize detector signals using common notion of time and frequency provided by the White Rabbit (WR) network. The time reference is provided by GPS/GLONASS receiver and backup precision frequency reference (Cesium or Rubidium clock). Timing Network structure and WR switches test stand are shown in Fig. 2.2.1.61.



Fig. 2.2.1.60. MCD (up) and Control Room (down)

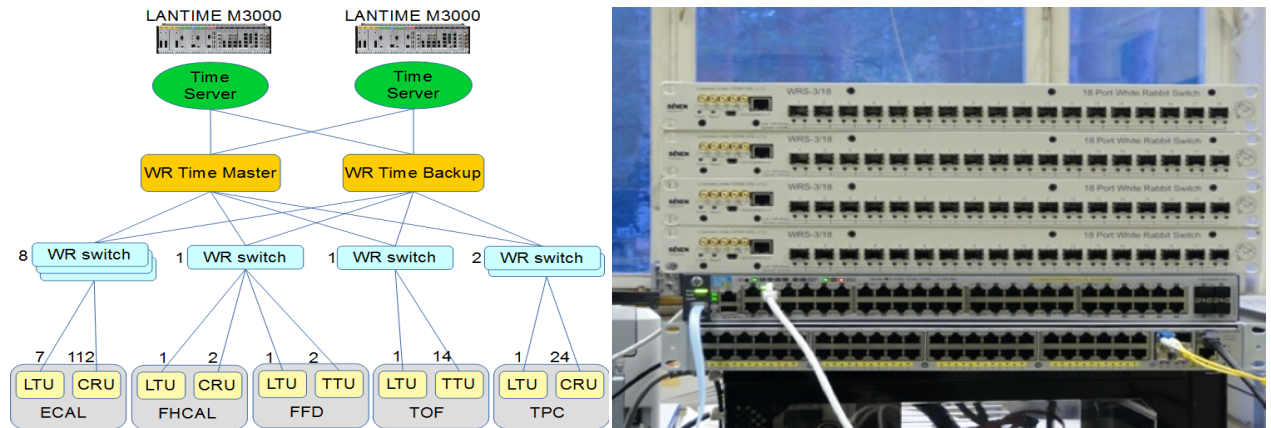


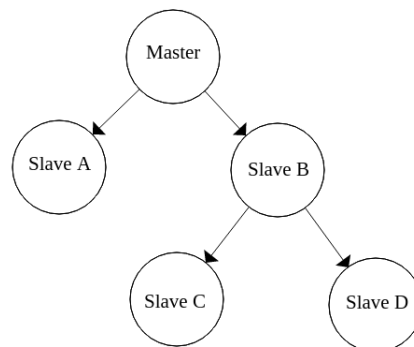
Fig. 2.2.1.61. The MPD Timing Network structure (left) and WR switches test stand (right)

10 WR switches were purchased till the end of 2019 and 10 will be purchased in 2020.

#### 2.2.1.10.4. MPD DAQ software

Each program participating in the experiment has its own configuration. A record in configuration is a data structure composed of a **field** and **value** pairs, named *document*, for example:

```
Document A: {program name: run control,           ← field: value
             status: run,                         ← field: value
             devices: {Document B, Document C, ...}, ← field: value
             ... }
```



It means that we design data in JSON-like documents. This is more expressive and powerful than the traditional row/record model. A typical number of documents in each program is 10 – 500, depth from 5 and more layers. We entrusted the management of such a data structure to the Mongo document-oriented database, which is open source. Programs participating in the experiment also represent a tree structure, like the left picture. Commands are transmitted from program to program on this tree from the parent program (run control program).

In the first and the second quarter of 2019 in all programs was added a function to recording their configurations to Mongo database. It was introduced a new entity called *Run*. *Run* is the parallel launch of several programs (typical 10 – 50), which are connected to each other in a tree structure and consistently perform one task. Also, we taught our programs to transfer their configurations up to the tree. What did it give us:

- we know exactly with what configuration programs were launched, and this information will not be lost after experiment.
- now we can restart the *Run* with exactly the same configurations.

In late 2019 – early 2020 planned to develop software for combining all previously written applications under single application monitoring (AM). Assumed, that this program will be able to monitor about 10-50 other programs (subprograms). It will contain the necessary information for a successful reproduction of subprograms.

The main functions will be:

- launch remote programs; aggregation, logging and visual representation of errors that occurred, during *Run*;
- work with the configuration database: applying previously saved configurations to executable subprograms;
- to help user understanding a hierarchical structure of *Run*.

*DevFlashProg*. This program can connect to 138exed138et device and write firmware image file into device flash memory and/or verify it. A log information is written in corresponding database after every success write.

*PNP protocol*. Any program that takes part in a run control system sends specific package to multicast. Another can find out what program is running at this moment and some information about it, host and port of TCP-server for remote control or with outgoing data.

*MLDP protocol*. All our 138exed138et devices support MLDP protocol. It allows up to avoid binding devices to the IP-address in programs. MLDP-message contains IP address, serial number, device type and other useful information. All our 138exed138et devices periodically sends it over multicast. One program can receive it and find out on what address we should establish a connection.

*Mstream*. This program receives data packages from 138exed138et device, perform defragmentation of Mstream data blocks, packs them into MpdRawData format and transmit them to outgoing TCP-server. In future it is planned to integrate this logic into control programs as separate threads.

*Event builder.* The task of this program is to collect data from several client programs (mstream program or another event builder), separate event blocks in every data flow, combines them together per events and further retransmits or writes to the file as united data block.

*TDC control.* This program sets up TDC72VXS device with proper configuration. Among the main parameter there are channel enable, readout window, trigger source. In debug mode it is capable to make specific adjustment of HPTDC setup. Although it starts mstream subprogram for reading data. In the future it is planned to make it as a slave of run control system.

*TTVXS control.* This program sets up TTVXS device with proper configuration. Among the main parameter there are enable slots of VME crate, trigger source. Although it starts mstream subprogram for reading data from this block. In the future it is planned to make it as a slave of run control system.

*ADC64.* This program sets up ADC-like devices with proper configuration. Among the main parameter there are channel enable, readout window, trigger source, DSP (digital signal processing) logic and sparse readout. This program can read data from device, visualize them and save data as an ASCII file. It is used just to prepare for run, in run execution adc64-system is used.

*Adc64-system.* This program writes configuration and handle data readout from list of ADC-like boards with error handle and remote control. This program can be used as slave one in run control system.

*Mpd-rawstat.* This program can perform specific data/device tests: presence of all devices in the final data file, absence of significant time discrepancy, etc. Data can be obtained from reading a file or form specific TCP-server of event builder program (monitor output).

*Adc64-viewer.* This program is similar to mpd-rawstat, but it performs just quick visualization of any signal from adc-like devices. Data source can be a file or monitor output.

*CRU control.* At this moment this program is under design. This program will be able to configure corresponding device and integrate other programs into the run control system.

### **2.2.1.11. Engineering Support**

The main task, which will be solved at the NICA accelerator complex, requires the design and construction of an experimental setup capable of: registration with high efficiency secondary particles born in the collision of heavy ion beams; identifying

the type and determine the energy of particles; restoring the vertices of the primary interaction and the coordinates of the birth of secondary particles – Multi-Purpose Detector MPD. The MPD-PLATFORM (Fig. 2.2.1.61) is an important part of the NICA project infrastructure. Mechanically connected to the MPD, the PLATFORM is designed to provide working conditions for power supply systems, DAQ electronics, monitoring and control elements of the subdetectors.



*Fig. 2.2.1.61. PLATFORM MPD Mechanical Support Structure with RACK's*

### ***2.2.1.11.1. Architecture of mechanical structure***

The MPD mechanical support consists of:

- RACK – main module of the mechanical structure designed to assemble elements of a system;
- AUXILIARY RACK – COOLING UNIT – air/water heat exchanger designed for cooling equipment installed in the connected RACK;
- UNIT – group of mechanically connected RACKs (4 RACKs with 2 or 3 AUXILIARY RACK – COOLING UNIT);
- CONTAINER – of mechanically connected UNITS (8 RACKs with 5 AUXILIARY RACK – COOLING UNIT) installed at the same level;
- PLATFORM – movable mechanical structure consisting of four levels, called CONTAINERS and connected to MPD.

### ***2.2.1.11.2. Technical description and equipment***

The RACK (Fig. 2.2.1.62) it is a demountable structure consisting of a steel frame, mounting rails with a distance between them 19", removable front and rear doors and side panels. The doors are equipped with mechanical and electronic locks and are connected by a flexible protective conductor PE Protective Earth. A 600x1200x2200 RACK was selected with a usable height of 47U (1U = 1,75 inches). The total mass of the structure with embedded devices should not exceed 1 500 kg.



*Fig. 2.2.1.62. RACK – the Main Module of the Mechanical Structure, AUXILIARY RACK – COOLING UNIT*

The RACK standard equipment:

- **FAS Fire Alarm System** – early fire detection and accurate location of fire hazard at RACK level, active extinguisher system and smoke extraction system;
- **PMS PLATFORM Management System** – real-time remote management and data acquisition;
- **IPD Intelligent Power Distributor** – power supply of devices installed in RACK. The control system performs the optimization of phase loading, provide overcurrent and electrical shock protection, failures detection, automatically switch-on and switch-off power of the devices and remote-control mode;
- **VAC Ventilating and Air Conditioning** – cooling system with closed air circulation in the RACK;
- **CCAS Cable Connection Authorization System** – marking cables with micro RFID elements and saving the described data in EqDb;
- **ACS Access Control System** – service technicians access managed by administrator to the RACKs using electronic keys registered in EqDb;
- Free space – 36U.

AUXILIARY RACK – COOLING UNIT 300x1200x47U can be installed with one or two RACKs. The control unit attempts to keep the temperature of the impelled cold air at 22 ° C. The necessary fan speed is determined and controlled by determining the temperature difference between the warm inlet and the cold outlet air (Fig. 2.2.1.63).

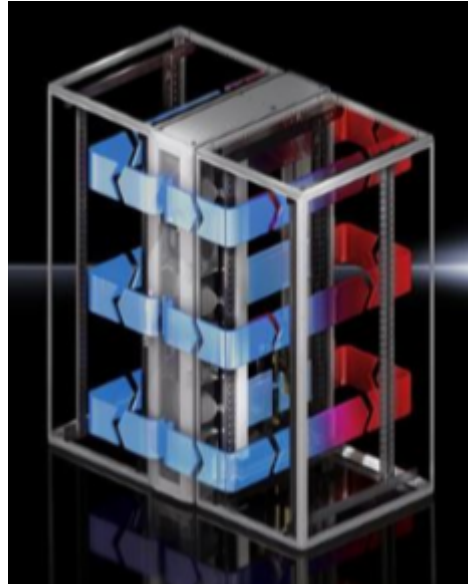


*Fig. 2.2.1.63. Air routing*

To achieve enough cooling in the server enclosure, it is important to ensure that the cooling air passes through the interior of the built-in units and is unable to flow past at the sides. To ensure targeted air routing in the system, the server enclosure is divided by foam strips into warm air and cold air section. Additionally, the system consisting of LCP DX, server enclosure and cold aisle containment should be well sealed to avoid a decrease of the cooling capacity due to mixing of cold and hot air. In addition, the system consisting of COOLING UNIT and attached RACK should be well sealed to avoid a decrease of the cooling capacity due cold air leakage. Existing cable entry glands are additionally sealed e.g. using suitable brush strips.

CONTAINER is a group of RACKs with its own infrastructure, which includes:

- **FAS – Fire Alarm System** – all closed spaces and cooling ventilation ducts will be equipped with appropriate smoke and fire detectors. All fire detectors will be connected to the global FAS-NICA system with automatic fire brigade notification system;
- **CRWS – Cable Race Way System** – cables arrangement on MPD-PLATFORM;
- **VAC – Ventilating and Air Conditioning** – COOLING UNITs are connected to external Ice-water aggregate;

- **CCTV** – Closed Circuit TeleVision – distributed system of weatherproof cameras in many locations, remotely controlled, connected to the CNNet converged IT network with writing data in EqDb;
- **SES** – Smoke Extraction System – connection with smoke exhaust ventilation of the NICA complex building;
- **SAS** – Sound Alert System – audio messages to personnel about hazards and the manner of the required response. Warnings should be accompanied by a light form e.g. flashing light with warning lamps.

PLATFORM is a four-tier steel structure, with a CONTAINER installed on each level.

LEVEL 1 (ELECTRIC DISTRIBUTOR) – power equipment, supplying MPD and the Platform itself. Power Supply automatically connect the PLATFORM NICA-MPD to one of two (working and emergency) Power Supply Lines 3 x 380 V, 50 Hz, 800 A (400kW). Further power distribution will be performed by a typical block provides 3 x 380 V, 50 Hz and 25 A at the output, which is enough to power one standard RACK.

LEVELs 2, 3 and 4 are for the SSC Slow Control System and DCS Detector Control System of the MPD-NICA project. The desired power consumption of the LEVELs 2 – 4 is about 200 kW.

### ***2.2.1.11.3. Management***

The control of the RACK takes place centrally from the Panel Operator in the WinCC SIEMENS SCADA system. There are two types of RACKs that can be handled remotely:

- RACK MASTER – manages all installed RACKs;
- RACK SLAVE – controlled from the MASTER RACK.

To facilitate the management of IT, a CLUSTER is a group of RACKS or devices installed in different RACKS, functionally designed for the same task and logically combined in the IT system that controls their structure.

*EqDB – Equipment Database ORACLE.* This EqDb system allows you to register administrative information, such as orders, deliveries and detector construction processes, the cost of its production, any movements of components for testing or maintenance. EqDb has a built-in connection authorization mechanism based on RFID Radio Frequency Identification technology. EqDb works online with a slow control system and is an important element of technical support for the entire MPD-NICA project.

*CNNet Convergent IT NICA Network* – interface for connecting the NICA-MPD-PLATFORM with the rest of the JINR network.

- remote administration at local and global levels;
- a virtual private network channel connecting CNNet to other cooperating DaCe Data Center, such as the WUT Warsaw University of Technology.

#### **2.2.1.12. Integration in MPD**

The installation of the TOF will begin after the finishing of the Ecal installation. Each module will be inserted in their position on both sides of the yoke of magnet. This will be done by means of a mobile support structure. The structure is equipped with adjustable rails of the same kind used inside the MPD barrel. To insert a module into the barrel it is enough to suspend the support structure with the hall crane in front of the chosen services sector and connect the rails together to form a unique sliding line that will allow pushing the module into the right position.

The design of part of integration equipment is finished. The production and assembling of integration devices in the MPD hall should be finished in summer 2020.

### 2.2.2. Detector for studies of Baryonic Matter at Nuclotron (BM@N)

BM@N (Baryonic Matter at Nuclotron) is the first experiment operational at the Nuclotron/ NICA accelerating complex. The purpose of the BM@N experiment is to study relativistic heavy ion beam interactions with fixed targets. The Nuclotron will provide the experiment with beams of a variety of particles, from protons to gold ions, with a kinetic energy ranging from 1 to 6 GeV/nucleon. The maximum kinetic energy of ions with the charge to atomic weight ratio of 0.5 is 6 GeV/nucleon. The maximum kinetic energy of gold ions with  $Z/A$  of 0.4 is 4.5 GeV/nucleon, while the maximum kinetic energy for protons is 13 GeV. Recently the BM@N experiment collected data in beams of carbon, argon, and krypton ions. The planned intensity of the gold ion beam at BM@N is  $10^6$  ions/s. The acceleration of the gold ion beam is planned in 2021, after the Nuclotron upgrade. In Fig. 2.2.2.1 the interaction rates are presented for different experiments with heavy ion collisions at different energies per nucleon-nucleon collision in the center of mass system. The beam energy of the BM@N experiment is in the intermediate range between experiments at the SIS-18 and NICA/FAIR facilities and partially overlaps the energy range of the HADES experiment. The acquisition rate of non-peripheral collisions, i.e., central or intermediate interactions is expected to range from 20 to 50 kHz at the second stage of the BM@N experiment in 2022 and later. The interaction rate is limited by the capacity of the data acquisition system and readout electronics.

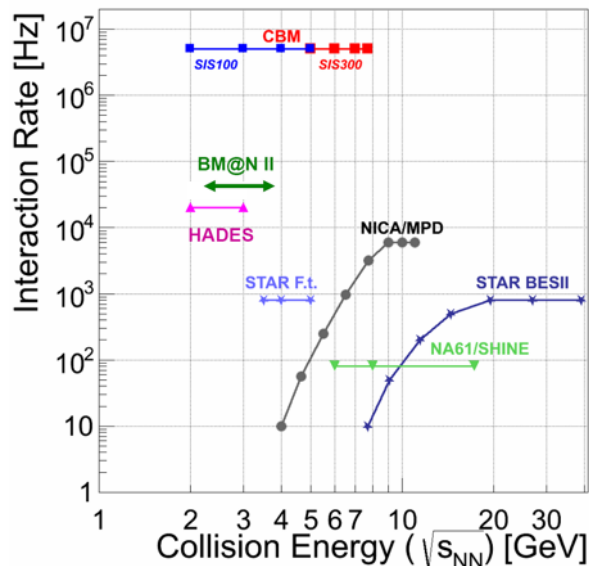


Fig. 2.2.2.1. Interaction rate and energy per nucleon-nucleon collision in c.m.s. in experiments with heavy ions. The range for BM@N is superimposed.

The layout of the proposed BM@N configuration for heavy ion program is shown in Fig. 2.2.2.2. The experiment combines high precision measurement of track parameters with time-of-flight information for particle identification and presumes a

measurement of the total energy by the hadron calorimeter to analyze the collision centrality. The charged track momentum and multiplicity will be measured using a set of forward silicon detectors (FwdSi), large aperture silicon tracking system (STS), 7 planes of two-coordinate GEM (Gaseous Electron Multiplier) detectors mounted downstream of the target inside of the analyzing magnet. The GEM detectors are operational at high particle densities and in strong magnetic fields. The vertical gap between the poles of the analyzing magnet for detector installation is about 1 m. The magnetic field can reach a maximum value of 1.2 T, which makes it possible to optimize the BM@N geometrical acceptance and resolution on momentum for different processes and energies of the beam. The outer tracking system consists of cathode chambers that will be supplemented with cathode strip chambers to increase the effectiveness of track measurement in Au+Au collisions. The time-of-flight detectors (ToF) based on the multi-gap Resistive Plate Chamber (mRPC) technologies with strip readout provide an opportunity to separate hadrons ( $\pi$ , K, p) and light nuclei with momentum up to few GeV/c. The Zero Degree Calorimeter (ZDC) detector is foreseen for the extraction of the collision impact parameter (centrality) by measuring the energy of the fragments of colliding particles. The Cherenkov modular quartz detector positioned around the target and partially overlapping the backward hemisphere is planned to generate a trigger signal for the data acquisition and a starting signal (T0) for the time-of-flight detectors. In 2022, at the second stage of the BM@N experiment, at least four planes of two-coordinate silicon strip detectors will be installed in front of the GEM detectors to improve track reconstruction in Au+Au collisions. Detectors of this type are currently under development for the CBM experiment, therefore the actual implementation of the BM@N tracker upgrade depends on the timetable of the CBM silicon tracker program.

The technical runs with the BM@N detector were performed in the deuteron beam in December 2016 and in the carbon beam in March 2017. The kinetic energy was 4 GeV/nucleon for the deuteron beam and was varied from 3.5 to 4.5 GeV/nucleon for the carbon beam. The starting configuration of the central tracker was based on a forward silicon strip detector and a set of GEM detectors. The experimental data from the central tracker, outer drift chambers, time-of-flight detectors, zero degree calorimeter and trigger detectors were read out using the integrated data acquisition system. The collected data were used to check efficiencies of sub-detectors and develop algorithms for the event reconstruction and analysis. In particular, experimental data of minimum bias interactions of the beam with different targets were analyzed with the aim to reconstruct tracks, primary and secondary vertices using the central tracking detectors. Since the GEM tracker configuration was tuned

to measure relatively high-momentum beam particles, the geometrical acceptance for relatively soft decay products of strange V0 particles was rather low. The Monte Carlo simulation showed that only  $\sim 4\%$  of  $\Lambda$  hyperons and  $\sim 0.8\%$  of  $K_s^0$  could be reconstructed.  $\Lambda$  hyperons were reconstructed using their decay mode into  $(p, \pi^-)$  pairs. Since particle identification at this stage of the analysis was not used, all positive tracks were considered as protons and all negative as  $\pi^-$ . The invariant mass distributions of  $p$  and  $\pi^-$  are shown in Fig. 2.2.2.3 for reconstructed interactions of the carbon beam with C, Al, Cu targets. The background under the signal will be reduced by introducing additional silicon tracking detectors to improve the primary and decay vertex resolution.

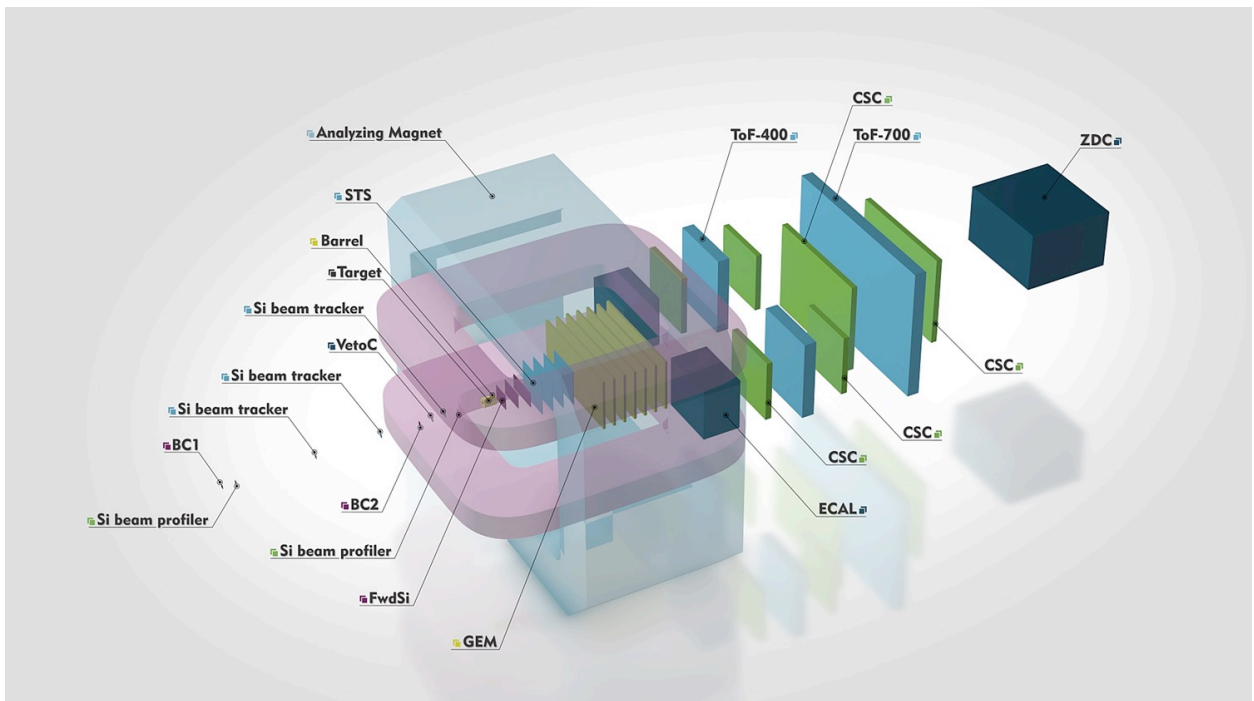


*Fig. 2.2.2.2. Schematic view of the BM@N setup for the heavy ion program (without vacuum beam pipe).*

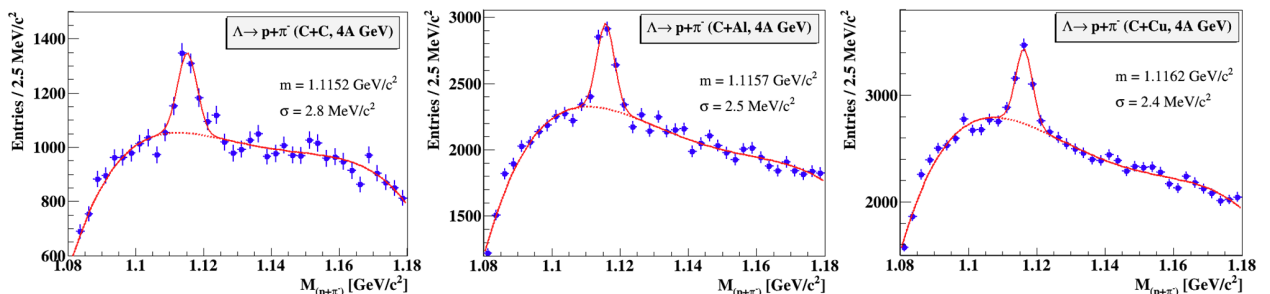


*Fig. 2.2.2.3. Invariant mass spectrum of proton and  $\pi^-$  pairs reconstructed in interactions of the carbon beam with C, Al, Cu targets.*

The yields of  $\Lambda$  hyperons in minimum bias interactions of the 4 AGeV carbon beam with the C, Al, Cu targets are measured in the kinematic range on the  $\Lambda$  transverse

momentum of  $0.1 < p_T < 1.05$  GeV/c and the  $\Lambda$  rapidity in c.m.s. of  $0.03 < y^* < 0.93$  (Fig. 2.2.2.4). The measured yields of the  $\Lambda$  hyperons in minimum bias C + C interactions are extrapolated into the full kinematical range using averaged predictions of the DCM-QGSM and URQMD models and compared in Fig.4 with the results of other experiments.

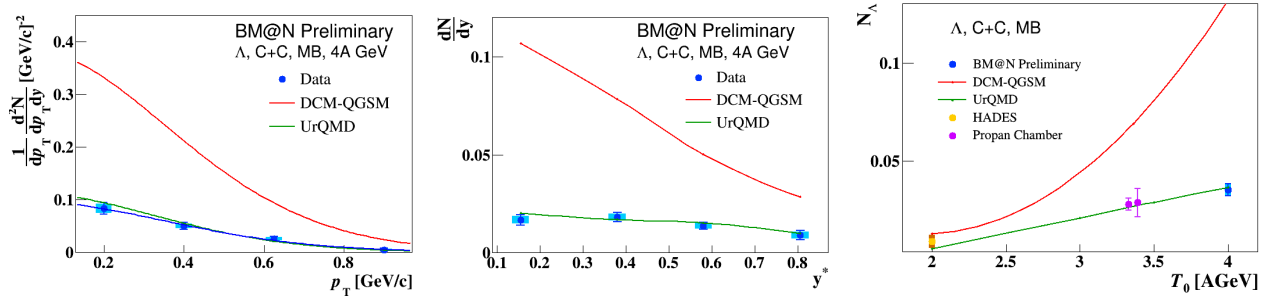


*Fig. 2.2.2.4. Yields of  $\Lambda$  hyperons in minimum bias C+C interactions vs transverse momentum  $p_T$  (right plot) and rapidity  $y^*$  in c.m.s. (central plot).*

*Energy dependence of  $\Lambda$  hyperon yields in C + C interactions measured in different experiments, including BM@N. The predictions of the DCM-QGSM and UrQMD models are shown as lines.*

The extended configuration of the BM@N set-up was realized in the recent runs with the argon and krypton beams performed in March 2018 (Fig. 2.2.2.5). The set-up comprised GEM detectors with the size of 163 x 45 cm<sup>2</sup>, forward silicon strip detectors, full time-of-flight system, extended trigger system, hadron and electromagnetic calorimeters. The first measurement of short-range correlations of nucleons in carbon nucleus was performed in inverse kinematics with the carbon beam and liquid hydrogen target.

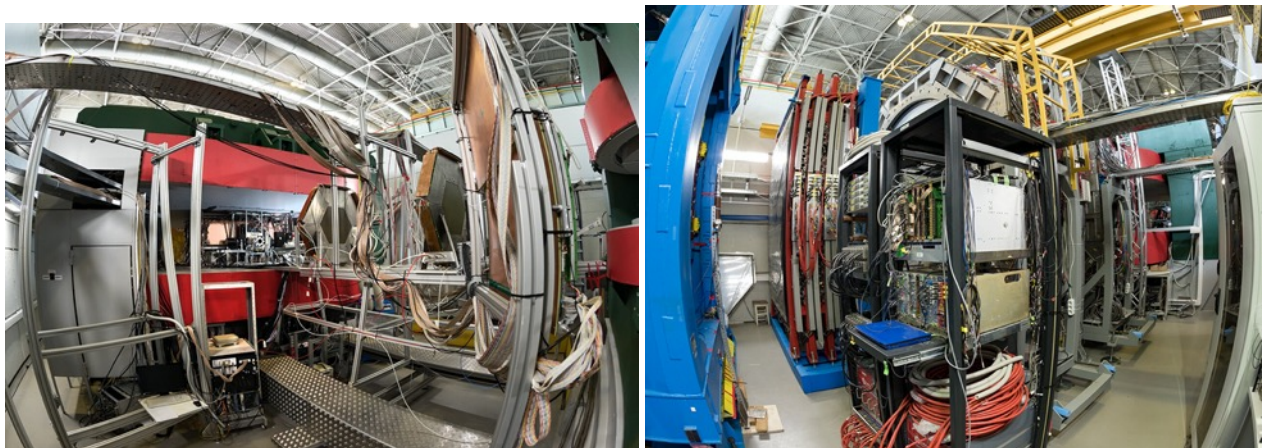


*Fig. 2.2.2.5. BM@N setup in front of the analyzing magnet (left plot) and behind the analyzing magnet (right plot) in the technical run in March 2018.*

### 2.2.2.1. Wide aperture Silicon Tracking System – STS

In 2022 BM@N experiment will be upgraded in order to fit occupancy challenge of Au+Au collisions with beam energies up to 4.5A GeV. A new hybrid tracking system based on four stations of double-sided microstrip silicon sensors of high granularity followed by 7 planes of two-coordinate GEM detectors and a vacuum beam pipe will be installed. Silicon planes are currently under development following the design used for the STS of the CBM experiment. The BM@N STS project will be performed in two steps: firstly, two stations with 44 modules will be assembled, installed and tried at the end of 2021 or early 2022, the full configuration will be ready a year later.

The final layout of the BM@N STS was fixed in the middle of 2019 after numerous simulations performed by our German partners (see Fig. 2.2.2.6). The system will consist of 292 modules with Double-Sided microstrip Silicon Detectors (DSSD) of the CBM STS family of sensors. Three different sizes of the sensors will be used: 256 modules with 62\*62 mm<sup>2</sup> size, 20 modules with 42\*62 mm<sup>2</sup> size, 16 “central” modules with sensors geometry cutoff allowing for the beam pipe passage through the STS. Strip occupancies for the central sensors located in the place of the maximum counting rate was estimated to be less than  $5 \times 10^{-4}$  per event. The total sensitive areas of the first and the last stations are 597\*398 mm<sup>2</sup> and 835\*517 mm<sup>2</sup>, respectively. The distance between the stations is 200 mm, the minimal distance from the target to the first station is 300 mm. The horizontal angular acceptance of the system is more than 260 degree.

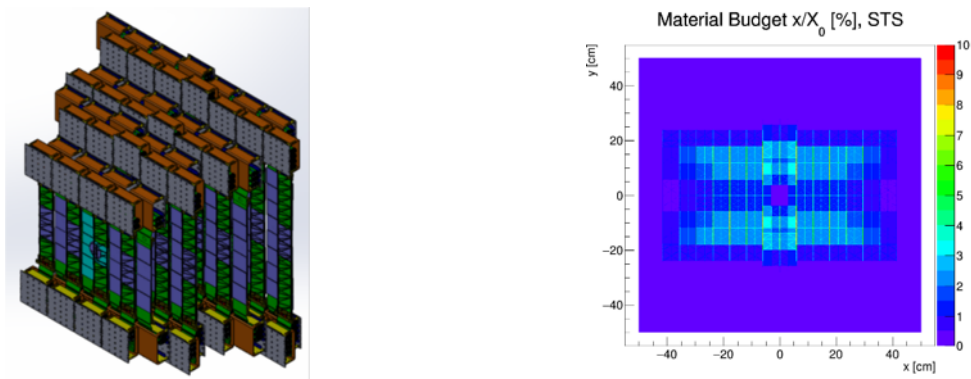


Fig. 2.2.2.6. Layout of the BM@N STS and its material budget distribution

The physics performance of the hybrid tracking system has been studied based on generated central Au+Au collisions with a beam kinetic energy of 4A GeV produced with the DCM-QGSM event generator. The primary tracks, which create only hits in 4 silicon stations, can be reconstructed with an efficiency of better than 90% above a momentum of 0.6 GeV/c (see Fig. 2.2.2.7, left). The momentum resolution for primary particles is shown in Fig. 2.2.2.7(right) as a function of the momentum.

Only for the momentum below  $p = 0.5$  GeV/c the momentum resolution is worse than  $\Delta p/p = 0.006$ .

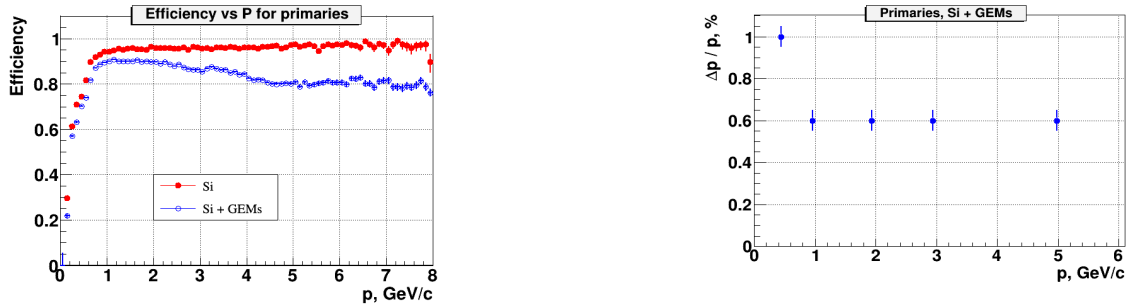


Fig. 2.2.2.7. Left: reconstruction efficiency as a function of the momentum of primary tracks with minimum 4 hits in the Si stations only (red histogram), and in the Si + GEM stations (blue histogram). Right: momentum resolution as a function of the momentum of primary tracks reconstructed in the silicon+GEM setup in central Au+Au collisions at a beam kinetic energy of 4A GeV

A signal of  $\Lambda$  hyperons was reconstructed with the track finder identifying the vertex of the hyperon decay. The resulting proton-pion invariant mass spectrum is shown in Fig. 2.2.2.8. The mass resolution of the  $\Lambda$  signal is  $\sigma = 1.1$  MeV/c<sup>2</sup>, the signal-to-background ratio is  $S/B = 5.2$ .

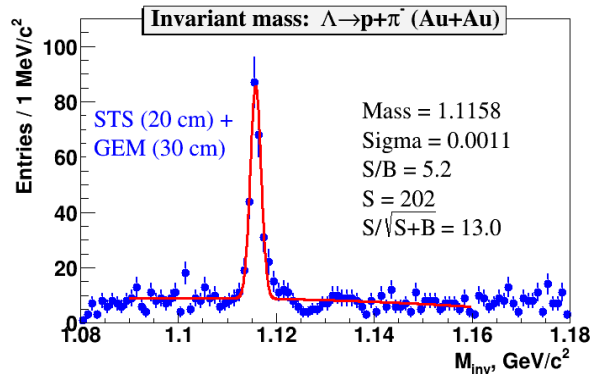
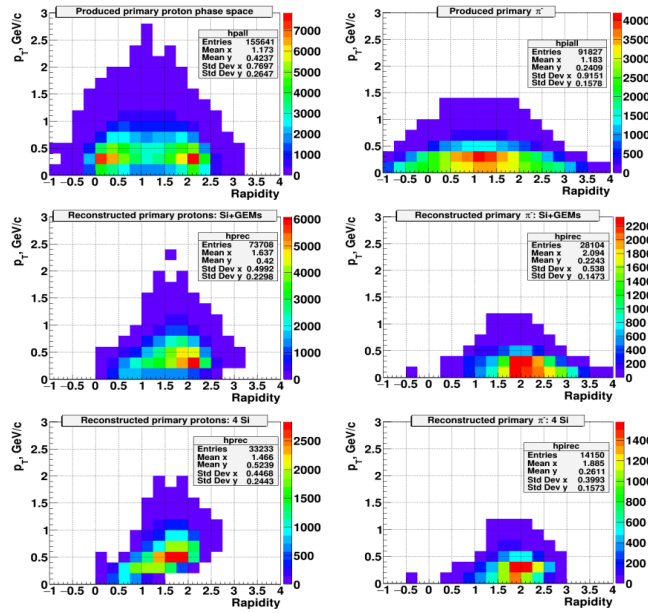


Fig. 2.2.2.8. Proton-pion invariant mass spectra using 4 silicon + 6 GEM stations

The phase space distributions of decay products of  $\Lambda$ -hyperons generated with the DCM-QGSM model in central Au+Au collisions at a beam kinetic energy of 4A GeV are shown in Fig. 2.2.2.9. The  $\Lambda$  hyperon reconstruction efficiency in the hybrid silicon+GEM detector system is above 10%.



*Fig. 2.2.2.9. Phase space distributions as function of transverse momentum and rapidity for protons (left column) and pions (right column) as generated with the DCM-QGSM code for central Au+Au collisions at a beam kinetic energy of 4A GeV (upper row); reconstructed in the silicon+GEM detectors (center row); reconstructed in the silicon stations only (lower row). The particle identification is based on the Monte Carlo information.*

The first draft of BM@N STS TDR is now available. The final version will be presented in the beginning of 2020. The TDR consists of the following main chapters:

1. The research program of the upgraded BM@N experiment;
2. The physics performance simulations of the hybrid STS+GEM tracking system;
3. Studies of the radiation environment;
4. The Silicon Tracking System;
5. The project organization and timelines.

In the 4<sup>th</sup> chapter the full configuration of the STS system, information about the components, assembly process, quality assurance and system integration are presented.

### **2.2.2.1.1. STS module**

A module (see Fig. 2.2.2.10) is the basic component of the STS. It consists of a double-sided microstrip silicon sensor, a set of multilayer ultra-thin aluminum microcables and two Front-end Boards (FEBs) with readout electronics.



*Fig. 2.2.2.10. Module without shielding*

The design of the STS sensors was finalized, all sensors have been acquired by JINR since 2017 except the central ones. The design of these sensors is being developed with a plan to get them produced in 2021 and 2022. That is agreed as an in-kind contribution of Germany to NICA. A custom designed probe automat (Fig. 2.2.2.11) was fully commissioned for full strip-by-strip DSSD QA testing with specially developed software and procedures.

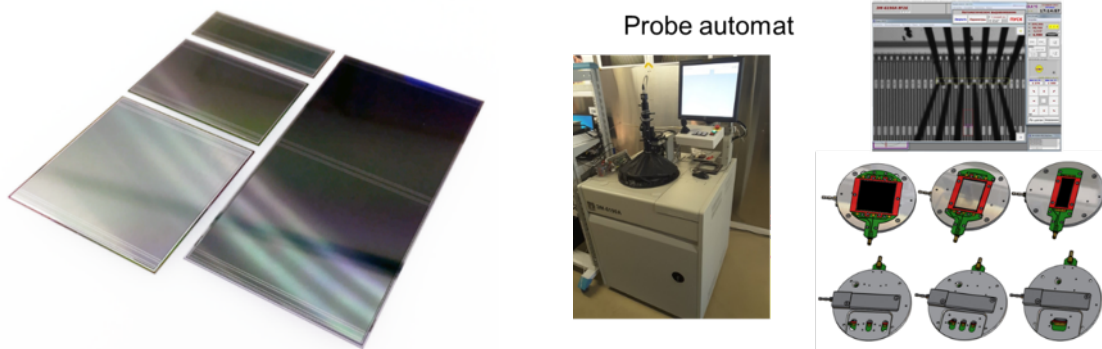


*Fig. 2.2.2.11. The CBM STS family of DSSD. The two middle-sized variants will be used in the BM@N-STC (left). Probe automat for the strip-by-strip QA tests of the DSSDs (right)*

The final specification of the ultrathin micro-cables (Fig. 2.2.2.12) was completed in 2019 after years of proto-typing undertaken both in GSI, JINR and LTU, Kharkov. A batch of the final 44 sets for the first two stations was ordered to be delivered to JINR in the beginning of 2020.

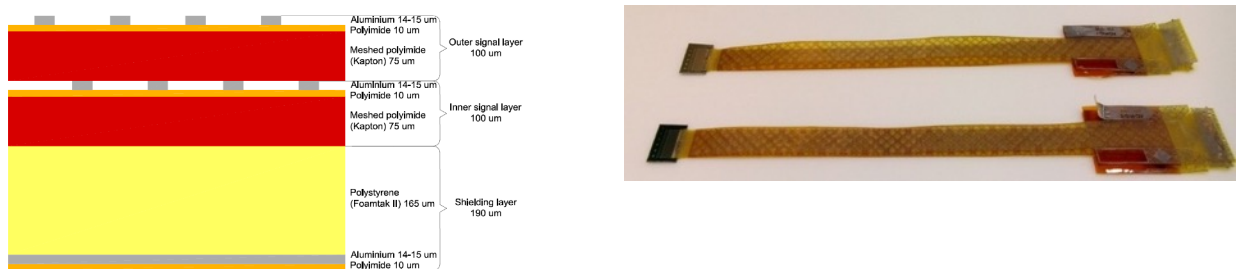


*Fig. 2.2.2.12. Cross-section of a micro-cable (left) and STS Xyter ASICs bonded with micro-cables (right)*

The readout electronics is based on state-of-the-art STS-XYTER ASIC (Fig. 2.2.2.13) developed at AGH, Krakov for the CBM STS. The last version of the chip – v. 2.1 was tested in JINR and GSI independently with recommendations put forward to the designers for the next, final, generation of the chip. 200 chips v.2.2 considered to be prefinal were shipped to JINR a where special equipment was tuned for their certification. All chips are certified and now being used for adjustment of the module assembly technology

The Front-End Boards (FEBs) with 8 STS-XYTER ASICs were produced and tested in 2018-2019. The existing FEB designed in GSI is found to be good for testing of electrical features of the circuit, but not suitable for its subsequent integration into the system due to the connectivity features. A new PCB for FEB was offered by JINR for the BM@N detector which is now under development together with the SINP MSU experts (supported by the RFBR Grant). A new version of FEB\_BMN should be ready in the beginning of 2020.

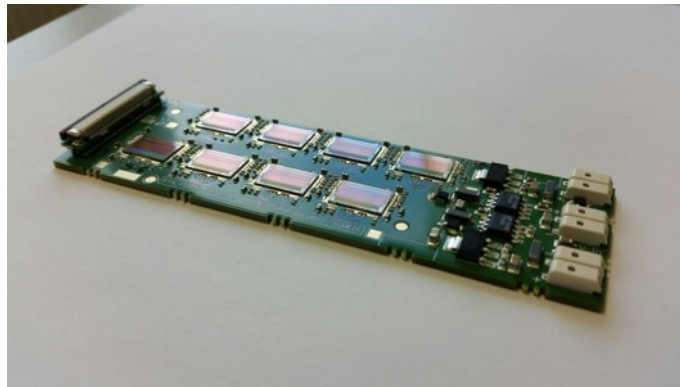


*Fig. 2.2.2.13. FEB with 8 STS XYTER ASICS*

One of the most time-consuming parts of the module assembly process is the test and selection of glues. The final list of glues is now ready, all glues were tested on the mechanical properties, influence on the detector performance, thermal and electrical conductivity and radiation hardness.

The module assembling site was prepared and equipped with wire bonding machines in 2014 -2016 (Fig. 2.2.2.13). All sets of jigs for the module assembling were developed, produced and tested during 2013-2018.

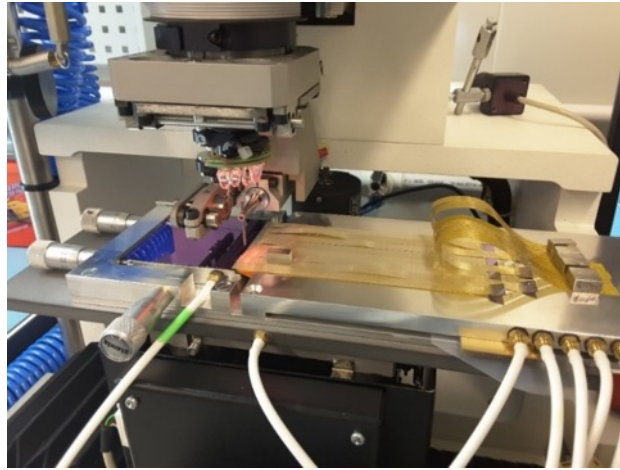


Fig. 2.2.2.13. TAB bonding process of micro-cable and Si-sensor

The quality assurance procedures for the bonding tests during the module assembly were developed in 2018-2019 (Fig. 2.2.2.14). Quality assurance tests for the FEBs and long-term stability tests of the modules are under development and will be finished in the beginning of 2020.

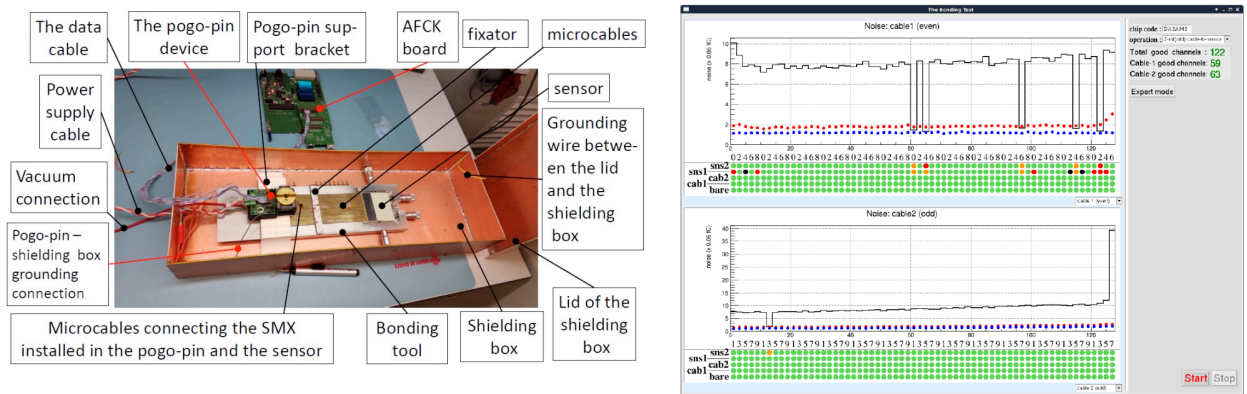


Fig. 2.2.2.14. QA tests during module assembly (left) and GUI of the Bonding test software showing not bonded channels (right)

Three modules were assembled and tested at the JINR assembly lab in 2019 (Fig. 2.2.2.15). Serial module production will start in 2020. Additional resources are needed for the implementation of detector production DB.

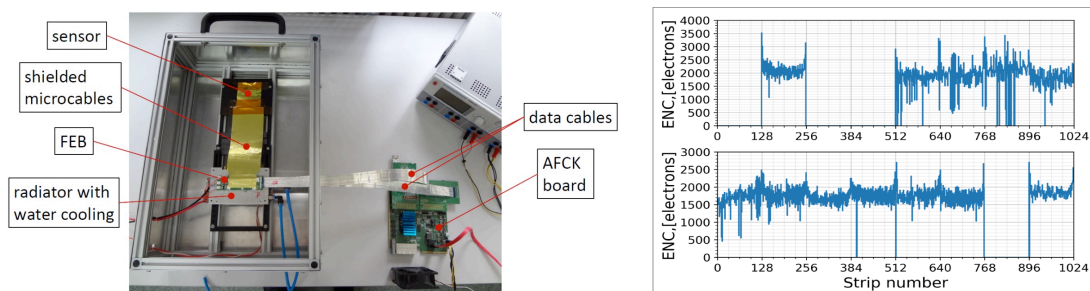


Fig. 2.2.2.15. Test bench for the tests of assembled module (left) and noise per channel measurements for N (top) and P (bottom) sides of the sensor (right)

### 2.2.2.1.2. Ladder assembly

Assembled modules will be mounted onto ultralight carbon fiber truss. Such super-module is called a ladder. The accuracy with which the positions of the sensors on the CF truss plays important role for the subsequent alignment procedures which in turn produce impact on the of track reconstruction efficiency. A custom designed device for the ladder assembly (Fig. 2.2.2.16) was developed and produced at the Planar facility (Minsk, Belorussia) within the period 2018-2019. It allows one to mount modules onto the CF truss with the accuracy as follows

Precision of the sensor orientation

X coordinate	$\pm 50 \mu\text{m}$
Y coordinate	$\pm 15 \mu\text{m}$ on 1200 mm base $\pm 12 \mu\text{m}$ on 180 mm base
Z coordinate	$\pm 50 \mu\text{m}$

Precision of the optical fiducials recognition system  $\pm 2 \mu\text{m}$

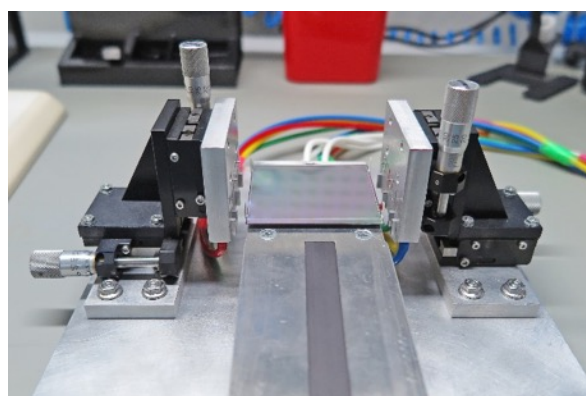
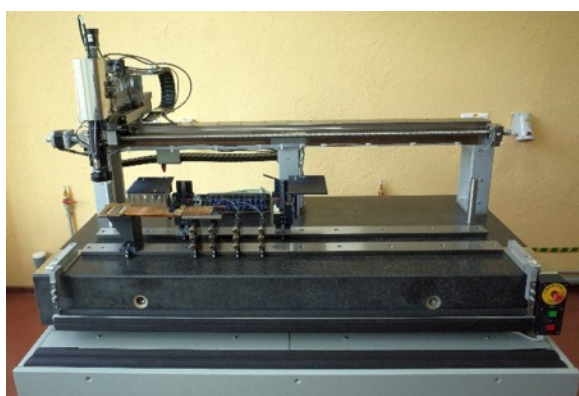


*Fig. 2.2.2.16. Device for the ladder assembly, photo from Planar facility Jig for gluing of fiber-glass L-legs, which are used for the fixation of the sensor on CF frame*

The Factory Acceptance Test (FAT) of the ladder assembly device took place in October of 2019. The Site Acceptance Test (SAT) was performed in November of 2019. The first prototype of the ladder will be assembled in the beginning of 2019. The start of the serial ladder production is planned in the middle of 2020, after additional clarifications of the ladder assembly technology are performed.

### 2.2.2.1.3. DAQ system

A contract on the developing of the data acquisition system was signed with GSI in 2017. But since that time the realization of the contract proceeds with the speed which do not satisfy us. Now measures are being taken to speed up this subproject. Nevertheless, a small prototype of the self-triggering readout system has been assembled in JINR and tested in the laboratory and in the beam in 2019.

Unfortunately, the optimization of the firmware and the TFC system which was expected to be shipped from Germany was delayed due to technical complications met by the German Party and an additional work is still needed in this direction. The final version of the system will be ready by the end of 2020. Due to the inaccessibility of GBTx ASIC in Russia, which is typically used to provide optical link between the on-detector electronics and the readout units located in radiation-free zone, it is planned to reduce the frequency of the throughput of the GBT and use 10 meter length low skew twinex cables to be able to operate with standard FPGA Controllers. Several types of cables are now under test. Set of cables for the first two stations has already been ordered.

#### ***2.2.2.1.4. System integration***

A tentative design of the STS mainframe is ready and now is under discussion with the manufacturer. The design is shown at Fig. 2.2.2.17. We expect the mainframe to be produced till the end of 2020.

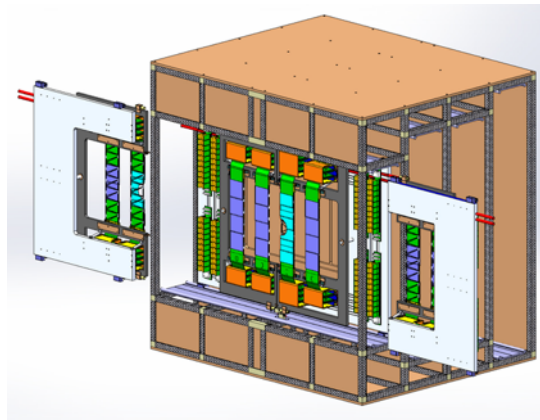


*Fig. 2.2.2.17. STS Mainframe*

The power dissipated by the electronics inside the STS box is estimated to be of the order of 15 kW. Most of this thermal power comes from the front-end electronics. Since the electronics has a wider temperature range for its operation, an absolute temperature specification for the ASICs is demanded mainly by the operating temperature of the sensors. In order to avoid excessive temperature gradients inside the STS box it is suggested to choose the operating temperature of electronics close to this level. The generated heat needs to be evacuated by the liquid cooling system. The total power dissipated by one FEB is on the level of 12 W. Since the size of the PCB is limited, it is important to provide a good thermal interface between the surface-mounted readout electronics and the heat exchanger. Each ASIC is glued to the PCB with a thermal and electrically conductive glue. To reduce thermal resistance of the PCB a Thermal Vias is used for each ASIC. The bottom side of the FEB is glued with a thermal conductive epoxy film to the aluminum fin of “L”

shape. All fins are mounted to the base plate of the FEB box, which is installed on the heat exchanger (Fig. 2.2.2.18). The heat exchanger is cooled by 157exed heat transfer fluid. Thermal Interface Materials (TIMs) are used to reduce heat resistance between each part of the thermal path.

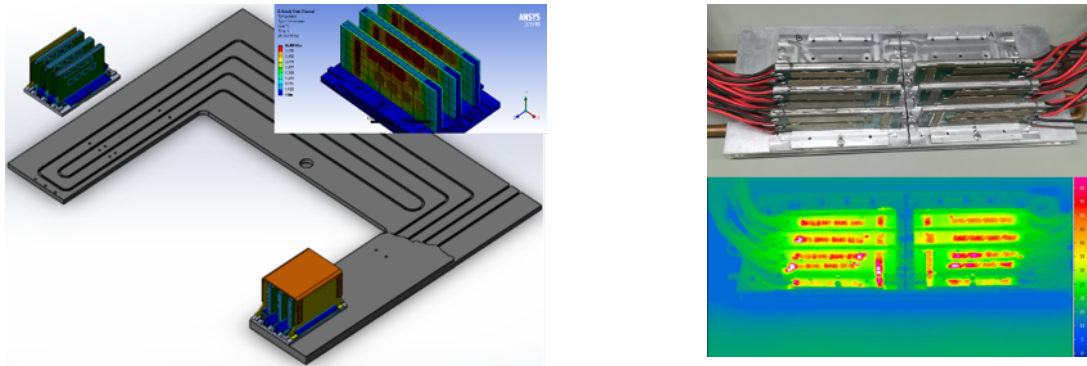


*Fig. 2.2.2.18. Schematic view of the thermal connection between front-end electronics and 157exed fluid cooled heat exchanger(left) and thermal prototypes of two FEB boxes as a test bench for different TIMs (right)*

The design of the FEB box is finished, several boxes were produced and now are being tested. Different types of materials of the thermal fin and TIMs were tested in 2019. The configuration of the thermal interface was finalized in the end of 2019. A prototype of the heat exchanger for one quarter of the first station was produced at Minsk and tested. Two 14 kW chillers produced by ATC were delivered in 2015 and used for these tests.

#### **2.2.2.2. Forward Silicon Detectors**

The major directions of the workplan for the development of the forward silicon detectors:

1. Design and development of three 2-coordinate planes based on Silicon Detectors for Forward Silicon Tracking Detectors.
2. Design and development of a coordinate plane based on a Silicon Detector for a Multiplicity trigger system.
3. Design and development of three 2-coordinate planes based on Silicon Detectors for a beam tracker placed inside the beam pipe in front of the target.
4. Design and development of two 2-coordinate planes based on Silicon Detectors for a beam profilometer placed inside the beam pipe in front of the target.

1. Development of three 2-coordinate planes for Forward Silicon Tracking Detectors based on Silicon Detector Modules consisted of Double-sided Silicon Strip Detectors (DSSD). Each side of the Silicon Detector Module has 640 strips. The Silicon Detector Modules have been designed for 2 years (2016-2017) in LHEP JINR. Each

module consists of two Silicon Detectors, two integrated circuits of Pitch Adapters (PA-640) for electrical decoupling of front-end electronics (FEE) inputs on each side of the detector, two FEE boards (each board has 640 channels) and low-mass mechanical support frames. All the components are commercially available. The module assembling can be done in the LHEP laboratory conditions. To manufacture silicon detectors, which are designed by joint efforts of JINR-LHEP and NIIMV (Zelenograd), float-zone (FZ) silicon wafers have been purchased by JINR in the SiMat company (Germany) and I to NIIMV to produce the silicon detectors. The detectors have the size of (63×63×0.3) mm<sup>3</sup> and consist of 640 strips on both p<sup>+</sup> and n<sup>+</sup> sides with a 95 and 103 μm pitch, respectively. Main parameters of all manufactured detectors have been measured at NIIMV as an output control and at LHEP as an input control (Fig. 2.2.2.19).

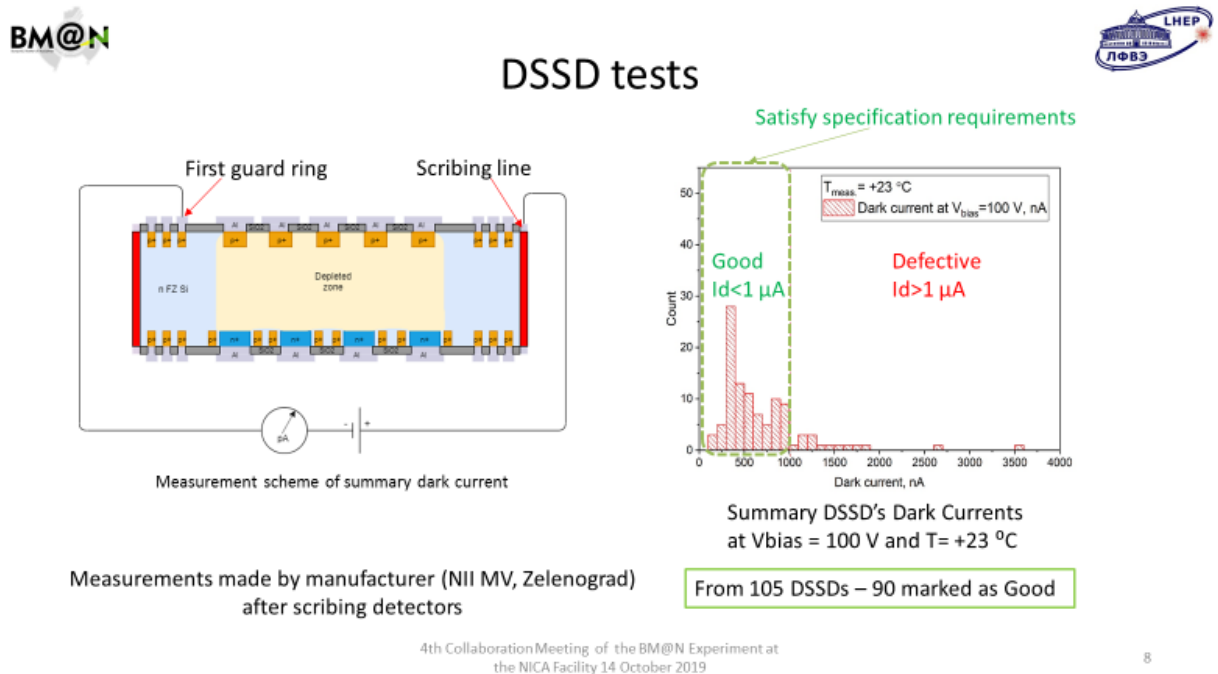
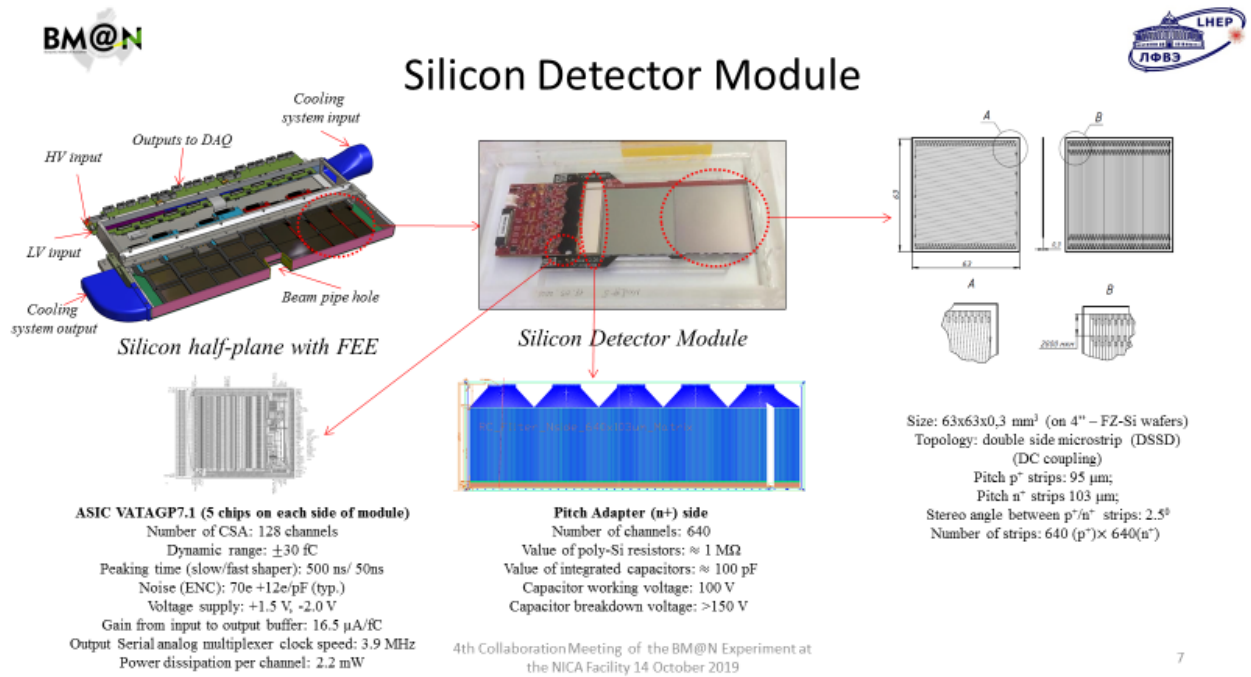


Fig. 2.2.2.19. Measurement scheme of the DSSD total dark current (left; dark current summary histogram for 105 DSSDs at  $V_{bias}=100$  V and  $T= +23$  °C

Main controlled parameters are a current-voltage characteristic (I-V) and a capacitance-voltage characteristic (C-V). A detector is marked as good for assembling if its summary dark current is less than 1000 nA at a bias voltage of 150 V and a temperature of +20°C. The results of the output control show that the yield of good detectors is between (50÷70) % for double-sided detectors. The DSSD manufacturing technology is one of the most difficult to accomplish because the technological processes (photolithography, doping, metallization, etc.) are carried out separately on two sides of the silicon wafers. To produce three 2-coordinate planes need for the “basic configuration” of the BN@N setup in the end of 2020, 42 two-

coordinate modules (Fig. 2.2.2.20) with the sensitive area of each module of  $120 \times 60 \text{ mm}^2$  are required. For this purpose, contracts for the supply of 85 DSSDs and 84 pitch adapters were signed with NIMV in 2018 and executed in 2019.



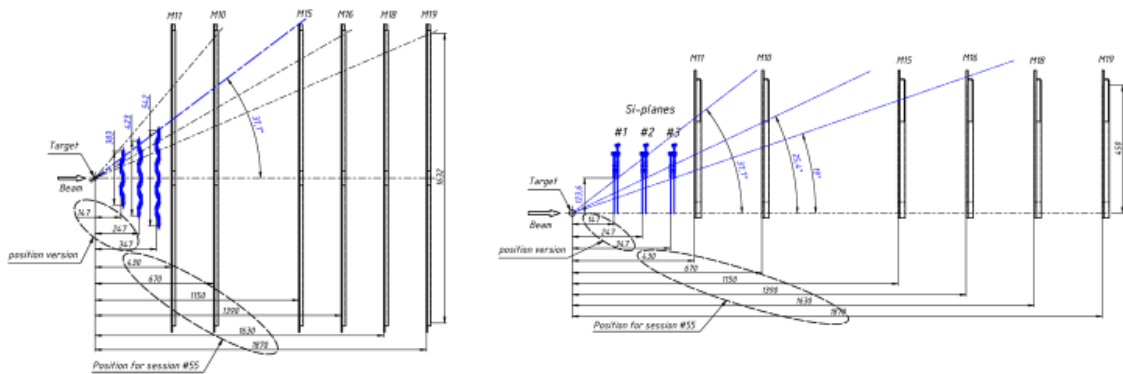
*Fig. 2.2.2.20. Silicon Detector Module components and an assembled coordinate half-plane consisting of 9 modules(left)*

The DSSD topology with a DC coupling doesn't contain integral resistors and capacitors (RC). Therefore, external R, C components are required to supply a bias voltage to each strip and to decouple electrically the DC current from the electronic inputs. This role is performed by a Pitch Adapter (PA-640). The PA modules are made on sapphire plates with an epitaxial layer of silicon (SOI) jointly by ZNTC (Zelenograd Nanotechnology Center) and the NIIMV company. PA-640 are required to sustain electric strength of 640 integrated capacitors with a 120 pF capacitance value. PA-640 has a low leakage current (less than 10 pA at 100 V per capacitor) and a breakdown voltage of 150 V, which is equal to a 3 MV/cm electric field strength. The resistivity of integrated polysilicon resistors is 1 Mohm. The aluminum metallization topology of PA-640 is fully compatible to ASIC's bonding pads. The front-end electronics is based on commercially available ASICs VATAGP7.1 (IDEAS, Norway): 400 ASICs have been delivered to JINR; 100 FEE PCBs have been produced by the PCB technology company; the MELT company has assembled ASICs to PCBs. 5 ASICs are mounted on each PCB to read-out signals from 640 detector strips. The main requirement for the "basic configuration" of the BM@N setup is the presence of a vacuum beam pipe with a diameter of 50 mm in the zone of the silicon coordinate planes. To meet this requirement, each silicon plane consists of

2 half-planes divided symmetrically relative to the beam pipe axis and has free space for the passage of a beam pipe with the diameter of 50 mm. This configuration allows one to assembly/disassembly the silicon planes independently from the beam pipe installation. The positions and a general view of assembled 6 half-planes are shown in Fig. 2.2.2.21, 2.2.2.22 and 2.2.2.23.



## New Forward Silicon Detectors Configuration (BM@N – 2020)



Positions of Si-planes on the beam-channel XZ (left) and YZ (right)

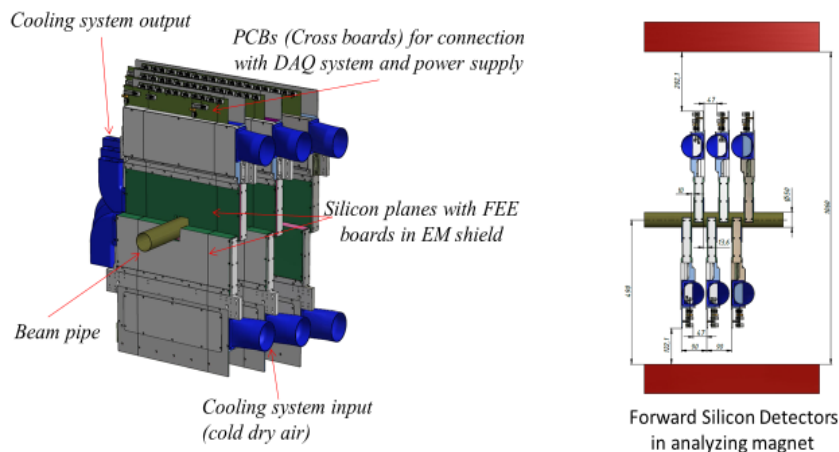
4th Collaboration Meeting of the BM@N Experiment at  
the NICA Facility 14 October 2019

5

Fig. 2.2.2.21. Positions of Silicon Detector components and assembled coordinate half-planes.



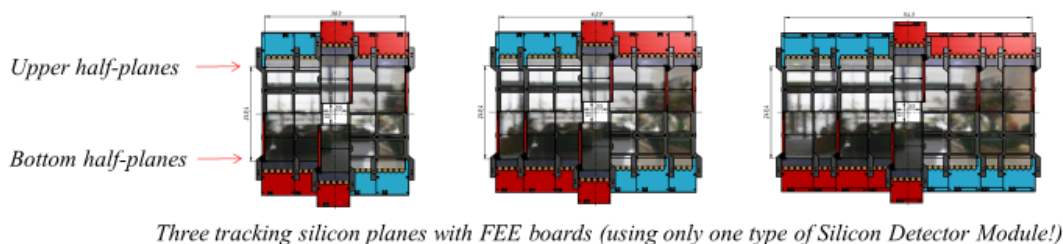
## New Forward Silicon Detectors Configuration (BM@N – 2020)



4th Collaboration Meeting of the BM@N Experiment at  
the NICA Facility 14 October 2019

4

Fig. 2.2.2.22. General view of Forward Silicon Detectors (without cables and cooling system pipes) around the beam pipe.



Number of	First Plane	Second Plane	Third Plane	Total
DSSDs	20	28	36	84
ASICs	100	140	180	420
PAs	20	28	36	84
FEE PCBs	20	28	36	84
Channels	12800	17920	23040	53760
Area, m <sup>2</sup>	0.073	0.102	0.132	0.307

4th Collaboration Meeting of the BM@N Experiment at  
the NICA Facility 14 October 2019

6

*Fig. 2.2.2.23. Design of three silicon planes (without electromagnetic shield) with the beam pipe holes of 51x51 mm<sup>2</sup>.*

The design of a first multiplicity trigger plane was based on the silicon detector with 64 azimuthal strips, which was used in the BM@N argon and krypton beam runs in March-April 2018. The multiplicity trigger plane had a ring shape and was made on one silicon wafer with an external diameter of 100 mm and an internal diameter of 28 mm. The hole in the center of the wafer was cut by a laser. This configuration cannot be used with the beam pipe of 50 mm. For the “basic configuration” of the BM@N setup a new multiplicity trigger detector has been developed with the same number of strips (64 strips to use the existing FEE boards) and a 50 mm diameter hole for the beam pipe. The new design is based on two symmetric half-planes, that simplifies the procedure of assembling of the multiplicity trigger plane around the beam pipe. A general view of the detector half-planes with read-out boards is shown in Fig. 2.2.2.24 and 2.2.2.25. Each half-plane consists of 4 detectors (total number of strips is 32), each detector has a shape of an isosceles trapezoid and consists of 8 azimuthal strips located at angles with an interval of 5.6°. After assembly of 8 such detectors an octagon is formed on the inner radius, which fits to the 50 mm diameter of the beam pipe. The outer diameter of the circumscribed circle is 186 mm. 16 trapezoid detectors for the multiplicity trigger plane were developed and manufactured in 2019 according to the contract between JINR and NIIMV (Zelenograd).

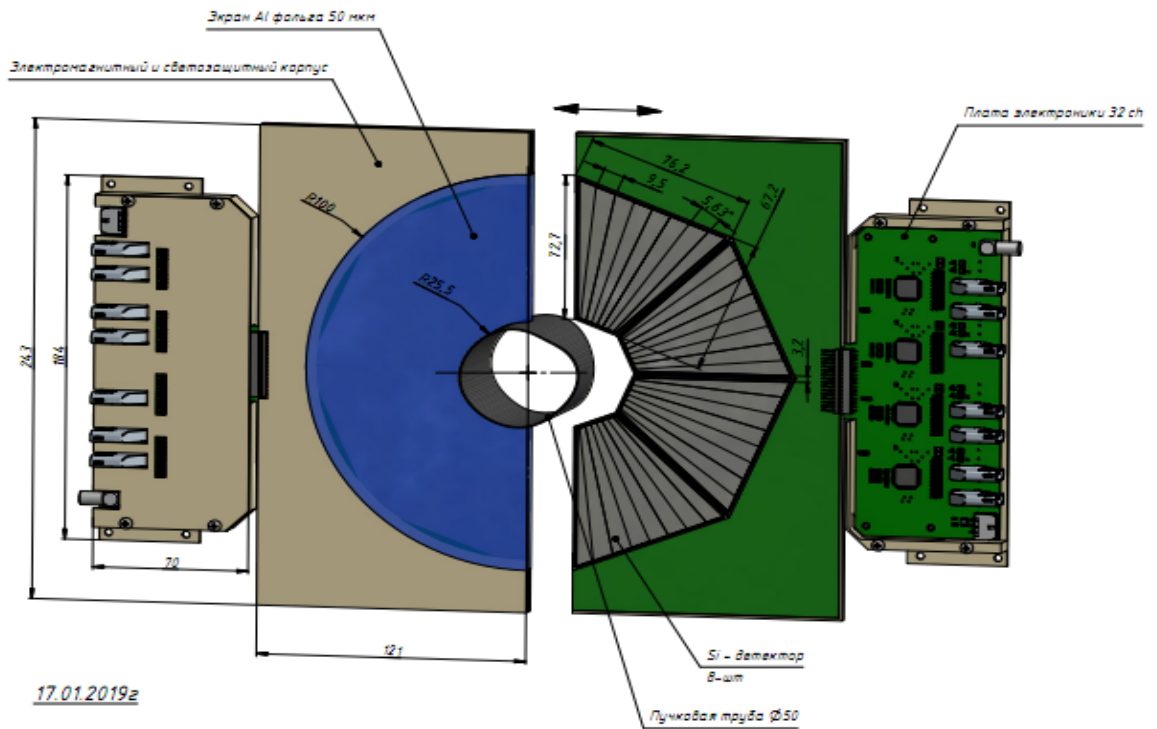


Fig. 2.2.2.24. A general view of the multiplicity trigger plane consisting of 2 half-planes (8 silicon strip trapezoid detectors) and 2 FEE boards.

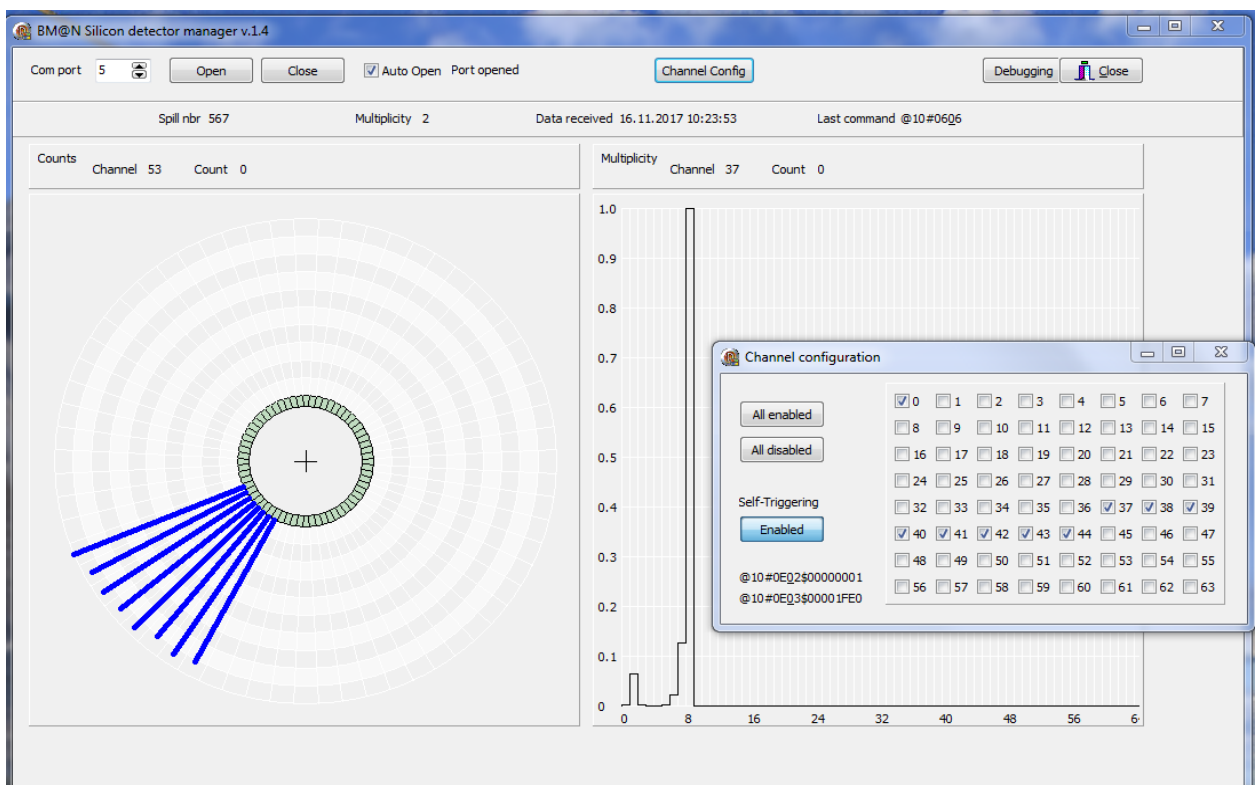


Fig. 2.2.2.25. Display of test events with the multiplicity equals to 8.

3. For the “basic configuration” of the BM@N setup, a decision was made to construct a beam tracker in front of the target to determine the (X, Y) coordinates and angles of the incident ion in the interaction point. Due to possible radiation

damage of detectors by heavy ions, various versions of detector materials have been considered (C, GaAs, SiC, Si). The diamond and silicon carbide detectors are the most radiation hard, but they are of little availability and have a small size. Based on the analysis of the data on radiation damage in silicon, the expected size of the beam of 20-30 mm and the initial intensity of the gold ion beam of about  $10^6 \text{ sec}^{-1}$ , it was decided to use thin (175  $\mu\text{m}$ ) double-sided silicon detector with the size of 63x63  $\text{mm}^2$  to cover the whole beam spot by the sensitive area of the detector. To justify this decision, the following arguments were taken into account: the signal from ionization of 4 AGeV gold ions is 6400 times larger than the signal from m.i.p. (Fig. 2.2.2.26). Therefore, thin detectors have been chosen to reduce effects of radiation damage (loss of the signal amplitude and increase of the dark current). The FZ-Si wafers with a thickness of 100  $\mu\text{m}$  and diameter of 100 mm, are commercially available, But the NIIMV company agreed to develop and manufacture thin silicon detectors using wafers with a thickness not less than 150  $\mu\text{m}$ . Thin detectors have less power dissipation, because the depletion voltage is proportional to the squared thickness of the detector, and current is linearly proportional to the thickness. Therefore detectors with a 2 times smaller thickness produce an 8 times smaller power dissipation. It's also necessary to control the power dissipation of detectors damaged by hard radiation, because of bad detector cooling in vacuum. Gold ions generate a huge signal in the silicon detector. Therefore a dark current noise and (5 ÷ 10)% decrease of the signal amplitude are less critical than the thermal breakdown of the detector. At fluences of gold ion beam greater than  $10^{13} \text{ cm}^{-2}$  which correspond to continuous irradiation of detectors for 4 months with the intensity of  $10^6 \text{ sec}^{-1}$ , the detectors will be replaced if it is necessary. For this purpose, a contract with the NIIVM company for a development of 15 DSSDs (128×128 strips and 175  $\mu\text{m}$  thickness) for the beam tracker and 10 DSSDs (32×32 strips and 175  $\mu\text{m}$  thickness) for the beam profilometer was signed in 2018 and was executed in 2019. The design of a coordinate plane based on thin silicon detectors, integrated into the beam pipe is shown in Fig. 2.2.2.27 and 2.2.2.28. An important part of the heavy ions beam tracker design is the choice of a suitable FEE ASIC. A special requirement for this chip is to register a large signal from a heavy ion at a high event rate. This requires a wide dynamic range (up to 20 pC), a short peaking time (less than 200 ns) for the pile-up rejection, at least 64 channels per chip, a possibility of the sample-and-hold mode from an external “trigger” and a multiplexed output for compatibility with the DAQ system of the BM@N setup.

Ionization energy loss and signal amplitude of Silicon Detector/175 $\mu$ m from Kr and Au ions with E = 4A GeV

**Au:**  $\Delta E = 452 \text{ MeV}/175\mu\text{m}/\text{Si}$ , signal (charge)=20 pC, current (20ns)=  $1 \times 10^{-3} \text{ A}$

**Kr:**  $\Delta E = 92 \text{ MeV}/175\mu\text{m}/\text{Si}$ , signal (charge)=4 pC, current (20ns)=  $0.2 \times 10^{-3} \text{ A}$

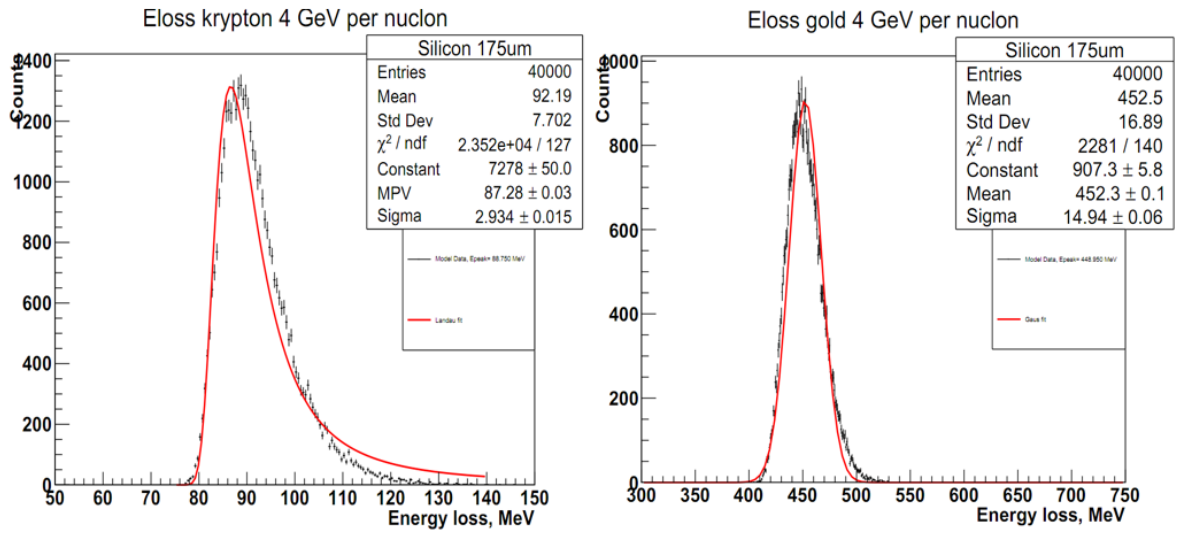


Fig. 2.2.2.26. Geant4 simulation of energy loss on ionization in a silicon detector with a thickness of 175  $\mu\text{m}$  for Kr<sup>36+</sup> (left) and Au<sup>79+</sup> (right) ions with an energy of 4A GeV.

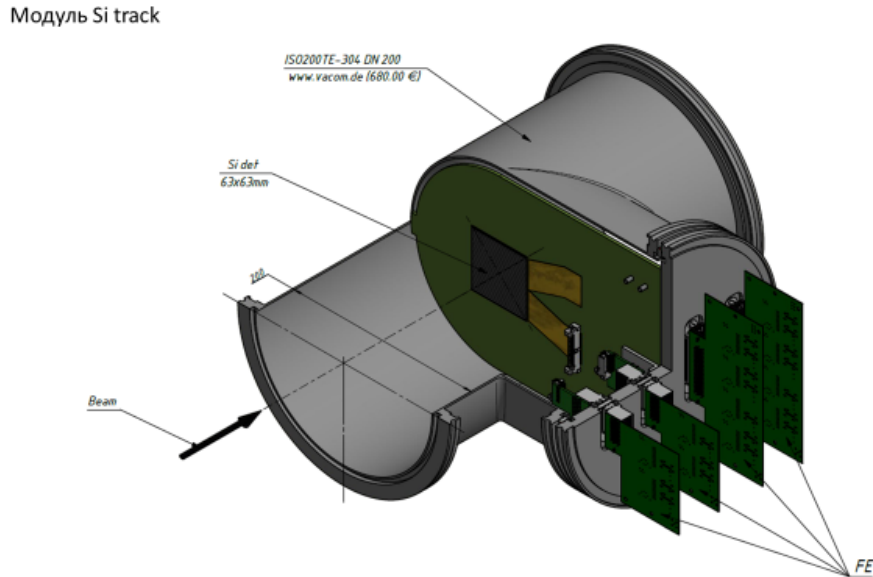
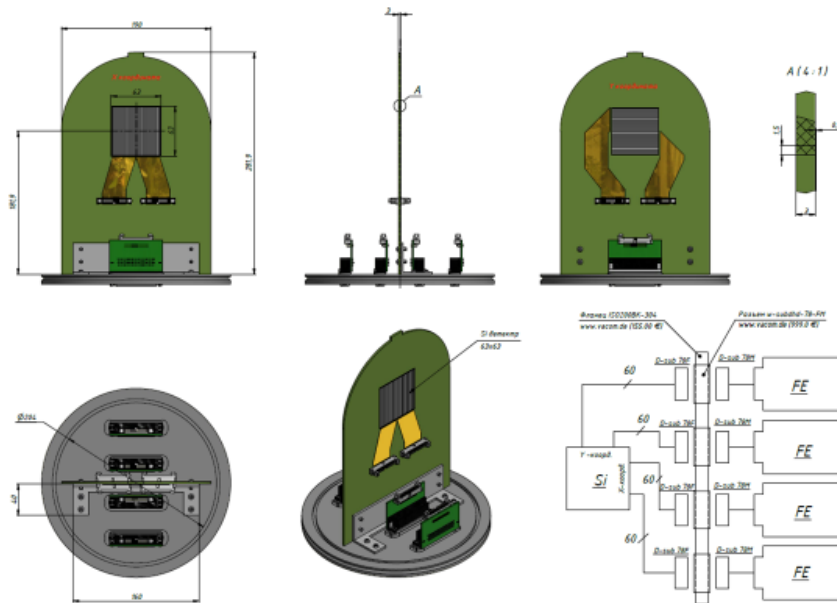


Fig. 2.2.2.27. Beam tracker position inside the vacuum station and FEE boards at the outer vacuum flange.



*Fig. 2.2.2.28. Beam tracker coordinate plane assembled at the outer vacuum flange.*

The ASIC chip of the IDEAS company VATA64-HDR16 was chosen, as it fits to the parameter requirements. The beam tracker based on this ASIC chip is being developed and will be installed onto the vacuum station flange incorporated into the beam pipe structure. The chip will be connected via vacuum multi-pin connectors with 256 detector strips. Twenty VATA64-HDR16 chips were purchased for the beam tracker,

The beam profilometer based on DSSD will consist of two planes. The distance between two planes is approximately 3m. The second plane is placed as close as possible to the target, but in front of the beam counter (BC1). The size of silicon detectors is  $60 \times 60 \text{ mm}^2$ , the thickness is  $175 \text{ }\mu\text{m}$ . Each detector has  $(32 \times 32)$  strips. The construction of the profilometer planes will be similar to the beam tracker planes, but their signals will be readout via an autonomous measurement system independent from the BM@N DAQ System. The mechanical construction of the profilometer planes has to be sophisticated due to need for automatic removal of these two planes from the beam zone after the beam tuning. Also, we have to design two versions of FEE – for light ions (to detect C ions) and for heavy ions (starting from Ar). ASIC VA163 will be used to measure ion beams with low charges in the range up to  $0.7 \text{ pC}$  per spill and ASIC VA32HDR11 will be used for beams with the ion charge range up to  $30 \text{ pC}$  per spill. This will allow us to work with profilometers at the initial stage of the carbon beam tuning. It will be necessary to change one type of FEE by another to provide proper work of the profilometer after switching from light to heavy ions. FEE boards have identical connectors and located on the flange

outside of the vacuum station. A profilometer prototype based on DSSD was developed to perform an autonomous measurement of beam profiles, display information in the form of a two-dimensional image and amplitude information. The profilometer prototype design and test results are presented in Fig. 2.2.2.29 and Fig. 2.2.2.30.

## Si beam profilometer prototype

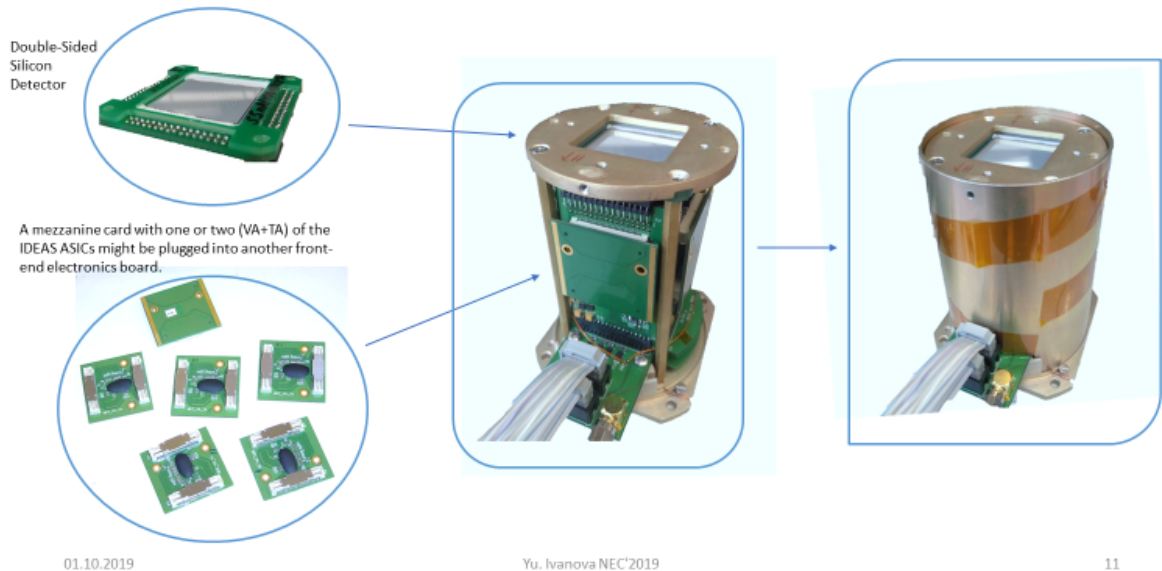


Fig. 2.2.2.29. Profilometer prototype based on Double-sided Silicon Strip Detector.

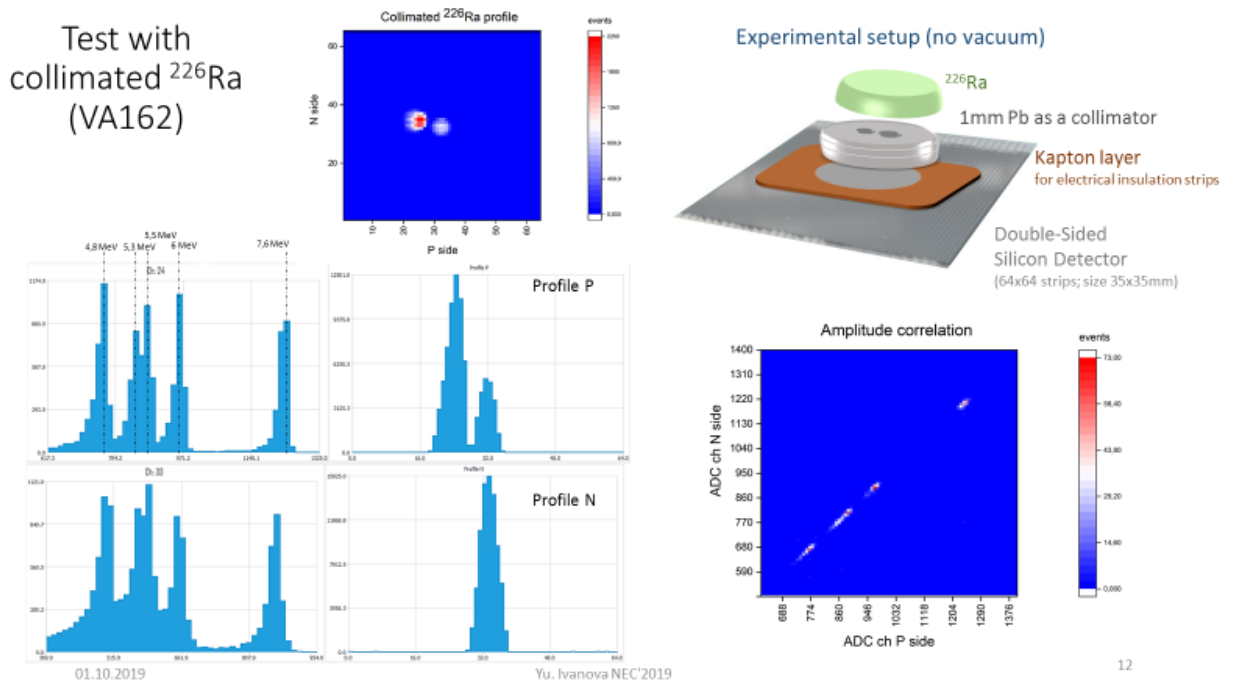


Fig. 2.2.2.30. Test results of the profilometer prototype with a source of alpha particles.

### 2.2.2.3. GEM central tracking system

Central tracking system of the BM@N experiment will provide precise momentum measurements of the cascade decays products of multi-strange hyperons and hyper-nuclei produced in central Au-Au collisions. All physics measurements will be performed in conditions of high beam intensities in collisions with large multiplicity of charged particles. This requires the use of detectors with the capacity to resolve multiple tracks produced at very high rate. The basic requirements for the tracking system are: capability of stable operation in conditions of high radiation loadings up to  $10^5$  Hz/cm<sup>2</sup>, high spatial and momentum resolution, geometrical efficiency better than 95%, maximum possible geometrical acceptance within the BM@N experiment dimension, operation at a 0.8 T magnetic field. Detectors based on the GEM technology possess all the mentioned characteristics combined with the capability of stable operation in a strong magnetic field up to 1.5T. Detectors of this kind are already widely used in such experiments as TOTEM, COMPASS, BNL and are planned for the CMS Muon Endcap upgrade. Production and assembly processes of the large size (up to 2m long) GEM-based detectors are well developed at CERN PH DT and MPT Workshop. Since non-glue «foil-stretching» technology is involved, one chamber can be assembled in several hours and easily re-opened for technical service if needed. For this reason, two coordinate triple GEM detectors were chosen for the central part of the BM@N tracking system, which is located inside the analyzing magnet downstream of the target.

Triple-GEM configuration performs low probability of discharge propagation and stable operation at gains above  $10^5$ . BM@N GEM detectors consist of three multipliers, with a drift gap of 3 mm, first transfer gap of 2.5 mm, second transfer gap of 2 mm and an induction gap of 1.5 mm, as shown in Fig. 2.2.2.31a. BM@N GEM tracking system final setup will consist of three types of the GEM chambers:  $660 \times 412 \text{ mm}^2$ ,  $1632 \times 450 \text{ mm}^2$  (Fig. 2.2.2.31b) and  $1632 \times 390 \text{ mm}^2$ . In order not to be flooded by the primary non-interacting heavy ion beam particles and near halo there is a hole in the central region of a big GEM detector. Because of large multiplicity near the beam line, readout layer is divided into outer and inner (hot) zones for all types of detectors.

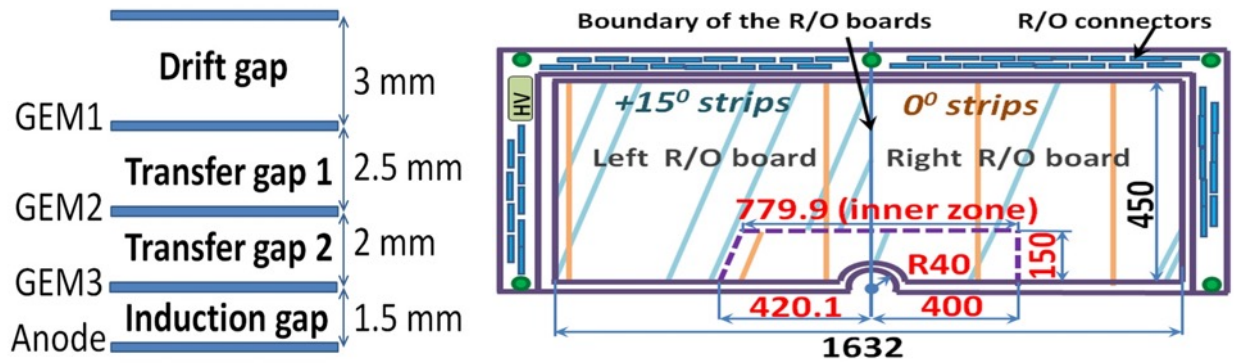


Fig. 2.2.2.31. a) Schematic cross section of BM@N triple GEM detector b) Schematic view of the  $1632 \times 450 \text{ mm}^2$  GEM detector.

Front-end electronics is based on the charge sensitive pre-amplifier chip VA162 and VA163 (IDEAS). The chip has 32 channels. Each channel contains a charge-sensitive preamplifier, a shaper with  $2 \mu\text{s}$  (VA-162 chip) and  $0.5 \mu\text{s}$  (VA-163 chip) peaking time and a sample-hold circuit. An analog multiplexer with 32 inputs allows one to perform serial read-out channel by channel. The chip can be used to amplify and read negative and positive charges in the range from  $-1.5 \text{ pC}$  to  $+1.5 \text{ pC}$ . The equivalent noise charge is  $1900e$  without load, and  $2000e$  at  $50 \text{ pF}$  input load. The integral linearity is 1% and 3% for positive and negative charge, respectively.

The multiplexed data from each board are transmitted through 13 m of twisted pair flat cable to the 12-bit analog-to-digital converter (ADC) readout by the BM@N data acquisition system.

The VA162 and VA163 chips are produced by IDEAS - Integrated Detector Electronics AS (Norway). The ASICs has 32 input channels. Each read out card includes four chips, which are installed, bonded and filled with black compound. Thus, we have 128 input analog channels read-out board (Fig. 2.2.2.32).



Fig. 2.2.2.32. 128 channel read-out board. Front and back side view.

GEM chambers can be operated with Ar(70)/CO<sub>2</sub>(30), Ar(90)/C<sub>4</sub>H<sub>10</sub>(10), Ar(80)/C<sub>4</sub>H<sub>10</sub>(20) gas mixtures. The gas system consists of two parts: 1) the mixer system which delivers quantity, mixing ratio and pressure conditioning to downstream elements; 2) the distribution system, which delivers the gas in well defined quantities to the individual detectors. The gas system is produced by Ltd «Eltochpribor» (Zelenograd, Russia).

Seven needed potentials are distributed to the GEM chamber through the HV divider. Such scheme of HV supply is very convenient, as only one channel of HV power supply is needed to power the chamber via a single cable. Thus, to power final GEM setup of 14 GEM chambers with the voltage of approximately -3kV, a 14-channel high-voltage system is required. For GEM HV power system two 12 channel CAEN AG550DN modules in CAEN SY5527lc\_p create are used.

The LV power system is based on four NTN 350-6,5 and six NTN 700-6,5 LV modules. NTN low voltage module has adapter for remote control via Ethernet connection. It is possible to use Ethernet control to integrate the low voltage source to the BM@N Slow Control System database.

First beam tests of five 660×412mm<sup>2</sup> and two 1632×450mm<sup>2</sup> GEM chambers were performed at BM@N technical runs in 2016 and 2017 years with the deuteron and carbon beams at the Nuclotron. The GEM detectors were arranged in 6 planes as it is shown in Fig. 2.2.2.33. The left and right parts of the 1632×450mm<sup>2</sup> GEM detectors were treated as independent detectors. The main goal of the tests was to study the performance of the GEM detectors and the FEE and readout electronics as a part of the BM@N experimental setup. The GEM detectors were filled with the flowed Ar(90)/C<sub>4</sub>H<sub>10</sub>(10) gas mixture and equipped with the VA162 based electronics. The measurements were made within the magnetic field varied from 0 up to 0.9. The tracks of charged particles were reconstructed and track detection efficiency of the GEM chambers was calculated (estimated average efficiency ~ 95%). Coordinate and momentum resolutions were calculated using data, collected without target and with magnetic field of 0.79 T. Gaussian fit of hit residuals distribution gives the standard deviation of 670 μm, which conform to the Monte-Carlo simulation.

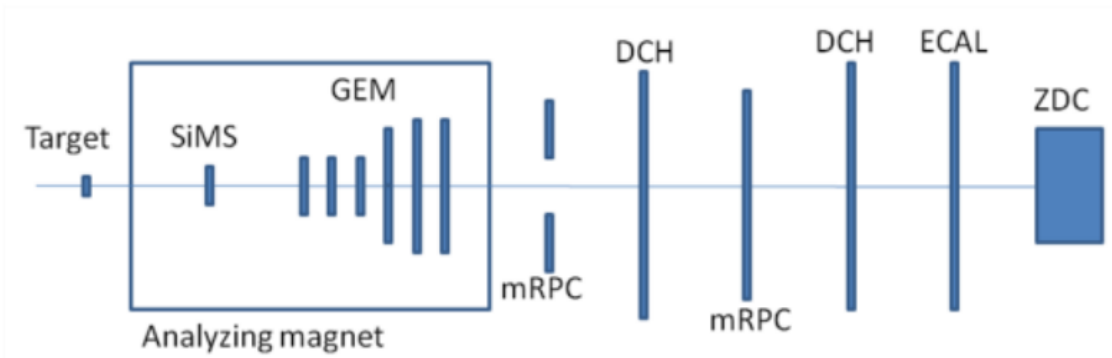


*Fig. 2.2.2.33. Schematic view of the BM@N experimental setup in the deuteron and carbon beam runs*

Momentum resolution for deuteron beam (9.7 GeV/c) is  $\sim 9\%$ . The resolution for protons from deuteron defragmentation is  $\sim 6\%$ .

Beam tests of seven  $1632 \times 450 \text{ mm}^2$  GEM chambers were performed in 2017 and 2018 years with the carbon, argon and krypton beams (Fig. 2.2.2.34). The GEM detectors were filled with the flowed Ar(80)/C<sub>4</sub>H<sub>10</sub>(20) gas mixture to increase the avalanche electrons velocity. The value of the electric field in drift gap was also increased to 1.5 kV/cm. The detectors were equipped with the faster VA163 based electronics. Gaussian fit of hit residuals distribution gives 3 times better standard deviation of 230  $\mu\text{m}$ .



*Fig. 2.2.2.34. GEM chambers integrated into BM@N experimental setup*

Four  $660 \times 412 \text{ mm}^2$  detectors were involved in SRC experiment for identification of correlated protons in 2018 year. The positions of GEM detectors in SRC experimental setup are shown on Fig. 2.2.2.35.

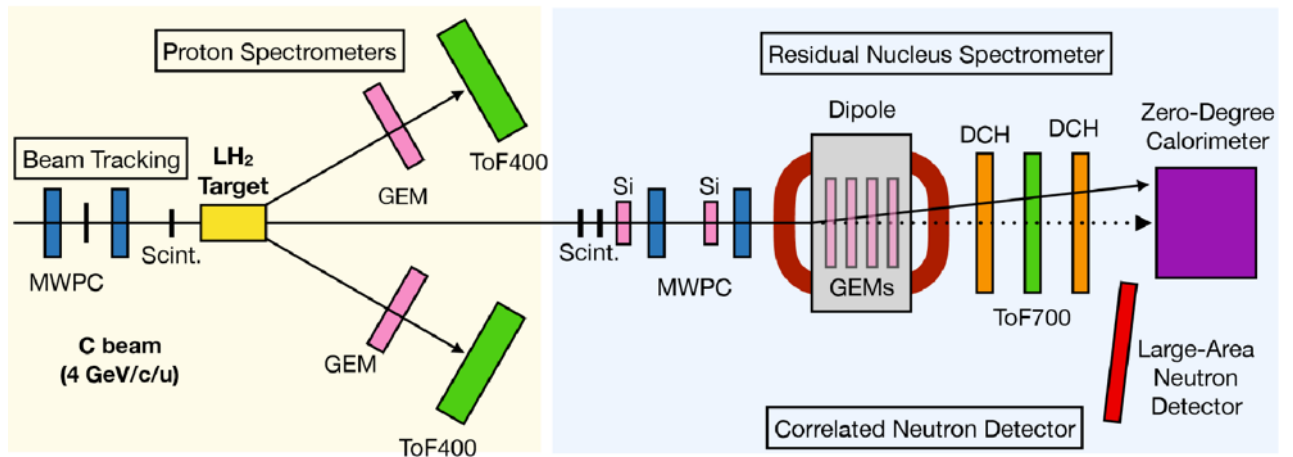


*Fig. 2.2.2.35. Schematic view of the SRC@BMN experimental setup*

The final configuration of the central tracking system consists of 14 GEM detectors (Fig. 2.2.2.36):

- 7 GEM detectors of the size  $1632 \times 450 \text{ mm}^2$  – above the vacuum beam pipe;
- 7 GEM detectors of the size  $1632 \times 390 \text{ mm}^2$  – below the vacuum beam pipe.

Since the magnetic field is perpendicular to the electric field direction inside the GEM chamber, electron avalanche in the gas gaps drifts at some angle (the Lorentz angle) with respect to the normal to the readout board. The electron cloud drift results in a displacement of the collected charge, which is called Lorentz shift. The shift value depends on the field strength and gas properties. To eliminate a systematic shift of the reconstructed tracks in the magnetic field, GEM detectors are oriented in alternating order so that the electric field for the neighboring planes has opposite directions (see Fig. 2.2.2.36).

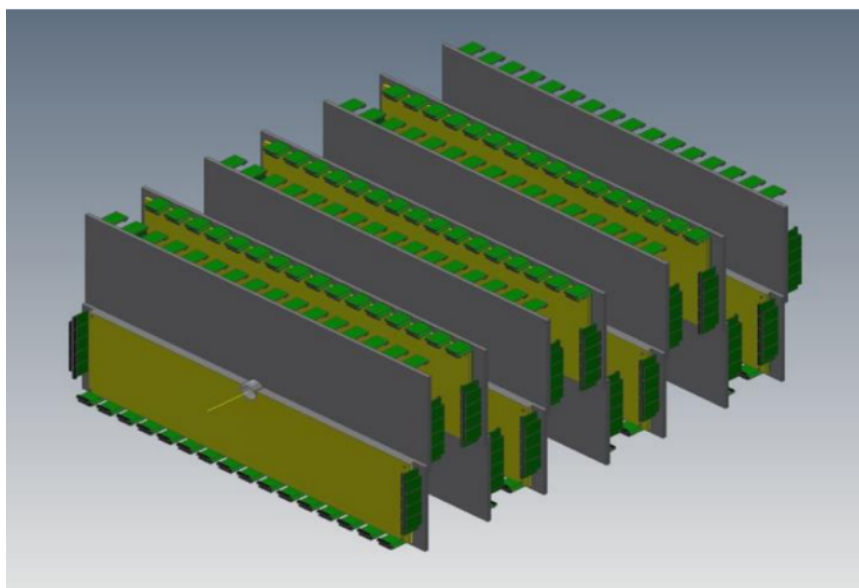


*Fig. 2.2.2.36. A technical drawing of the BM@N GEM tracking system.*

The full configuration with 14 GEM detectors (~90000 readout channels) is planned to be integrated in the BM@N experimental setup at the middle of 2020 with the electronics based on VA-163 chips.

Seven top GEM detectors have been studied using d, C, Ar, Kr beams of the Nuclotron accelerator. Three bottom GEM detectors of the BM@N central tracking system have been assembled and tested using cosmic rays. The last four bottom GEM detectors were assembled at the end of 2019 at CERN DT and MPT Workshop. Seven GEM chambers with the size of 1632×450 mm<sup>2</sup> are currently the biggest GEM detectors in the world.

The development of the mechanics design to provide GEM planes precise installation inside the magnet will be performed by Ltd «Pelcom-Dubna» (Dubna, Russia) till the end of 2019. The production will be performed till 04.2020.

For heavy ion program (up to Au-Au collisions) with the beam intensities up to few 10<sup>6</sup> Hz GEM electronics is to be upgraded to faster. VMM3a and TIGER ASICs are considered as possible candidates. First tests of FEE based on both chips are already started. Before 2022 new electronics will be integrated into the BM@N experimental setup.

#### **2.2.2.4. Outer tracker based on DCH chambers**

The purpose of the outer tracker is to provide link between tracks measured in the central tracker and hits in the ToF detectors. It consists of big drift chambers which will be complemented with CSC detectors (cathode strip chambers) to perform track measurements in Au+Au collisions.

The Drift Chamber (DCH) consists of 4 double coordinate planes with the following parameters: the wire inclination angles of 0, 90, ±45°, the wire pitch of 10 mm, the outer dimensions of the sensitive area of  $Y_{\text{out}} \pm 1.2$  m,  $X_{\text{out}} \pm 1.2$  m, the beam hole radius of  $R_{\text{min}} = 10$  cm, 256 wires per coordinate plane, 2048 wires per chamber. The outer view of the DCH chambers is shown in Fig. 2.2.2.37. The performance of the DCH chambers to measure the angular distribution and momentum of the deuteron beam in the first technical run are illustrated in Fig. 2.2.2.38 and 2.2.2.39.



Fig. 2.2.2.37. Two DCH chambers installed in the BM@N experimental zone.

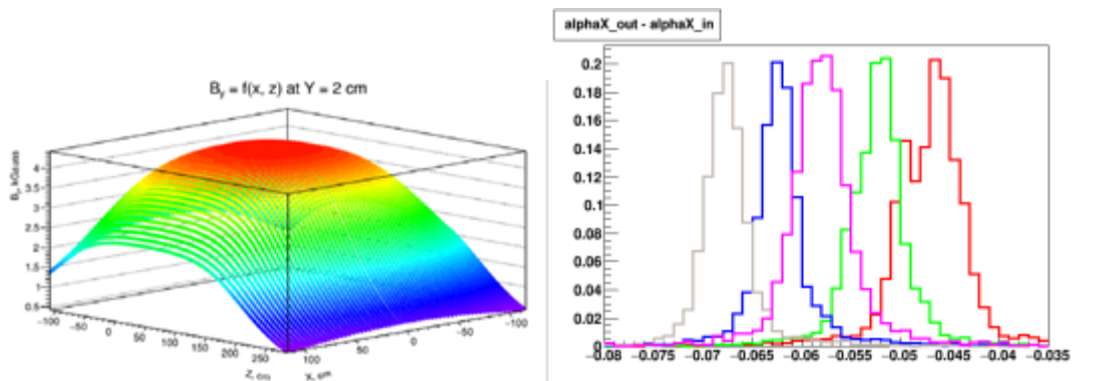


Fig. 2.2.2.38. Right plot: map of the vertical component of the magnetic field of the spectrometric magnet measured at the horizontal plane of the beam. Left plot: angular distributions of the deflected deuteron beam measured in two DCH chambers for different values of the magnetic field.

In 2014 - 2016 the Drift Chambers (DCH 1,2) were installed into the experimental setup in full configuration (4096 channels):

- 1) HV and Low voltage supplies: MPOD Mini crate with ISEQ EHS F 040n HV module (16 channels) and 3 Low voltage modules (+5V) MPV 8008 D (Fig. 2.2.2.40, left);
- 2) Low voltage supplies (8 pieces, -5V): FuG Elektronik NLN 700 - 6.5 (Fig. 2.2.2.40, right);
- 3) VME crates (4 pieces) with readout modules (64 pieces) TDC64V (Fig. 2.2.2.41).

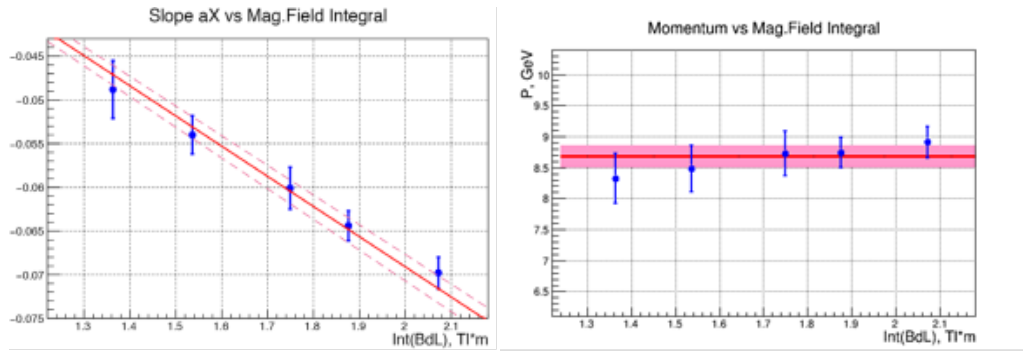


Fig. 2.2.2.39. Right plot: mean angles (radians) and r.m.s. of the deflected deuteron beam measured in two DCH chambers for different values of the magnetic field integral. The red and dash lines show the nominal value of the momentum of the deuteron beam of 8.68 GeV/c with the accelerator momentum uncertainty of 2%. Right plot: momentum of the deuteron beam calculated from the angular distributions for different values of the magnetic field integral. The red line with the colored error bar gives the nominal value of the beam momentum with the accelerator uncertainty.

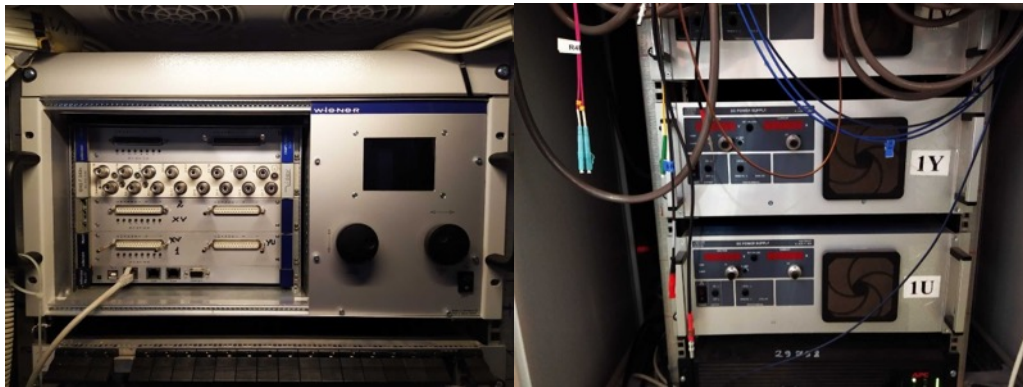


Fig. 2.2.2.40. Left - MPOD Mini crate with HV and LV modules; right - Low voltage supplies FuG Elektronik



Fig. 2.2.2.41. VME crates with readout modules TDC64V.

Due to the high occupancy of the DCH chambers in high multiplicity Au+Au collisions, the Drift Chambers will be supplemented by CSC detectors for experimental runs in 2020 and after.

### 2.2.2.5. Gas system for central and outer trackers

The gas system for the central and outer tracker was installed into the experimental setup in 2016 (Fig. 2.2.2.42).



Fig. 2.2.2.42. The gas system for central and outer tracker.

The gas system consists of two parts: 1) the mixer system which delivers a mixture of gases in a required ratio and pressure to downstream elements; 2) the distribution system, which delivers the gas in well defined quantities to the individual detectors.

The detector is supplied with a constant gas mixture with a precision better than 1%. Each primary gas line is equipped with a Mass Flow Controller to measure the flow of gas components with appropriate accuracy and is equipped with purifier cylinders. The gas from the mixer is distributed to the distribution rack. The major design criterion of the distribution system is to provide a uniform gas supply to each detector. The gas line for the central and outer trackers is shown on Fig. 2.2.2.43 and Fig. 2.2.2.44.

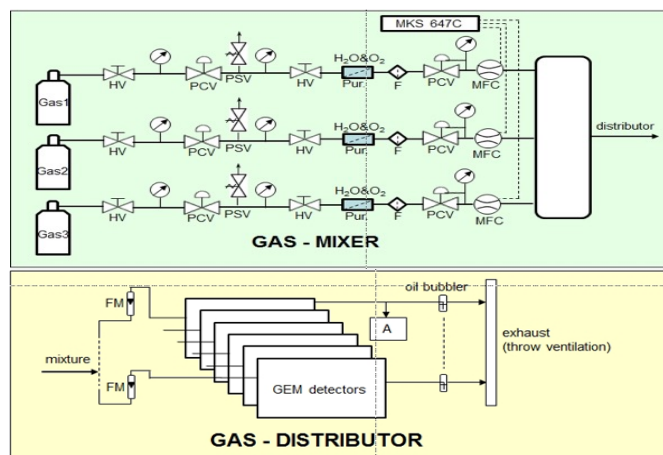


Fig. 2.2.2.43. The gas line for the central tracker. The layout of the mixer module: HV – on/off valve, PCV – pressure control (constant) valve, PSV – pressure safety valve, Pur. – Purifier (H<sub>2</sub>O and O<sub>2</sub>), F – filter, MFC – mass flow controller (MKS Instruments firm), MKS 647C – power supply and readout (MKS Instruments firm). Component layout of the distributor module: FM – flowmeter (manually flow adjustment), oil bubbler – pressure and air protection, A – oxygen analyzer.

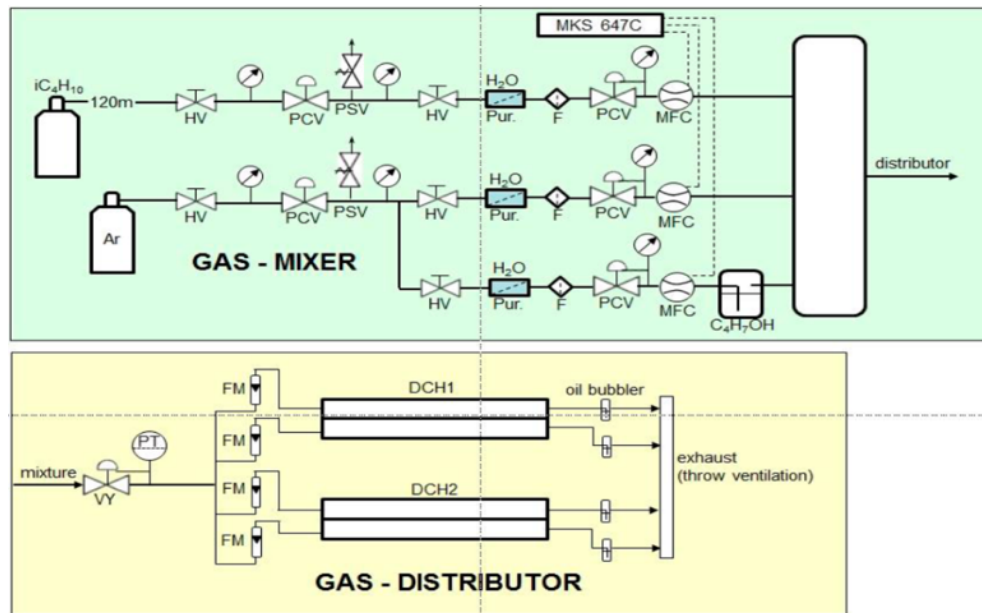


Fig. 2.2.2.44. The gas line for the outer tracker. The layout of the mixer module: HV – on/off valve, PCV – pressure control (constant) valve, PSV – pressure safety valve, Pur. – Purifier (H<sub>2</sub>O and O<sub>2</sub>), F – filter, MFC – mass flow controller (MKS Instruments firm), MKS 647C – power supply and readout (MKS Instruments firm). Component layout of the distributor module: FM – flowmeter (manually flow adjustment), oil bubbler – pressure and air protection.

Some modification of the gas system should be implemented in 2019 - 2020.

### 2.2.2.6. Outer tracking system based on CSC chambers

The full configuration of the outer tracking system for heavy ion program will consist of four planes of 1129×1065 mm<sup>2</sup> CSC (cathode strip chamber) and two planes of 2190×1453 mm<sup>2</sup> CSC. The CSC detectors are situated outside the magnetic field with the aim to make precise link to the tracks, reconstructed in the GEM detectors inside the analyzing magnet. Tracks refined in CSC are used to improve particles momentum reconstruction and to find corresponding hits in the time-of-flight systems ToF400 and ToF700.

The first CSC detector with the size of the active area of 1129×1065 mm<sup>2</sup> was designed and assembled at LHEP JINR in 2018. It consists of an anode plane located between two cathode planes (see Fig. 2.2.2.45 a). The anode plane is a set of gilded tungsten wires with the diameter of 30 μm which are fixed on the plane with a step of 2.5 mm. The gap between the anode plane and each cathode plane is 3.8 mm. There is a spacer between the cathode planes to prevent deformation of the chamber due to the gas pressure inside. The anode wires are supported by two special wires strained across in the middle. A schematic view of the CSC detector is shown in Fig. 2.2.2.45a. Both cathode planes are made from PCBs (printed circuit boards). A two-coordinate readout of the signal is performed on two cathode boards using sets

of parallel metal strips. The inclination angles of the cathode strips to the vertical axis are 0 degrees (X coordinate) and 15 degrees (Y coordinate). The pitch of the X and Y strips is 2.5 mm. PCBs are glued to the support honeycomb. Because of a large multiplicity of charged particles in Au-Au collisions, readout layer is divided into outer (cold) and inner (hot) zones.

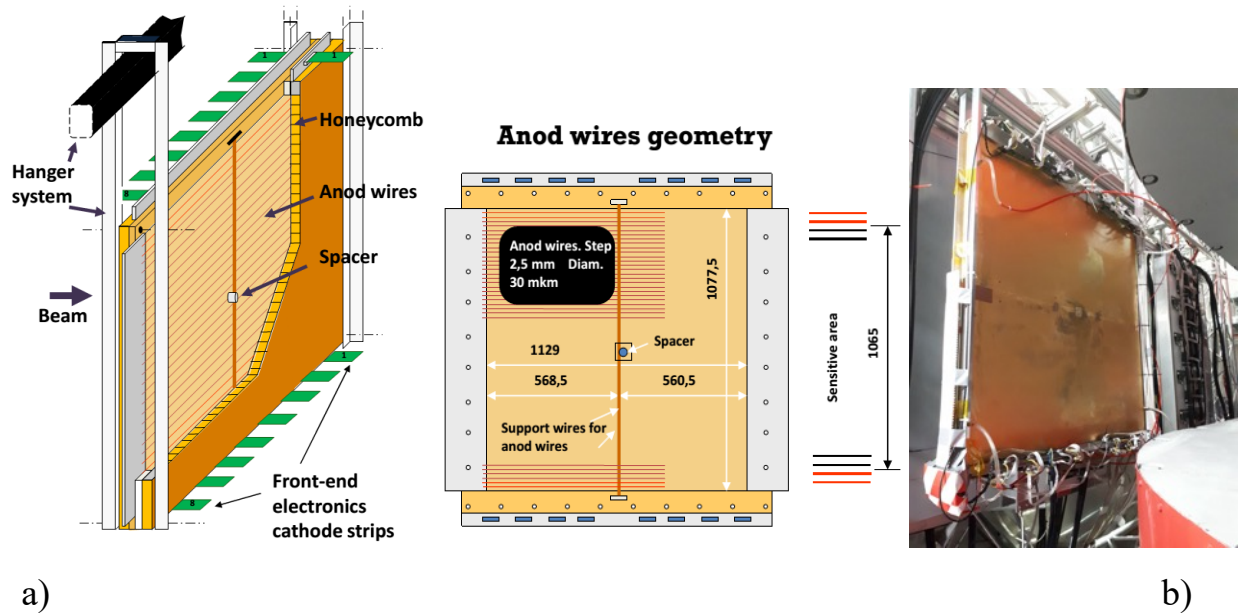


Fig. 2.2.2.42 a) Schematic cross section of  $1129 \times 1065 \text{ mm}^2$  CSC b)  $1129 \times 1065 \text{ mm}^2$  CSC integrated into the BM@N experimental setup.

Front-end electronics is based on the charge sensitive pre-amplifier chip VA163 produced by IDEAS – Integrated Detector Electronics AS (Norway). The chip has 32 channels. Each channel contains a charge-sensitive preamplifier, a shaper with  $0.5 \mu\text{s}$  (VA-163 chip) peaking time and a sample-hold circuit. An analog multiplexer with 32 inputs allows one to perform serial read-out channel by channel. The chip can be used to amplify and read negative and positive charges in the range from  $-1.5 \text{ pC}$  to  $+1.5 \text{ pC}$ . The equivalent noise charge is  $1900e$  without load, and  $2000e$  at  $50 \text{ pF}$  input load. The integral linearity is 1% and 3% for the positive and negative charge, respectively. Each read out card includes four chips, which are installed, bonded and filled with black compound. Thus, we have 128 input analog channels read-out board (Fig. 2.2.2.43). The multiplexed data from each board are transmitted through 13 m of twisted pair flat cable to the 12-bit analog-to-digital converter (ADC) readout by the BM@N data acquisition system.



*Fig. 2.2.2.43. 128 channel read-out board. Front and back side view.*

The CSC chambers can be operated with Ar(50)/CO<sub>2</sub>(50)/C<sub>3</sub>H<sub>8</sub>O(vapour), Ar(75)/C<sub>4</sub>H<sub>10</sub>(25)/C<sub>3</sub>H<sub>8</sub>O(vapor) gas mixtures. The gas system consists of two parts: 1) the mixer system which delivers a mixture of gases in a required ratio and pressure to downstream elements; 2) the distribution system, which delivers the gas in well defined quantities to the individual detectors. The gas system is produced by Ltd «Eltochpribor» (Zelenograd, Russia).

The LV power system is based on NTN 350-6,5 and NTN 700-6,5 LV modules. NTN low voltage module has adapter for a remote control via the Ethernet connection. The Ethernet control is used to record the low voltage value in the BM@N Slow Control System database.

First beam tests of the 1129×1065 mm<sup>2</sup> CSC were performed in 2018 in the argon beam with kinetic energy of 3.2 AGeV and the krypton beam with kinetic energy of 2.3 AGeV at the Nuclotron. The CSC was installed upstream the ToF-400 time-of-flight detectors as it is shown in Fig. 2.2.2.44. The main goal of the tests was to study the performance of the CSC detector and the FEE and readout electronics as a part of the BM@N experimental setup. The CSC was filled with the flowed Ar(75)/C<sub>4</sub>H<sub>10</sub>(25)/C<sub>3</sub>H<sub>8</sub>O(vapor) gas mixture and equipped with the VA163 based electronics. The signal clusters were reconstructed as groups of adjacent strips with amplitudes of signals above the threshold. For the reconstructed clusters, the center of gravity, the width and the total charge were calculated. The average cluster width is 6 strips which is equal to 15 mm. The gap size between the anode and cathode is planned to reduce to 3 mm instead of 3.8 mm in order to improve the spatial resolution in multitrack events.

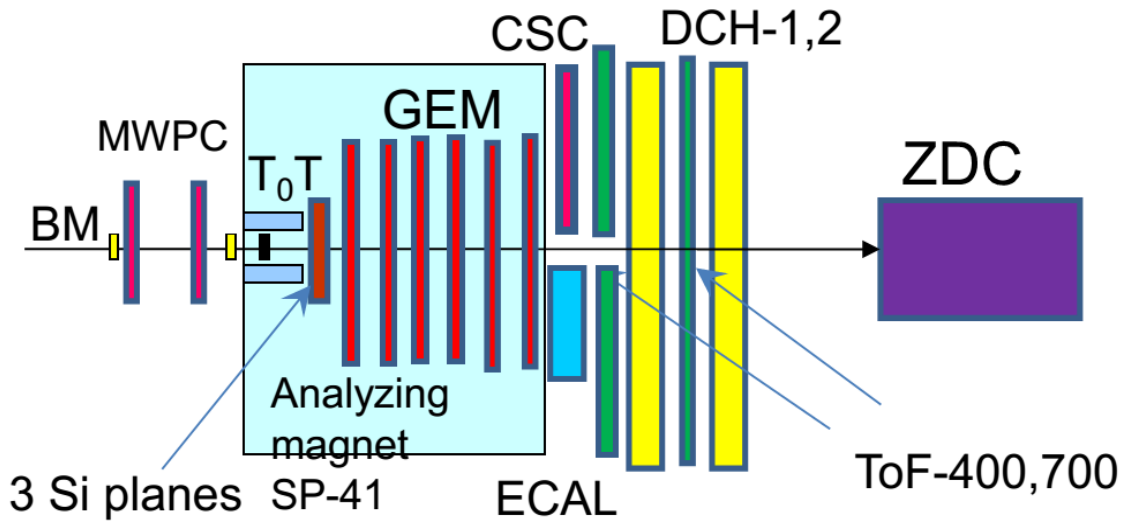


Fig. 2.2.2.44. Schematic view of the BM@N experimental setup in March 2018

Tracks of charged particles were reconstructed in the GEM central tracking system and extrapolated into the CSC. The efficiency distribution over the chamber surface is presented in Fig. 2.2.2.45 (left). The efficiency for the area  $y < -5$  cm was not estimated because of the relative location of the CSC and GEM detectors: the GEM detectors were covering the phase space only above the beam. The yellow vertical strip at  $x = 110$  cm is an effect of the support wires. The green area at the left upper corner is due to a problematic front-end board. The combined tracks reconstructed from GEM and CSC hits were extrapolated to the TOF-400. Such procedure improves the momentum resolution and helps to separate secondary particles ( $\pi$ ,  $p$ ,  $K$ , light nuclei) in the momentum range 0.5-3.5 GeV/c (see Fig. 2.2.2.45, right).

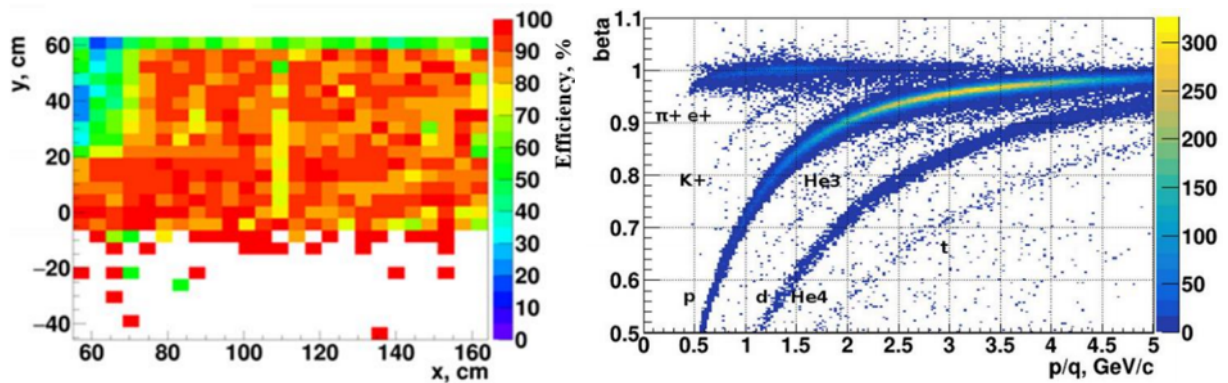
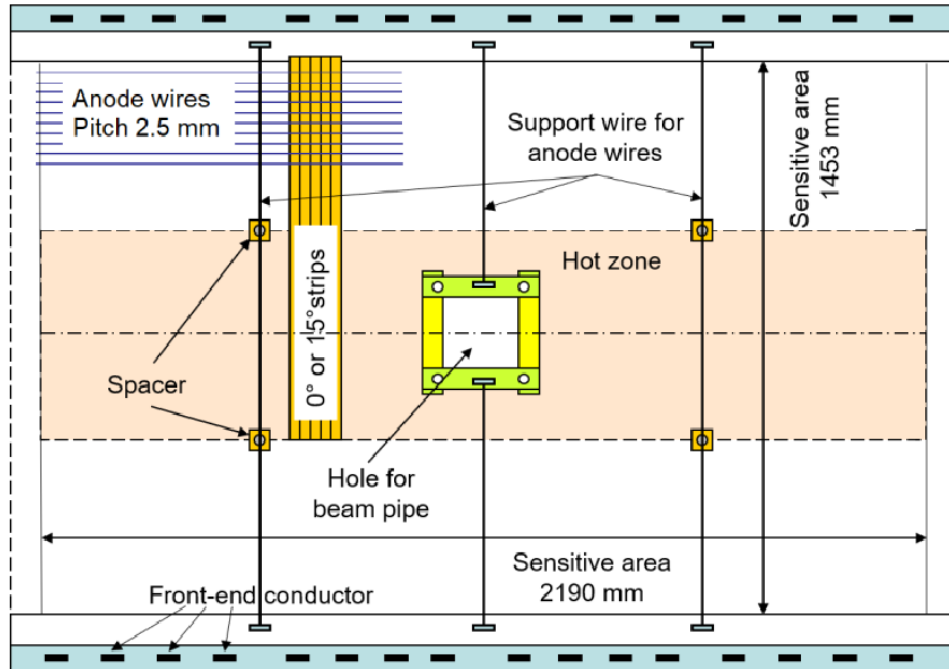


Fig. 2.2.2.45. Efficiency distribution for CSC (left); preliminary particle identification of GEM+CSC tracks extrapolated to the ToF-400 (right).

Two CSCs of the size  $2190 \times 1453$  mm<sup>2</sup> have been designed to cover the ToF-700 system on both sides and replace the existing DCH-1.2 chambers (Fig.2.2.2.44). The design of these cathode strip chambers is shown in Fig. 2.2.2.46. One cathode plane consists of 8 PCBs, each PCB is divided into hot and cold zones. The hole in the

center of the chamber is designed for the vacuum beam pipe. The gap size between the anode and cathodes is planned to be 3 mm. A two-coordinate readout of the signal is performed using sets of parallel metal strips with the inclination angle of 0 degrees for the X coordinate and 15 degrees for the Y coordinate. The pitch of the X and Y strips is 2.5 mm.



*Fig. 2.2.2.46. A technical drawing of the cathode strip chamber of the size  $2190 \times 1453 \text{ mm}^2$  (15-degree strips are not shown in this picture).*

The full configuration of the outer tracking system consists of 6 CSC: four  $1129 \times 1065 \text{ mm}^2$  CSC – to cover the ToF-400 system and two  $2190 \times 1453 \text{ mm}^2$  CSC – to cover the ToF-700 system.

One  $1129 \times 1065 \text{ mm}^2$  CSC has been studied using Ar and Kr beams of the Nuclotron accelerator and cosmic rays. All components for the assembly of three  $1129 \times 1065 \text{ mm}^2$  CSCs are delivered to JINR. The assembly of the chambers is planned to be finished in the first quarter of 2020. After passing quality assurance and cosmic tests three  $1129 \times 1065 \text{ mm}^2$  CSCs will be integrated into the BM@N setup in the middle of 2020.

Technical drawings of the  $2190 \times 1453 \text{ mm}^2$  CSC are ready. The design of the cathode planes is being performed at the moment. The production of the cathode planes is planned to be performed before middle of 2020. The technological equipment for the assembly is under development. The assembly process of the first  $2190 \times 1453 \text{ mm}^2$  CSC is planned to be finished by the end of 2020 and of the second one – in the middle of 2021.

The full configuration with 6 CSC detectors with the electronics based on VA-163 chips (~35000 readout channels) is planned to be integrated into the BM@N experimental setup at the end of 2021. To improve the performance of the FEE, two new ASICs (VMM3a and TIGER) with the capability to measure both time and amplitude information are considered. First tests of FEE based on both chips have already started. In 2022 the new FEE electronics is planned to be integrated into the BM@N experimental setup.

#### **2.2.2.7. Time of Flight System TOF-700**

Time-of-flight wall (ToF-700) placed at 7m from the target provides BM@N with the pion/kaon separation up to 3 GeV/c and proton/kaon separation up to 5 GeV/c.

The design of the ToF-700 wall is based on our experimental results obtained during multiple tests of various modifications of the glass multigap Timing Resistive Plate Chamber (mRPC) exposed in charge particles beam.

The wall size of 3.2x2.2 m<sup>2</sup> is defined to satisfy the geometrical acceptance of the tracking detectors. A glass mRPC, a detector with high time resolution, good detection efficiency and relatively low cost, is the best choice as a basic element of the ToF-700. Glass mRPCs have been chosen to construct TOF systems in such experiments as ALICE, HARP, STAR and PHENIX. High resolution of ~60 ps was achieved with an efficiency above 97% and a crosstalk signal in the adjacent strips about few percent.

##### ***2.2.2.7.1. Design of the ToF-700 wall***

Conventional glass mRPC suffers from serious shortcomings – low hit rate capability. Because of high bulk resistivity, 10<sup>12</sup> - 10<sup>13</sup> Ω/cm, mRPC made of ordinary (“window”) glass works well only up to several hundred Hz/cm<sup>2</sup>. But Monte-Carlo simulation of Au-Au collisions shows that the rate of particles going through region of the ToF-700 wall the around beam can be up to few kHz/cm<sup>2</sup>. To increase the mRPC hit rate capacity it is necessary to decrease the resistivity of glass electrodes. There are two ways to decrease the resistivity of “window” glass – to minimize its thickness or/and to heat the glass electrode. Our studies showed that the “warm” mRPCs can provide us with good time resolution even at a rate of ~20 KHz/cm<sup>2</sup>.

Two types of mRPC were chosen for the construction of the wall plane: a “warm” mRPC for the central “hot” region with high rate of tracks, and a conventional “cold” mRPC for the “cold” region with low rate of tracks. An arrangement of 58 mRPCs in the wall plane is shown in Fig. 2.2.2.47. The hole in the wall center is for the beam pipe.

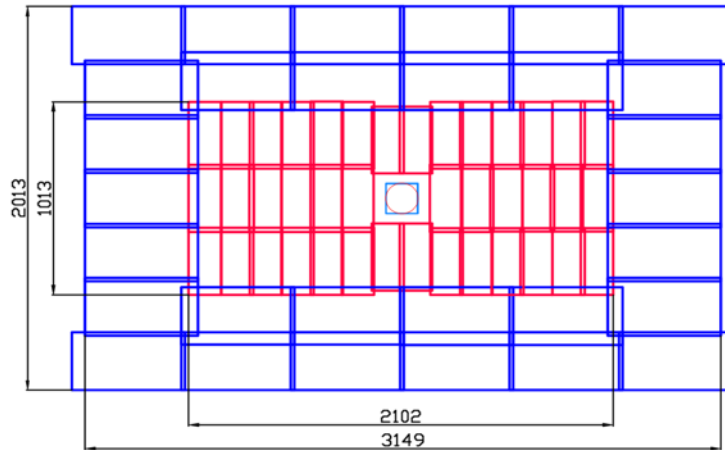


Fig. 2.2.2.47. Arrangement of 40 “warm” and 18 “cold” mRPCs on the wall plane.

### 2.2.2.7.2. mRPC’s design and assembling

To reduce the fraction of events with double-hit in one strip, the chambers with different strip area (length) are mounted in the “hot” / ”cold” regions of the wall.

To optimize the number of chambers types and sizes, only two types of mRPC were proposed: 18 “cold” mRPCs, each with the active area of  $17.6 \times 56 \text{ cm}^2$  (16 strips of  $1 \times 56 \text{ cm}^2$ ), for the region with the low hit rate and 40 “warm” mRPCs, each with the active area of  $16 \times 35.1 \text{ cm}^2$  (32 strips of  $1 \times 16 \text{ cm}^2$ ) for the region with the high hit rate and occupancy. The total number of chambers is 58, the number of strips - 1568.

A schematic cross section of the “cold” mRPC is shown in Fig. 2.2.2.48: it consists of two identical five-gap stacks with an anode strip readout plate in between.

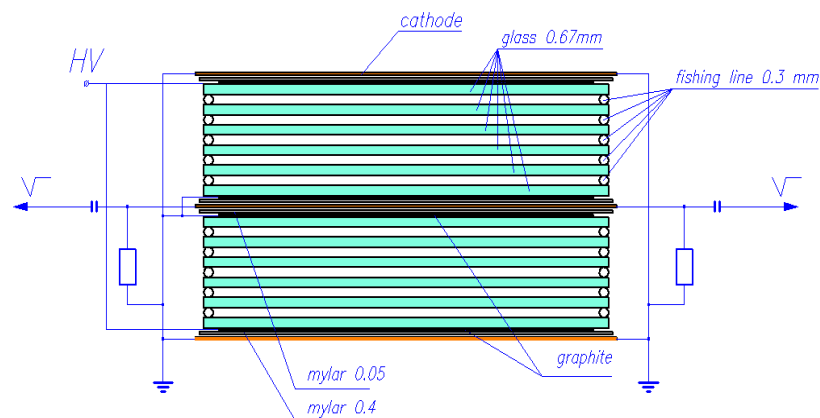


Fig. 2.2.2.48. Schematic cross-section of the ten-gap mRPC.

Each stack is formed by six glass plates with the bulk resistivity of  $2 \times 10^{12} \Omega/\text{cm}$ . The gap of 0.3 mm between the glasses is fixed by spacers – usual fishing-lines, which ran directly through the RPC working area. A graphite conductive coating with the surface resistivity of  $\sim 1 \text{ M}\Omega/\text{cm}^2$  is painted to the outer surfaces of the external glass

plates of each stack to distribute both the high voltage and its separate ground and to form the uniform electrical field in the stack sensitive area.

The anode readout strips plate is a one-sided printed PCB with the thickness of 100  $\mu\text{m}$ , the thickness of the copper is 35 microns. Signals are taken from both ends of the anode strips. The entire mRPC assembly is put into a gas-tight box.

A special workshop was prepared for production of mRPCs. It has space for washing, painting and stoving of glasses and a clean room for assembling mRPCs.

#### ***2.2.2.7.3. Heating and thermal stability of “warm” mRPC***

In order to provide good time resolution for a high particle rate the “warm” mRPC should be operated at about 40 degrees Celsius. To warm the chamber a special surface heaters were designed. The required temperature inside the “warm” mRPC is achieved with the heaters installed on both sides, top and bottom. The heaters are covered with a 10 mm thick heat-insulated material to reduce the loss of heat. The mRPC thermo-stabilization system includes the digital thermometers soldered on the motherboard inside the mRPC box. Each chamber has two temperature-controlled heating channels. The thermometers are connected to microcontroller boards, which in turn are connected to a master controller. Each master controller has 32 channels to steer the power supplies which are connected to the heaters of the mRPC.

The master controller receives temperature setting from the data acquisition computer and reads an actual temperature from the digital thermometers in the mRPC box. For smooth temperature stabilization a proportional-integral-differential regulator algorithm is implemented into the controller firmware.

#### ***2.2.2.7.4. Front-end electronics (FEE) of mRPC***

A number of FEE channels for ToF-700 is 3136. As FEE for mRPCs readout the AddOn board developed for the HADES experiment was chosen. The 32-channels FEE module (32RPC board) designed for our mRPCs is based on the NINO chip. The output signal of the NINO amplifier-discriminator is the time-over-threshold pulse whose leading edge provides the time of the hit while its pulse width is proportional to the input signal charge.

The signals from mRPC are delivered to the 32RPC module by 50 $\Omega$  coaxial cables with the MMCX connectors. Output LVDS signals are transmitted to the digitization module with the DHR-78F sockets. At present, a 64-channel VME time-to-digital converter TDC64VHLE based on the HPTDC chip is used for digitization.

Controls of the power supply, threshold settings, stretch time settings and hysteresis settings of the 32RPC boards are done by a special designed power and control

module (PWR&CTRL). The PWR&CTRL module is controlled by the U-40 VME module via a digital SPI interface.

#### **2.2.2.7.5. The support of ToF-700 wall**

The construction of the wall support is shown in Fig. 2.2.2.49. To ensure an overlap between active areas of the mRPCs, the chambers should be arranged on the wall in four layers.

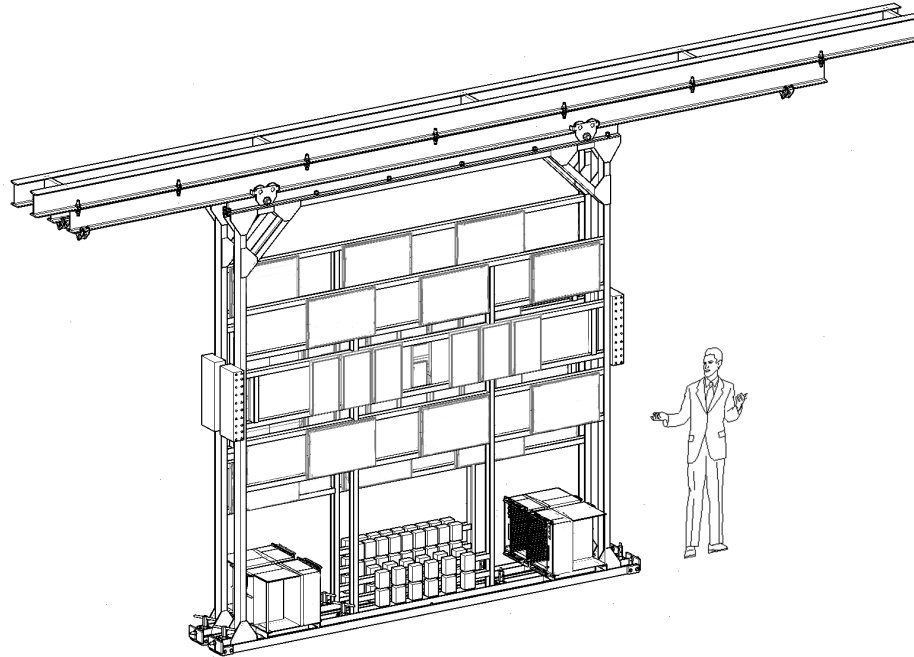


*Fig. 2.2.2.49. The design of the ToF-700 wall (model).*

The wall consists of two subwalls. The chambers are located on both sides of the sub walls. Both subwalls can move relative to each other to provide access for installation and maintenance.

#### **2.2.2.7.6. ToF-700 data analysis**

TOF-700 data analysis software was developed in the BMNROOT package framework. The analysis includes few stages and takes into account: INL (TDC non-linearity) corrections, VME crates Time Stamp differences, time corrections versus the T0 pulse width, time corrections versus the TOF pulse width, equalization of each strip time response for the main time peak. Finally, we use tracks reconstructed in GEM+DCH detectors and ToF-700 time data to reconstruct proton tracks and calculate the time correction for each strip (this correction shifts the reconstructed particle mass to the nominal proton mass). Fig. 2.2.2.50 and Fig. 2.2.2.51 illustrate the quality of the fragment separation versus the track momentum and the ToF registration efficiency versus the track coordinate in DCH, respectively

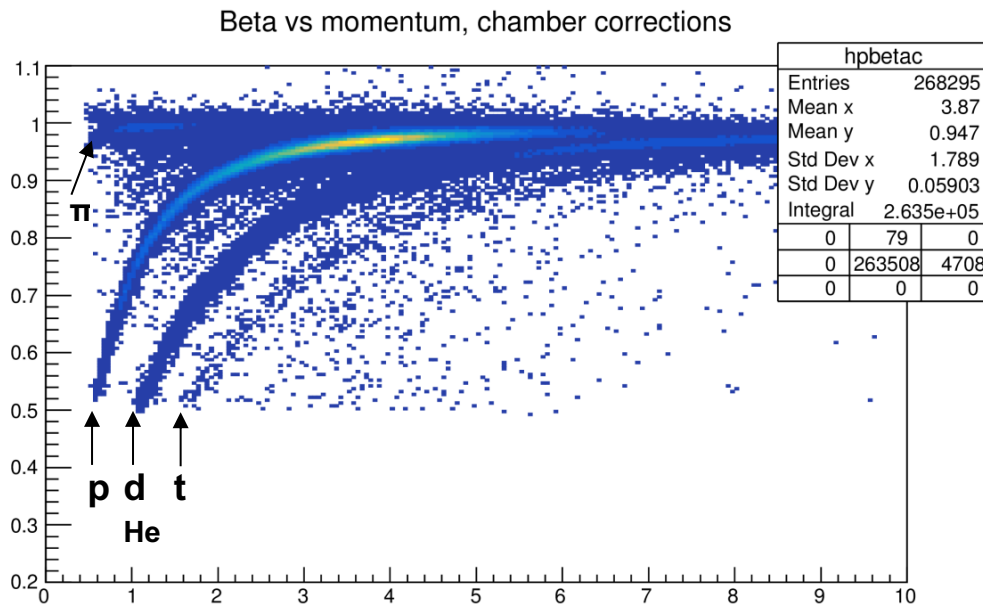


Fig. 2.2.2.50. Separation of hadrons and nuclear fragments in the plot of the particle beta vs momentum.

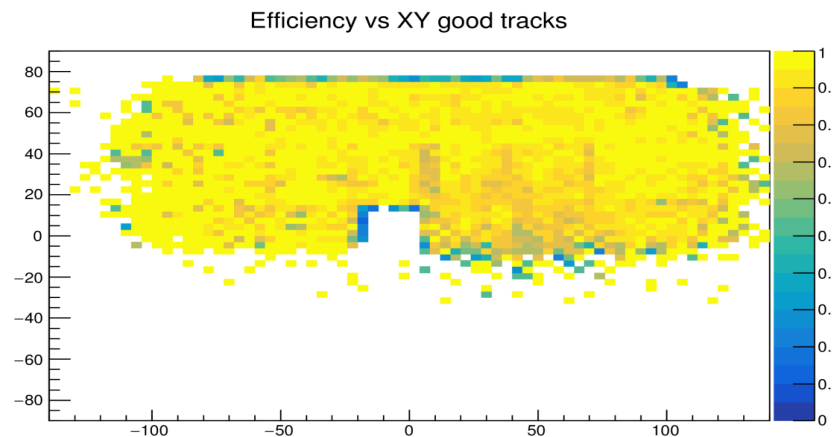


Fig. 2.2.2.51. ToF-700 registration efficiency vs XY coordinate of tracks reconstructed in the DCH chambers.

### 2.2.2.8. Time-of-Flight system ToF-400

The Time-of-Flight system for charged particles identification consists of two walls of Multi-gap Resistive-Plate Chambers. The first wall will be positioned at 4 meters from the target (ToF-400), and the second one at the distance of 7 meters (ToF-700). The ToF-400 wall will cover about 3 m<sup>2</sup> (Fig. 2.2.2.52). The main idea of ToF-400 is identification of charge products of interactions with small momentum deflected at big angles relative to the beam direction.

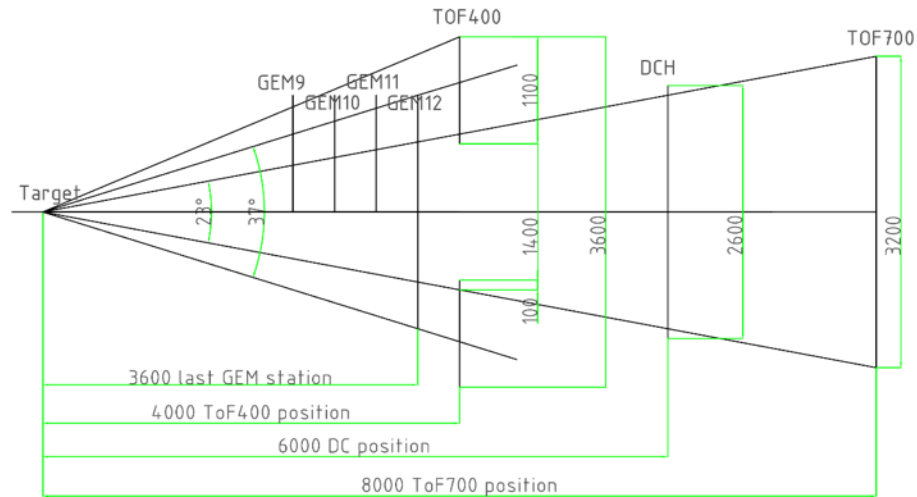


Fig. 2.2.2.52. Schematic view of the position of TOF-400 in the XZ plane

The TOF-400 wall consists of two parts (left and right) placed symmetrically to the beam. Every part consists of two gas boxes (modules) with 5 mRPCs each (Fig. 2.2.2.53, left). The active areas of the mRPCs overlap on 50 mm inside the box. The gas box is made from aluminum frame and covered by aluminum honeycomb for reduction of radiation length. The overlap of the gas boxes ensures crossing of the active areas of the detectors by 50 mm. The size of every part is 1.15 x 1.3 m<sup>2</sup> (Fig. 2.2.2.53, right) defined to satisfy the geometrical acceptance of the tracking detectors. The gas boxes are mounted on the aluminum farm via the Bosch profiles for the box position adjustment.



Fig. 2.2.2.53 Gas box (module) with packed detectors (left) and a left part of ToF-400 wall mounted in BM@N hall (right).

The operation of the ToF400 system was started in the BM@N run at the Nuclotron in March 2018. The design of the supporting farm should be changed during 2020 to be able to mount the CSC detectors foreseen in the full configuration of BM@N.

### 2.2.2.8.1. Construction of mRPC, assembling and testing of ToF modules

The scheme of mRPC is presented in Fig. 2.2.2.54. The detector consists of three stacks with 5 gas gaps each. As resistive electrodes we use common float glass. The outer glass electrodes have a thickness of 0.42 mm. The internal glass electrodes have a thickness of 0.27 mm. The fishing line used as a spacer defines the 200  $\mu\text{m}$  gap between all resistive electrodes. The outer part of the external glass electrode is covered by conductive paint with the surface resistivity about 2 – 10  $\text{M}\Omega/\text{cm}^2$  to apply high voltage. All internal glasses are floating. The pickup electrodes look like strips and are made on the PCB board. The main feature of the proposed triple-stack mRPC is that the readout strips are located only in the inner stack. This ensures that the construction is symmetric, and the speed of the signal transmission to the anode and cathode is the same. That prevents the dispersion of the signal.

A differential analog signal from a strip is transferred by a twisted pair cable to front-end electronics. The signal is read out from both ends of the strip. It provides a better time resolution and a determination of the coordinate of a particle along the strip. To get stiff structure, we glue paper honeycomb with a thickness of 10 mm on outer part of the external PCBs. The dimension of the active area of one mRPC is 300\*600  $\text{mm}^2$ . It has 48 readout strips, is 10 mm wide and 300 mm long. To reduce crosstalk the gap between strips is 2.5 mm. Thus, the pitch of strips is 12.5 mm.

All the required mRPC are produced in 2017. Two additional detectors should be assembled to replace failed ones during 2020.

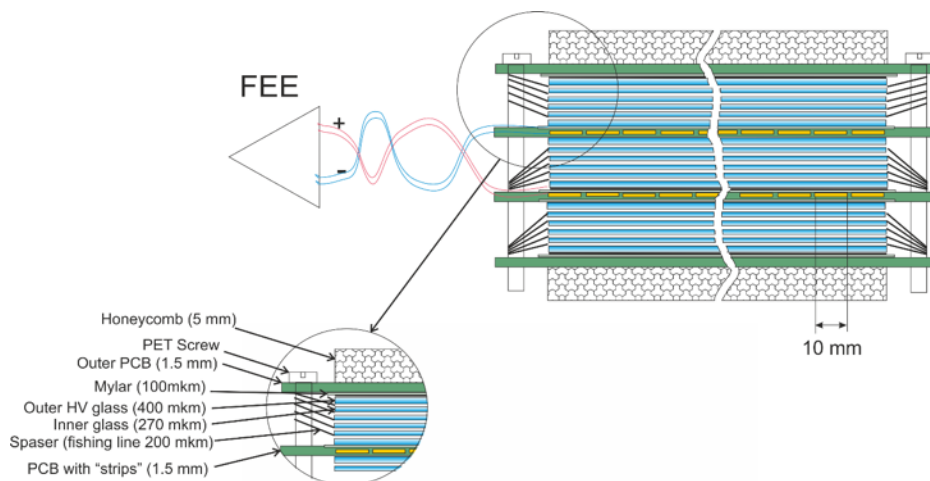


Fig. 2.2.2.54. Sectional view of the triple stack strip mRPC for ToF-400.

Assembling of mRPCs and modules was performed in building 42 of LHEP. The assembling area consists of three clean rooms for washing and drying glasses, assembling and optical control of mRPC. Also, there is a room for assembling of

ToF-400 modules. The test setup for modules was located in the building 202 of LHEP. Each assembled module is tested immediately after production. Tests include HV test, signal transition test to control reliability of soldering and connections inside the module. After that, all modules are tested in a cosmic ray test setup. We foresee four weeks in total to test one 2-module stack, including two weeks reservation time for setting up HV and detectors conditioning and 2 weeks for data taking.

All ToF-400 modules were produced in 2017.

#### ***2.2.2.8.2. Electronics for ToF-400***

The fast front-end preamplifier discriminator NINO chip developed for the ALICE TOF were used in the BM@N Time-of-Flight system. The chip has 8 channels and processed on 0.25  $\mu\text{m}$  technology. Each channel includes an ultra-fast preamplifier with a peaking time less than 1 ns, a discriminator with a minimum detection threshold of 10 fC and an output stage which provides the LVDS output signal. The output signal has time jitter less than 25 ps. Its pulse width depends on the input signal charge. Each channel consumes less than 30 mW. The 24-channel amplifier-discriminator FEE board was developed in LHEP JINR during 2015 – 2017 (Fig. 2.2.2.55, left). The distinctive features of the ToF preamplifier board are the following: the stabilized voltage supply of the NINO chip, the input impedance matched to the impedance of the mRPC, capacitors at the inputs for two-side strip readout, the threshold remote monitoring and control, the board and the gas space thermal monitoring.

All FEE cards (80 pcs + 10 pcs reserve) were produced in 2017.

72-channel time-to-digital converters (TDC72VHL) based on HPTDC chip were developed and produced in LHEP JINR for data acquisition (Fig. 2.2.2.55, right). It is used for digitizing LVDS signals coming from the output of the NINO amplifier using cables Molex P/N 11102512xx with connectors Molex 76105-0585. Time sampling of the TDC72VHL is 24.4 ps per bin. The TDC72VHL provides the ability of the precise “White Rabbit” synchronization with other timing devices. Native time resolution of a TDC72VHL channel reaches 20 ps after applying the calibrations.

All TDC boards (27 pcs + 10 pcs reserve) are produced in 2017. Two VME crates were purchased and delivered in 2017.



*Fig. 2.2.2.55. 24-channel amplifier-discriminator board based on NINO ASIC (left) and View of the TDC72VHL module (right)*

### **2.2.2.8.3. Gas system**

The mRPC works with a non-flammable Freon-rich gas mixture containing 90% C<sub>2</sub>H<sub>2</sub>F<sub>4</sub> + 5% i-C<sub>4</sub>H<sub>10</sub> + 5% SF<sub>6</sub>. The flows of component gases are metered by MKS mass flow meters, which have an absolute precision of 0.3% under constant conditions. Flows are monitored by a process control computer, which continuously calculates and adjusts the mixture percentages supplied to the system. The flow of the gas mixture can be adjusted in the range from 6 l/hour up to 90 l/hour, but running flows are expected to be typically about 40% of the full-scale flow on the mass flow controllers. For this flow the volume exchange rate is 2.0 per day. Gas will successively blow modules and go out to air through an oil flap. This simple open gas loop system based on MKS 1479A controller are designed and produced. The same system is also used for ToF-700.

### **2.2.2.8.4. HV & LV power supply and Slow control system**

To provide high voltage power to the ToF modules, a 40 channels high voltage system produced by HVSys is used. The current system is not stable. The local connection to the HV device was disconnected several times during BM@N data taking. This leads to the need to stop the data set and gain access to the experimental area for a hard reboot of the device. New high voltage system produced by ISEG and WIENER companies (Germany) will be used in future. Ten iSeg EHS4080p(n) (4 channels, up to 8 kV and 1 mA) modules and one MPOD crate will be purchased during 2019-2020.

Three low voltage supply modules iSeg MPV 8016I in one MPOD crate are used to power all FEE of the ToF system.

To control the Time-of-Flight system of the BM@N it is necessary to monitor several parameters of different subsystems such as temperature monitoring, voltage and current monitoring, gas flow monitoring, etc. At present, the slow control system has been developed. The data of the slow control system are used during experimental data analysis. All of the slow control equipment components are acquired in 2017.

### **2.2.2.9. Detector T0 and Trigger System**

Beam Line and Target Area Detectors, T0 detectors, and fast trigger systems are important part of the BM@N experiment for its heavy ion program and for studies of Short Range Correlations (SRC).

The detector system provides transport of heavy ions to a target, effective triggering of nucleus-nucleus collisions, and monitoring beam characteristics. T0 detectors have a pico-second time resolution and they are used as start detectors for ToF measurements. Special modules of trigger electronics T0U based on FPGA were developed for these two experimental programs.

#### ***2.2.2.9.1. Detector for BM@N heavy ion program***

In period 2014 – 2017 the BM@N had technical runs with *d*- and C- beams without a vacuum pipe. In these runs the first beam counter BC1 was based on 70×70×5 mm<sup>3</sup> plastic scintillator coupled with PMT FEU-87, the second beam counter BC2 had a small size scintillator which defined the size of the beam spot on the target. The veto-counter (VC) was build from a 10- mm plastic scintillator with a diameter of 100 mm and a hole with a diameter of 27 mm.

Two different concepts to get the T0 pulse signal are considered:

- 1) Cherenkov or scintillation beam counters based on MCP-PMTs applicable for beam intensity up to 10<sup>6</sup> ion/s;
- 2) for higher beam intensity, a modular array of Cherenkov detectors with MCP-PMT readout located at small distance from a target with the aim to detect secondary relativistic charge particles and high-energy photons.

Three different versions of the T0 counter with quartz radiators and fast scintillator BC-418 were tested with deuteron and carbon beams. The Cherenkov modular array consists of detectors with 10- mm lead converters for photon detection, 15- mm quartz radiators, MCP-PMTs XP85012/A1-Q from Photonis and boards of front-end electronics.

The first experimental test of the T0 array was carried out during the BM@N run in 2015 with carbon ions interacting with a copper target in the magnetic field of 0.5T. In this experiment the T0 beam counter was a Cherenkov detector with a 8-mm

quartz radiator inclined at  $47^\circ$  to the beam axis. The time resolution  $\sigma_t = 27$  ps was obtained for this counter detecting carbon ions.

In the BM@N run with Ar and Kr ions performed in 2018, BC1 counter was produced from a scintillator of 150- mm in diameter and 3- mm in thickness with PMT XP2020 used as a light detector. The T0 pulse was produced by a beam counter with scintillator of 20 mm in diameter, and 0.8 mm in thickness and MCP-PMT PP0365G as a light detector.

Nuclear interactions in a target are triggered by detection of charged particles in a wide angular range by a barrel detector (BD) and a multichannel Si-detector (SiD). The BD consists of 40 scintillation strips produced from BC-418, connected on one end with SiPM  $6 \times 6$  mm<sup>2</sup> from Sensl. A view of BD is shown in Fig. 2.2.2.56.

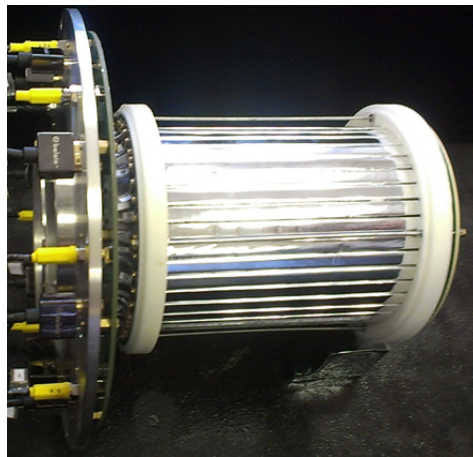


*Fig. 2.2.2.56. A view of a new BD detector prepared for run 2018.*

The first version of the trigger electronics unit (T0U) was developed for the BM@N run in 2015. The T0U, shown in Fig. 2.2.2.57, has a modular structure. It has a motherboard and 4 different types of mezzanine boards. The T0U device distributes input signals to external electronics (TDC72VHL) and to a trigger processor, generates the L0 trigger signal (trigger processor is build using Altera Cyclone V GX FPGA), provides the LV power supply for FEE modules of the T0 detector and accumulates the trigger monitoring information. It also has four discriminator cards to discriminate input pulses originated from the beam detectors, four TTL-NIM convertor cards, one Ethernet interface card.

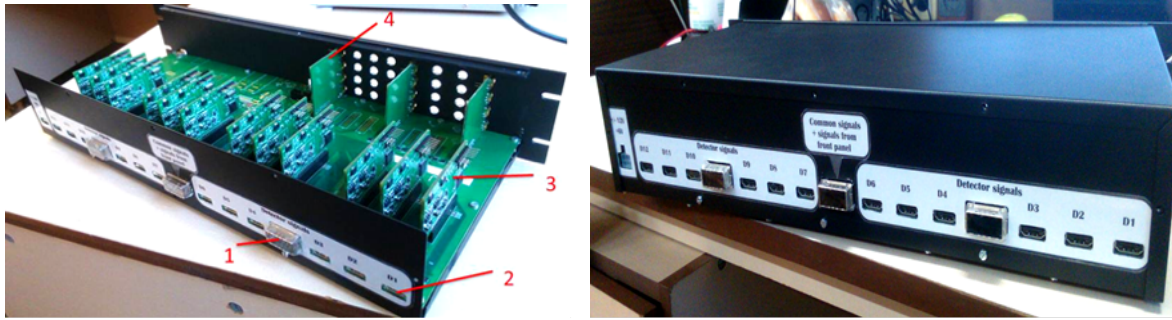


Fig. 2.2.2.57. A view of the T0U module: 1 – the output connector for pulses to TDC72; 2 – the input connector for HDMI cable from detector FEE; 3 – the power supply board; 4 – the board of output trigger pulses.

A T0U software manager controls the hardware of the T0U module and reads out the summary of the spill data containing counts from input channels and from some internal points of the trigger logic. A window of the trigger interface is shown in Fig. 2.2.2.58.

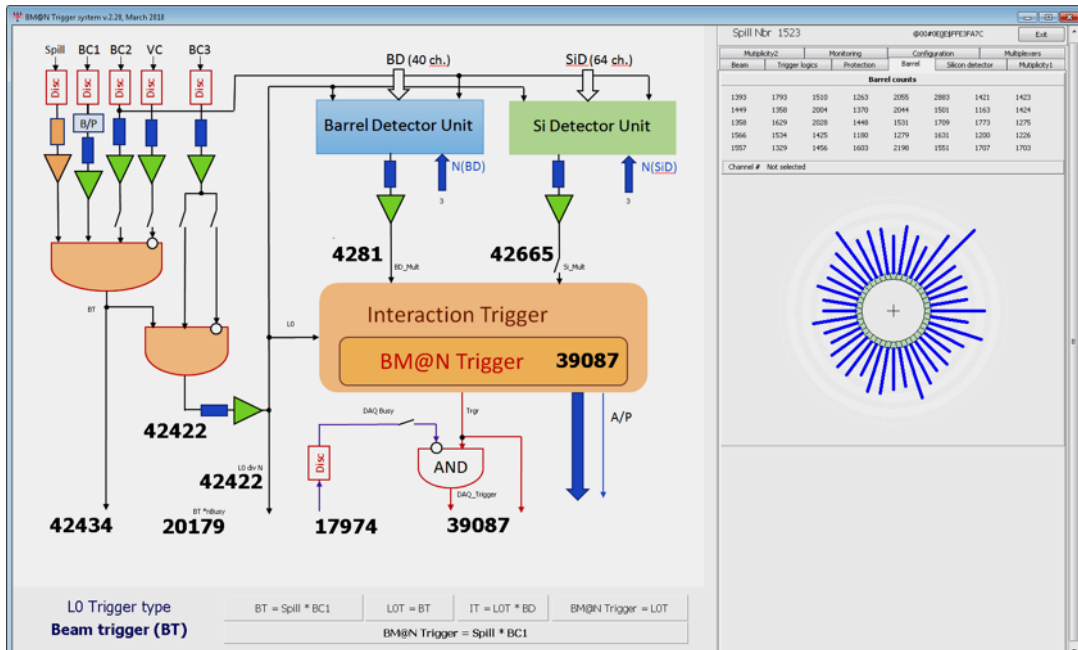
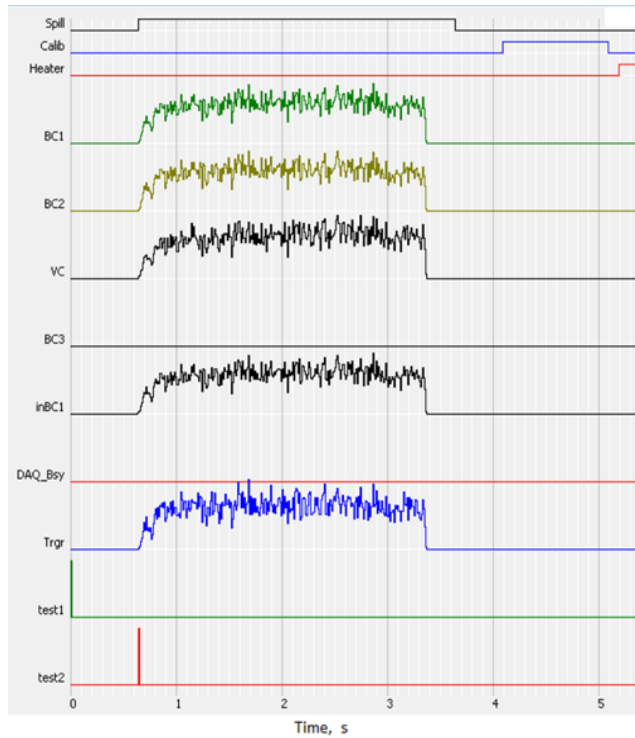


Fig. 2.2.2.58. A window of the trigger interface in the BM@N run 2018.

The SpillView TCP/IP server has been developed for control of the spill intensity in a real time mode. The time structure of Ar ion spills and the counting rates of the beam detectors and of the final trigger are shown in Fig. 2.2.2.59.



*Fig. 2.2.2.59. A window of the SpillView monitor.*

A number of fired channels in the BD and SiD detectors correlates with the centrality of nucleus-nucleus collisions. But the background of delta-electrons produced in the beam line materials and the target also gives some contribution to responses of BD and SiD. This background increases rapidly with the charge of beam ions. For future runs with heavy nucleus beams a new vacuum beam line with a new system of beam detectors is being developed in 2019 – 2020.

In 2019 we studied the dependence of the rate of this background on the geometry and shielding of detectors in the target area and on the magnetic field by performing simulations with the QGSM + GEANT4 code. It was shown that additional lead shielding for BD and some shift of the SiD position can suppress the delta-electron background. Even for Au + Au collisions the system of the BD and SiD detectors provides effective triggering of nucleus-nucleus interactions.

A new project of the beam detectors and trigger for run 2020 – 2021 includes a set of scintillation beam counters BC1 and VC with PMTs Hamamatsu R2490-07 and BC2 (T0) with two MCP-PMT XPM85112/A1-Q400, a target area BD + SiD detectors with total granularity of 104 channels. The scintillators of the beam counters are installed into a vacuum beam pipe. A lead shield is used around the BD scintillation strips as an absorber of delta-electrons. The electronics consists of the T0U module, the SiD module, the NIM crate with digitizer CAEN mod. N6742 and the power supply module for SiPMs of the BD detector, the HV crate from WIENER with HV

modules EHS F6 30n\_SHV from ISEG. All timing LVDS pulses are fed to the TDC72VHL module. Also, some modification of trigger logic of T0U is required.

#### 2.2.2.9.2. Detector for SRC experiments

A set of beam and trigger detectors used in the SRC experimental run in 2018 is shown in Fig. 2.2.2.60. A beam of carbon ions interacted with a liquid hydrogen target. All detectors are scintillation counters with PMTs. Beam counter BC2 based on fast scintillator  $60 \times 40 \times 0.8 \text{ mm}^3$  and MCP-PMT served as T0 counter. Two pairs of large-scale counters X1 – Y1 and X2 – Y2 were used for triggering high-energy recoil protons.

A special trigger unit with SRC trigger logic was developed. A window of the trigger module manager is shown in Fig. 2.2.2.61.

The data obtained in 2018 run are under analysis.

For future runs in 2020 – 2021, a new set of trigger detectors BC1, BC2-1, BC2-2, BC3, BC4 are designed and produced. In BC2-1 (T0-1) two MCP-PMT XPM85112/A1-Q400 are used. The second T0 counter BC2-2 is based on two MCP-PMT XP85012/A1. An upgrade of electronics and cable system will be carried out in 2020.

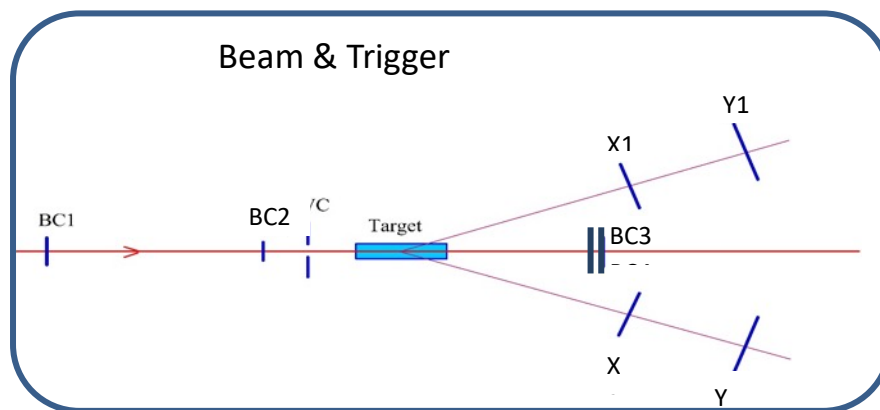


Fig. 2.2.2.60. The beam and trigger detectors of the SRC experiment.

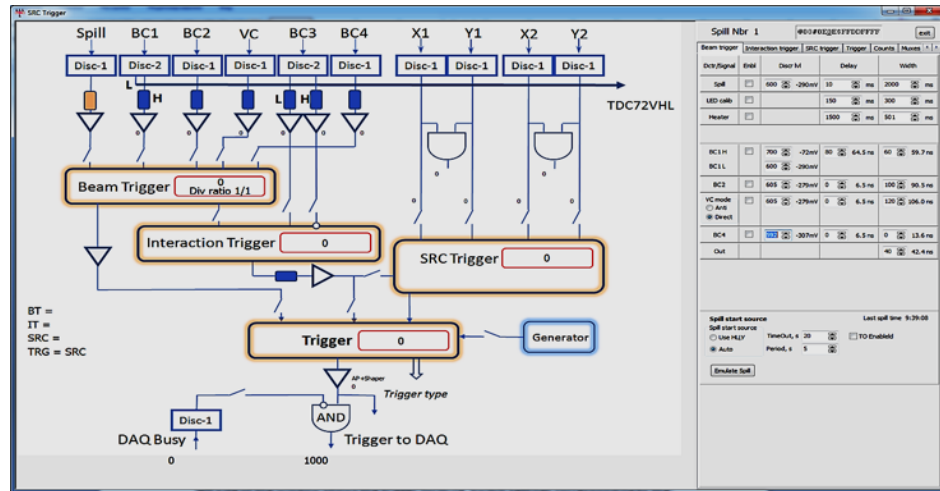


Fig. 2.2.2.61. A window of the SRC trigger module manager.

### 2.2.2.10. Zero degree calorimeter ZDC

Zero degree calorimeter (ZDC) consists of 104 hadron calorimeter modules: 68 and 36 modules with the cross section  $15 \times 15 \text{ cm}^2$  and  $7.5 \times 5.7 \text{ cm}^2$  correspondently, as shown in Fig. 2.2.2.62.

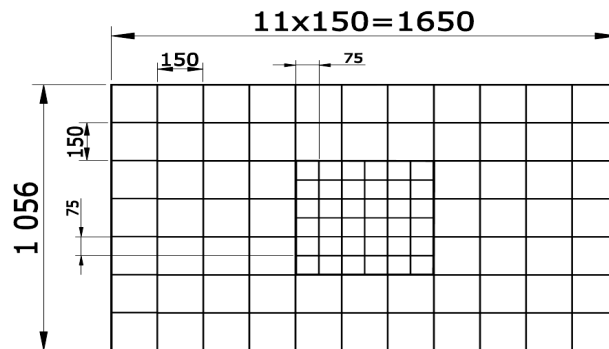
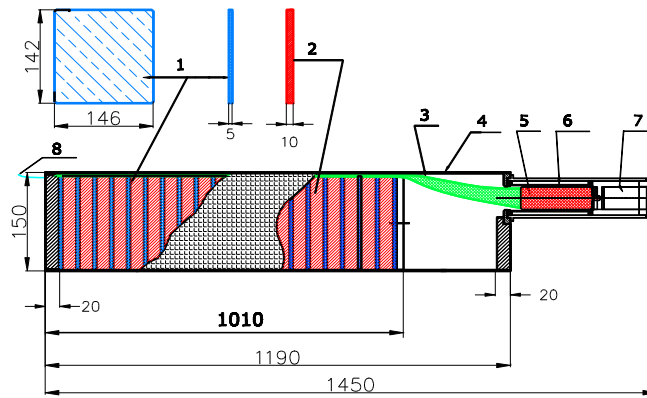


Fig. 2.2.2.62. ZDC layout: central part consists of 36 modules with sizes  $7.5 \times 7.5 \text{ cm}^2$ , peripheral part contains 68 modules of  $15 \times 15 \text{ cm}^2$

The central part consists of 36 modules with sizes  $7.5 \times 7.5 \text{ cm}^2$ , peripheral part contains 68 modules of  $15 \times 15 \text{ cm}^2$ . Small granularity in the ZDC center allows one to operate with the nuclear beam intensities up to 1 MHz, which is sufficient for the first stage of the experiment, and improve the space calorimeter resolution up to 7 mm.

A schematic view of the ZDC module is shown in Fig. 2.2.2.63. The active module components are the PMT with the voltage divider, scintillation plates, lead absorber, light guide with the wave length shifter (WLS) placed in the light protective box which serves also as the module housing.



*Fig. 2.2.2.63. ZDC module design. 1, 2 – 64 scintillator/lead layers, 3 – WLS, 4 – iron housing, 5 – PM (FEU-84) tube, 7 – PM high voltage base, 6 – mu-metal screen, 8 – fiber with an optical connector for LED light.*

### **2.2.2.10.1. Moving platform**

ZDC is located in a special moving platform manufactured for this purpose. The drawing of the platform and a general view of ZDC is shown in Fig. 2.2.2.64. The platform design and production were performed in Novo Kramatorsk, Ukraine in 2014.

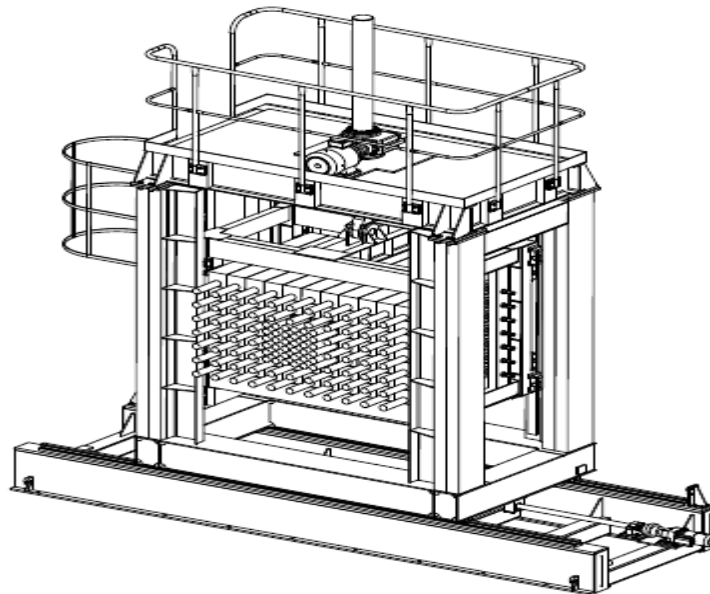


*Fig. 2.2.2.64. ZDC setup inside of moving platform.*

ZDC was fully assembled in end of 2015. The ZDC on the platform is shown in Fig. 2.2.2.65.



Fig. 2.2.2.65. ZDC from 104 modules completely assembled.

The first results were obtained with Carbon ion beam in December 2015 (Fig. 2.2.2.66).

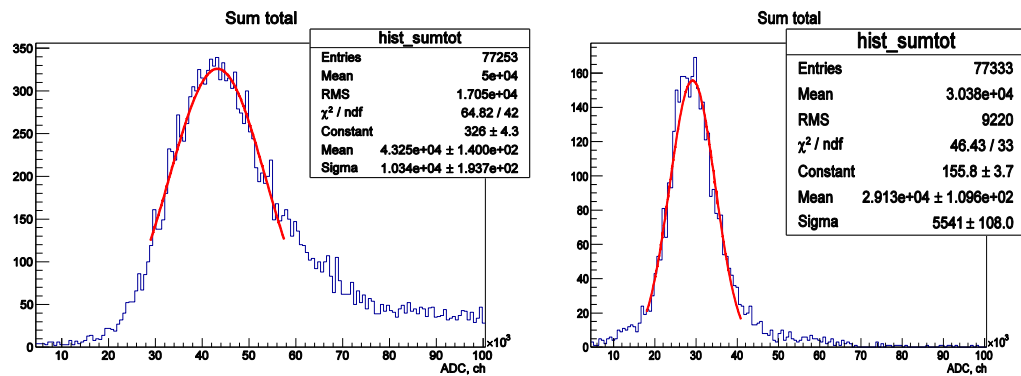


Fig. 2.2.2.66. Total ZDC energy for Carbon beam with energy 3.5 GeV/Nucleon impact in ZDC center; right –  $^{12}\text{C}$ arbon, left –  $^6\text{Li}$  nuclei, correspondently.

A ZDC layout scheme is shown in Fig. 2.2.2.67. Colored cells shown ZDC layers. Signals from all modules of the layers are combined to get a total sum. The summation boards were assembled in IHEP, Protvino.

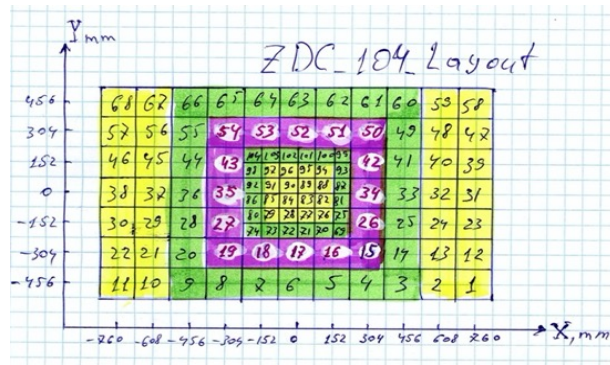


Fig. 2.2.2.67. Mapping of 104 cells. Colored cells represent five layers for signal summation.

The HV system for ZDC-104 was developed and 198 manufactured at LHEP, JINR.

### 2.2.2.10.2. Readout electronic and ZDC calibration

The ADC64s unit (<https://afi.jinr.ru/ADC64>) is used as ZDC readout electronics. ADC64 (Fig. 2.2.2.68). is a 64-channel 12-bit 50MS/s ADC device with signal processing core and Ethernet interface. It has dedicated serial links for the clock synchronization and data readout that allows system scalability to an arbitrary number of channels.



Fig. 2.2.2.68. The ADC64s board

Zero Degree Calorimeter was calibrated in Carbon beam with energy of 4.5 GeV/nucleon (see Fig.2.2.2.69).

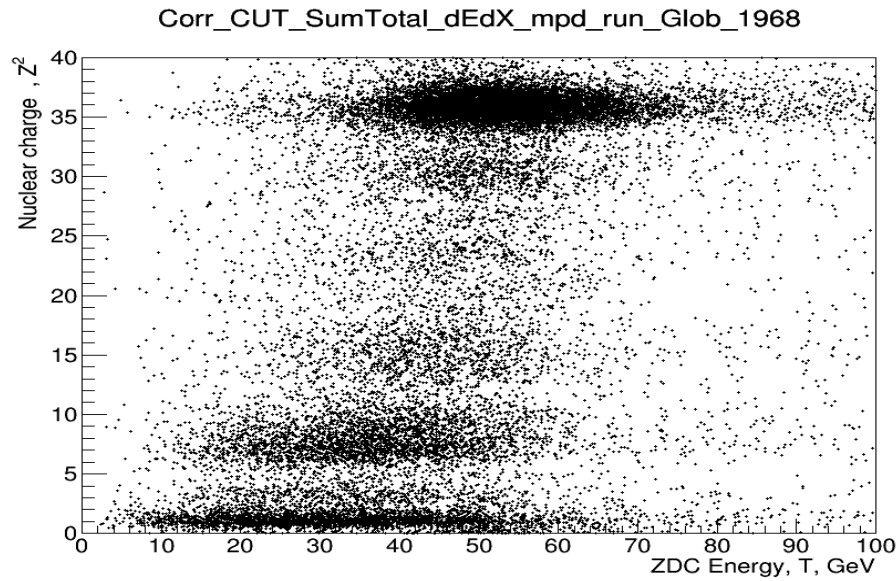


*Fig. 2.2.2.69. ZDC energy spectra versus nuclear charge. The charge was measured by  $dE/dX$  counter  $10 \times 10 \text{ cm}^2$  situated in front of the ZDC centre module; the Carbon beam of 4 GeV/nucleon interacts with Pb target.*

The ZDC energy distribution in the Inner and Outer parts of the calorimeter can be used for estimation of the interaction centrality. The Energy asymmetry (see, Fig. 2.2.2.70) is calculated as the ratio:

$$\text{Asymmetry} = (E_{\text{Inner}} - E_{\text{Outer}}) / (E_{\text{Inner}} + E_{\text{Outer}}).$$

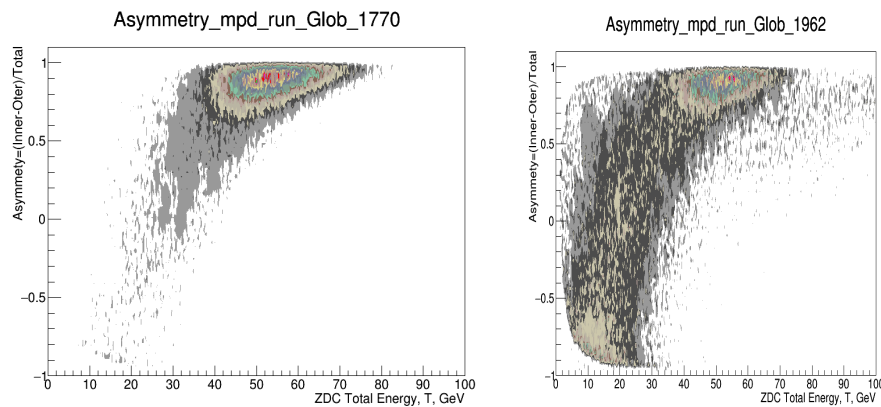


*Fig. 2.2.2.70. The Energy Asymmetry distribution for different Run conditions: Left: – carbon beam without interaction with a target, Right: – carbon beam interacts with a Pb target of 9.9 mm thick.*

### 2.2.2.11. Forward Hadron Calorimeter FHCAL

During 2018 – 2019, the following works were carried out to modernize the ZDC forward hadron calorimeter FHCAL:

- Calculation of doses and neutron fluxes of the ZDC calorimeter using FLUKA program. It was shown that for experiments with heavy ion beams, the dose and neutron fluxes in the scintillators of the modules in the central region of

the calorimeter significantly exceed the acceptable levels, which would lead to the degradation of calorimeter characteristics such as the energy resolution and linearity of response. Therefore, for the BM@N heavy ion program it was decided to replace the existing ZDC calorimeter with a new hadron calorimeter with a beam hole in the center of the calorimeter which has a better energy resolution. The existing ZDC calorimeter can be used to measure the energy of forward going neutrons.

- In September 2019 a new forward hadron calorimeter was assembled and installed in the BM@N setup. The inner part of the new calorimeter is assembled from 34 modules with transverse dimensions of 150x150 mm manufactured at INR RAS. These modules are similar to the modules of the MPD calorimeter described in section 2.2.1.6. To assemble the outer part of the new calorimeter, 20 modules of the hadron calorimeter designed for the CBM setup, which is under construction at the FAIR accelerator complex in Darmstadt, were used. These modules were also manufactured at INR RAS. Temporary use of these modules for the BM@N calorimeter is regulated by a special agreement signed by the management of INR RAS, JINR, CBM and BM@N collaborations.

- The new hadron calorimeter is assembled on a platform specially made for this purpose.

- 54 boards to readout avalanche photodetectors with analog electronics were manufactured and tested. All the boards with this type of electronics were installed in calorimeter modules in September 2019.

- The digital electronics for data readout from the calorimeter modules based on ADC64 boards was produced.

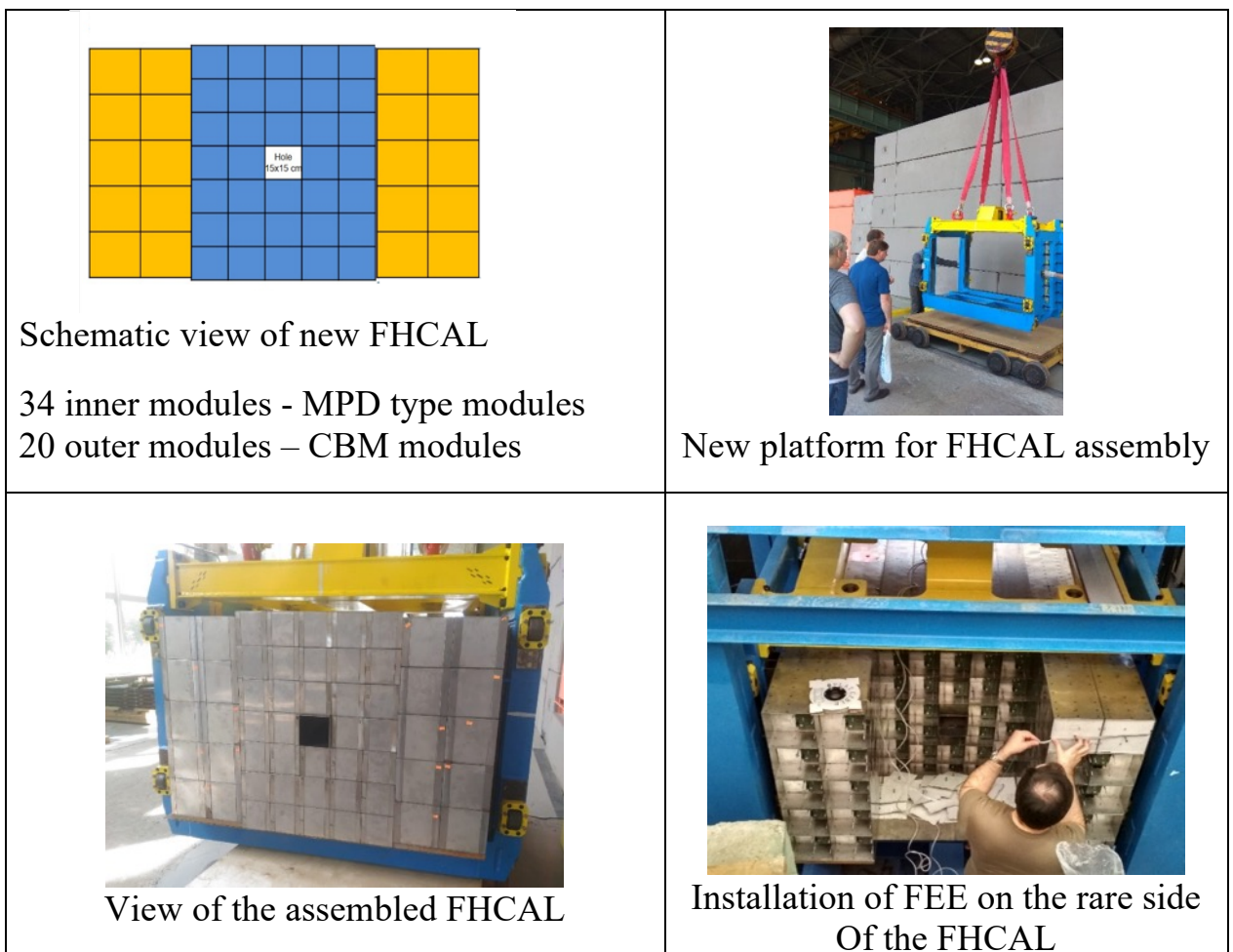
- A technique has been developed for energy calibration of calorimeter modules, which uses longitudinal segmentation of modules. During 2018 – 2019, a work was also carried out on the development of the forward beam hodoscope for measuring the charge of fragments in the beam hole of the new forward hadron calorimeter. Two prototypes of such a hodoscope were made. Both prototypes were made of radiation resistant quartz. One of the hodoscopes was assembled with four quartz plates with dimensions of 40x4x480 mm, in which light from each of the plates was detected using a PMT. This hodoscope was tested in Ag ion beam during the physics run of the HADES experiment in 2019. Another prototype of the hodoscope detector with a quartz plate with a size of 3 x 5x 80mm was tested with cosmic muons at INR RAS. Cherenkov light was detected using a micropixel avalanche photodiode fixed at one of the edges of the

quartz plate. For both prototypes, a light output was obtained for particles with a charge of one.

The future plans for the new forward hadron calorimeter and forward hodoscope are the following:

- Integration of data readout from the calorimeter modules and the detector slow control into the general BM@N DAQ and slow control systems.
- Testing the response of all the calorimeter modules with cosmic particles.
- Energy calibration of the calorimeter modules with cosmic particles.
- Perform a research on the light output of the hodoscope prototype based on the LFS crystal.
- Production and testing of a full-scale beam hodoscope.

All these works are planned to complete in the first half of 2020. Photos in Fig. 2.2.2.71 illustrate the present status of the new forward hadron calorimeter FHCAL.



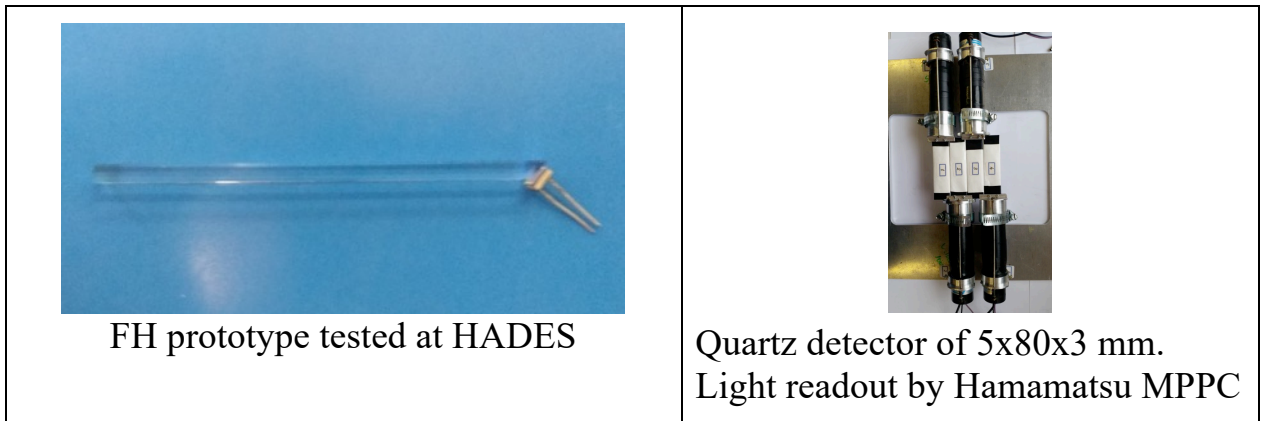


*Fig. 2.2.2.71. Illustration to the new front calorimeter status*

### 2.2.2.12. Electromagnetic calorimeter ECAL

The design of the ECAL modules and readout electronics was based on the “shashlyk” modules developed for the MPD ECAL calorimeter (see section 2.3.1.2). In the BM@N run in the argon and krypton beams of the Nuclotron performed in Spring 2018 one arm of the ECAL calorimeter consisting of 49 modules was operated. The photo of the one-arm ECAL calorimeter inside the BM@N analyzing magnet and the schematic view of one “shashlyk” module are given in Fig.2.2.2.72.

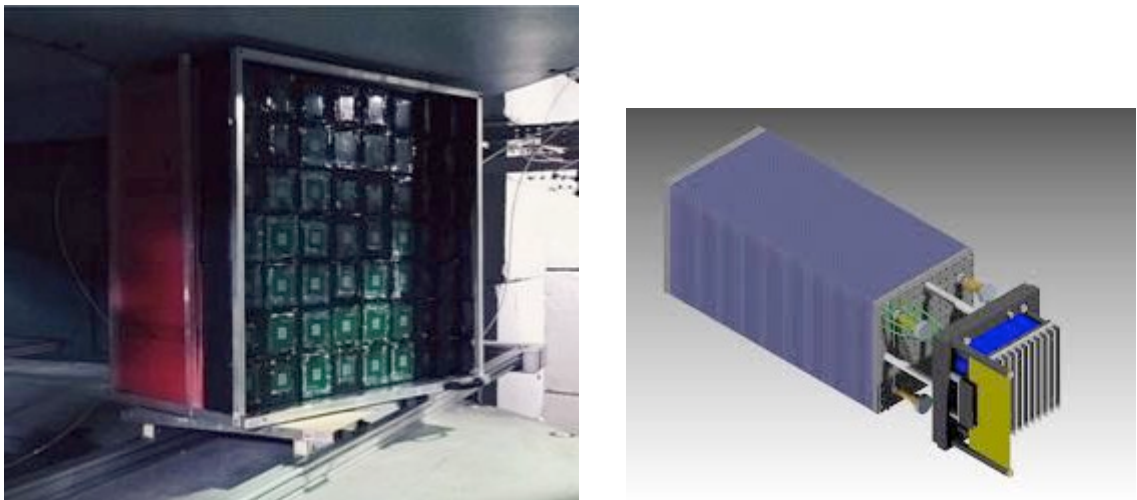


*Fig. 2.2.2.72. Left: One arm of the ECAL calorimeter inside the BM@N analyzing magnet. Right: schematic view of one module of the ECAL calorimeter.*

The task of the ECAL group in 2019 was to process data from the electromagnetic calorimeter obtained in the argon and krypton beam runs. The main effort was focused on the separation of signals from gamma against the background signals from neutrons and charged particles. The most effective method of separation of particles is based on the signal time analysis. The Monte Carlo simulation showed that the time distribution of signals in clusters produced by gamma rays and other particles are significantly different.

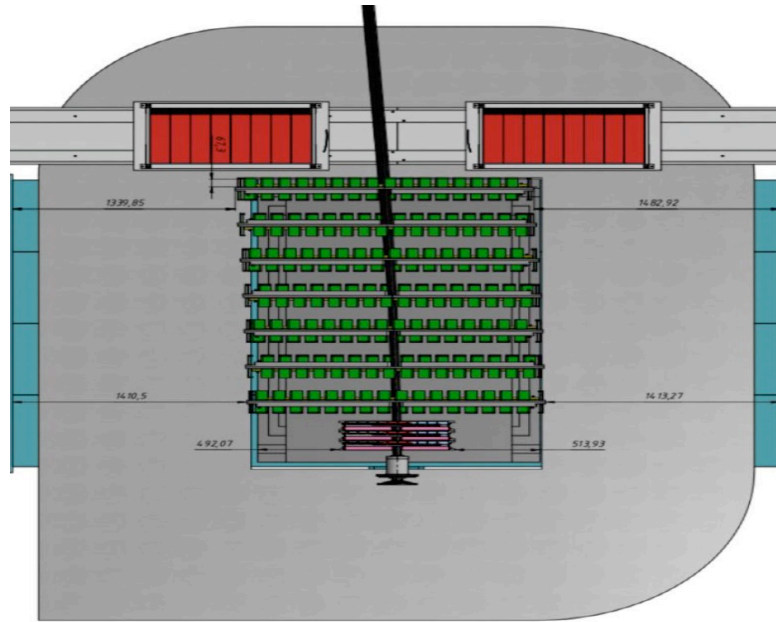


Fig. 2.2.2.73. Location of the two arm ECAL calorimeter (red boxes) behind the GEM detectors (green figures) inside the BM@N analyzing magnet foreseen for next experimental runs in 2020-21

Subsequent analysis of experimental data and simulation results showed that the vast majority of detected events in ECAL are background from charged particles, neutrons and gammas produced outside the target. Monte Carlo simulation shows that the difference in time of signals in a pair of clusters from gamma originated from  $\pi \rightarrow \gamma\gamma$  decay does not exceed 0.5 ns. For background events, this value is much larger. Fig. 2.2.2.74 shows the simulation results for  $\pi \rightarrow \gamma\gamma$  decay and the signal time difference  $dT$  for any two clusters in the experimental data.

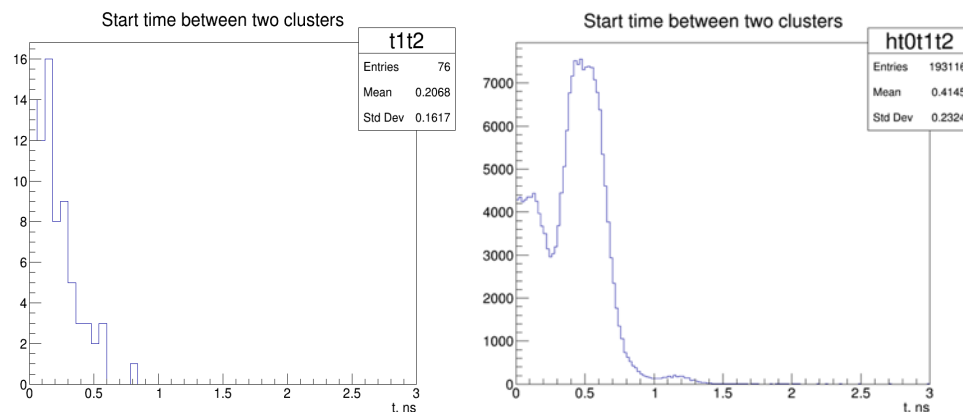


Fig. 2.2.2.74. Time distribution of the difference in the arrival of signals from a pair of clusters: the  $\pi \rightarrow \gamma\gamma$  simulation (left) and the experimental data (right).

Using the criteria on the cluster time difference together with the analysis of the energy and shape of the clusters, it was possible to suppress the background by 3-4 orders of magnitude. As a result, more pure events containing two gamma quanta

remained for the final analysis. An example of such an event is presented in Fig. 2.2.2.75.

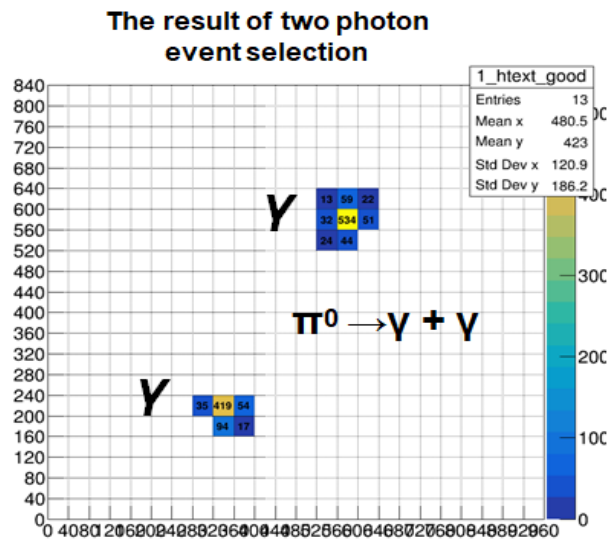


Fig. 2.2.2.75. Selected event according to the formulated criteria.

The final analysis of the data of the selected events was carried out according to the standard procedure, namely, by constructing the effective mass from a pair of clusters, reproducing the background mass distribution by a “mixing event” method, and then subtracting the background from the effective mass spectra. The result of this analysis is presented in Fig. 2.2.2.76. The chosen method of selecting of 2-gamma events using the time analysis made it possible to select decays of  $\pi^0$  mesons. Unfortunately, due to the small acceptance of the one-arm calorimeter located rather away from the beam in the BM@N argon and krypton runs, the overwhelming number of events included in the effective mass spectra shown in Fig. 2.2.2.76 are from decay photons of different particles. To increase the acceptance of the calorimeter for detection of  $\pi^0$  mesons it is foreseen to add a second arm to the ECAL installation (Fig.2.2.2.73). The installation of the two-arm calorimeter is planned in 2020.

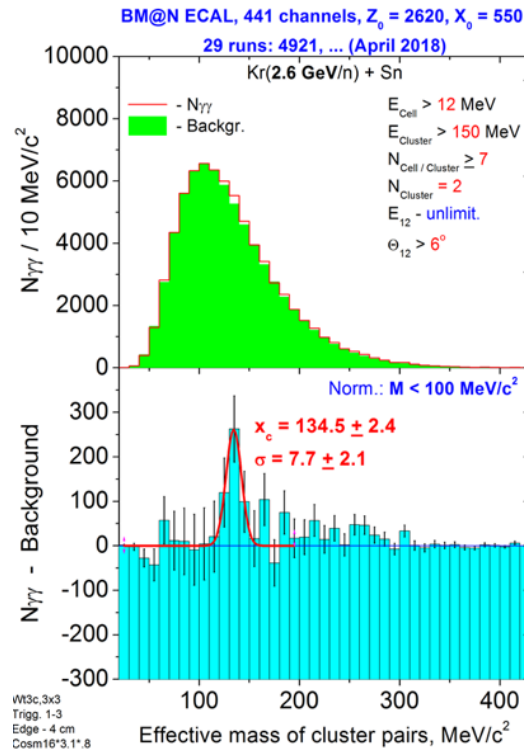


Fig. 2.2.2.76. Separation of the  $\pi^0$  meson in the spectrum of effective masses of  $\gamma\gamma$ .

### 2.2.2.13. BM@N DAQ system and computing

The core function of the DAQ system is realization of data transfer from the detector to the storage system. It includes the data flow from readout electronics to the First Level Processor (FLP) fabric, to the Event Building (EB) and to the Storage System. Main DAQ components are data transfer networks, data processing servers, online storage system, software packages, network communication protocols and data formats. Readout electronics interface, Clock and Time Synchronization (Timing) System and Trigger Distribution

DAQ system at BM@N consist of 3 large parts:

- Electronic modules, developed by DAQ group, which include DAQ electronics, digitizing modules for all detectors at BM@N, detector control modules, front-end electronics and specific modules;
- Network infrastructure includes White Rabbit Network, Data Transfer Network, Slow Control Network and First Level Processors (FLP).
- Data processing, management, analyzing, utility and control software.

#### 2.2.2.13.1. Electronics modules

##### DAQ Electronics.

FVME2 Controller is a VME64x bus controller module, which collects data from VME modules, transmits the data to the server (FLP) via optical link and controls modules within one VME crate.

PEXML-4 (Fig. 2.2.2.77, left) is PCI-E interface module. It's mounted into FLP, receives data from FVME Controller and transmits setups for VME modules to Controller using M-Link protocol.

FVME2 TMWR module (Fig. 2.2.2.77, middle) is used for clock and trigger distribution and time synchronization via White Rabbit protocol within one VME crate. Every FVME2 TMWR module at different VME crates are synchronized between each other by White Rabbit network.

UT24VE RC (Fig. 2.2.2.77, right) is universal 24 TTL I/O VME64x board with White Rabbit support, which used for implementation trigger logic.

For 2013-2019 years 16 FVME2 Controllers, 16 FVME2 TMWR, 20 PEXML-4 and 16 UT24VE RC were produced for BM@N, detector and DAQ test stands and for reserve.



*Fig. 2.2.2.77. PEXML-4 (left), FVME2 TMWR (middle), UT24VE RC (right)*

#### Digitizing modules for detectors.

There are two large family of digitizing modules: time to digital converters (TDC) and waveform digitizers (ADC).

TDCs are used at TOF400, TOF700, DCH and FFD detectors and ADCs – at ECal, ZDC, GEM, STS and CSC detectors.

TDC72VHL and TDC64VHLE (Fig. 2.2.2.78, left and middle) is 72-channels and 64-channels VME64x modules with 25 ps resolution. The first one digitizes signals from TOF400 and FFD, the second one – from TOF700.

TDC64V (Fig. 2.2.2.78, right) is 64-channels VME64x module with 100 ps resolution and used for digitize signals from DCH.

For 2013-2019 years 69 TDC64V, 55 TDC64VHLE and 35 TDC72VHL were produced for BM@N, detector and DAQ test stands and for reserve.



*Fig. 2.2.2.78. TDC72VHL (left), TDC64VHLE (middle), TDC64V (right)*

ADC64VE and ADC64s2 (Fig. 2.2.2.79) are 64-channels 62.5 MSps waveform digitizers. ADC64VE is used at GEM, STS and CSC detectors, and ADC64s2 – at

ZDC and Ecal. For 2013-2019 years 42 modules ADC64s2 and 50 modules ADC64VE were produced for BM@N, detector and DAQ test stands and for reserve.



*Fig. 2.2.2.79. ADC64VE (left) and ADC64s2 (right)*

Detector control modules.

Front-end electronics at GEM, STS, CSC and TOF700 needs a remote control for tuning threshold and other specific parameters. Therefore U40VE (Fig. 2.2.2.80) module is applied. It's a universal 40 I/O VME64x board with White Rabbit support. It has personal firmware for different kinds of front-end electronics. For 2013-2019 years 40 modules were produced for BM@N, detector and DAQ test stands and for reserve.



*Fig. 2.2.2.80. U40VE*

Front-end electronics.

ADC64Amp electronic module (Fig. 2.2.2.81, left) was developed for amplification and shaping signals from Ecal and ZDC detectors. It's a 64-channels ADC driver with unipolar inputs, which connects to the digitizer like a mezzanine board.

MAPD\_FEB module (Fig. 2.2.2.81, right) is intended for placing 9 MPPCs Hamamatsu at the Ecal module. It connects to ADC64Amp amplifier by flex kapton cable.

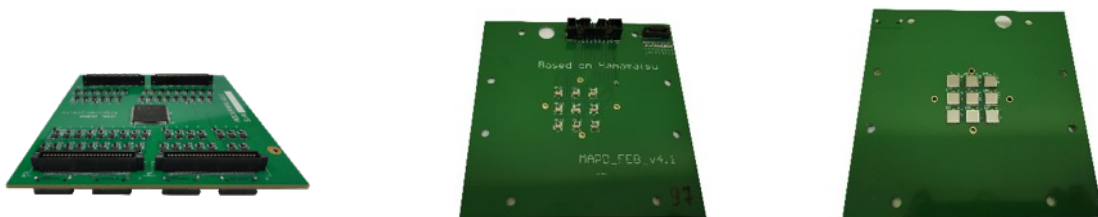


*Fig. 2.2.2.81. ADC64Amp (left), MAPD\_FEB – top and MAPD\_FEB bot*

For 2013-2019 years 120 MAPD\_FEB modules and 20 ADC64Amp modules were produced for BM@N, detector and DAQ test stands and for reserve.

### Specific modules.

For readout signals from MWPC HRB6ASD module (Fig. 2.2.2.82, left) is used. It's a 128-channels readout board with adjustable thresholds. Synchronization of these boards is implemented by TTB9 (Fig. 2.2.2.82, right) – trigger and timing distribution module. For 2013-2019 years 36 HRB6ASD and 8 TTB9 were produced for BM@N, detector and DAQ test stands and for reserve.

Some analog signals from T0 unit of FFD detector are digitized and counted by TQDC16VS (Fig. 2.2.2.83, left) and MSC16VE (Fig. 2.2.2.81, right). TQDC16VS is a VME64x 16-channel time and amplitude digitizer and MSC16VE is a VME 64x 16-channel scaler with RAM. For 2013-2019 years 4 MSC16VE and 8 TQDC16VS were produced for BM@N, detector and DAQ test stands and for reserve.



*Fig. 2.2.2.82. HRB6ASD (left) and TTB9 (right)*



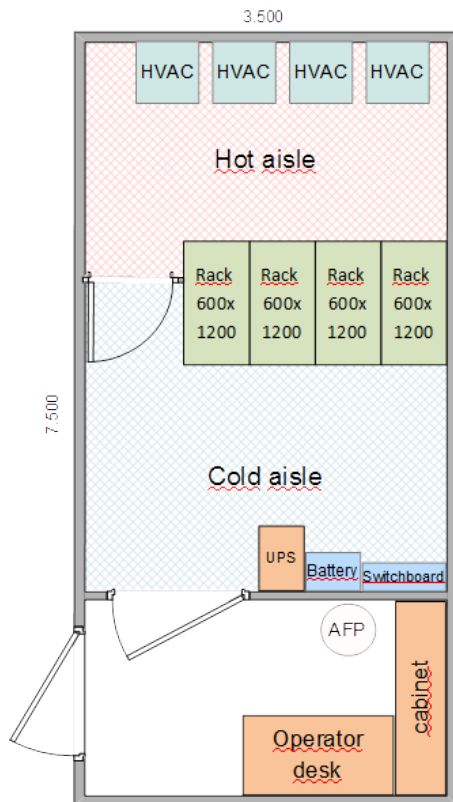
*Fig. 2.2.2.83. TQDC16VS (left) and MSC16VE (right)*

### **2.2.2.13.2. Network infrastructure**

#### Data Transfer Network, Slow Control Network and First Level Processors.

Switches with SFP ports for optical transceivers and RJ45 ports for cooper Ethernet cables were acquired to collect and aggregate data from readout electronics. The “white rabbit” network was rebuilt and reconfigured. All optical fiber lines between the BM@N experimental site and the switching racks were replaced by new one.

New optical cable path was paved for in Mini Data Center (MDC, Fig. 2.2.2.84). This one has allowed to move all FLPs from BM@N experimental site to MDC. The fiber optic communication lines replacement is giving a unexpected big reserve of optical connections for additional devices. It allowed to scale network (see Fig. 2.2.2.85) very easy. For 2018-2019 MDC was built and launched in test mode.



Specifications	
Input power	50 kW
IT power	24 kW (N+1) / 30 kW max
Rack count	4 racks
Redundancy	N+1 (UPS, HVAC)
Battery backup	8 minutes
Rack size	600 x 1200 x 42U

Stage-1 Equipment	Rack Units
Passive network	16
Active network (switches, controllers)	18
Infrastructure nodes	4
FLP, Event Builder nodes	44
Transient Flash Storage	13
Message Logging and Search	5
Reserve (Stage-2)	68

Fig. 2.2.2.84. MDC (mini data center) specifications.

20 nodes of FLP were acquired for the BM@N. It's a computer node that receives raw data stream from detector electronics, performs data validation and reassembles data fragments. MStream protocol receivers are run on FLP nodes.

The BM@N Storage System has two stages: the Transient Data Storage (TDS) 285 TB and Permanent Data Storage (PDS) 1,8 PB. It utilizes a two-tier software architecture and data migration from TDS and PDS is transparent to the user. The storage system exposes standard interfaces to the applications. POSIX compatible cluster file system as well as a raw Object Storage are available.

The TDS will perform the temporary storage of raw data produced by Event Builder system.

The data are recorded to the TDS during data-taking phase of BM@N and is continuously migrated to permanent storage.

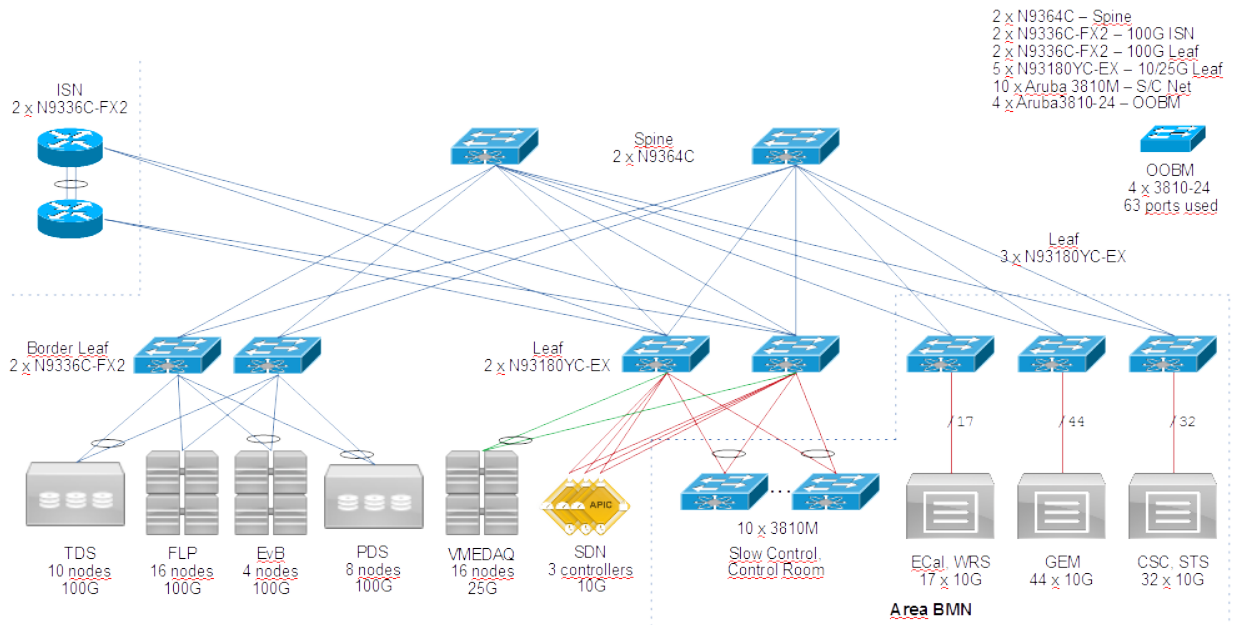


Fig. 2.2.2.85. BM@N DAQ Network

White Rabbit Network.

White Rabbit provides sub-nanosecond accuracy and picoseconds precision of synchronization for large distributed systems. It also allows for deterministic and reliable data delivery. DRE boards digitize detector signals using common notion of time and frequency provided by the White Rabbit (WR) network (Fig 2.2.2.86). The time reference is provided by GPS/GLONASS receiver and backup precision frequency reference (Cesium or Rubidium clock).

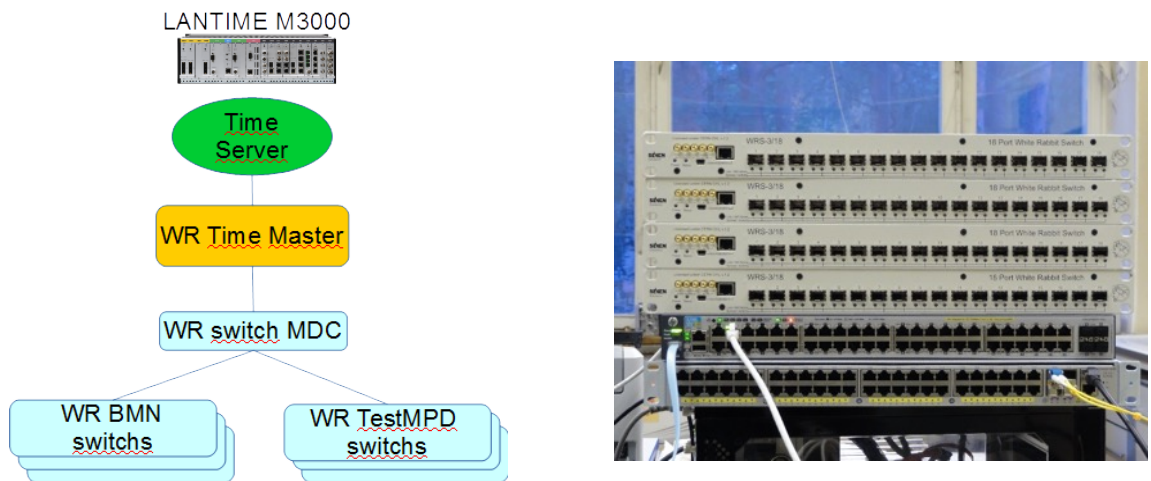


Fig. 2.2.2.86. White Rabbit Network structure (left) and WR switches test stand (right)

The Mini Data Center views are shown in Fig. 2.2.2.87.



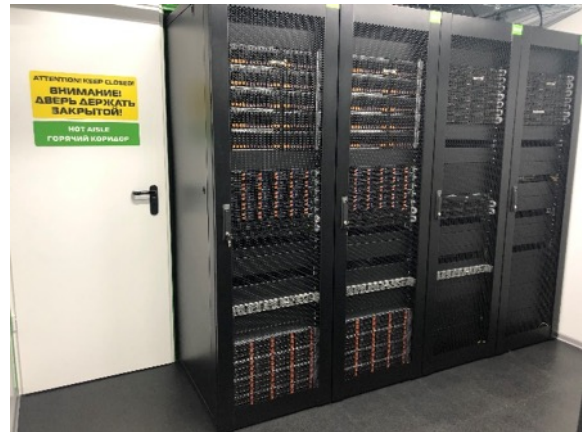
MDC outside view.



MDC inside view 1.



MDC inside view 2.



MDC inside view 3.

*Fig. 2.2.2.87. MDC outside view (top left) and inside views*

### **2.2.2.13.3. DAQ Software**

#### DevFlashProg

This program can connect to Ethernet device and write firmware image file into device flash memory and/or verify it. A log information is written in corresponding database after every success write.

#### PNP protocol

Any program that takes part in a run control system sends specific package to multicast. Another can find out what program is running at this moment and some information about it, host and port of TCP-server for remote control or with outgoing data.

#### MLDP protocol

All our 211thernet devices support MLDP protocol. It allows up to avoid binding devices to the IP-address in programs. MLDP-message contains IP address, serial number, device type and other useful information. All our 211thernet devices

periodically sends it over multicast. One program can receive it and find out on what address we should establish a connection.

### Mstream

This program receives data packages from 212thernet device, perform defragmentation of Mstream data blocks, packs them into MpdRawData format and transmit them to outgoing TCP-server. In future it is planned to integrate this logic into control programs as separate threads.

### Event builder

The task of this program is to collect data from several client programs (mstream program or another event builder), separate event blocks in every data flow, combines them together per events and further retransmits or writes to the file as united data block.

### TQDC control

This program sets up TQDC16VS-E device with proper configuration. Among the main parameter there are channel enable, thresholds, readout window, trigger source. In debug mode it is capable to make specific adjustment of HPTDC setup. Although it starts mstream subprogram for reading data. Perform some data analyze.

### ADC64

This program sets up ADC-like devices with proper configuration. Among the main parameter there are channel enable, readout window, trigger source, DSP (digital signal processing) logic and sparse readout. This program can read data from device, visualize them and save data as an ASCII file. It is used just to prepare for run, in run execution adc64-system is used.

### Adc64-system

This program writes configuration and handle data readout from list of ADC-like boards with error handle and remote control. This program can be used as slave one in run control system.

### Mpd-rawstat

This program can perform specific data/device tests: presence of all devices in the final data file, absence of significant time discrepancy, etc. Data can be obtained from reading a file or form specific TCP-server of event builder program (monitor output).

### Adc64-viewer

This program is similar to mpd-rawstat, but it performs just quick visualization of any signal from adc-like devices. Data source can be a file or monitor output.

### HRB-system

This program writes configuration and handle data readout from list of HRB6ASD and TTB9V boards with error handle and remote control. This program can be used as slave one in run control system.

### Vme DAQ program kit

There are two main programs: vmedaq and vmegui.

*VmeDaq* is a daemon that communicate with modules in single VME-crate, write configuration, perform data readout, support remote control protocol.

*VmeGui* is a GUI application for changing saved configuration of modules and for basic data analysis.

### U40ve-ideas and u40ve-8spi

These programs configures and controls corresponding devices.

### Afi-run-control (aka u40ve-rc)

This program combines two tasks: first one is configuring U40VE-RC and UT24-RC boards, the second one is management slave programs and perform run execution.

## **2.2.2.14. The experimental hall of BM@N setup**

The experimental hall of the BM@N setup is an area in the building №205, which is located on channel 6B of the extracted beam from the Nuclotron accelerating complex. This hall has 5 magnetic elements (Fig. 2.2.2.88):

1. 2 quadrupole lenses K-200, which provide the focusing of accelerated beam on the target;
2. 2 correction magnets: VKM (magnet for vertical correction) and SP-57 (magnet for horizontal correction). These magnets provide fine-tuning of the beam position on the target;
3. an analyzing magnet SP-41 with an aperture of 1070 mm and a pole size of 1360x2490 mm. The maximal magnetic field value is 1 T.

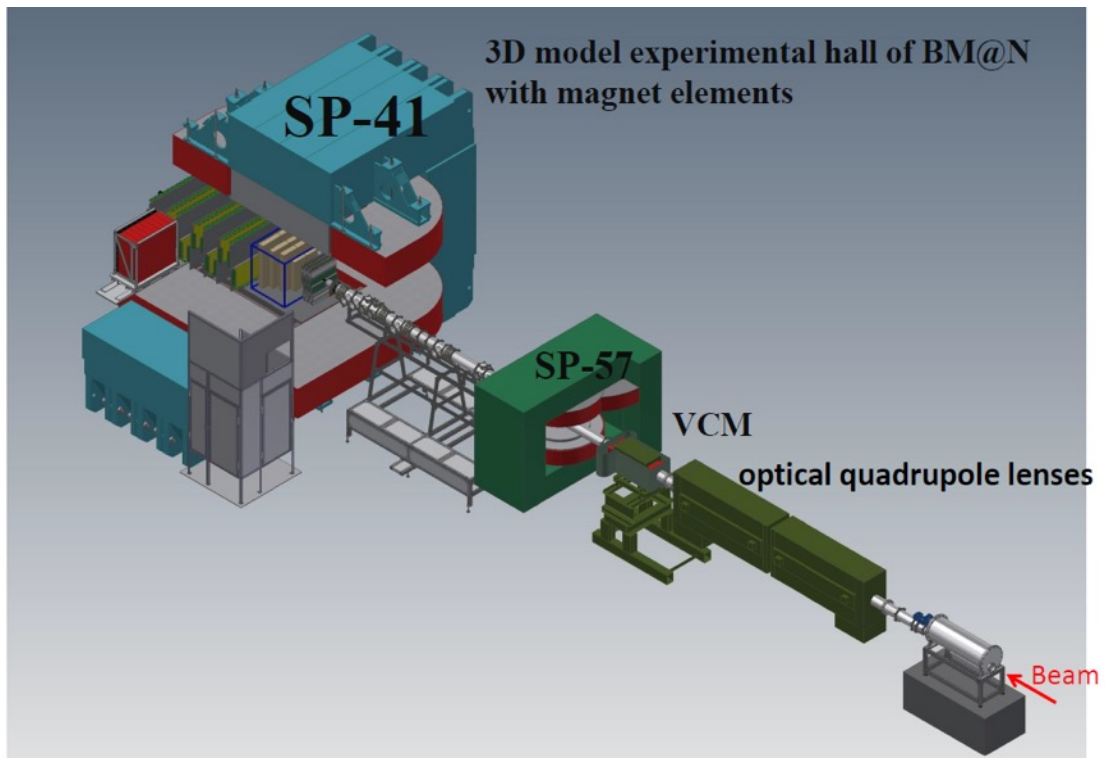


*Fig. 2.2.2.88. BM@N experimental hall with 5 magnetic elements*

In 2013, a biological protection was designed and installed around the experimental hall. It includes: a beam stopper, 3 doors with locks, information boards, a beam dump, reinforced concrete walls. Biological protection is the border between the prohibited area and controlled area during the test and physical runs at the BM@N. It excludes entering of unauthorized personnel to the prohibited area. The beam stopper was designed, manufactured and installed. To minimize the interaction of the beam with air molecules, the beam stopper is made in a vacuum box.

A quick-detachable roof was installed over the experimental hall of the BM@N. The modular system of the metal roof was designed for fast relocation of detectors and other elements using a crane. Also in 2013, a two-story Control Room with the necessary infrastructure was designed and installed. Personal computers and visualization system of slow control are located inside. Online monitoring and operation can be performed from the control room during BM@N runs.

In 2014, an adjustment device (platform) was designed and mounted to install ZDC modules with a total weight of 15 tons in the BM@N experimental hall. This device provides online precise installation (with an installation accuracy of 1 mm) of each ZDC module to the beam axis to perform the calibration procedure for all modules. The adjustment device is controlled by electric drives and ACS (automatic control system), which allows quick installation of each ZDC module without stopping the beam acceleration.

To mount two DCH drift chambers inside the BM@N experimental hall as an outer tracker, mechanical supports were designed. These supports allow one to perform an independent alignment of both DCH detectors.

Cable channels were mounted along the entire perimeter of the biological protection, taking into account the location of all the detecting elements of the BM@N setup.

To locate the DAQ system inside the BM@N installation hall, twelve 19-inch racks were installed. Taking into account all the subsystems, detectors, LV, HV of the necessary equipment for conducting experiments at the BM@N, the power supply was designed and installed. Uninterruptible power supplies are used in every rack to ensure high voltage stability in the common network inside the experimental hall.

A mechanical support, which is designed to mount all beam detectors before the target, was made. Since it was planned to test and use various beam detectors at the installation, this support was made of BOSCH aluminum profile. Thus this universal support was used in all runs of the BM@N. All trigger detectors were installed on this support. Currently, it is used as a mechanics to install and align a vacuum beam pipe with boxes for beam detectors.

The BM@N setup includes two ToF detectors. To position the ToF system at a distance of 400 cm and 700 cm from the target, mechanical structures with support on the side walls of biological protection were mounted. As the density of the detection elements in experimental hall is high, the need for maintenance of the detectors using this mechanical support was taken into account during development.

The first technical run at the BM@N experimental setup was performed in 2015 with the deuteron beam. The characteristics of the detector subsystems and read-out electronics were investigated, an integrated data acquisition system was tested, and the algorithms for data analysis were developed. The first physical data were recorded in 2017 with the carbon beam, the analysis process is at the final stage. After the heavy ion source “Kryon” was launched, relativistic argon and krypton beams were accelerated and transported to the BM@N setup in February–March 2018 for the first time. About 130 million events were recorded. The analysis of the experimental data will provide the information about the products of interaction of “medium” ion beams with various targets (carbon, aluminum, copper, tin, lead).

Currently, work is underway to prepare the BM@N setup for data taking with the relativistic heavy ion beams. The expected maximal intensity of Au ions is  $2 \times 10^6$  Hz by 2022. By the first runs with heavy ion beams, the existing experimental setup will be expanded and supplemented with new detectors, taking into account the experience gained at previous Nuclotron runs.

A vacuum beam pipe will be integrated into the experimental setup to minimize the amount of scattering material on the way of heavy ions.

Beam pipe will consist of three parts: before the target, inside the analyzing magnet and after the analyzing magnet.

Beam pipe before the target is already produced and installed into BM@N experimental setup in October 2019. It is performed from stainless steel and consists of vacuum standard modules and boxes for all beam detectors (Fig. 2.2.2.89).

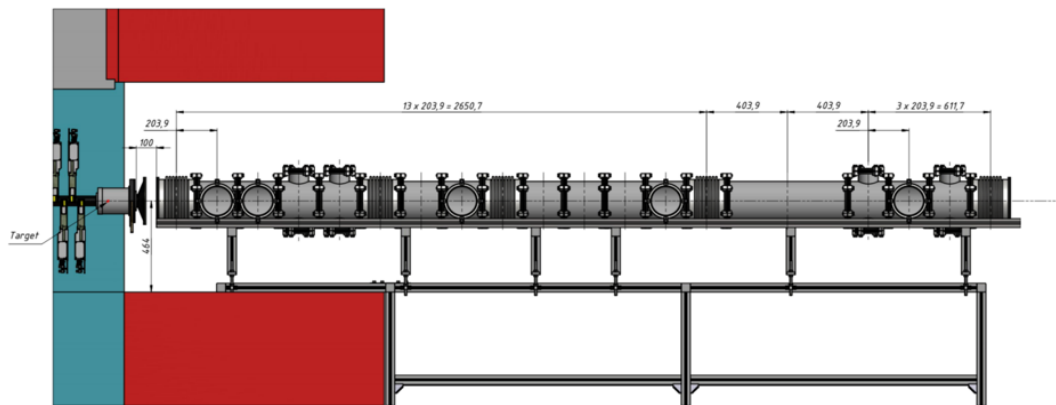


*Fig. 2.2.2.89. Beam pipe before the target*

This configuration of beam pipe was manufactured and tested by LLC “Vacuum systems and technologies” (Belgorod, Russia). At present this company develops mechanics for beam profilometers, which will be used at the beginning of the Nuclotron run and have to be removed when the physical data acquisition start.

After this beam pipe the target station will be located. At present, the design of the target station is being developed (Fig. 2.2.2.90). The target station will allow changing the target without breaking the vacuum.

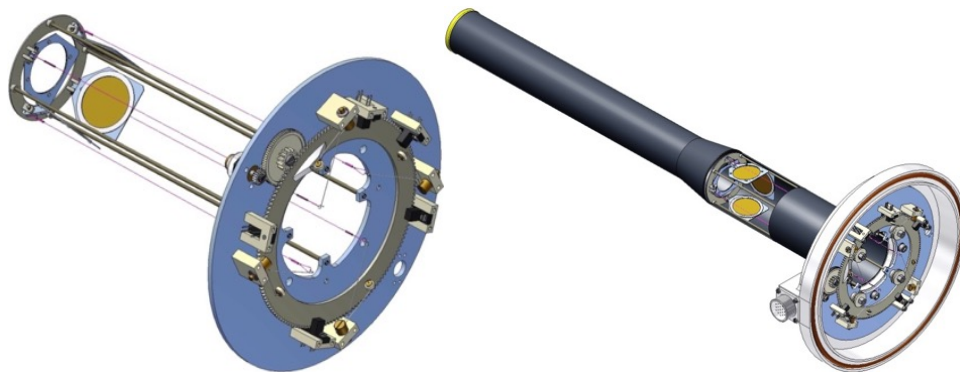


*Fig. 2.2.2.90. Target station*

The carbon beam pipe will be installed inside the analyzing magnet. It will consist of the parts, that are shown in Fig. 2.2.2.91. Such configuration will allow to perform different scenarios of tracking detectors installation. Total length of the carbon beam pipe is 5 m. The thickness of the walls is 1 mm. It has to sustain vacuum up to  $10^{-3}$  Torr. Production of first prototype of carbon beam pipe is started by DD “Arkhipov”.

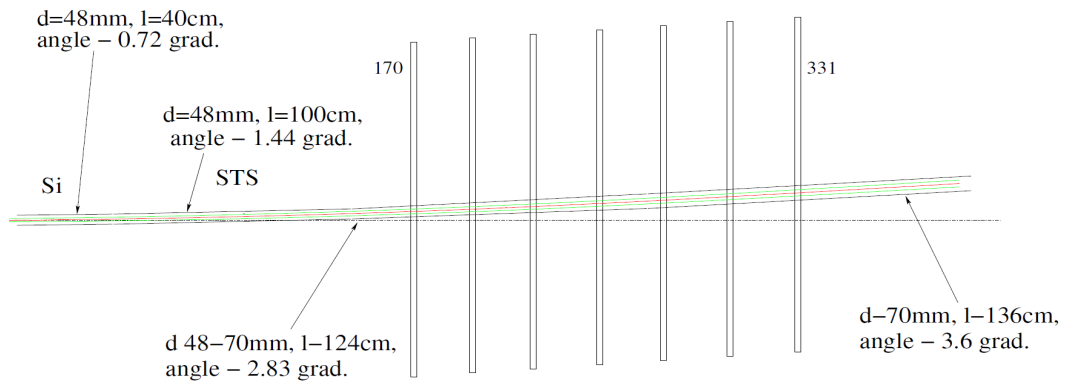


*Fig. 2.2.2.91. Carbon beam pipe configuration inside the analyzing magnet*

Development of aluminum beam pipe downstream the analyzing magnet is started. To finish the development precise 3d measurements of all the detector subsystems after the magnet are to be done (Fig. 2.2.2.92).



*Fig. 2.2.2.92. Experimental area downstream the magnet*

For physical program with heavy ion beams with intensities few  $10^6$  ion/s additional reinforced concrete blocks for personnel biological protection are to be installed.

Power supply system has to be upgraded for full detector configuration.

### **2.2.2.15. First experimental runs and BM@N status**

Collected statistics of experimental events in BM@N technical runs with deuteron, carbon, argon and krypton beams of different energies performed in 2016-2018 is shown in Fig. 2.2.2.93 below.

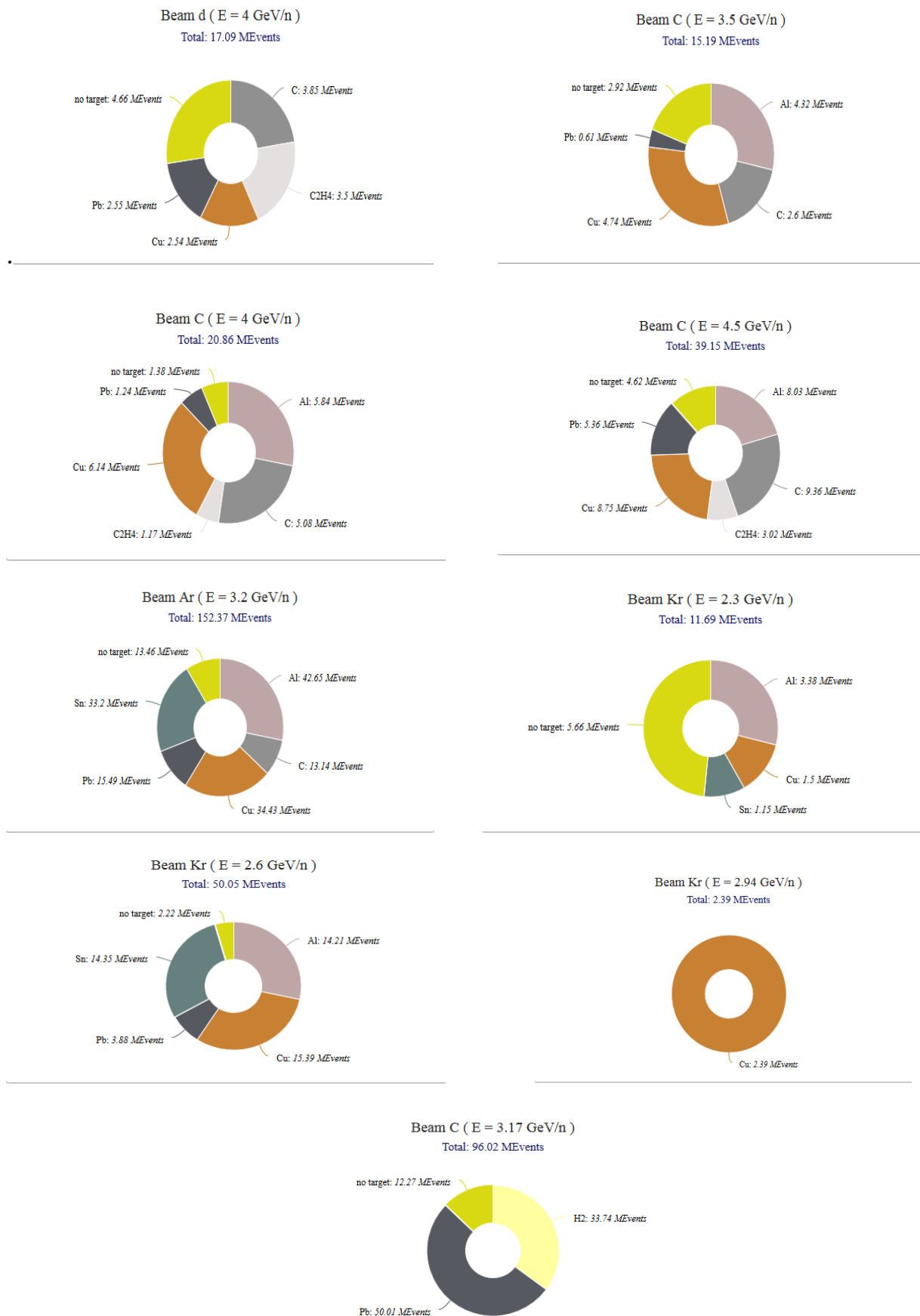


Fig. 2.2.2.93. Collected statistics of events in the BM@N experimental runs

Configuration of the BM@N central tracker, beam parameters and event rates in in the performed and future BM@N experimental runs are shown in Table 2.2.2.1.

Table 2.2.2.1. Configuration of the BM@N central tracker, beam parameters and event rates in BM@N experimental runs

Year	2016	2017 spring	2018 spring	2021	2022 and further
Beam	d(↑)	C	Ar,Kr, C(SRC)	Kr,Xe	up to Au
Beam intensity, Hz	0.5 M	0.5 M	0.5 M	0.5 M	2 - 5 M
Data rate, Hz	5 k	5 k	10 k	10 k	20 k→50 k
Central tracker configuration	6 GEM half- planes	6 GEM half- planes	6 GEM half- planes + 3 FwdSi planes	6 GEM planes + 3 FwdSi planes	7 GEM planes + 3 FwdSi planes + 4 STS planes
Status of the experiment	Technic al run	Technic al run	Technical and physical run	physical run, first stage	physical run, second stage

### 2.2.3. Spin Physics Detector (SPD) for study of nucleon spin structure

Preliminary version of the SPD (Spin Physics Detector at the NICA collider) conceptual project was presented at the JINR PAC on Particle Physics in January 2019. The PAC expressed support of the activity and recommended to approve the proposal of the Laboratory for preparation of technical project the SPD for the 3 year period (2019-2021). The analysis of the SPD concept was performed taking the remarks formulated by the PAC into account and the further progress has achieved by November 2019:

1. New options of the magnetic system based on three pairs of superconducting coils, for the barrel and the end parts respectively. The results were published in «Письма в ЭЧАЯ» and presented at the European Conference on Applied Superconductivity (EUCAS2019, Glasgow, September 2019). Some illustrations are shown in Fig. 2.2.3.1 and 2.2.3.2.

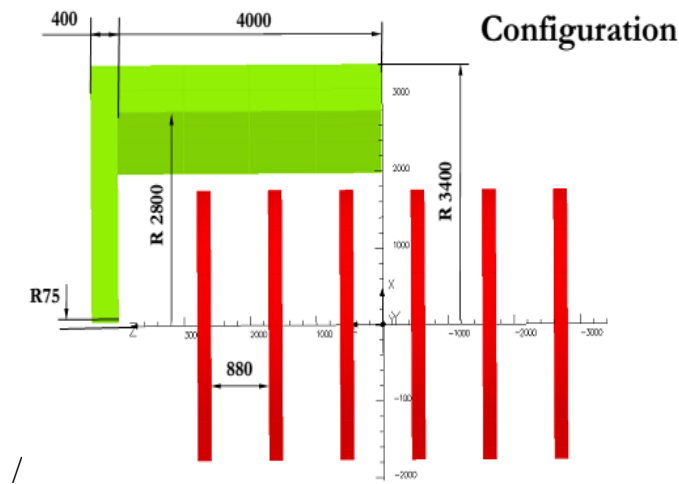


Fig. 2.2.31. General composition of the SPD (left) and scheme of coils generated the magnetic field (right).

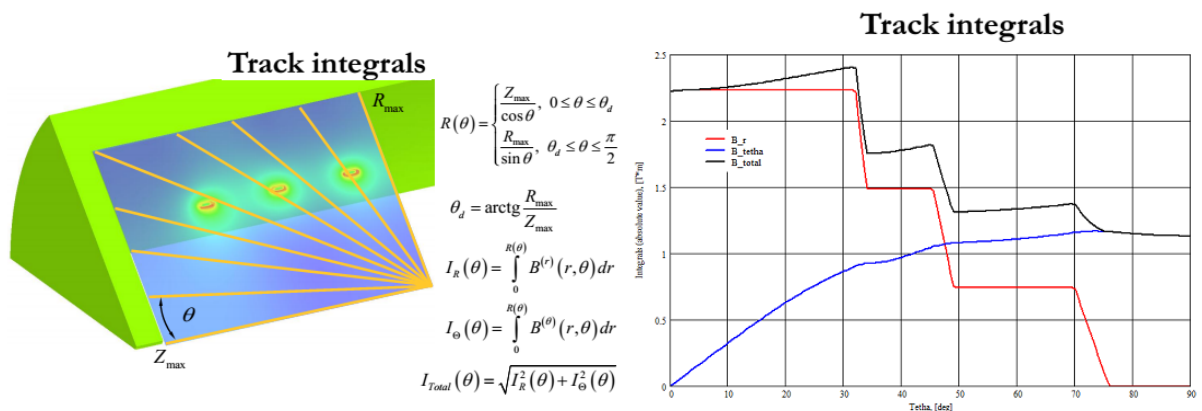


Fig. 2.2.3.2. The magnetic field integrals along different tracks of the particles.

Some of general parameters of the magnetic system in comparison with the CMS set-up at LHC are shown in Table 2.2.3.1.

General parameters of the magnetic system in comparison with the CMS at LHC

Parameter	Unit	SPD/NICA	CMS/LHC
Volume: dia./length	m/m	3.6/8.0	6.5/12.7
Magnetic system		6 coils	solenoid
Peak magnetic field	T	2.0	4.5
Field volume	m <sup>3</sup>	~ 80	~ 414
Stored energy	MJ	~ 80	~2800
Coil turns		6x40	2112
Operating current	kA	10	20
Total inductance	H	~ 2.2	12,6

2. The computer code for simulation of the particle tracking in SPD base on the Kalman-filter method was developed. Test modeling for the SPD tracking system was performed. The particle momentum resolution for different configurations of the magnetic systems was calculated. The package was adopted into the SPD-Root system. The tests are continued. The results of calculations of the momentum resolution are shown in Fig. 2.2.3.3.

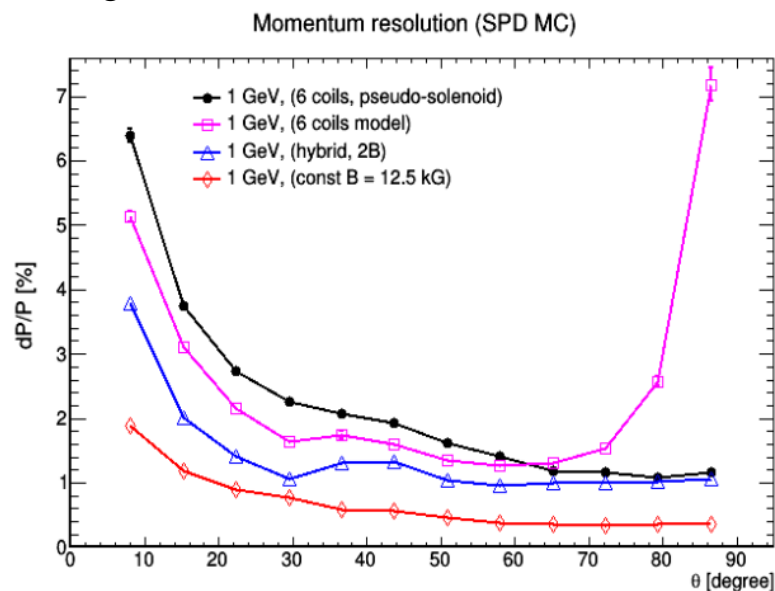


Fig. 2.2.3.3. The dependences of momentum resolution of 1 GeV particle in the case of different magnetic systems on the particle trajectory angle to the SPD axis.

3. Two versions of the muon range system were proposed. The both should be further used in the analysis by Geant4 и SPD-Root for getting detailed modeling results the physics processes of interest. It was shown that muon system of 4 nuclear

lengths thickness + electro-magnetic calorimeter improves signal-to-noise ratio substantially in comparison with the start one. The modeling of Drell-Yang processes, charmonium and direct photons production is continuing.

4. The project was prepared and construction work on the beam test area, aimed at the SPD detectors testing at the Nuclotron extracted beam in Build. 205, have been started.

5. Works on the design, prototyping, manufacturing and tests of the SPD detectors, namely: silicon, straw-tubes, muon system, electromagnetic and hadron calorimeters, beam-beam counter (BBC) system et al. are started or in progress.

6. Work on the SPD data acquisition system was started also.

7. International Workshop on the SPD scientific program (Dubna, June 2019) was carried out, organization of the SPD collaboration was started, working group for the preparing of the collaboration documents, the “SPD Constitution”, in particular, was organized.

8. Results of the SPD physics program development and the CDR preparation were reported at DSPIN2019 (September — 3 reports) and NICA-DAYS2019 (October — 2 reports).

## **2.3. Scientific and engineering infrastructure**

### **2.3.1. Buildings of the Collider complex (Building No. 17)**

In 2009 works on the design of building No. 17 for placement of a collider complex was started. KOMETA company (Russia) was chosen as the designer. In 2013 the first design (stage “P”) was completed and in 2015 construction began. As a general contractor (as a result of an international competition) the Austrian company Strabag was chosen (Agreement 100/2795 of 09/18/2015 for the amount of 3 620 181 414.5 rubbles). As a result of clarification of the terms of reference by JINR specialists at the design stage and at the initial stage of construction, significant changes took place in the 2013 project, which led to an increase in the area of the building No. 17 from the originally planned 19 900 m<sup>2</sup> to 30 800 m<sup>2</sup>. The change in the area of the building led to an increase in the pile field, reinforced concrete and metal structures, the area of walling and roofing, with a corresponding increase in the volume of engineering equipment (ventilation, refrigeration, power). The demand for electric capacities increased from 4 MW to 9 MW. Additionally, the forces of the general contracting organization carried out the removal of five cable lines, the substation No. 13 in building 1A was reconstructed, and work was also done on the construction of a closed cold supply system with the dismantling of the existing river water supply system. Taking into account the additional volume of work, the preliminary cost of the building No. 17 is currently estimated at 7 billion rubbles. Design changes are reflected in four additional agreements to the General Contract. (No. 1 dated 06/23/2016, No. 2 dated March 21, 2017, No. 3 dated August 15, 2017, No. 3.1 dated October 25, 2017) and 10 additional agreements to the Agreement for the provision of technical audit of the project documentation and development of working documentation (No. 1 dated 12/01/2014, No. 2 dated September 24, 2015, No. 3 dated September 25, 2015, No. 4 dated February 10, 2016, No. 5 dated January 20, 2017, No. 6 of December 29, 2017, No. 7 of May 29, 2018, No. 8 of October 20, 2018, No. 9 of May 13, 2019, No. 10 of September 25, 2019).

By the beginning of the fourth quarter of 2019, the construction of a pile field (100%), reinforced concrete structures (93%), installation of metal structures (75%), installation of facades (10%), roofing (30%), earthworks and temporary roads (90%) were completed. Dismantling of the extension of building No. 1 was completed taking into account the increased volumes to ensure the possibility of connecting this building to the building No. 17. To the purpose of installing equipment to transfer the beam from the Booster to the Nuclotron, an aperture in the ceiling of the building No. 1 is equipped.

At the completion stage are tenders for the selection of companies for installation of ventilation and power supply systems, finishing work and landscaping.

A general view of the construction site as of August 2019 is shown in Fig. 2.3.1.1. Deadline for the building No.17 according to the schedule of works (taking into account the increase in construction volumes) is December 2020. This is 1.5 years later than the scheduled date. However, to date, there are risks of deviation even from this new schedule for the following reasons:

1. delay in the approval by JINR of companies for the production and installation of power supply and cold supply systems;
2. the lack of sections of the working documentation that is necessary for the installation of facade systems, stained-glass windows and roofing pie, as well as for the beginning of tender procedures for the installation of the following internal engineering systems: ventilation, water supply, sewage, power electrical equipment, cold supply, automation, dispatching and low-voltage systems .

In view of the foregoing, the completion date of the construction is not finally clear.



*Fig. 2.3.1.1. General view of the construction site (August 2019).*

### **2.3.2. The Cryogenic compressor station**

In 2017 by efforts of “CryogenMash” company (Contract No. MV-421-2015-025 dated 03/31/2016) the design and passed a non-state examination of the project for the construction of the Cryogenic Compressor Station was completed. As a result of the tender, the company “PSJ” (Czech Republic) was selected as the general contractor. (Contract No. 100-539 dated November 22, 2017), however, this

company was not able to implement the project due to bankruptcy. As a result, being in a tight timeframe, the project managers decided to change the conditions for choosing a contractor, according to which it was necessary to choose a company or group of companies with the task of constructing a station building and assembling, commissioning and launching cryogenic equipment purchased by JINR. In the course of the work done and the procurement procedures, “SK Stroytekhinvest” company was selected as a new general contractor (Contract Agreement No. 100-1789 of 05/30/2019) with the condition that the organization should be involved to the installation of equipment, which was necessarily agreed with JINR.

By the beginning of the fourth quarter of 2019 a foundation pit was developed, columnar foundations were concreted, electrical, low-current and sewer networks were removed from the construction site, installation of metal structures of the building frame began. Partially backfilling was completed.

The deadline for completion of the facility in accordance with paragraph 3 of the contract is January 2020.

### **2.3.3. A building of the NICA Centre**

In April 2018, based on the results of the tender, an agreement was signed on the development of design estimates for the NICA Centre facility (Contract No. 1 / 03-2018 of 04/11/2018). The Institute of Unique Structures Design LLC was selected as the General Designer "ARENA". In the framework of the project, the concept of the future building was agreed upon, technical and technological tasks are being formed, the necessary environmental, geodetic and geological surveys have been carried out and the architectural appearance and internal layout of the building have been agreed. At the stage of approval are decisions on a choice of materials and technologies for the implementation of internal and external engineering systems. Landing of the building was carried out. The coordination of external engineering systems is being carried out: household and storm sewers, drinking and fire water supply, low-current cable routes, power cable lines. At the coordination stage are issues of internal fire extinguishing systems, access control systems, heating, air conditioning and ventilation systems. Soon, the Institute’s services will be presented with Project “P” stage documentation for the purpose of agreeing and submitting documents to the Main State Expertise of the Russian Federation.

In the process of working on the project, two additional agreements appeared on the postponement of the deadlines for the submission of design documentation (DS No. 1 dated 06/14/2019 and DS No. 2 in the coordination stage) with a deadline of September 30, 2020. The reasons for the postponement of the implementation of the design work are as follows:

1. long approval of the proposed design solutions by JINR services.
2. bringing the concept and architectural decisions of the designed building in line with the volume of planned financing.

The agreed conceptual view of the future NICA Centre building is shown in Fig. 2.3.3.1.



*Fig. 2.3.3.1. The agreed conceptual view of the future NICA Centre building*

#### **2.3.4. Other building and experimental pavilions**

In order to implement the megaproject, NICA facilities are being created and will be operated on the basis of existing buildings and structures located on the technical site of LHEP. The reconstruction and modernization of existing buildings is carried out in accordance with the tasks set forth in Table 1 of the Passport of the NICA Complex object (see [http://nica.jinr.ru/docs/TDR\\_spec\\_Fin0\\_for\\_site\\_short.pdf](http://nica.jinr.ru/docs/TDR_spec_Fin0_for_site_short.pdf)).

##### **Building No. 1**

The existing building No.1 is part of the accelerator complex being created, requiring technological reconstruction. Building No. 1 is a capital building - an industrial building of circular shape, with a diameter of 87.3 meters, a height of 30 meters in the domed part and a total area of 23 931 square meters with two extensions. The building will house: a magnetic cryostat Booster's ring system with a perimeter of 251.5 m located in a tunnel around the foundation of the synchrotron magnet, a system for diagnosing beams, monitoring and

control, a vacuum ring system, an RF system for accelerating beams in the Nuclotron, a system for slow resonant output of accelerated beams in the main experimental hall (building 205) with the initial section of beam transportation from the exit window of the Nuclotron cryostat to the “focus F3” point, transportation channels of the extracted beams from point F3 to experimental installations in the building No. 205. Taking into account the task in the building, the following reconstruction activities have been carried out and continue to be carried out: inspection, design, reconstruction of engineering systems, general construction work to create the necessary building structures and redevelopment of premises, replacement of reflective structures, opening equipment in concrete floors, works on restoration of facades, replacement of a roofing cake, creation of a concrete contour of biological protection, construction measures to connect building No. 1 with building No. 17 under construction, arrangement of entrance groups, reconstruction of the loading and unloading zone with replacement of the gates, improvement of the adjacent territory.

### **Building No. 1A**

The building is an existing one requiring technological reconstruction. Building No. 1A is a capital structure - an industrial four-story freestanding rectangular building equipped with a supporting, two-beam, electric crane with a lifting capacity of 30.0/5.0 tons. The main purpose is the location of power supplies for magnets, lenses of the Nuclotron ring, beam transport channels and power cable routes. As part of the planned work, the substation No. 13 located in the building was reconstructed, as well as the construction of a closed cold supply system with the dismantling of the existing river water supply system was completed. The reconstruction of the building involves the replacement of technological equipment (power sources), in the building it is necessary to place: the MPD control room, the power supply control room, the server room, office premises for staff. To accomplish the tasks, the following measures have been taken and are underway for the reconstruction of the building: examination, design, reconstruction of engineering systems. replacement of reflective structures, general construction work on the creation of the necessary building structures and redevelopment of premises, replacement of the roofing cake, reconstruction of the entrance group, necessary measures for the replacement of technological equipment, improvement of the adjacent territory.

### **Building No. 1B**

The building is an existing one requiring technological reconstruction. Building No. 1B is a capital building - an industrial building directly adjacent to building No. 1, and involves the location of the cryogenic support system of the Nuclotron. The

building houses helium refrigerators with the necessary infrastructure for storing and circulating gaseous helium, as well as containers for storing liquid nitrogen and its transportation lines. Reconstruction of the building is carried out in order to install additional cryogenic equipment on the newly created platform. Additional equipment will increase the performance of the cryogenic system. As a part of the reconstruction, measures have been taken and are being carried out to examine, design, reconstruct engineering systems, general construction work to create a platform for cryogenic equipment and other necessary building structures, redevelopment and repair of technological premises, necessary measures to replace technological equipment with the involvement of specialists in the field of industrial design.

#### **Building No. 4**

The existing building is part of the accelerator complex being created and requires technological reconstruction. Building No. 4 is a capital building - an industrial one-two-story detached building, in which the experimental production workshop (EPW) is located. On the basis of this EPW it is necessary to create a site for the assembly of thermal screens for SP magnets of the NICA accelerator complex. For this reason it is planned to reconstruct the left wing of the hull. A survey was conducted, according to the results of which the design was completed. The roofing pie was replaced, reconstruction of engineering systems, restoration of the facades, general construction work on the preparation of premises for the installation of technological equipment - ultrasonic baths, an oven, etc. are carried out. Creation of a system of industrial supplies and exhausts ventilation, installation of an external vestibule and expansion of the existing window opening for the installation of metal gates, improvement of the surrounding area are going as well.

#### **Building No. 14**

The existing building is part of the accelerator complex being created and requires technological reconstruction. Building No. 14 is a capital building - an industrial two-story detached building, in which it is planned to create the engineering infrastructure of the on-line LHEP cluster. The on-line cluster is designed to host telecommunications equipment, server equipment, data storage systems, and engineering infrastructure is necessary to ensure the conditions for the continuous and uninterrupted operation of IT equipment of the public sector. Engineering infrastructure should provide a round-the-clock operation mode of the fixed assets in the 7x24x365 mode. According to the results of the survey, the design for the modernization of engineering systems, supporting and enclosing structures of the building, the replacement of the roofing cake, general construction work on the

preparation of premises for the installation of technological and computer equipment are ending.

### **Building No. 32**

The existing building, building No. 32, is a capital building - an industrial three-story detached building, in which the express section of the central economic center is created, with the installation of CNC machines and the modernization of the crane beam (increase in carrying capacity from 3 to 5 tons) with an industrial safety review to produce the necessary parts from various materials (metals, textolite, polycarbonate, etc.) for the needs of the physical-technological equipment of the created NICA complex. As part of the reconstruction, a survey, design, reconstruction of engineering systems, general construction work to modernize crane tracks, create a platform to accommodate CNC machines and other necessary technological structures, replace the roofing pie, redevelop and repair technological and office premises, replace technological equipment, replace reflective structures, restoration of facades, arrangement of entrance groups, improvement of the adjacent territory.

### **Building No. 42**

The existing building is a capital industrial two-story detached building in which will be created: a section for assembling time-of-flight detectors for MPD and BM@N, a section for assembling an electromagnetic calorimeter, a section for testing accelerator elements, as well as specially prepared storage rooms superconducting magnets. As a part of the reconstruction, inspection, design, reconstruction of engineering systems, general construction works on modernization of crane tracks with an examination of industrial safety and other necessary technological structures were carried out, re-planning and repair of technological and office premises, necessary measures for the installation of technological equipment, replacement of reflective structures, work on the insulation of external walls and the installation of ventilated facades, replacing the roofing pie, arranging in the entrance lobby, the reconstruction of the loading and unloading zone with replacement of the doors, landscaping of the adjacent territory.

### **Building No. 203A**

The existing building is part of the accelerator complex being created, requiring reconstruction. Building No. 203A is a capital building - an industrial one-story freestanding building, in which a complex will be created for preparing accelerator parts for the final assembly consisting of an ultrasonic wash, a vacuum heating furnace and a "clean room". A survey was conducted at the reconstruction events, the results of which are designing taking into account the reconstruction of

engineering systems, general construction works on the creation of crane tracks and other necessary technological structures, redevelopment and repair of technological and office premises, necessary measures for the installation of technological equipment, replacement of reflective structures, replacement roofing cake, arrangement of entrance groups, reconstruction of equipment movement area with gate replacement.

### **Building No. 205**

The existing building is a capital one - an industrial building for conducting physical experiments, consisting of a one-story industrial part for the location of the set-ups involved in the experiments, two eastern and western outbuildings with offices and power elements of the collider in them. In building No. 205, it is planned to create, with further development, the BM@N installation, the test zone MPD, SPD, the zone for improving the ROC technology for MPD cameras of the MPD project, the modernization of the RB protection zone, and the creation of power supply systems of the building. Following measures for the reconstruction of the building carried out and planned to carry out: survey, design, reconstruction of engineering systems, general construction work on the construction of crane tracks and other necessary technological structures, redevelopment and repair of technological and office premises, replacement of hoisting mechanisms (elevators), necessary assembly measures technological equipment, replacement of reflective structures, replacement of a roofing pie, work on the insulation of external walls and installation in ventilated facades, reconstruction of the loading and unloading zone with the replacement of the gates, improvement of the adjacent territory.

### **Building No. 216**

The existing building is part of the accelerator complex being built that falls under reconstruction. Building No. 216 is a major building - an industrial two-story one connected to the building No. 215 by a gallery in which several “clean rooms” have already been created and are being created in the process of assembly: an area for assembling modules of silicon track systems for BM@N and MPD set-ups; a site for assembly and certification of track systems; a site for gluing and machining of structural elements of track systems. Also in a room of the building has already created the LHEP off-line computer cluster. As a part of the reconstruction, the following works have been carried out: inspection, design, reconstruction of engineering systems, general construction work on the modernization of the necessary technological structures, measures to strengthen floors and foundations for installed equipment, redevelopment and repair of technological and office premises, necessary measures for the installation of technological equipment, replacement reflective structures, work on insulation of external walls and installation of

ventilated facades, replacement of roofing pyro and, construction input groups, reconstruction of loading and unloading areas, landscaping of the adjacent territory.

### **Building No. 217**

The existing building is part of the accelerator complex being created. Building No. 217 is a capital building - an industrial two-story detached one. An industrial workshop has been created and continues to develop in the building for assembling and testing superconducting magnets of the NICA project, non-serial elements of the magnetic cryostat system of the NICA accelerator complex, as well as a “clean room” in which the time-projection camera TPC for MPD set-up is assembled. As a part of the reconstruction, the following works were carried out: inspection, design, reconstruction of engineering systems, creation of an industrial supply and exhaust ventilation system, general construction work on the creation of crane runways and other necessary technological structures, redevelopment and repair of technological and office premises, necessary measures for the installation of technological equipment, replacement of reflective structures, replacement of roofing cake, arrangement of entrance groups, reconstruction of loading and unloading zones with replacement of gates improvement of the adjacent territory.

#### **2.3.5. Auxiliary and technological equipment**

In order to ensure installation work at the NICA accelerator complex, they were designed and manufactured:

- mechanical 4 crane beams with a load capacity of 2 tons for Booster, have been in operation since 2016 (Fig. 2.3.5.1, left);

- mechanical 18 crane girders with a loading capacity of 3.2 – 5.0 t for accelerator tunnels, are stored at the factory, 3 of them are planned to be installed in October 2019;

- overhead cranes with a lifting capacity of 80/20 t for the MPD and SPD pavilions, the crane in the MPD pavilion was installed, tested (Fig. 2.3.5,1, right), the Acceptance Certificate was put into operation by JINR supervisory structures and a representative of Gostekhnadzor; an exceptional feature of this crane is that with a crane lifting capacity of 80 tons, its minimum travel speed is only 0.05 m / min.; the low speed of the crane hook allows comfortable and safe installation of “delicate and gentle” detectors and their parts; the second positive point is the radio control of the crane from the floor;

- installation of the same crane for assembling the SPD detector, started in October 2019;

- 8 bridge cranes with lifting capacity 3.2 - 10 t for auxiliary premises;

- traverse for 75 tons for mounting a cryostat in the magnetic circuit;



*Fig. 2.3.5.1. Installation and testing of booster crane beams, May 2016 (left) and static tests of crane with lifting capacity of 80 tons. The weight of the control load is 100 tons, June 2019 (right).*

- a crosshead with a lifting capacity of 50 tons for tilting the poles and installing them on transport supports (under construction at the Atom NPO, Dubna);
- 14 special power (reinforced) concrete blocks, the dimensions and weight of which are indicated in the assembly technology of the magnetic circuit;
- technological support for the cryostat;
- slings, spiders, earrings, eyebolts and other lifting equipment were purchased and a 2x4x4 m container was made, for storage;
- 4-storey mobile platform for electronics (production at Pelkom Dubna Engineering Plant LLC is nearing completion).

To test cranes under load, in 2019 a set of stacked test weights with a total weight of 100.5 t was manufactured, which made it possible to test cranes with lifting capacity from 3.2 t to 80 t.

Until the end of 2019, it is planned:

- to install an overhead crane with lifting capacity of 80/20 t and 3 mechanical cranes of beams;
- complete the manufacture of a movable platform;
- complete the manufacture of traverse with lifting capacity 50 t;
- other.

The following work is scheduled for 2020:

- transportation of magnetic circuit elements and technological equipment to the MPD pavilion;
- control assembly of the magnetic circuit in the MPD pavilion;
- disassembly of the magnetic circuit up to 13 beams;

- acceptance of a cryostat;
- installation of a cryostat;
- final assembly of the magnetic circuit;
- assembly of poles with coils;
- assembly of transport poles and their joint ventures;
- installation of a magnetic measurement system;
- magnetic measurements of the magnet field;
- adjustment of the position of the cryostat;
- installation, commissioning, commissioning of a joint venture, training of JINR staff to work with it;
- manufacturing and installation of the upper platform;
- assembly of a mobile platform with equipment;
- manufacture and installation of an electric lift on a movable platform;
- installation and testing of cranes.

### 2.3.6. Cryogenic complex

The existing cryogenic system of the Nuclotron is based on two modernized helium refrigerators KGU–1600/4.5, commissioned at the earlier 90th. To provide cooling of two more accelerators, it is necessary to increase of cooling capacity of cryogenic system from 4000 to 10000 W. The cryogenic system of the future accelerators (Booster and Collider) will consist of the central helium liquefier OG-1000 and satellite refrigerators RSG-2000/4.5 This task will decide by commissioning of the new liquifier OG-1000 with capacity of 1000 l/h and three satellite refrigerators RSG–2000/4.5. Satellite refrigerators operating jointly with central big liquefier due to liquid helium supplying from it. Two satellite refrigerators RSG–2000/4.5 located close to the collider, one - at the central cryogenic plant in 1B building. OG-1000 liquifier located in 1B building too.

Basic parameters of the NICA helium cryogenics

- |   |                           |
|---|---------------------------|
| - Refrigerating capacity at 4,5 K                 | - 10000 W;                |
| - Cold mass at 4,5 K                              | - 290 t;                  |
| - Total power of electric motors (kW)             | - 11,4 MWatt;             |
| - Total volume of helium storage                  | - 34932 nm <sup>3</sup> ; |
| - Liquid nitrogen liquifying capacity             | - 2300 kg/h;              |
| - Total volume of nitrogen storage                | - 61676 nm <sup>3</sup> ; |
| - Total area taken by cryogenic complex equipment | - 4000 m <sup>2</sup> .   |

The main elements of the cryogenic complex listed below.

1. Central platform of the cryogenic station:

- Helium refrigerators KGU-1600/4.5	- 2 units;
- OG-1000 helium liquefier	- 1 unit;
- RSG-2000/4.5 helium satellite refrigerator for Booster	- 1 unit;
- Nitrogen re-condenser RA-0,5	- 1 unit;
- Nitrogen liquefier OA-1.3	- 1 unit;
- draining and oil-purification units MO-800	- 4 units;
2. Machine hall:	
- Helium screw compressors “Kaskad-80/25”	- 2 units;
- Helium piston compressors “305GP-20/31”	- 3 units;
- Helium piston compressors “2GM4-12/31”	- 2 units;
- Helium piston compressors “6GSH1,6/1,1-200-1”	- 3 units;
3. Machine hall cooling towers	- 2 units;
4. Helium isochoric gasholder	- 1 unit;
5. Helium high pressure receivers	- 10 units;
6. Liquid nitrogen tank	- 2 units;
7. Liquid helium transport tank	- 1 unit;
8. Helium pipelines system	
9. Nitrogen pipelines system	
10. New machine hall	
- Helium screw compressors “Kaskad-110/30	- 2 units;
- Nitrogen compressor aggregates “Aerocom2-179/18”	- 1 unit;
- Nitrogen compressor aggregates “SAMSUNG SM5000”	- 2 units;
11. Nitrogen gasholder	- 1 units;
12. Nitrogen high pressure receivers	- 5 units;
13. RSG-2000/4.5 helium satellite refrigerator for collider	- 2 units;
14. Nitrogen re-condenser RA-0,5	- 1 unit;
15. Liquid nitrogen tank	- 1 unit;

General view of the cryogenics for the NICA complex is shown in Fig. 2.3.6.1.

### 2.3.6.1. Helium compressors and helium facilities

Helium compressors are needed to provide of cryogenic facilities with compressed helium. By now:

- Two screw compressors “Kaskad-110/30 manufactured and delivered to JINR. Compressors are not commissioning yet because new machine hall are building now;
- Piston compressor “405GP-20/30” are manufactured and commissioned;
- Piston compressor “305NP-20/31” are manufactured and commissioned (Fig. 2.3.6.1.);

- Three piston compressors “6GSH-200/1,6” are manufactured and commissioned (Fig. 2.3.6.1).

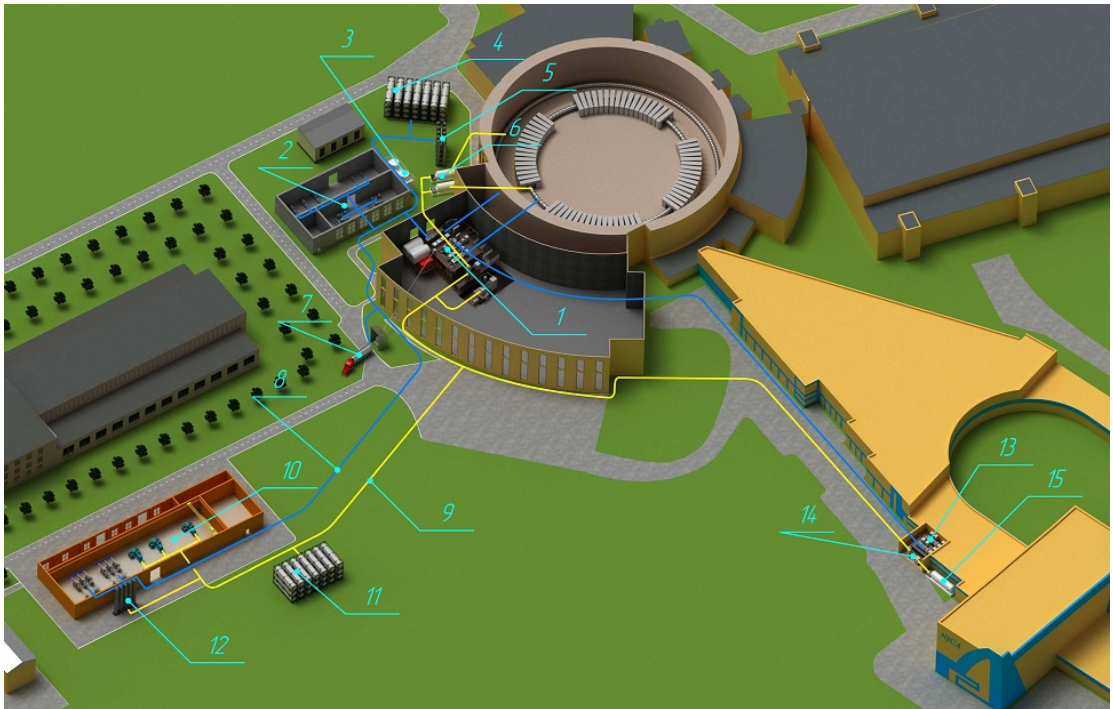


*Fig. 2.3.6.1. General view of the cryogenics for the NICA complex*



*Fig. 2.3.6.2. Piston compressor “305NP-20/31”*



*Fig. 2.3.6.3. Piston compressor “6GSH-200/1,6”*

Cryogenic helium facilities provide cooling of the superconducting magnets of the accelerator complex to an operating temperature of 4.5 K. By now:

- Helium liquefier OG-1000 manufactured and in trial operation now (debugging of control system);

- Three satellite refrigerators RSG–2000/4.5 are manufactured at 2019. Installation of one (for cooling the booster) is carried out in the 1B building. The deadline is December 2019. Two more refrigerators for cooling the collider are in storage at the manufacturer, because a room for it not ready;

- Four blocks of draining and oil-purification MO–800 are manufactured. Unit MO-800 is used for purification of helium after compression in the compressor from impurities of oil and moisture. Final purification from oil vapor is carried out in this block by means of two coal adsorbers. Purification from moisture is carried out in two zeolite adsorbers. The oil purification unit has a capacity of 800 kg / h of gaseous helium. One unit already working. Platform for the remaining blocks placement are designed. Installation work will begin in 2020.

- 40 m<sup>3</sup> Liquid helium transport reservoir manufactured at 2019. This tank will be able to increase capacity of the existing equipment to store helium by more than 4 times; to provide a rather cheap delivery of helium from the manufacturer by own transport. Commissioning planned at the first half of 2020.

- Purification unit KV910 (Fig. 2.3.6.4). Designed for fine purification of helium during testing of magnets and gas supply to the bearings of turbo expanders. Commissioning planned at the first half of 2020.



*Fig. 2.3.6.4. Purification unit KV910*

- Helium 1000 m<sup>3</sup> gasholder. Isochoric gas holder needs to provide ensure the maintenance of excess pressure on the suction of the compressors and their technological start-up. This device is a complex of vessels with a total volume of 1000 m<sup>3</sup> connected by a collector. Delivery planned at second half of 2020.

### **2.3.6.2. Nitrogen compressors and nitrogen facilities**

Nitrogen compressors are needed to provide of liquefier and re-condensers with compressed nitrogen. To date:

- Nitrogen compressor “AeroCom2-179/18” manufactured and delivered to JINR. Compressor is not commissioning yet because new machine hall is building now. Assembling planned at second half of 2020;
- Nitrogen compressors “Samsung SM5000” manufactured and delivered to JINR. Compressors not commissioning yet because new machine hall is building now. Assembling planned at second half of 2020;

Facilities of the nitrogen system are designed to supply liquid nitrogen to consumers of the accelerator complex - cryogenic plants, thermal shields, nitrogen traps, etc., as well as the reception and condensation of cold nitrogen vapors from consumers. Already made:

- Nitrogen liquefier OA-1.3; it is not mounted because the platform for its placement in building 1B is not yet ready; installation scheduled for 2020;

- two RA-500 nitrogen re-condensers; they are not mounted because the platform and the room for their placement in building 1B and room No. 177 of building No. 17 are not ready; their installation scheduled for 2020;
- Five nitrogen receivers "Rv-20/3,5" for storing gaseous nitrogen; they were delivered; their installation will be carried out after the readiness of the new machine hall, commissioning scheduled for 2020;
- Three 30 m<sup>3</sup> containers for storing liquid nitrogen; they were delivered; their placement project is being developed; installation scheduled for 2020;
- Nitrogen 1000 m<sup>3</sup> gasholder; isochoric gas holder needs to provide ensure the maintenance of excess pressure on the suction of the compressors and their technological start-up; this device is a complex of vessels with a total volume of 1000 m<sup>3</sup> connected by a collector; Its production scheduled for the second part of 2020.

### 2.3.7. Infrastructure of energy-supplying and energy-saving engineering systems

#### 2.3.7.1. Energy supply systems

A large amount of work has been done to supply energy to all objects of the created research infrastructure. An increase in electricity demand led to the reconstruction of the main step-down substation GPP-1 (110/6 kV). During the reconstruction, its capacity will increase to 40.8 MW.

Table 2.3.7.1 shows the planned distribution of the GPP-1 power among the facilities of the Complex after its modernization.

Table 2.3.7.1.

Planned power supply facilities for the NICA Complex objects

Objects	Capacity, MW
Booster	1.6
Collider	9.0
New cryogenic station	9.0
Computer cluster	1.0
Nuclotron	1.4
Channel for extracted beam experiments (Building 205)	1.6
Facility for assembling and testing of SC-vagnets (Building 217)	1.1
Lhep infrastructure	5.0
East boiler home	0.8
NICA centre	1.8
External consumers	8.5
In total	<b>40.8</b>

The required capacity of GPP-1 will be provided by two new transformers manufactured by Siemens Transformers LLC, Voronezh. The design work on the reconstruction of the GPP-1 is carried out by the organization Kostroma Office - a branch of JSC Electrocentromontazh. At present, working documentation has been issued for approval at JINR, it is planned to receive budget documentation in December of this year, and by the spring of next year choose a general contractor for the construction and installation work. The reconstruction of GPP-1 is supposed to be carried out in 2020.

In fig. 2.3.7.1. are shown reconstructed and put into operation 6 kV power substations No. 11, No. 13, No. 42 and “K”.

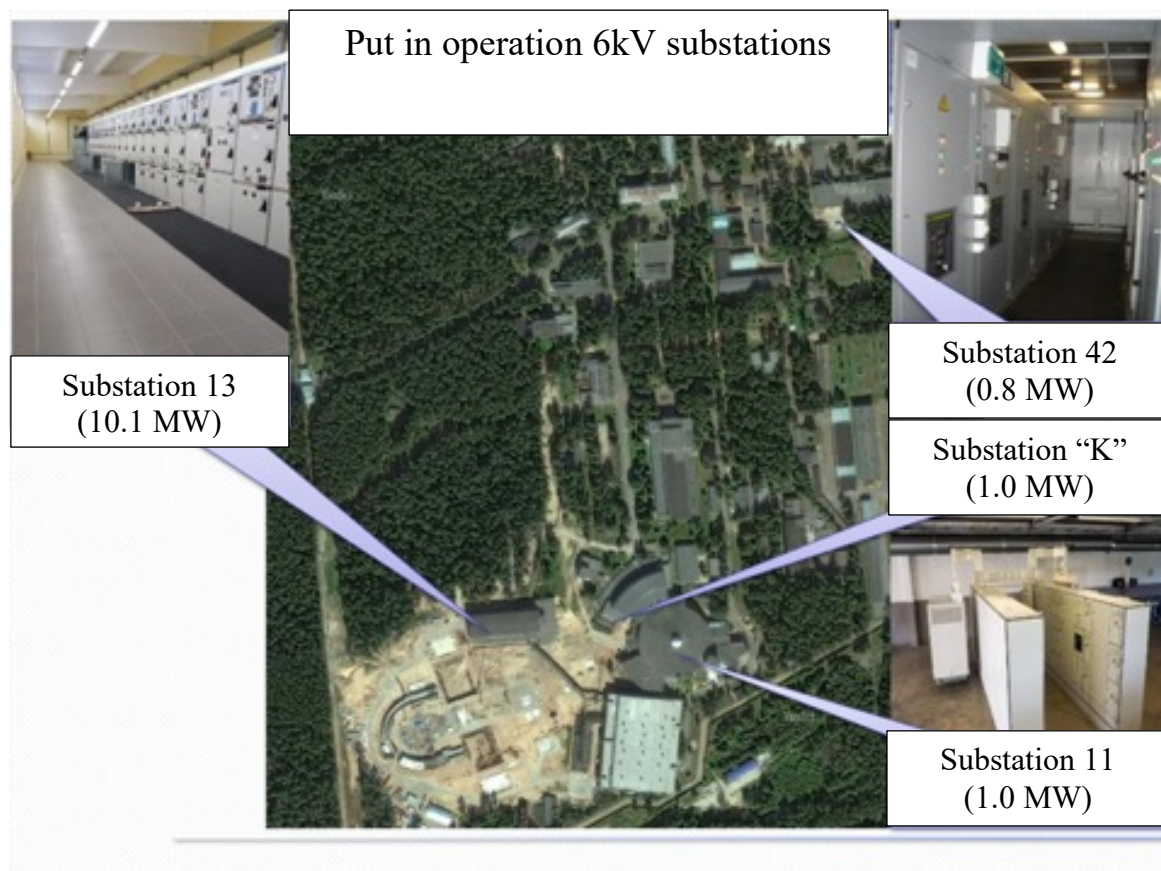


*Fig. 2.3.7.1. Reconstructed and put into operation 6 kV power substations No. 42, 11, 13 and subject to reconstruction – substations No. 11 and “K”.*

In fig. 7.3.7.2 shows reconstructed 6 kV power substations No. 12, No. 15, No. 21, No. 31 and five Collider substations.

Substation No. 12 will provide power to the Nuclotron and Booster.

Substation No. 15 is the second power center of the Collider, and the channels of the building No. 205.

Substation No. 21 power supply of the new cryogenic compressor station.

Substation No. 31 of the Laboratory for creating MPD detector elements.

Five substations under construction (RTP-1, TP-2, RP-2, TP-3, TP-4) will provide power to building No. 17.

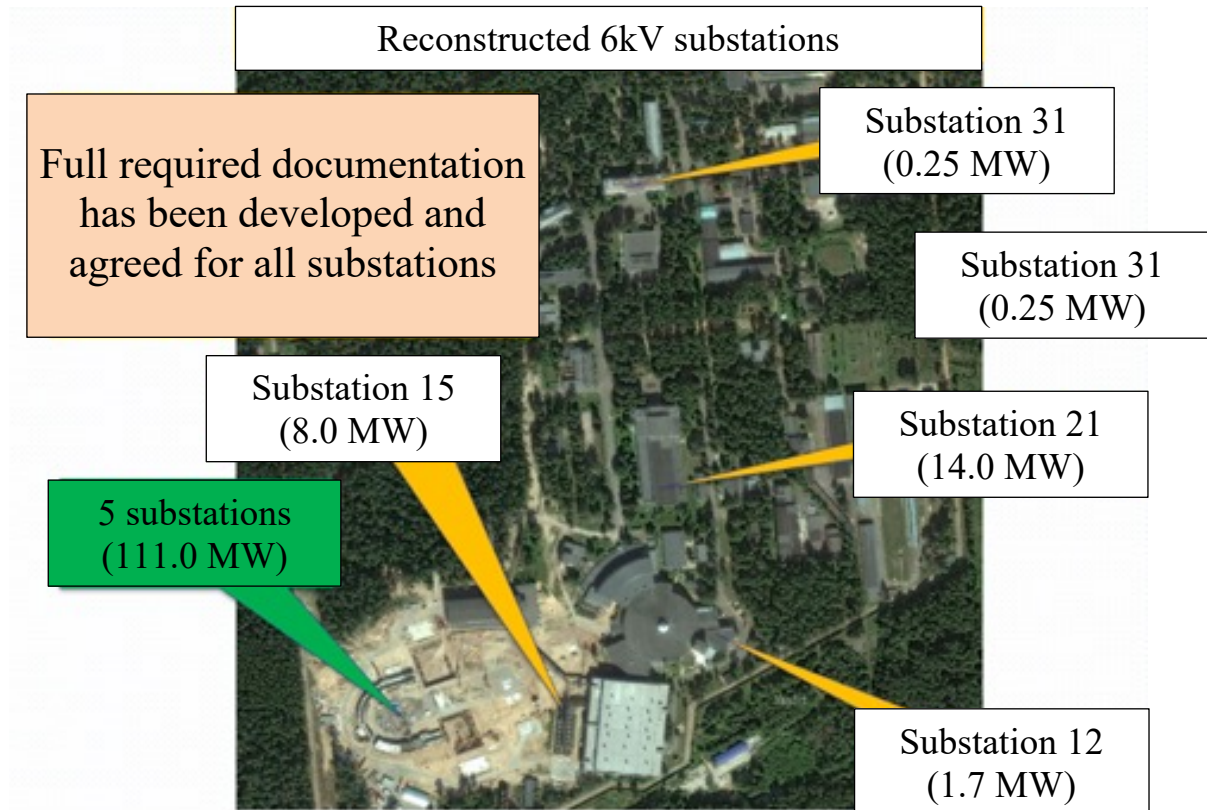


*Fig. 2.3.7.2. Reconstructed 6 kV power substation No. 12, 15, 21, 31 and five Collider substations.*

The upgrade of the laboratory operating current system has been completely updated (Fig. 2.3.7.3).



*Puc. 2.3.7.3. Equipment for the reconstruction of the operational current system.*

Work in the framework of the development of energy-supplying and energy-saving engineering systems involves the modernization of external network facilities, which are constantly being worked on (see, for example, Fig. 2.3.7.4).



*Puc. 2.3.7.4. Reconstructed switchgear of buildings No. 205 (left) and No. 217 (right).*

In connection with the construction of new buildings and structures, as well as the development of the operational resource of existing external networks, projects for their reconstruction have been prepared and are being implemented in the Laboratory.

Works on the water supply and sewage network Collider were completed. The sewage pumping station (SPS) No. 15 was modernized to accept additional volumes from the Collider buildings and the NICA Center.

As of the end of 2018, water pipelines were replaced in the amount of 75%, heating networks in the amount of 90%, sewer networks in the amount of 10%. As a result, more than 12 km of new routes were laid. The end of the modernization of heat and water networks is planned in 2019, of sewer networks in 2021.

A number of other works are planned, the most important of which are:

- installation of the Collider heat supply network and backup input to the VBLHEP site, implementation - 2019, an agreement has been concluded;
- reconstruction of external heat supply of VBLHEP, implementation - 2019-2020, documents were prepared for the start of the tender for the selection of a contractor;
- the heat supply system of the NICA Center, implementation - 2019-2020, the project is being approved;
- an external water supply system and sewage network of VBLHEP to provide the building with the NICA Center, implementation – 2019 – 2020; a preparation for a design contract is underway.

### 2.3.7.2. The power supply system of the beam output channel from the Nuclotron to the Measuring pavilion

The power supply system is designed to supply a precision DC current to the magnetic elements (ME) to form the magneto-optical axis of the trajectory of the passage of charged particles from the ring of the Nuclotron through the Measuring pavilion in the building 205. The channel consists of dipole and quadrupole magnets designed to control the movement of charged particles through the transport channels. Existing ME are cooled with water and have a system of technological protections for overheating, disruption of the cooling system, the maximum current, etc. In normal mode, one power supply supplies ME only one of the channels. The electrical parameters of the magnetic elements are given in table 1 below.

The main features of the power supply system are high indicators for the accuracy of maintaining high current values (current from 600 to 4000 A) at relatively low voltage values (from 75 to 230 V DC). The power supply system has redundancy on the supply voltage side and on the DC side.

Table 2.3.7.1

Parameters of magnetic elements.

Magnetic element	I (A)	U (V)	R (Om)	L (H)	the beam output channel from the Nuclotron
20K100	3500	75	0.021	0.010	2
20HK100	4000	84	0.021	0.010	2
20K200	3500	130	0.037	0.017	2
СП-94	635	212	0.334	0.870	1
СП-12А	1700	215	0.126	0.600	1
ВКМ	1600	200	0.125	0.630	1

The schematic diagram of the power supply system is shown in Fig. 2.3.7.1 and consists of the following elements:

- feeding switchgear SG-6kV substation «K»;
- power transformers 6/0, 69 kV;
- high precision power supplies;
- switching cabinets;
- cable communications;
- automated control system.

Connection of the projected power supply system to the power grids of the JINR provided at the voltage level of 6k V to two cells of the outgoing lines of substation No13. The nominal operating power of the power supply system is accepted in the amount of up to 3200 kVA.

The equipment of the power supply system is located in the existing room of the switching point adjacent to the room of the housing 1B, the layout solutions are given in the graphic part of the project.

#### **Switchgear 6kV substation "K".**

For the organization of the power supply system according to the adopted scheme, it is assumed to carry out the reconstruction of substation 6kV "K" with the replacement of outdated equipment with the modern D-12P "Classic" series without increasing the permitted power up to 3500kVA.

#### **0.69 kV switchgear and power transformers.**

As the main voltage of the power supply line of the magnetic elements of the channel output beam of charged particles from the Nuclotron adopted a voltage of 0.69 kV, for which in the adjacent room with the switching point of the housing 1B provides for the installation of three dry power transformers TSZ 6/0, 69 kV with a capacity of 1600kVA with their power from the reconstructed substation "K". In the normal operation of the power supply system of magnetic elements, it is provided with power from two dry power transformers, the third transformer is used as a backup, its inclusion is provided in the event of an accident at one of the workers. The distribution of electricity at the level of 0.69 kV and the organization of the power supply system directly to the sources is carried out in the SG-0.69 kV of the switching point building.



All switching devices are equipped with motor drives with the possibility of remote-control automated control system via RS485 channels

### Power supplies (PS).

The power supply is built on the principle of AC/DC Converter and has a modular structure. The Converter power of one module is 100 - 150 kW. The modules are connected in series or in parallel depending on the parameters of the ME. The Converter unit as part of the module has a single circuitry and design for all types of sources. The parameters of the transformer and rectifier block are consistent with the parameters of the ME. The source is equipped with channels for receiving protections and locks from ME. All sources are equipped with remote monitoring and control equipment included in the automated control system. The power supply system consists of 11 PS of which 9 working sources and two reserves. The main technical parameters of power supplies are given in table 2.3.7.2, weight and size data in table 2.3.7.3.

Table 2.3.7.2

Main technical parameters of power supplies

№	Parameter name	parameter value	note
1.	Input parameter		
1.1.	Supply voltage	three-phase voltage 690 (+/-10%) V	For all PS
1.2.	The frequency of the mains	50 (+/- 2%) Hz	
1.3.	efficiency factor	not lower 0.92	
2.	Output parameter		
2.1.	output voltage	Постоянное, 75-220 В	In accordance with the parameters of the ME
2.2.	output current	635-4000 А	
2.3.	Rated power	140-600 кВт	
2.4.	Operating mode	Статический	For all PS
2.5.	The setting range of the output current	From 5% to the nominal value of PS	In accordance with the parameters of the ME
2.6.	The relative stability of the current	$10^{-4}$	For all PS
2.7.	The resolution changes the output current	$10^{-4}$	
3.	The inductance of the load	0,01 – 0,87 Гн	determined by the parameters of the ME
4.	Load resistance	10...100 МОм	
5.	Cooling method	Forced liquid	For all PS
6.	Cooling liquid	Deionized water	
7.	Dimensions	1400x2000x800мм	For all PS except PS for ME type СИ-94
		800x2000x800мм	PS for ME type СИ-94

Weight and size parameters of power supplies

ME	I (A)	U (B)	P (кW)	Dimensions (mm)	Weight (kg)
20K200	3500	130	455,0	1400x800x1800	800
20K100	3500	75	262,5	1400x800x1800	600
20K100*	4000	100	360,0	1400x800x1800	700
BKM	1600	200	320,0	1400x800x1800	700
СП-12А	1700	215	365,5	1400x800x1800	700
СП-94	635	212	134,6	800x800x1800	400

PS cabinets are supposed to be placed in the existing electrical room of the switching point in the immediate nearby of the SG-0.69 kV.

### **Switching cabinets.**

Switching cabinets (SC) are intended for the organization of power backup of ME sources on DC circuits. Backup of power supply of ME is organized by means of transfer system of busbar which allows to make connection of ME to reserve power supplies. In SC installation of disconnectors with nominal currents of 2000 A (SC-1 line) and 4000A (SC-2 line), with motor drives is provided.

Cabinets SC-1 and SC-2 are designed for switching high-current DC circuits during absence current. SHP cabinets are connected to each other in rows and include busbars for rated current, which are connected to the reserve PS through a disconnector. The output circuits of the SC cabinets have in their design the technical possibility to change the polarity of the power terminals on the load cables.

Cabinets SC-1 and SC-2 are equipped with locks that do not allow the simultaneous inclusion of two disconnectors. All SC are equipped with the equipment of remote monitoring and control included in system of automatic control system.

The main technical characteristics of the SHP are given in table 2.3.7.4.

### **Cable communications.**

The power supply system of the ME is provided with busbars, power and control cables. For the organization of high-current circuits from power supplies to SC cabinets with rated current loads up to 2000A and 4000A it is assumed to use complete busbar bridges. Technical characteristics of the busbar and the choice of cable and wire products is based on the rated current loads of power circuits, the length of the network and the possible method of laying. The total length of power cable lines is more than 6.5 km.

Main technical characteristics of SHP

№	Parameter name	parameter Value
1	voltage	DC, 250V
2	current	
	SC-1	DC, 2000A
	SC-2	DC, 4000A
3.	Control voltag	AC, 50Hz, 220V
4.	dimensions of cabinets	1400×600×2000 MM
5.	Degree of protection cabinets	IP20

### **Automated control system.**

An automated process control system is created that performs the functions of monitoring and controlling the equipment of the power supply system. The automated control system consists of 7 cabinets of data acquisition and transmission devices, automated workstations of the operator and the engineering station.

Stand-alone cabinets are networked with the ability to transfer data to remote workstations via a server. Communication between power system objects and SCADA via Modbus-RTU protocol, and between SCADA and operator via Ethernet. The automated control system provides information exchange with other levels of the hierarchy of management and operation of electrical networks. For the organization of uninterruptible power supply the equipment of automated control system is equipped with uninterruptible power supplies.

The project for the power supply system was made in 2017. In 2018, power supplies were purchased in the company "LM Inventor", Russia, a high-voltage switchgear of the 6kV network in «Tavrida Energo Stroy», Russia, switchgear of the 0.69 kV network in the company "sp.z o. o. Frako Term" Poland, switching cabinets in "NIEFA-ENERGO, LLC", Russia. During 2019, automated control system equipment was purchased, company "EPP-T", Russia, performed construction, installation and commissioning works on the entire complex of equipment except for laying power cables to the magnetic elements of the channel. Photos of the power system equipment are shown on Fig. 2.3.7.2



Power transformers



SG 0.69kV



CS and PS



Switchgear 6kV substation "K"

*Fig. 2.3.7.2. Equipment of the power supply system of the beam output channel from the Nuclotron.*

### 2.3.7.3. The power supply system for the transport of a beam of charged particles in the building 205

The power supply system is designed to supply a precision DC current to the ME to form the magneto-optical axis of the trajectory of the passage of charged particles in the building 205. The channel consists of dipole and quadrupole magnets designed to control the movement of charged particles through the transport channels. Existing ME are cooled with water and have a system of technological protections for overheating, disruption of the cooling system, the maximum current, etc. In normal mode, one power supply supplies ME only one of the channels. The electrical parameters of the magnetic elements are given in table 1 below.

Table 2.3.7.5

Parameters of magnetic elements.

ME	I (A)	U (V)	R (Om)	L (H)	Quantity ME
K-100	3500	75	0.021	0.010	7
K-200	3500	130	0.037	0.017	16
СП-94	635	212	0.334	0.870	5
СП-57	600	171	0.285	0.400	5
СП-12	1100	190	0.173	1.020	1
СП-12А	1700	215	0.126	0.600	6
СП-40	1100	220	0.200	1.710	3
СП-41	2500	300	0.120	1.800	1
МЛ-17	1280	160	0.125	0.027	1

The main features of the power supply system are high indicators for the accuracy of maintaining high current values (current from 600 to 4000A) at relatively low voltage values (from 75 to 230V DC). The power supply system has redundancy on the supply voltage side and on the DC side.

The schematic diagram of the power supply system is shown in Fig. 2.3.7.3 and consists of the following elements:

- 6kV network switchgear (SG) substation №15;
- power transformers 6/0.69kV;
- 0.69kV network switchgear;
- high precision power supplies;
- switching cabinets;
- cable communications;
- automated control system.

Connection of the projected power supply system to the power grids of the JINR provided at the voltage level of 6kV to five cells of outgoing lines of the

reconstructed substation №15. The rated power of the power supply system is accepted in the amount of up to 5000kVA.

The equipment of the power supply system is located in the existing premises No. 108 and No. 111, the experimental room along the wall and the new modular transformer building located next to the building 205.

### **0.69kV switchgear and power transformers.**

As the main voltage of the power supply line of magnetic elements of the channel output beam of charged particles from the Nuclotron adopted a voltage of 0.69 kV, for which the new modular building of transformers provides for the installation of 5 dry power transformers TC3 6/0.69 kV with a capacity of 1600kVA with their power from the reconstructed substation No. 15. In the normal operation of the power supply system of ME, it is provided with power from 4 power transformers, the 5th transformer is used as a backup, its inclusion is provided in the event of an accident at one of the workers. The distribution of electricity at the level of 0.69kV and the organization of the power supply system directly sources, is carried out in switchgear SG-0.69 kV in room No. 108 and No. 111.

The distribution device at the voltage level is created similarly to the power supply system of the beam output channel from the Nuclotron.

The mode of operation of the installation: 4 transformers workers, working on their own sections of tires, one transformer is in hot standby, and if necessary, feeds any of the four working section of busbar by switching its power to power from the fifth, reserve, section of busbar. Operation modes are controlled both in automatic and manual mode.

All switching devices are equipped with motor drives with the possibility of remote-control automated control system via RS485 channels.

### **Power supplies (PS).**

The power supply system consists of 32 PS, of which 27 working and 5 standbys.

Main line of 30 PS is built on the principle of AC/DC Converter and has a modular structure. The Converter power of one module is 100 - 150kW. The modules are connected in series or in parallel depending on the parameters of the ME. The Converter unit as part of the module has a single circuitry and design for all types of sources. The parameters of the transformer and rectifier block are consistent with the parameters of the ME. The source is equipped with channels for receiving protections and locks from ME.



All sources are equipped with remote monitoring and control equipment included in the automated control system. The main technical parameters of power supplies are given in table 2.3.7.6, weight and size data in table 2.3.7.7.

Table 2.3.7.6

Main technical parameters of power supplies

№	Parameter name	parameter value	note
1.	Input parameter		
1.1.	Supply voltage	three-phase voltage 690 (+/-10%) V	For all PS
1.2.	The frequency of the mains	50 (+/- 2%) Hz	
1.3.	efficiency factor	not lower 0.92	
2.	Output parameter		
2.1.	output voltage	Постоянное, 75-220 V	In accordance with the parameters of the ME
2.2.	output current	635-4000 A	
2.3.	Rated power	140-600 kW	
2.4.	Operating mode	Статический	For all PS
2.5.	The setting range of the output current	From 5% to the nominal value of PS	In accordance with the parameters of the ME
2.6.	The relative stability of the current	$10^{-4}$	For all PS
2.7.	The resolution changes the output current	$10^{-4}$	
3.	The inductance of the load	0,01 – 0,87 H	determined by the parameters of the ME
4.	Load resistance	10...100 МОм	
5.	Cooling method	Forced liquid	For all PS
6.	Cooling liquid	Deionized water	
7.	Dimensions	1400x2000x800мм	For all PS except PS for ME type СИ-94
		800x2000x800мм	PS for ME type СИ-94

Table 2.3.7.7

Weight and size parameters of power supplies

ME	I (A)	U (V)	P (kW)	Dimensions (mm)	Weight (kg)
20K200	3500	130	455,0	1400x800x1800	800
20K100	3500	75	262,5	1400x800x1800	600
20K100*	4000	100	360,0	1400x800x1800	700
BKM	1600	200	320,0	1400x800x1800	700
СИ-12А	1700	215	365,5	1400x800x1800	700
СИ-94	635	212	134,6	800x800x1800	400

PS cabinets are supposed to be placed in the room №108 and №111 in the immediate nearby of the SG-0.69kV.

**Switching cabinets.**

Switching cabinets (SC) are intended for the organization of power backup of ME sources on DC circuits. Backup of power supply of ME is organized by means of transfer system of busbar which allows to make connection of ME to reserve power supplies. In SC installation of disconnectors with nominal currents of 2000A and 4000A, with motor drives is provided.

Cabinets SC are designed for switching high-current DC circuits during absence current. SC cabinets are connected to each other in rows and include busbars for rated current, which are connected to the reserve PS through a disconnector. The output circuits of the SC cabinets have in their design the technical possibility to change the polarity of the power terminals on the load cables.

Cabinets SC are equipped with locks that do not allow the simultaneous inclusion of two disconnectors. All SC are equipped with the equipment of remote monitoring and control included in system of automatic control system.

The main technical characteristics of the SC are given in Table 2.3.7.8.

Table 2.3.7.8

Main technical characteristics of SC.

№	Parameter name	parameter Value
1	voltage	DC, 250V
2	current	DC, 2000A, 4000A
3.	control voltag	AC, 50Hz, 220V
4.	dimensions of cabinets	1400×600×2000 MM
5.	degree of protection cabinets	IP20

**Cable communications.**

The power supply system of the ME is provided with busbars, power and control cables. For the organization of high-current circuits from power supplies to SC cabinets with rated current loads up to 2000A and 4000A it is assumed to use complete busbar bridges. Technical characteristics of the busbar and the choice of cable products is based on the rated current loads of power circuits, the length of the network and the possible method of laying. The total length of power cable lines is more than 8 km.

**Automated control system.**

An automated process control system is created that performs the functions of monitoring and controlling the equipment of the power supply system. The

automated control system consists of 7 cabinets of data acquisition and transmission devices, automated workstations of the operator and the engineering station.

Stand-alone cabinets are networked with the ability to transfer data to remote workstations via a server. Communication between power system objects and SCADA via Modbus-RTU protocol, and between SCADA and operator via Ethernet. The automated control system provides information exchange with other levels of the hierarchy of management and operation of electrical networks. For the organization of uninterrupted power supply the equipment of automated control system is equipped with uninterruptible power supplies.

Stage "P" of the project for the power supply system was approved in 2019. In the process of developing working documentation on the stages of creating a power supply system. In 2018, a contract was signed for the manufacture of power supplies in the company "LM Inventor" Russia. A contract with the company "EPP-T" Russia for the manufacture of switching cabinets. In the process of concluding a contract for the manufacture of 0.69kV network switchgear in the company "sp.z o. o. Frako Term" Poland. Signed in 2019 contract with the firm "DSS engineering" for the development of automated control system. Contracts are being prepared for construction, installation and commissioning with company "EPP-T" Russia on the stages of creating a power supply system. In 2019, the partial dismantling of building 208 was carried out, on the site of which work is being prepared for the construction of new modular buildings substation No. 15 and Transformers. Photos of the building 208 are shown in pic.2.3.7.3.



August 2018г.



August 2019г.

*Fig. 2.3.7.3. Dismantling of the building 208*

### 2.3.8. Facility for assembly and testing of sc-magnets

In frame of NICA project special facility for assembly and testing of superconducting (sc) magnets was developed and commissioned at LHEP JINR. It's intended for assembly and test the cryo-modules with sc-magnets for booster synchrotron and collider of the NICA project and for assembly and test of magnets' units for SIS-100 synchrotron of the FAIR project. As well, full testing program should be performed for all assembling at the facility sc-magnets.

Totally it is necessary to process 258 main and 168 correction sc-magnets for NICA booster and collider (see Table 2.3.8.1) and 166 units of sc-magnets for SIS100 synchrotron.

Table 2.3.8.1

Number of sc-magnets to be processed at the LHEP testing facility.

	Booster	Collider	SIS-100
Dipoles	40	88	-
Quadrupoles	48	82	166
Total	88	170	166

Construction of the facility began in 2010. In November 2016 its' commissioning was done. By the end of 2019 all cryo-modules with sc-magnets for NICA Booster would be completed. Testing of the NICA collider magnets should be finished at second half of 2021, magnets for SIS-100 – at the end of 2023. Thus, average performance of the facility should be 12 magnets per month starting from 2020.

The facility located in the building #217 of LHEP. Its' area is 2600 m<sup>2</sup>. It has several halls specified for procedures of the technological workflow (see Fig. 2.3.8.1).

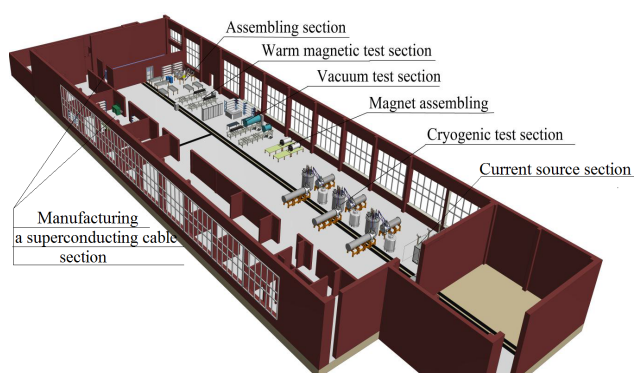


Fig. 2.3.8.1. Facility for assembly and testing of sc-magnets: schematic view (left), general view (right)

It includes:

- sc-cable production hall
- sc-coil production hall
- magnets mechanical assembly hall

- room temperature magnetic test hall
- vacuum test bench
- assembling magnets to cryostat bench
- cryogenic tests' hall
- power supplies' hall.

Facility equipped with overhead crane.

Schematic view of NICA Booster synchrotron magnet is presented in Fig. 2.3.8.2.

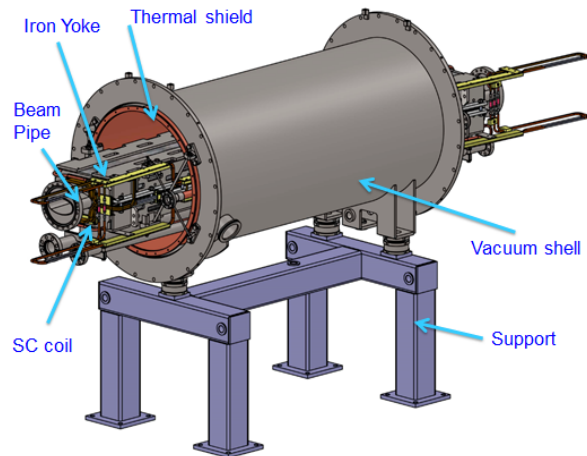


*Fig. 2.3.8.2 NICA Booster dipole module schematic view.*

The equipment for cable production allows producing a Nuclotron-type hollow composite superconducting cable with the capacity of up to 50 m/h. The diameter of the cooling channel of the cable can vary from 3 to 5 mm. The number of sc-wires in the cable are up to 32. The wire diameter may be up to 1 mm.

Three halls for manufacturing of sc-coils are equipped with a rotating table and toolings for winding of various types of coils. There are two ovens for coils with length up to 6m long heat treatment.

The hall for the sc-magnets' mechanical assembly is equipped with a few tables and tooling for rotating the magnets round the longitudinal axis to ease welding and brazing the cooling channels, devises for electrical insulation test, resistance and inductance measurement, hydraulic of cooling channels test and adjustment.

Two granite-plate-tables aligned in the one base reference plane is located at this hall as well. They are used for incoming control and precise geometrical measurements of the magnets' yokes and other parts. These measurements performed by 3D-arm (ROMER Absolute Arm) and laser tracker with the accuracy 2-3 $\mu$ m.

The hall for "warm" (room temperature) magnetic measurements is equipped with different magnetic measurement systems, pulsed linear regulated power converter with the current up to 100 A and DAQ based on National Instruments PXI measuring electronics and LabVIEW software.

The bench for checking of magnets' cooling channels, beam pipes and cryostats vacuum tightness is equipped with tables, vacuum chamber (cylindrical chamber with rails for rolling the trolley with the magnet), pumping systems, a leak detection system and a helium high pressure system. The pumping system is based on diffusion pumps PDI250-W HSR, rotary vane pumps DUO35, TPR280 and IKR251 gages produced by Pfeiffer Vacuum, a helium leak detector, manometers, valves and reducers. A string measuring stand is also used for magnetic measurements, it consist of special tables, wire equipment and electronic rack.

The bench for assembling magnets in cryostats is equipped with two tables, tooling for mounting, adjustment and fixing the magnets in the cryostat, devices for mounting and verifying the temperature sensors and voltages taps.

Hall for cryogenic tests of the magnets equipped with 3 helium satellite refrigerators (HSR) (Fig. 2.3.8.3), 6 feed boxes with 12 high temperature superconductor (HTS) current leads [9] on 18 kA pulse operation, a system for «cold» (at temperature of the liquid helium – 4.5 K) magnetic measurements, vacuum and control systems. It is intended to provide cryogenic tests of superconducting magnets simultaneously at 6 benches. Each pair of low-temperature test bench includes: satellite helium refrigerator, main and starting heat exchangers, tank with liquid nitrogen, tank with liquid helium, two current leads cryostats, sub-cooler of liquid helium flow, HTS current leads.

Satellite helium refrigerator cools down the superconducting magnet from 300 K to 4.5 K, provides cooling at the operating temperature about 4.5 K and warms up from 4.5 K to 310 K. Cooling capacity of satellite helium refrigerator is 100 W.

The test bench use HTS current leads. These HTS current leads are operated at high intensity current up to 18 kA. Their operation is pulsed. HTS current leads have three cooling stages. The top of the HTS current lead is cooled with water.

Cold magnetic measurements are carried out during cryogenic tests under the control of a data acquisition system, using specially designed sensors. Special equipment is used to control rotation with the help of a motor sensor and information collection, it controls the power source. The system records and processes the data.

For cryogenic tests various power sources are used. Power equipment were designed, developed and manufactured by special companies. During tests power supply gives power from the sources to the current leads via copper buses cooled by special cooling system.

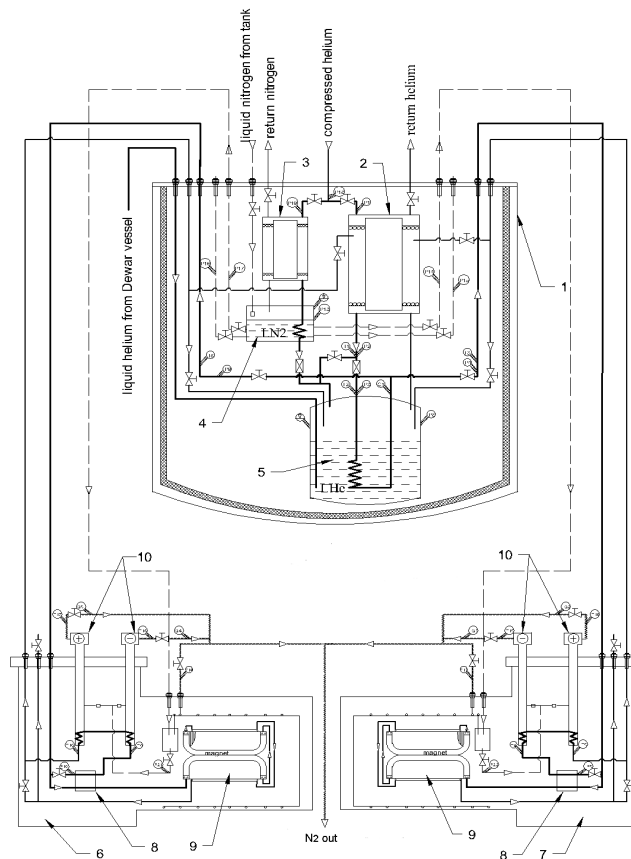


*Fig. 2.3.8.3. Satellite refrigerator unit with two test benches scheme: 1 - vacuum shell of the satellite helium refrigerator; 2 and 3 – main and starting heat exchangers; 4 – bath with liquid nitrogen, 5 – bath with liquid helium, 6 and 7 – left and right feed boxes; 8 – subcooler of liquid helium flow; 9 – SC magnet; 10 – HTS current leads.*

The developed testing facility was commissioned with a time-delay of 1 year to the original project plan. But tests of FoS sc-magnets and start of serial testing program for NICA booster synchrotron were done before the commissioning the facility at the full range. To perform all testing program for NICA collider and SIS-100 synchrotron the facility has to operate at 12 magnets per month performance.

## **2.4. Computer unit and computer networks of the distributed information and computing cluster of the NICA project**

### **2.4.1. General structure of the computer unit and network**

The computer unit of the NICA Complex project is being constructed using modern technologies as a geographically distributed information and computing cluster, which allows one to more fully satisfy the project participants' requirements in the field of theoretical studies, as well as in the field of experimental data processing and analysis. It is noteworthy that such a distributed platform enables one to integrate both the JINR common computing resource and specialized clusters in a more efficient way. This computer unit is aimed at accumulating, transferring and storing physical data acquired from the main nodes of the NICA Complex, i.e. accelerators, BM@N, MPD and SPD detectors, the computing equipment of experimental facilities for innovations and applied research, as well as at processing data and analysing them, monitoring and modelling processes under study and systems used.

The main technological elements of the basic configuration of the distributed information and computing cluster are located in four specialized rooms, three of which are situated at the site of the Veksler and Baldin Laboratory of High Energy Physics (LHEP) and one – in the Laboratory of Information Technologies (LIT) at the DLNP site being part of the JINR Multifunctional Information and Computing Complex (MICC). The structure of the cluster presupposes its connection with computing complexes of other organizations involved in the implementation of the project NICA Complex.

The general scheme of the distributed computer unit of the project NICA Complex is presented in Fig. 2.4.1.

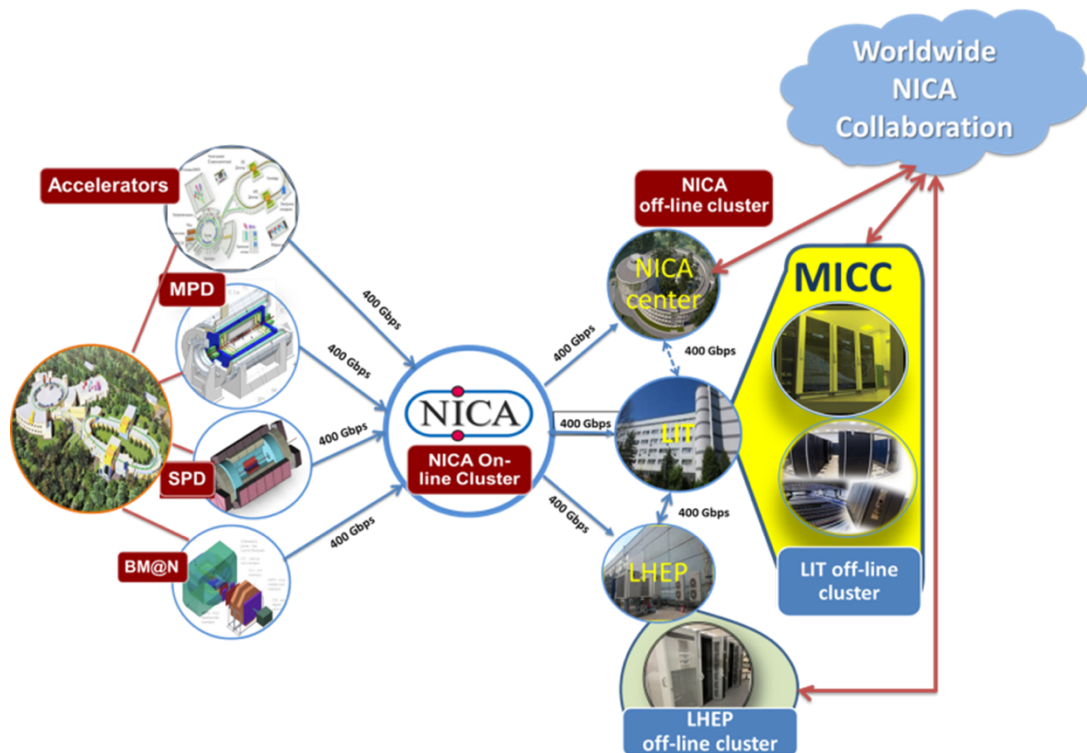


*Fig. 2.4.1. Scheme of the distributed computer unit of the NICA cluster.*

#### **2.4.2. Distributed computing network**

One of the uppermost components of the NICA Complex computer unit is a computer network combining clusters and servers within clusters, as well as computer subnets of physical buildings, into a unified computing infrastructure of the complex.

The equipment of the central telecommunication node, i.e. the core of the switching and routing system of on-line and off-line clusters, is implemented on four multifunctional switches Cisco Nexus 9504 with a full-mesh topology for maximum reliability and performance. Fig. 2.4.2 illustrates the implemented scheme of the computing network of the NICA Complex distributed cluster.

In 2019, four 100 Gbps network core switches Cisco Nexus 9504 and ten 10 Gbps access switches Cisco Nexus 9336C-FX2 were purchased, installed and configured to implement the cluster network. Three nodes ACI Multisite Fabric, namely LIT off-line, LHEP off-line and on-line, are organized on the basis of this equipment using the Cisco ACI (Application-Centric Infrastructure) technology aimed at combining physical and virtual computing infrastructures and creating an environment that is automated, scalable, programmable, cost-effective and meets both the application requirements and network security. In the following years, it is planned to further expand the ACI Multisite Fabric to all data sources of the NICA Complex:

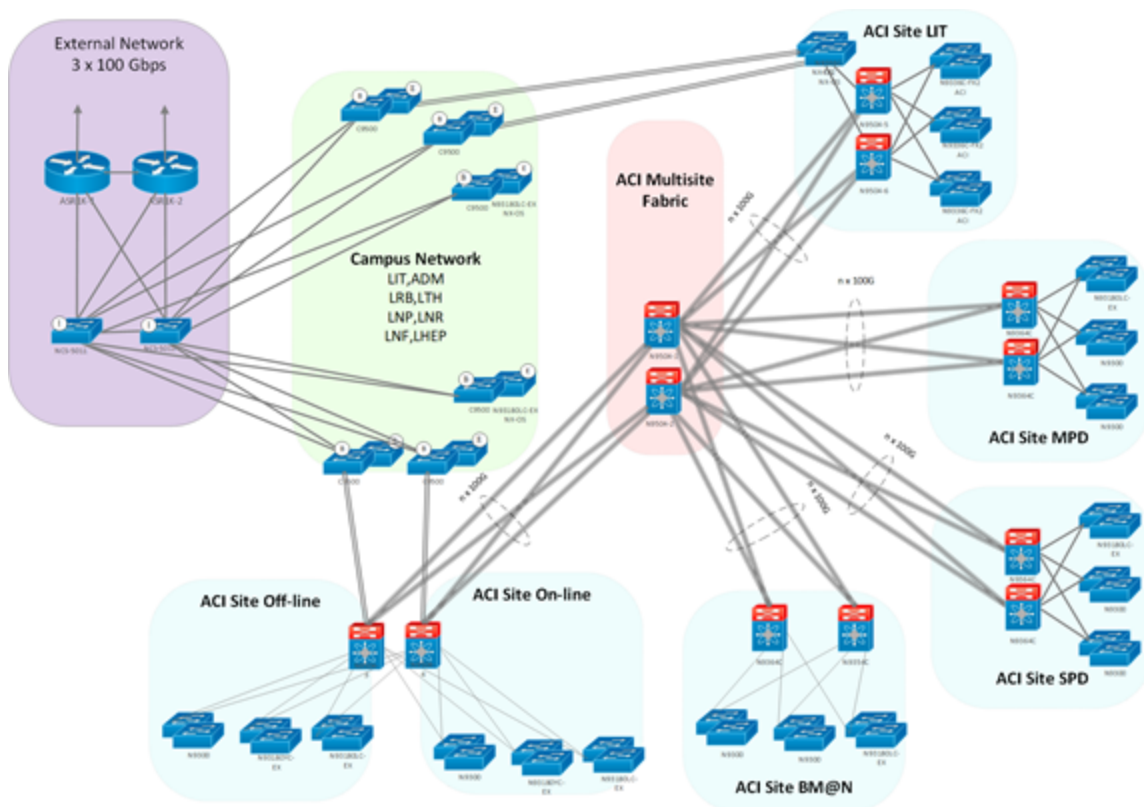


*Fig. 2.4.2. Scheme of the cluster network of the NICA Complex.*

- ACI Multisite Fabric, which provides network security (right levels of control and protection against malicious agents) regardless of how or where users are connected;
- ACI Site On-line;
- ACI Site Off-line;
- ACI Site MPD;
- ACI Site BM@N;
- ACI Site SPD;
- ACI Site LIT.

To provide reliable operation meeting modern standards and requirements, in 2019 the following work was performed in the LHEP network infrastructure:

- the core of the NICA Complex computing network was built;
- a telecommunication channel between the sites was launched at a speed of 400 Gbps with the ability to easily expand to 800 Gbps;
- switches with access to the ACI Multisite Fabric were installed;
- the LHEP off-line and LIT off-line computing clusters were connected;
- preparatory work to connect all elements of the MultiSite network cluster was done.

This work is aimed at creating a unified information space of the resources existing in LHEP, i.e. computing, information, data storage, as well as at providing access to

the centralized resources of the JINR IT structure and to the resources of individual subdivisions, enabling high-speed access to Internet resources.

The most important stage in the development of the LHEP network infrastructure was implemented, namely, the organization of optical backbones between two sites of DLNP and LHEP with a bandwidth of 4x100 Gbps. Fig. 2.4.3 shows an implemented scheme of the information and computing network between two JINR sites.

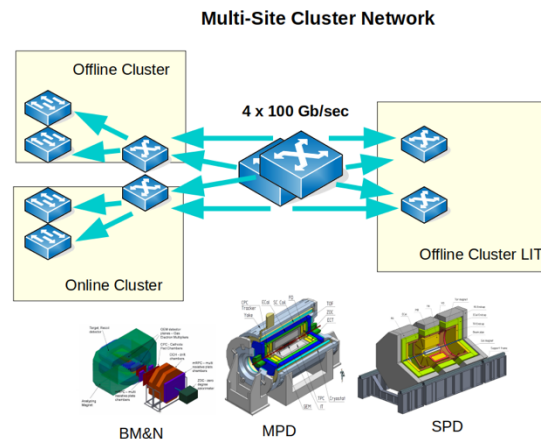


*Fig. 2.4.3. Scheme of interaction between the networks of LHEP and LIT.*

The second independent optical telecommunication channel between the DLNP and LHEP sites was planned within the basic configuration of the NICA Complex in 2019, but it was not implemented due to the complexity of coordinating the project. The work will be carried out in 2020.

### **2.4.3. On-line cluster**

The on-line cluster of the NICA Complex has several primary and secondary functions. The primary function is to get data from the NICA data acquisition system (DAQ). The function of not less importance is to acquire data from and for monitoring and diagnostics of physical facilities.

Goals and objectives of the LHEP NICA cluster:

- obtaining information from systems of acquiring data of physical facilities;
- sorting and packaging raw data;
- express data processing (not more than 5% of the total volume);
- temporary storage of “packed” data (no more than 24 hours);
- data transfer for further storage and processing on off-line clusters;
- acquiring data from and for monitoring and diagnostics of physical facilities.

The distributed information and computing cluster of the NICA Complex in its basic configuration should enable processing and storage of at least 10 petabytes of data per year.

In 2019, to implement the on-line cluster of the NICA Complex, a project of the reconstruction of the building №14 for its final placement was completed. The prototype of the cluster was installed in the building 201, necessary network packages were installed and configured for the safe and reliable operation of network resources of the computer unit (DNS, DHCP and others). The completion of work on the building 14 and the installation of the main equipment of the on-line cluster in it is planned for 2020.

#### **2.4.4. The NICA off-line cluster**

The off-line computer cluster of the NICA Complex is aimed at processing, storing and analyzing data from experimental setups of the accelerating NICA Complex. Like all large-scale centers for processing and storing data from physical facilities, such a cluster was built as geographically distributed (multi-site), combining all components located both at the LHEP site and in LIT at the DLNP site, using a unified local computer network N x 100 Gbps.

##### **2.4.4.1. LHEP NICA off-line cluster**

The off-line computer cluster of the NICA Complex is aimed at processing, storing and analyzing data from experimental setups of the accelerating NICA Complex. Like all large-scale centers for processing and storing data from physical facilities, such a cluster was built as geographically distributed (multi-site), combining all components located both at the LHEP site and in LIT at the DLNP site, using a unified local computer network N x 100 Gbps.

The implemented LHEP off-line cluster (Fig. 2.4.4) has 4500 CPU cores and 2 x 5.0 PB disk arrays.



*Fig. 2.4.4. Implemented LHEP off-line cluster.*

At the LHEP site, the cluster is located in the building 216 (room 115) and is subsequently expanded by the cluster of the new building of the NICA Center. In addition, the off-line cluster will be connected with the working prototype situated in the building 215, the on-line cluster (building 14) and the JINR MICC. When designing the off-line cluster, the experience of creating the large-scale JINR MICC, the simulation results and experience gained in creating a prototype of the off-line cluster are taken into account. The work on designing the off-line cluster was started with the creation of the prototype to gain such experience in creating a computer and network component, as well as an engineering infrastructure of the cluster.

To connect LHEP off-line to the power supply and put it into operation, a complex of the design documentation of engineering systems and fire suppression systems of the cluster was elaborated. All the equipment of the engineering infrastructure belongs to the Ripal company (Germany). For financial reasons, the supply of the equipment was divided into 2 parts. The first half (1 chiller, 2 LCPs, 4 racks and 1 UPS) was received and installed in the second quarter of 2017. The second half of the equipment was received by the end of 2018. The necessary repairs were made in the room; the area of the room is  $5.7 \text{ m} \times 8.8 \text{ m} = 50,16 \text{ m}^2$  and a height of 6 m.

The whole off-line cluster consists of 8 racks with the computer and telecommunication equipment, 2 UPSs, cooling, power supply and fire suppression systems.

The cluster consists of four identical modules, each of which consists of two racks (cabinets) with the server and air-water cooling device (LCP) between the racks. To create a “cold corridor”, the modules stand in two lines. Above, between the racks, there is a glass roof 1200 mm wide and side glass doors. The equipment in the racks receive power from two uninterruptible power supplies (UPS), which, in turn, receive power through cables from the switchboard. The arrangement of the equipment in the room 216-115 is presented in Fig. 2.4.5:

- The racks (S1-S8) for servers are 1200 x 600 x 2000 mm,
- LCP (L1-L4) - 1200 x 300 x 2000 mm,
- UPS (U1-U2) - 1000 x 800 x 2000 mm,
- Weight of the racks (cabinets): 300 (cabinet itself) + 20 servers (20-25 kg)  $\leq$  800 kg,
- Weight of LCP - 300 kg,
- Weight of UPS - about 1100 kg ( $407 + 2,65 \times 240=1043$  kg).

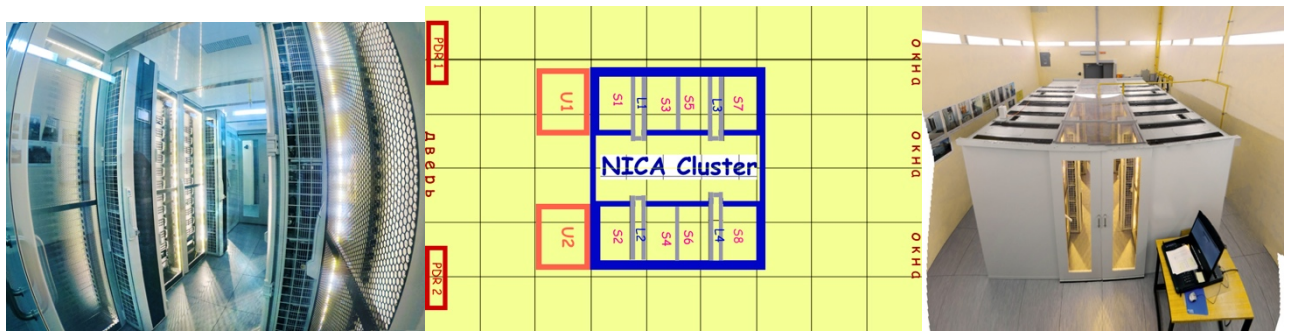


*Fig.2.4.5. Arrangement of the equipment in the room 216-115.*

The server rooms have a special raised floor made of calcium sulfate plates with a steel plate at the bottom of the plate and an antistatic coating on top of the plate. The thickness of the plate is chosen so that the floor can withstand the required distributed load. In our case, the load is up to 1500 kg/m<sup>2</sup> in the UPS area, and up to 1000 kg/m<sup>2</sup> in the rest of the room. All these requirements were satisfied by the plates of Lindner Nortec U 36 ST/PVC. Under the cabinets, a frame of C-profiles (SZ-2mm) is installed to provide the ability to remove a part of the plates for access from the cabinets to the underfloor space. Wire trays for cable routing are installed along the cabinets in the underfloor space. The size of the trays is 300 x 35 x 3000 mm.

One of the main components of the cluster is a cluster file system. Currently, several cluster file systems are used: EOS, Ceph, Luster, dCache, GlusterFS, etc. The scheme of using the distributed file system on the NICA Complex off-line cluster is shown in Fig. 2.4.6.

The cluster has a 100 Gbps internal network and is connected to the cluster network at a speed of 200 Gbps and to the laboratory network at a speed of 100 Gbps.

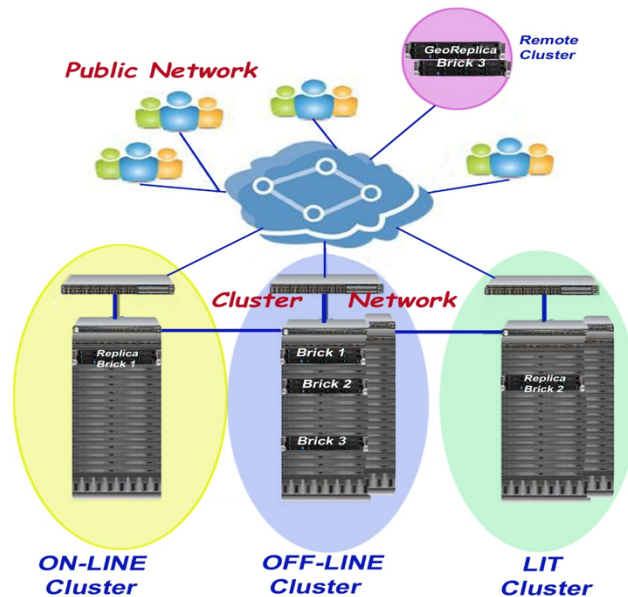


*Fig. 2.4.6. File system of the off-line cluster of the NICA Complex.*

#### **2.4.4.2. LIT NICA off-line cluster**

The developed computing models should take into account the development trends of network solutions, computing architectures and IT solutions that allow combining supercomputer (heterogeneous), grid and cloud technologies, and creating distributed software-configurable HPC platforms on their basis. The NICA computing and

information off-line cluster in LIT is organized on the basis of the JINR MICC as a distributed scalable hybrid cluster, which allows one to organize computing for the NICA project efficiently and without additional labor costs at the request of a different class of tasks and users. The main objective of the LIT off-line cluster is to create a two-layer (disk and tape) storage system for the NICA experiments, since after the first stage of these experiments significant storage volumes (from 2.5 PB to 10 PB per year) will be required.

The JINR Multifunctional Information and Computing Complex currently has the main components enumerated below.

1. JINR central information and computing complex (CICC) with built-in computing and memorizing elements.
2. Tier2 cluster for all experiments at the Large Hadron Collider (LHC) and other virtual organizations (VOs) in the grid environment.
3. Tier1 cluster for the CMS experiment.
4. HybriLIT heterogeneous platform for high-performance computing (HPC) with the “Govorun” supercomputer.
5. Cloud infrastructure.
6. Data storage system based on the EOS file system.

At present, the NICA computing and information off-line cluster in LIT is organized on the basis of Tier1, Tier2/CICC, the “Govorun” supercomputer and the EOS-based storage system.

The implementation of different computing models for the NICA megaproject requires the confirmation of their performance, i.e. meeting the requirements for the temporal characteristics of acquiring data from detectors with their subsequent transfer to processing, analysis and storage, as well as the requirements for the efficiency of event simulation and processing in the experiment. For these purposes, it is necessary to carry out tests in a real software and hardware environment, which should contain all the required components. The “Govorun” supercomputer commissioned as part of the MICC, containing the most up-to-date computing and data storage resources, including the ultrafast data storage system that provides a high speed of data acquisition up to hundreds of gigabytes per second, with the possibility of linear expansion of system performance and capacity, can become such an environment.

One of the main components of the computer unit of the project NICA Complex is a cluster file system. Currently, several systems are used in this capacity: GPFS, Lustre, dCache, Ceph, EOS, GlusterFS, etc. The EOS file system is the best option for on-line and off-line clusters. EOS is a distributed, parallel, linearly scalable file

system with the possibility of protecting it from failures. In 2019, EOS was installed and successfully integrated into the MICC structure (Fig. 2.4.7). At present, 3740 TB of disk space is available for EOS. The NICA experiments are using EOS to store data. Currently,  $\sim 81$  TB of raw data from the BM@N experiment and  $\sim 2$  TB of simulated data of the MPD experiment are stored in EOS in the MICC. EOS is displayed as a local file system on the MICC working nodes and allows authorized users (via the kerberos5 protocol) to read and record data.

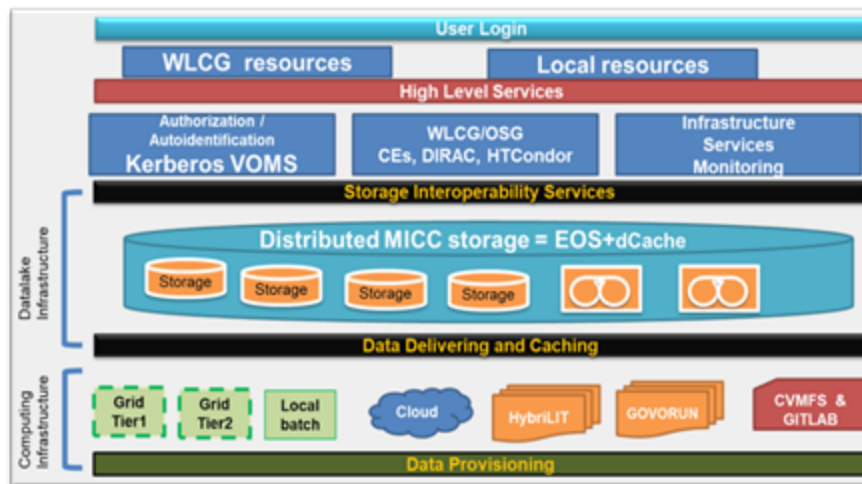


Fig. 2.4.7. Scheme of integrating EOS in the LIT MICC.

At present, the process of authentication and authorization of NICA users is unified on the following LIT MICC resources: the CICC/Tier2 counting farm, the Tier1 counting farm, cloud infrastructure resources, EOS data storage and access resources, CVMFS software update and access resources. Access to all of these resources is authorized through Kerberos5 protocols for all users registered in the JINR Kerberos and LDAP databases. This access option is most convenient for data processing and modeling, as it does not require any additional data manipulations from the user (copying from EOS storage to local disks, rewriting from local disks to EOS).

An important component of the computing and information system for NICA is the availability of a unified common software repository. For these purposes, in 2019, the CVMFS subsystem was installed. The NICA MPD and BM@N software packages were placed in CVMFS. The repository stores several versions of the same software package, and only an authorized person can change it on the CVMFS server. Read access from the repository was configured on all MICC working nodes, and it can be used around the world using the CVMFS client. The MPD and BM@N software repository occupies 9.5 GB on the CVMFS MICC servers.

Since 2019, the “Govorun” supercomputer has been used as part of the NICA LIT off-line cluster to solve problems requiring massive parallel calculations in lattice

quantum chromodynamics for the study of properties of hadron matter at high energy density and baryon charge and in the presence of supramaximal electromagnetic fields, for mathematical modeling of interactions of antiprotons with protons and nuclei using DPM, FTF and UrQMD+SMM generators developed at JINR and of interest for the NICA-MPD experiment, for the simulation of dynamics of collisions of relativistic heavy ions. In addition, the work related to the development of computing for the project NICA Complex is carried out on the basis of the supercomputer.

In 2019 another component of the off-line cluster for NICA - an ultrafast data storage system (UDSS) implemented in the “Govorun” supercomputer under the Lustre file system has been purchased and installed (Fig. 2.7.4, right). At present, UDSS has five storage servers with 12 SSD drives with the NVMe connection technology, which reduces the time of access to data. The total capacity of UDSS is currently 256 TB and the acquisition/transfer rate of data is 300 GB per second. It is noteworthy that UDSS has the ability to linearly increase productivity (speed of working with data) and the storage volume without changing the principles of the architectural design of the system. At the same time, hyperconvergence and the software-defined architecture of UDSS allow providing the maximum flexibility of data storage system configurations, including creating data storage domains, which meet the requirements of specific tasks, as well as connecting external disk fields to expand and develop the UDSS capacities.

Fig. 2.4.8 illustrates storage systems of the LIT off-line cluster (the data storage system of the LIT cluster is on the left, and the ultrafast disk memory system is on the right).

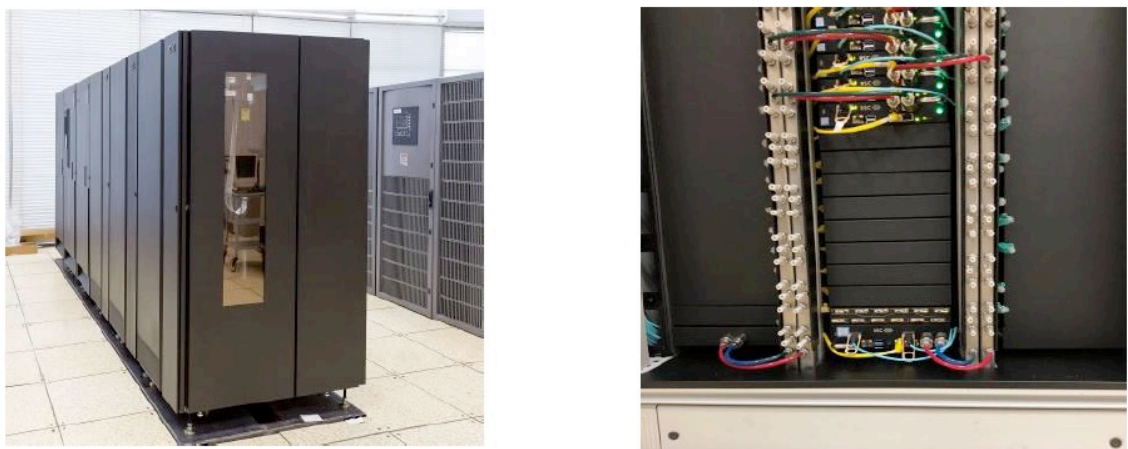


*Fig.2.4.8. Data storage system of the LIT cluster on tapes (left) and ultrafast disk memory system (right).*

At the first stage of modeling computing for the NICA megaproject, it is supposed to use computing resources of the “Govorun” supercomputer, the Skylake and KNL sections to generate data, save them to UDSS and transfer to “semi-cold” storages managed by the EOS and ZFS file systems (Fig. 2.4.9). It will allow checking the basic stack of data storage and transfer technologies, as well as modeling data flows, choosing optimal distributed file systems and increase the efficiency of event modeling and processing. This work was carried out in 2019 to simulate events of the MPD experiment, in addition, it is planned to use the DIRAC software to manage jobs and the process of reading/recording data from different types of storages and file systems (Fig. 2.4.9).

In 2019, more than 220000 jobs were completed on the “Govorun” supercomputer for the NICA needs, which amounted 85% of the total number of jobs. Fig. 2.4.10 shows the distribution of jobs performed on the supercomputer within the MPD, BM@N and SPD projects.

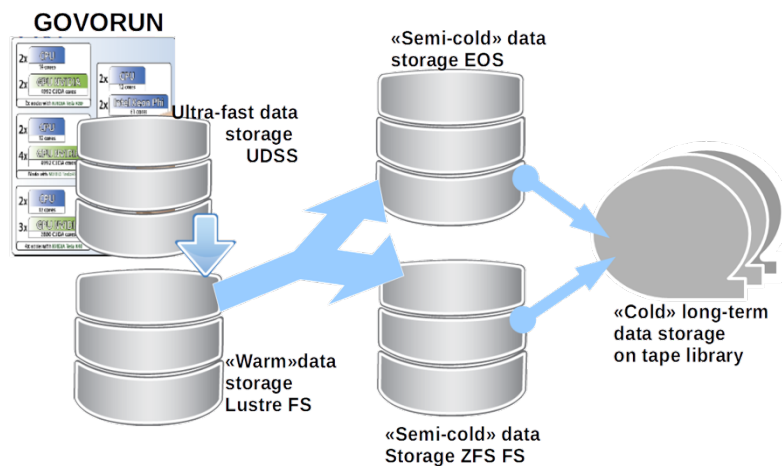


*Fig. 2.4.9. Data transfer scheme on the “Govorun” supercomputer to model calculations for the NICA megaproject and simulate events for the MPD experiment, which was implemented using the DIRAC software.*

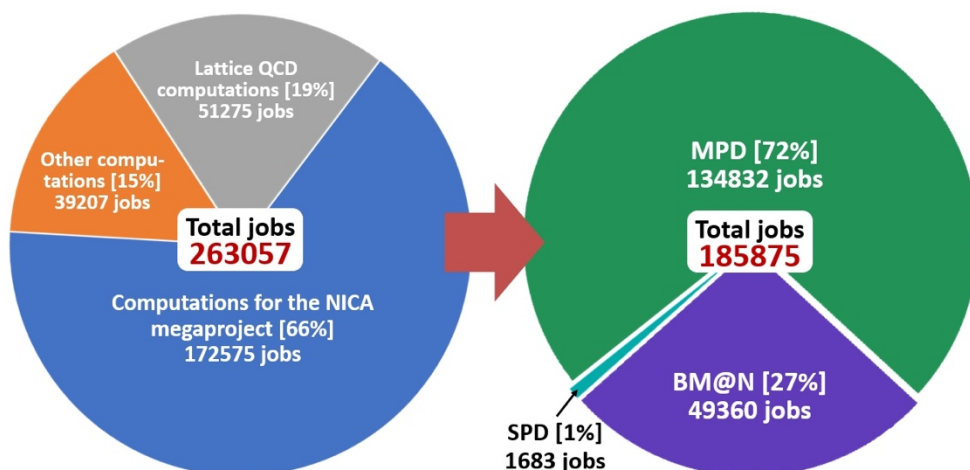


*Fig. 2.4.10. Distribution of jobs performed on the supercomputer within the MPD, BM@N and SPD projects in 2019.*

More than 80 million events have been generated for the MPD experiment using different types of generators. Currently, nearly 30 million events have been reconstructed. To solve these problems, the CPU and UDSS components are used.

In addition to the computing resources of the “Govorun” supercomputer, the computing resources allocated for NICA on the Tier1 and Tier2 components of the MICC were integrated on the basis of DIRAC, and the procedure for recording and reading data to the tape robot was checked and tested.

The DIRAC Interware is a product for integrating heterogeneous computing and data storage resources into a unified platform. Resource integration is based on the use of standard data access protocols (xRootD, GridFTP, etc.) and pilot jobs. Thanks to this, a unified environment in which is possible to run jobs, manage data, build processes and control their implementation, is provided to users. In the framework of DIRAC, batch processing systems, grid computing elements, clouds, supercomputers and even separate computing nodes can act as computing resources. Storage resources are limited only to those that support file transfer protocols used in grid systems.

Pilot jobs are an important concept in DIRAC. One can integrate almost any computing resource with their help. The idea of a pilot job is that a “pilot” job, which is always the same, is sent to the computing resource queue instead of user jobs. Only the way pilots can be run on different resources can differ. Once on the working node, the pilot loads basic data utilities, checks the environment and asks the DIRAC central service for the job that the resources occupied by the pilot would do. Having received the job, the pilot transfers control to it. After completing the job, the pilot can either ask for the next job or complete its work. Having a pilot guarantees the job some basic set of functions with which the job can work. If the resource on which the pilot works cannot provide these functions, the job will not even start and the error of the pilot launch will not hinder the user. Due to it, users see only errors related to their jobs, and only administrators should worry about the pilots not starting on the resource.

When working with data, DIRAC provides all the required set of commands. For the correct operation of all commands, the storage system should support grid data transfer protocols. It allows the pilot to acquire data on any of the resources and download them back. However, the user can always send his job to the specific computing resource and then work with the local file system on the resource. In this case, additional efforts may be required to make data accessible from anywhere. The

integration of computing resources and different data storage systems of the JINR MICC is presented schematically in Fig. 2.4.11.

Thus, with the help of DIRAC, the computing resources of the JINR MICC, i.e. Tier1/Tier2, the “Govorun” supercomputer, the JINR cloud, and storage resources, i.e. UDSS Lustre, dCache and EOS, were combined. As part of the Monte-Carlo data generation for the MPD experiment, 70000 jobs were performed on the MICC Tier1/Tier2 components using the DIRAC platform, and 15000 jobs were carried out on the computing resources of the “Govorun” supercomputer using UDSS. As a result, 4.5 TB of data were generated and sent to dCache.



*Fig.2.4.11. DIRAC Interware workflow for the NICA megaproject.*

At present, the NICA hybrid off-line cluster in LIT includes 500 CPUs (slots in batch) on the Tier2/CICC component of the MICC and 447 slots on the Tier1 component. 500 TB is reserved on the MICC EOS storage for the MPD experiment, 300 TB for BM@N and 250 TB for SPD. At the end of 2019 a tape robot with a capacity of 40 PB, in which 16 PB – dedicated for the NICA project, has been purchased.

The main objective in the near future is to combine the counting resources and storage/data access resources from all off-line clusters to conveniently use for the needs of the NICA experiments. It is supposed to use the resources located in two JINR laboratories, i.e. LIT and LHEP, for modeling, reconstruction and analysis of the NICA experiments. For convenient job launch and data access, the existing infrastructure requires refinement, modification and unification of different components of user authentication and authorization when accessing different services of data processing systems. In the future, it is planned to expand the use of

resources, with the possibility of attracting the resources of organizations that are somehow interested accessing data from the NICA experiments.

#### **2.4.5. File systems of the distributed cluster**

One of the key components of the computer unit of the project NICA Complex is a cluster file system. At present, several cluster file systems are used, namely Lustre, dCache, Ceph, EOS, GlusterFS, etc. The most appropriate one for on-line and off-line clusters is the EOS file system. EOS is a distributed, parallel, linearly scalable file system with the opportunity to protect it from failures.

Special attention is paid to novel perspective directions in creating distributed data storages (Data Lake), integrating Big Data and supercomputer technologies, methods of machine learning.

In 2020-2023 a significant increase in the amount of information is expected, which is needed to be stored and processed. At the same time, it is very difficult to evaluate the requirements to storage systems due to the evolution of data and processing models. However, the following requirements should be met:

- to provide a sufficient resource for storage and fast access to the information during processing;
- to provide a constantly expandable resource for long-term data storage, the volume and speed of which should be balanced with the corresponding flows of information;
- to provide the ability to use a data management system that automates the processes of interaction with storage systems;
- to automate support for the storage system to optimize and minimize costs.

In the coming years, it is necessary to increase the information storage capacity on the EOS system, which was put into operation in 2019. This data storage and access system should become the major system for all components of the NICA Complex and, in the future, for all JINR computing resources. The system has already been used to store data from BM@N. Storing uppermost data or data distributed territorially requires the creation of replicas, which reduces the available space multiple to the number of replicas.

One of the options for developing storages is to combine and import local site installations into a “Data Lake”, such projects are already at the development and testing stage.

Due to the significant increase in the needs of the NICA experiments and the extended use of EOS, it is necessary to plan a substantial growth in the storage capacity.

For long-term storage nothing but tapes is foreseen. At the beginning of the planning period, the cartridge capacity is equal to 12-20 TB for LTO8 – TS1160. By the end of the period, it will amount to 50-60 TB. It means that the capacity of the existing library TS3500 can be upgraded to 50-60 PB, and the capacity of the planned library for 2023 will reach up to 120-150 PB to the purchased one in 2019.

#### **2.4.6. Software of the NICA Complex**

Software for modeling, reconstruction and analysis of particle physics data is an important part of the computer unit of the NICA megaproject. For experiments on the BM@N facilities, which began in 2018, and MPD, on which it is planned to start experiments in 2021, software frameworks, such as BmnRoot and MpdRoot respectively, have been developed and are being used. The SpdRoot system is being developed as well and partially used to create a conceptual project of the SPD setup. The purpose of such computing systems is to provide modeling of primary particles, ion interactions and the resulting response of the detector, reconstruction and analysis of data from simulated and real interactions. When constructing detectors, the optimization of the hardware design, preparation of the code and the computing infrastructure require a reliable chain of modeling and reconstruction implemented by the distributed computing environment. MpdRoot and BmnRoot were used to carry out research and modeling of the technical design of all sub-detectors of both facilities in order to optimize their constructions. They were also used to study the realizability of physical problems on facilities, and BmnRoot was used for event reconstruction and analysis of physical data acquired in the BM@N experiments.

#### **2.4.7. Engineering infrastructure of the computer unit**

The main objective of the engineering infrastructure of the computer unit is to provide the necessary energy and climate conditions for the computing and network equipment, as well as to maintain the computing power in working condition. The engineering infrastructure includes:

- system of guaranteed and uninterruptible power supply;
- cooling system;
- ventilation and gas removing system;
- automatic fire suppression system;
- structured cabling system;
- video surveillance system;
- access control and management system;
- alarm system;
- dispatch system.

The main work in 2019 on the engineering systems of the NICA Complex computer unit was carried out while creating the LHEP off-line cluster.

Two chillers and external air conditioning units measuring 5 m x 10 m were installed on the prepared site (Fig. 2.4.12) outside the building 216. Size of chillers (W x H x D): 1100 x 1606 x 3240 mm, weight: 1058 kg. Size of external air conditioning units (W x H x D): 900 x 1540 x 320 mm, weight: 134 kg.



*Fig.2.4.12. Arrangement of the equipment for chillers and external air conditioning units.*

Cluster cooling system. The cooling system is air-water and includes two chillers Rittal with a cooling capacity of 88 kW, internal free cooling up to 110 kW and 4 LCP InLine Rittal heat exchangers of 40-55 kW. LCPs are indoors and connected by pipes with chillers installed on the street. The pipes pass through the external wall of the building and go under the raised floor in the center of the room to LCP. It should be especially noted that the cooling system must work around the clock, in a 24/7 mode and year-round. Therefore, winter sets are installed in the chiller and pipes. The chiller also has devices that automatically restart the chiller when power is applied after a short power failure. Back-up cooling and general conditioning of the room is ensured by two inverter split systems ToShiba Digital InVerter RAV-SM2804AT8-E with a total cooling capacity of 50 kW.

Cluster power system. The server and telecommunication equipment, as well as chiller control electronics, is connected to two UPSs Conceptpower DPA 150 with a

capacity of 96 kW each, to which PDR power distribution racks with installed PDM modules of secondary power distribution, having the main switch and protected 3-phase outputs to the equipment racks, are connected. In turn, UPSs receive power via cables from the electrical panel (room 216-113) through cable channels. The list of loads of the cluster power equipment is shown in Table 2.4.1.

Table 2.4.1.

List of loads of the cluster power equipment.

№	Element	Function	Weight, kg	Connection / consumption
1	Cabinet UPS-1	Uninterruptible power supply for 1-4 server cabinets	1100	96 kW
2	Cabinet UPS-2	Uninterruptible power supply for 5-8 server cabinets	1100	96 kW
3	Cabinets LCP	Air-water cooling of servers	4 x 300	4 x 1 kW
4	Ventilators	Ventilation system	2 x 10	2 x 0.5 kW
5	Air conditioners	Air-conditioning system	2 x 135	2 x 10 kW

Total power consumption of the complex: 280-300 kW 380v = 192 (UPS) + 60 (chillers) + 4 (LCP) + 20 (air conditioners) + 1 (ventilator).

Fire detection and suppression system. The integrated fire detection and suppression system is designed on the basis of automatic (smoke, heat, combined, etc.) fire detectors and an automatic gas fire suppression system (AGFSS), which is capable of monitoring and sending notifications via cellular communications and to the fire department. It is necessary to ensure ventilation of the room after the AGFSS operation.

The LIT off-line cluster is provided by the JINR MICC engineering infrastructure, which is being developed in accordance with the plans approved at JINR.

Fire detection and suppression system. The integrated fire detection and suppression system is designed on the basis of automatic (smoke, heat, combined, etc.) fire detectors and an automatic gas fire suppression system (AGFSS), which is capable of monitoring and sending notifications via cellular communications and to the fire department. It is necessary to ensure ventilation of the room after the AGFSS operation.

The LIT off-line cluster is provided by the JINR MICC engineering infrastructure, which is being developed in accordance with the plans approved at JINR.

## **2.5. NICA innovation block**

Three new areas are organized for applied researches within the of “NICA complex” project. Area-1 is created for Nuclotron extracted beams at medium energies of 150 - 800 MeV/u. Two stations are under development for radiobiological researches and tests of microelectronics that suffered radiation damage by heavy ions. The new Nuclotron transport beamlines will be created for these stations. Special area-2 will be constructed for relativistic nuclear power and utilization of radioactive waste at light ion energy 0.3 - 4.5 GeV/n. Special area-3 will be developed for investigations of radiation damages in microelectronics based on a heavy ion linac (HILAc). Heavy ions with the energy of 3.2 MeV/u will be used for irradiation of decapsulation microchips.

### **2.5.1. New nuclotron applied beamlines**

Area-1 is under development for applied researches with the extracted Nuclotron beams (Table 2.5.1) with medium energies of 150 - 800 MeV/u. The old part of the Nuclotron channel consists of the septum, the Lambertson magnet, the triplet of quadrupole lenses, the duplet of lenses, and the vertical deflection dipole magnet.

Two new beamlines will be constructed for radiobiological researches and chip irradiations. The new part of each channel involves an SP-94 dipole magnet, four quadrupole lenses (Table 2.5.2), and a pair of scanning magnets (Table 2.5.3). Two additional octuplets magnets are used for chip irradiation applied channel. Two exiting deflection dipole magnets SP-94 are used for beam transportation to both stations. The maximal magnetic field in these magnets is 1.5 T and the length of the magnets is about 1.3 m. The scanning vertical and horizontal magnets serve to from a uniform dose distribution with a large chip target area of 200×200 mm and radiobiological target area of 100×100 mm. The beam diagnostics of applied transport channels will operate in the “tuning” and “irradiation” modes. The diagnostics provides measurements of the following parameters: the ion beam profiles, the primary ion fluency, the primary ion density flux. The pressure in new applied channels corresponds to  $10^{-3}$  Torr. The conceptual project of new applied channels was prepared by ITEP - JINR collaboration in 2018. The tender procedure was started in October 2019 to choose a Supplier of the new applied transport channels. The equipment of applied channel should be installed in end of 2021.

Table 2.5.1.

## Applied stations' ion beams parameters

Ion beam parameters		
Parameters	SODIT	SODIB
Ion types:	$^{12}\text{C}^{6+}$ , $^{40}\text{Ar}^{18+}$ , $^{56}\text{Fe}^{26+}$ , $^{84}\text{Kr}^{36+}$ , $^{131}\text{Xe}^{54+}$ , $^{197}\text{Au}^{79}$	
Energy of ions, extracted from the Nuclotron, MeV/n	150-350	400-800
Energy spread at the Nuclotron exit, %	0,02	
Momentum spread (95%), less than, %	$\pm 0.1$	
Pulse duration of extracted beam, sec	2-20	
Homogeneity of ion flow in time inside the pulse, %	99	
Intensity variation from pulse to pulse, %	10	
Vacuum, Torr	$10^{-3}$	
Extracted beam intensity, ion/impulse	$3 \times 10^4 - 10^8$	$10^6 - 10^8$ (Xe, Kr, Fe, Ar) $10^7 - 3 \cdot 10^9 (^{12}\text{C}^{6+})$
Ion flux density, particles/( $\text{cm}^2 \cdot \text{s}$ )	$10^2 - 3 \cdot 10^5$	$10^3 - 10^5$
Maximum fluency per irradiation session, ion/( $\text{cm}^2$ )	$2 \times 10^7$	$10^7$
Duration of exposure per session, min	10 - 20	1 - 5
Radiation dose, Gy		1 - 3
Normalized emittance, (95 %) $\varepsilon_x/\varepsilon_y \pi \cdot \text{mm} \cdot \text{mrad}$	4.7/12.5 (working) 15.7/23.5(maximum)	
Beam emittance at the entrance to the stand at maximum energy, (95 %) $\varepsilon_x/\varepsilon_y \pi \cdot \text{mm} \cdot \text{mrad}$	5/13.3 (working) 16.6/24.9(maximum)	3/8 (working) 10/15(maximum)
Target irradiation area without scanning, mm	$20 \times 20$ (10 %)	$\varnothing 10$ (5 %)
Maximum irradiation area in scanning mode, mm	$200 \times 200$	$100 \times 100$
Homogeneity of ion flow at the maximum irradiating area	$\pm 15\%$	$\pm 10\%$
Beam full width at half maximum on the target, mm	30 - 57 (73 mm for Gaussian beam)	25 - 35

Table 2.5.2.

## Main parameters of quadrupole lenses of applied channels

Type	I, A	U, V	B, T	G, T/m	Bore diameter, m	Power, kW	Effective length, m	Weight, kg
Q21/ Q22	300	45	0.918	17	0.108	13.5	0.48	900
Q23/ Q24	300	60	0.780	9.8	0.16	18.0	0.48	900

Table 2.5.3.

## Main parameters of scanning magnets for applied channels

Type	I, A	B, T	Pole width, m	Interpolar gap, m	Effective length, m	Weight, kg	Frequency, Hz
SMX	395	0.8	0.17	0.14	0.373	750	3
SMY	395	0.8	0.17	0.14	0.373	750	3

### 2.5.2. Stations for chip irradiation and radiobiological researchers

Ion beams with energies of 150 - 800 MeV/u extracted from the Nuclotron will be used for radiobiological researches and modeling of cosmic ray interactions with microchips. Two stations will be constructed for chip irradiation (SODIT) and radiobiological researches (SODIB). The ions  $^{40}\text{Ar}^{18+}$ ,  $^{131}\text{Xe}^{54+}$  and  $^{197}\text{Au}^{79+}$  at the energy of 150 - 350 MeV/u are decelerated in a degrader and the surrounded microchip capsule to the energy of 5 - 10 MeV/u corresponding to the Bragg peak. The linear energy transfer (LET) is 60 - 70 MeV·cm<sup>2</sup>/mg for  $^{197}\text{Au}^{79}$  ions in the Si chip for this energy. A reduction of LET at capsulated chip irradiation results from the straggling effect at the ion energy degradation in the chip capsule. The second problem is related to production of secondary particles in its capsule.

The SODIT beam diagnostics will operate in the “tuning” and “irradiation” modes. The diagnostics provides measurements of the following parameters at the chip irradiation, the ion beam profiles, the primary ion fluency, the primary ion density flux, the secondary particle density flux and the radiation dose. The tuning diagnostic (Table 2.5.4) consists of ionization chambers with different working fields of 10 x 10 mm, 80 x 80mm and 250 x 250 mm and scintillation detector with working field of 80 x 80 mm. The online diagnostic in irradiation modes involves three scintillation detectors and one silicon detector installed at a large aperture to measure and control peripheral ion characteristics.

Table 2.5.4.

Tuning SODIT diagnostic

Parameter	Value
Intensity, fluence, profile and flow density measurement in non-scanning mode	
Ionization chamber, scintillation detector	
Input port diameter, mm	90
Working field, mm	80 × 80
Ion energy range, MeV/n	10 - 500
Accuracy of ion flux measurement	±10%
The beam time structure measurement, polling rate, Hz	20
Fluence measurement	Yes
Space resolution, mm	2-3
Accuracy of beam inhomogeneity measurements	±10%
Ionization chamber for scanning regime	
Working field, mm	250 × 250
Ion energy range, MeV/n	10 - 500
Accuracy of ion flux measurement	±10%
Fluence measurement	Yes
Accuracy of beam center gravity definition, mm	3
Accuracy of dispersion definition, mm	5
Accuracy of beam inhomogeneity measurements, mm	±15%

The conceptual project of chip irradiation station SODIT was prepared by ITEP - JINR collaboration in 2018. The equipment of experimental station SODIT is under development since autumn 2019 by the JINR - ITEP collaboration. The equipment of station SODIT should be installed in beginning of 2022.

The accelerator-based researches in radiobiology are important for improving radiotherapy and ensuring protection in cosmic space. Heavy ions extracted from the Nuclotron at the energy of 0.4 - 0.8 GeV/u are a tool for modeling biological action of cosmic space radiation. Heavy charged particles from Galaxy are the most dangerous type of cosmic radiation. The more probable energy of the galactic bare nuclei corresponds to 0.5 - 0.8 GeV/n. Exposure to the galactic heavy ions may cause incidence of cancer and formation of genetic and structural mutations, violation of visual functions, lesions of retina, and incidence of a cataract. Different ion beams extracted from the Nuclotron can be used for producing a typical dose of one Gy required for radiobiological researches. The equipment of the radiobiological station SODIB permits ion irradiation of biological samples and animals like rats and monkeys. A uniform dose distribution will be formed in the target with the maximal size of 100·100 mm and depth of 100 mm. Scanning magnets are used for this dose formation. The diagnostic system is used for measuring of the ion flux, the horizontal and vertical profiles and controlling the beam position relative to the target optical axes, dose space distribution and received dose. The tuning diagnostic consists of ionization chambers and scintillation detectors. The special chair for monkey 3D positioning with accuracy better than 1mm. The microclimate and special temperature will be prepared inside of the SODIB irradiation cabin. The conceptual project of station SODIB was prepared by ITEP-JINR collaboration in 2018.

### **2.5.3. Station for investigation in the field of nuclear energetic and transmutation SINET**

Nuclear power production as a substitution of the conventional power plants is becoming more and more attractive. However, there are the problems of safety, nuclear waste storage, utilization of spent nuclear fuel, as well as natural and depleted uranium and thorium, in the energy production cycle. Accelerator driven systems (ADS) imply after-burning of nuclear fuel with the help of neutron fluxes produced by an external neutron source in fission of natural and depleted uranium, thorium and other heavy elements. They provide safe operation, transmutation of minor actinides in nuclear waste, short (as compared to fast reactors) cycle of fissionable materials recovery. With increasing beam energy and corresponding hardening of the secondary neutron spectrum it becomes possible to re-utilize spent nuclear fuel for power production. Low energy (and highly charged) particles are

promptly stopped in a target, thus, the probability of inelastic collisions, and correspondingly, power gain of the system, drop. Energy release in a quasi-infinite target for 10 GeV/nucleon particles approaches an asymptotic near-linear function of the ion mass number from protons to  $^{40}\text{Ca}$ . It should be noted that the asymptotic dependence (integral energy release proportional to the ion mass number) in a 1 GeV/n range is applicable for protons to lithium, while in a 2 GeV/nucleon range, up to carbon. The numerical analysis shows that 0.5 GeV/n deuteron beam gives the same energy deposition as 1 GeV proton beam, and 0.5 GeV/n  $^7\text{Li}$  beam is equivalent to 3 GeV protons.

The energy deposition in a target also depends on the target size and materials. For light ions a converter from Be or C substantially increases the energy deposition in the target. Thus, according to numerical estimations, the energy deposition from 0.3 GeV/n  $^7\text{Li}$  beam is higher by a factor of 2 for Be converter and by a factor of 1.4 for C converter.

The study of energy conversion and redistribution in a big bulk target under the impact of an accelerated particle beam was performed in the framework of the JINR. A hydrodynamic model of generation and propagation of acoustic perturbations in a target irradiated by a high energy ion beam was constructed. The simulations demonstrated the role of different converter materials in energy redistribution inside the target. It was shown that frequency characteristics of acoustic waves are defined by the details of energy deposition and the speed of sound in the target materials. This study created the basis for development of the new acoustic method of diagnostics of the energy fields inside bulk targets irradiated by relativistic ion beams.

The influence of the target size and structure, as well as ion specie and energy, on the secondary particle spectrum and energy conversion in the target requires thorough experimental and theoretical investigation. The project of the Station for Investigation in the field of Nuclear Energetics and Transmutation ( applied area-2) at extracted beams of the NICA accelerator complex (SINET) will be developed especially for the purpose of obtaining new nuclear physics data on interaction of relativistic 0.3 - 4.5 GeV/n proton, deuteron, and light ion beams (intensities  $10^5$  -  $10^{10}$  p/s) with prototype ADS targets and fuel assemblies for verification of physical models and codes in design of ADS facilities and neutron sources. The SINET station will be built in the space between the old measurement pavilion and building 205. It will be applicable for irradiation of large compound targets at extracted beams of the NICA accelerator complex. A 3 - 3.5 m air gap in the vacuum beam line closed by two gates designated for installation of the diagnostic vacuum box in front

of the experimental irradiation zone is designed. This diagnostic box with detectors for nondestructive measurement of the time and space structure of the beam will be applied to provide reliable determination of beam parameters both for experiments in building 205 and at the SINET station upon irradiation of big compound targets. The spacing between the buildings (about 9 m) is sufficient to create reliable biological shielding both for irradiation of big targets and subsequent storage of irradiated samples. The station will include a remote controlled movable platform for positioning heavy targets/shields, and the vacuum beam line will be re-connected by a 3 m tube.

The SINET project is currently at the stage of approval of the Requirements Specifications for development of the Technical Design Project.

#### **2.5.4. Chip irradiation by low energy ions in SOCIT**

Special area-3 will be developed for investigations of radiation damages in microelectronics based on a heavy ion linac. Within the framework of the NICA project, the SOCIT station (area-3 of applied researches) will be constructed for chip irradiation by short-range ions extracted from the HILAc at the energy of 3.2 MeV/n. The HILAc-Booster beamline will be used for beam transportation to SOCIT. A dipole magnet will be installed in the middle of this channel to deflect the ion beams to SOCIT.

The ion energy after the HILAc is insufficient to pass through the microchip-surrounded capsule. Therefore, the chip decapsulation will be done before its irradiation. The  $^{197}\text{Au}^{79+}$  ions provide the linear energy transfer of  $95 \text{ MeV} \times \text{cm}^2/\text{mg}$  in the silicon chip at the energy of 3.2 MeV/n. The maximum ionization dose rate during one HILAc beam pulse should be less than  $10^6 \text{ rad/s}$  in the silicon chip. This requires to reduction of the beam current from milliamperes after the HILAc to several tenth of nanoamperes at the chip irradiation. A diaphragm with several holes of 20  $\mu\text{m}$  in diameter will be installed in front of the triplet of quadrupoles in the HILAc-Booster channel to reduce the beam current by five orders of magnitude. The HILAc-SOCIT channel optics involves a triplet of quadrupole lenses, a dipole magnet, and two quadrupole lenses. It permits formation of the round-shaped ion beam with the FWHM size of 70 mm on the irradiation target. The beam inhomogeneity is less than 10% at the chip target size of 20×20 mm.

The vacuum pressure in the SOCIT will be less than  $10^{-5}$  Torr and 3 orders of magnitude higher than the pressure of  $10^{-8}$  Torr in the HILAc-Booster channel. The HILAc-SOCIT channel should be designed to allow differential pumping in the area behind the dipole-deflecting magnet and prevent heavy gases like CO and H<sub>2</sub>O leaving SOCIT and penetrating to the HILAc-Booster channel. To solve these

problems, a cryogenic trap, a pulsed diaphragm crossing vacuum chamber and pumps will be installed in this applied channel behind the deflection dipole magnet.

The beam diagnostics will operate in the “tuning” and “irradiation” modes. The diagnostic equipment is designed to measure the following beam characteristics: the ion flux density, the flux, the fluence and the beam profiles. The silicon detector will be controlled average beam energy (Table 2.5.5).

Table 2.5.5

Parameters of SOCIT silicon detector

Parameter	Value
Input port diameter, mm	15
Working field, mm	10×10
Ion energy range, MeV/n	3.2
Time variation of ion energy at beam pulse to pulse	±5%
Beam pulse duration, μs	30
Repetition frequency, Hz	1
Area of detector displacement, mm	100 ×100
Accuracy of detector position, mm	1
The beam time structure measurement, polling rate, Hz	20
Fluence measurement	Yes
Space resolution, mm	2-3
Accuracy of beam inhomogeneity measurements	±10%

The tender procedure was started in October 2019 to select a Supplier of station SOCIT. The equipment of station SOCIT should be installed in 2021.

### **3. Personnel issues, mobility and activity of project participants**

The decision to establish the NICA Complex project within the framework of the Seven-year Plan for the Development of JINR 2010-2016 was made at the session of the Committee of Plenipotentiaries of the Governments of JINR Member States on 19-21 November 2009.

The project is implemented mainly by the staff of the Laboratory of High Energy Physics (LHEP JINR) named after V. I. Veksler and A. M. Baldin. A large amount of work is carried out under contracts signed on the basis of competitive procedures with companies of JINR Member States and high-tech companies from other countries. The number of participants is constantly expanding due to the development of international cooperation and the involvement in the project of representatives of scientific centers both from JINR member countries and from other countries. This is facilitated by active participation in international conferences, seminars and workshops including those held at JINR. Thus, in 2019, more than 100 students from 13 countries participated in student workshops in the framework of the NICA project, 190 representatives of universities and organizations from different countries participated in short-term business trips to JINR. In 2019, 88 employees, 61 of whom are under 35 years old, were hired to work on the NICA project at LHEP.

In 2019, about 150 scientific articles on the subject of the project have been published in scientific journals.

### **4. International cooperation**

In 2019, meetings of the BM@N and MPD international collaborations started to be held on a permanent basis. On April 16-17, 2019, the 3rd joint meeting of MPD and BM@N experiment collaborations was held in Dubna, where the scientific problems of experiments, the status of works on the development of the accelerator complex and subsystems of experimental facilities were discussed. The BM@N collaboration meeting reviewed and discussed the first results and progress of the analysis of experimental data taken in the 2018 Nuclotron run.

The 4th BM@N collaboration meeting was also held in Dubna on 14-15 October 2019. On October 22-25, the 3rd conference "NICA days" was held in Warsaw, where the physical program of experiments of the NICA complex was discussed, as well as the 4th meeting of the MPD collaboration.

Currently, the BM@N collaboration includes 234 representatives of 21 institutes from 11 countries; 476 scientists and specialists from 38 institutes and 11 countries participate in the MPD collaboration.

In 2019, works on the preparation of the project of the second facility on the collider of the NICA complex (SPD) were actively conducted; with the purpose to carry out experiments with polarized particle beams. On June 4-8, JINR held an international workshop on this project, discussed scientific issues, possible configuration of the set-up, plans for the formation of an international collaboration.

## Conclusion

Work on the development of the basic configuration of the "NICA Complex" project within the mega-science project "Complex of Superconducting Rings with Colliding Beams of Heavy Ions"(NICA Complex) is carried out in accordance with the agreement between the Government of the Russian Federation and JINR and its updating within the framework of the national project of the Russian Federation "Science". The intensity of the work is shown in Fig. 1 by the diagram of their conduct, obtained using the project management system EVM.

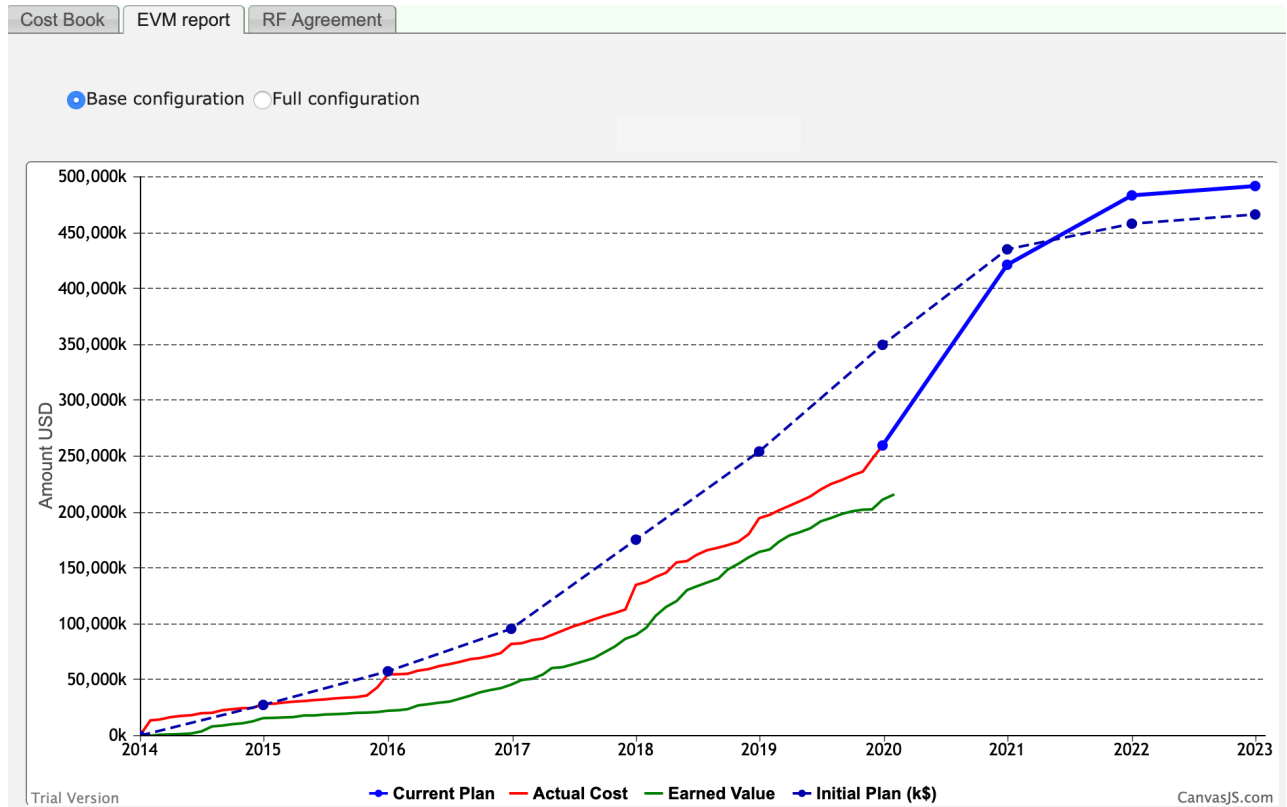


*Fig. 1. EVM-diagram of evaluation of the implementation of the "NICA Complex" project for the period 2014 – 2019 The blue curve – planned resources, the red curve – real costs, the green curve – the percentage of work performed, normalized to the financial scale.*

The main achievements of 2019 are listed below.

In 2019, first physical results of the successful implementation of the first significant phase of the NICA Complex project were obtained, an experiment at the BM@N facility, during which about 200 million events were collected.

The effective work of two international collaborations to conduct experiments on BM@N and MPD facilities has begun, work on the formation of the SPD collaboration still continues.

The assembling of the Booster is close to its completion, its technological launch planned for the end of 2019 in accordance with the planned target dates of the

Agreement. The expansion of international cooperation, attraction of new participants and implementation of grant programs are the most important components of successful implementation of the project. A constant work is conducted in these directions.

A number of new international agreements have been signed. New institutions and countries are involved in the project.

On 01.11.2019, the completed works account for about 52% of the total amount of work on the development of the basic configuration of the complex.

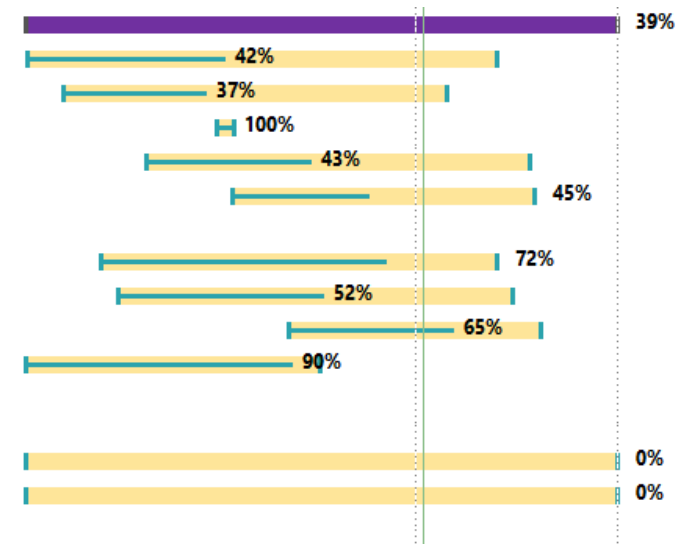
In general, the establishment of the basic configuration of the "NICA Complex" project is proceeding at a pace that allows us to count on the successful implementation of the main tasks of the Agreement between the Government of the Russian Federation, JINR, and the national project "Science". At the same time, in the process of project implementation, risks of under-performing in the terms of commissioning of its individual elements are accumulated. First of all, these risks are associated with construction works. Incomplete readiness of the main structures of building 17 for the start of MPD facility, unexpected delay in the construction of the cryogenic compressor station due to the change of the General Contractor may lead to a shift in the timing of the project as a whole. Unforeseen delays in the conclusion and / or execution of a number of other contracts for the supply of necessary materials and equipment are also accumulated and cannot but affect these deadlines.

At the same time, due to the inclusion of the "NICA Complex" project in the national project "Science" of the Russian Federation and the federal project "Development of Advanced Infrastructure for Research and Development in the Russian Federation", there are real opportunities to complete the basic configuration of the complex in time.

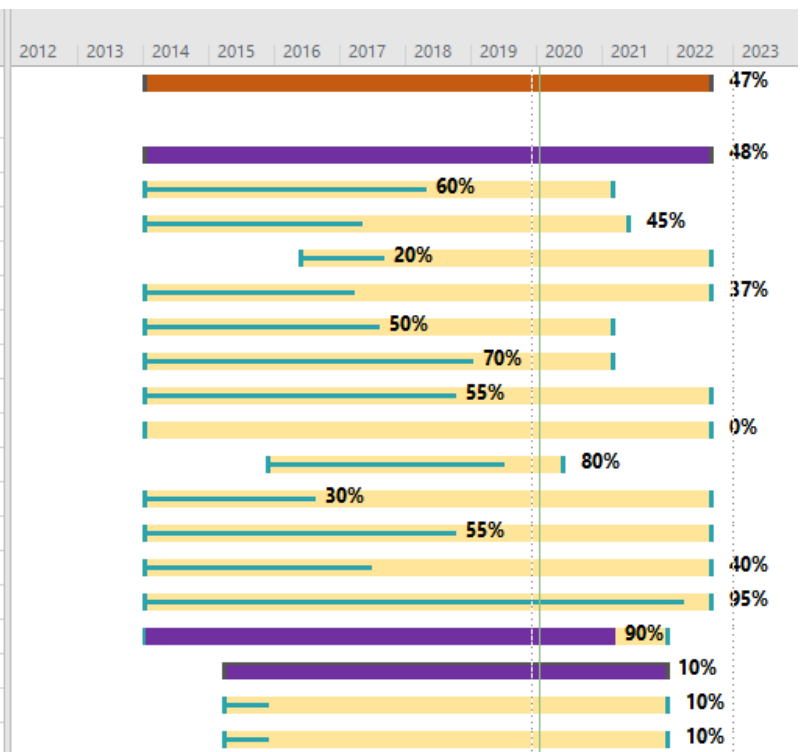
The diagram of implementation of the basic configuration of the "NICA Complex" project with the indication of the status of the main objects is shown in Fig. 2.

Structure	Task name	% completion	Start	Ending	2012	2013	2014	2015	2016	2017	2018	2019	2020	2021	2022	2023
<b>WBS</b>	<b>↙ NICA</b>	<b>56%</b>	<b>Чт 10.01.13</b>	<b>Пт 30.12.22</b>												
<b>1</b>	<b>↙ Construction of an accelerator complex including a booster synchrotron and a collider</b>	<b>67%</b>	<b>Чт 10.01.13</b>	<b>Пт 30.12.22</b>												
<b>1.1</b>	<b>↙ Light ion injection complex</b>	<b>84%</b>	<b>Ср 01.01.14</b>	<b>Вт 30.06.20</b>												
1.1.1	Light ion source	58%	Ср 01.01.14	Вт 30.06.20												
1.1.2	Laser source	100%	Ср 01.04.15	Вт 31.07.18												
1.1.3	Source of Polarized Particles	97%	Ср 01.01.14	Вт 30.06.20												
1.1.4	Linac LU-20M	100%	Ср 01.01.14	Сб 31.03.18												
1.1.5	Light ion linear accelerator (LILAC)	65%	Ср 01.01.14	Вт 30.06.20												
1.1.6	Engineering systems	97%	Ср 01.01.14	Вт 30.06.20												
<b>1.2</b>	<b>↙ Heavy ion injection complex</b>	<b>86%</b>	<b>Чт 10.01.13</b>	<b>Вт 31.03.20</b>												
1.2.1	Heavy Ion Source KRION - 6T	75%	Ср 01.01.14	Вт 31.03.20												
1.2.2	HILAc	100%	Чт 10.01.13	Вт 09.01.18												
<b>1.3</b>	<b>↙ Booster</b>	<b>81%</b>	<b>Пт 10.01.14</b>	<b>Вс 01.11.20</b>												
1.3.1	Cryo-magnetic system	97%	Пт 10.01.14	Пт 20.12.19												
1.3.2	Electron cooling system	95%	Пт 10.01.14	Чт 30.04.20												
1.3.3	Beam injection and extraction systems, beam transfer lines	47%	Пт 10.01.14	Вс 01.11.20												
1.3.4	Booster magnets power supply system	80%	Пт 10.01.14	Вт 10.12.19												
1.3.5	Radio-frequency system	97%	Пт 10.01.14	Пн 30.03.20												
1.3.6	Control and diagnostic system	77%	Пт 10.01.14	Пт 30.10.20												
1.3.7	Vacuum system	60%	Пн 12.01.15	Чт 01.10.20												
1.3.8	Energy-technological and engineering systems of Booster	96%	Пт 10.01.14	Вс 01.11.20												
<b>1.4</b>	<b>↙ Nuclotron</b>	<b>77%</b>	<b>Ср 01.01.14</b>	<b>Пт 31.12.21</b>												
1.4.1	Nuclotron-N	62%	Ср 01.01.14	Вт 31.03.20												
1.4.2	Injection and slow extraction system	85%	Сб 10.01.15	Вт 31.03.20												
1.4.3	Fast extraction system	80%	Сб 10.01.15	Вт 31.03.20												
1.4.4	Extraction channels to 205 bld.	70%	Ср 01.01.14	Пт 31.12.21												
1.4.5	Injection channel LU-20 Nuclotron	100%	Сб 10.01.15	Ср 18.07.18												

1.5	▾ Collider	39%	Ср 01.01.14	Пт 30.12.22
1.5.1	Cryo-magnetic system	42%	Пт 10.01.14	Пн 01.03.21
1.5.2	Stochastic cooling system (SCS)	37%	Пт 01.08.14	Пн 01.06.20
1.5.3	Electronic cooling system (project)	100%	Чт 01.12.16	Ср 01.03.17
1.5.4	Collider magnets power supply system	43%	Пн 02.11.15	Ср 01.09.21
1.5.5	Beam channels from Nuclotron, beam injection system	45%	Ср 01.03.17	Пт 01.10.21
1.5.6	Radio-frequency system	72%	Вс 01.03.15	Пн 01.03.21
1.5.7	Collider control and diagnostic system	52%	Пн 01.06.15	Вт 01.06.21
1.5.8	Vacuum system	65%	Пн 08.01.18	Пн 01.11.21
1.6	Scientific and technological base of the assembly, testing, certification and storage of SC magnets	90%	Ср 01.01.14	Сб 30.06.18
1.7	Operating expenses and staff	0%	Ср 01.01.14	Пт 30.12.22
1.8	Additional financing for project documentation	0%	Ср 01.01.14	Пт 30.12.22



Structure	Task name	% completion	Start	Ending
2	▾ Construction of experimental set-ups (MPD, BM@N)	47%	Пт 10.01.14	Чт 01.09.22
2.1	▾ MPD, including:	48%	Пт 10.01.14	Чт 01.09.22
2.1.1	TOF	60%	Пт 10.01.14	Пн 01.03.21
2.1.2	TPC	45%	Пт 10.01.14	Вт 01.06.21
2.1.3	ECAL	20%	Ср 01.06.16	Чт 01.09.22
2.1.4	ITS	37%	Ср 15.01.14	Чт 01.09.22
2.1.5	FFD	50%	Пт 10.01.14	Пн 01.03.21
2.1.6	Straw	70%	Пт 10.01.14	Пн 01.03.21
2.1.7	ZDC	55%	Пт 10.01.14	Чт 01.09.22
2.1.8	CPC	0%	Пт 10.01.14	Чт 01.09.22
2.1.9	MPD solenoidal magnet	80%	Вт 01.12.15	Пн 01.06.20
2.1.10	Data acquisition system	30%	Пт 10.01.14	Чт 01.09.22
2.1.11	Slow control system	55%	Пт 10.01.14	Чт 01.09.22
2.1.12	Engineering infrastructure	40%	Пт 10.01.14	Чт 01.09.22
2.1.13	Experimental test zone	95%	Пт 10.01.14	Чт 01.09.22
2.2	BM@N	90%	Пт 10.01.14	Чт 30.12.21
2.3	▾ SPD, including:	10%	Ср 01.04.15	Чт 30.12.21
	SPD	10%	Ср 01.04.15	Чт 30.12.21
2.3.1	SPD test zone	10%	Ср 01.04.15	Чт 30.12.21



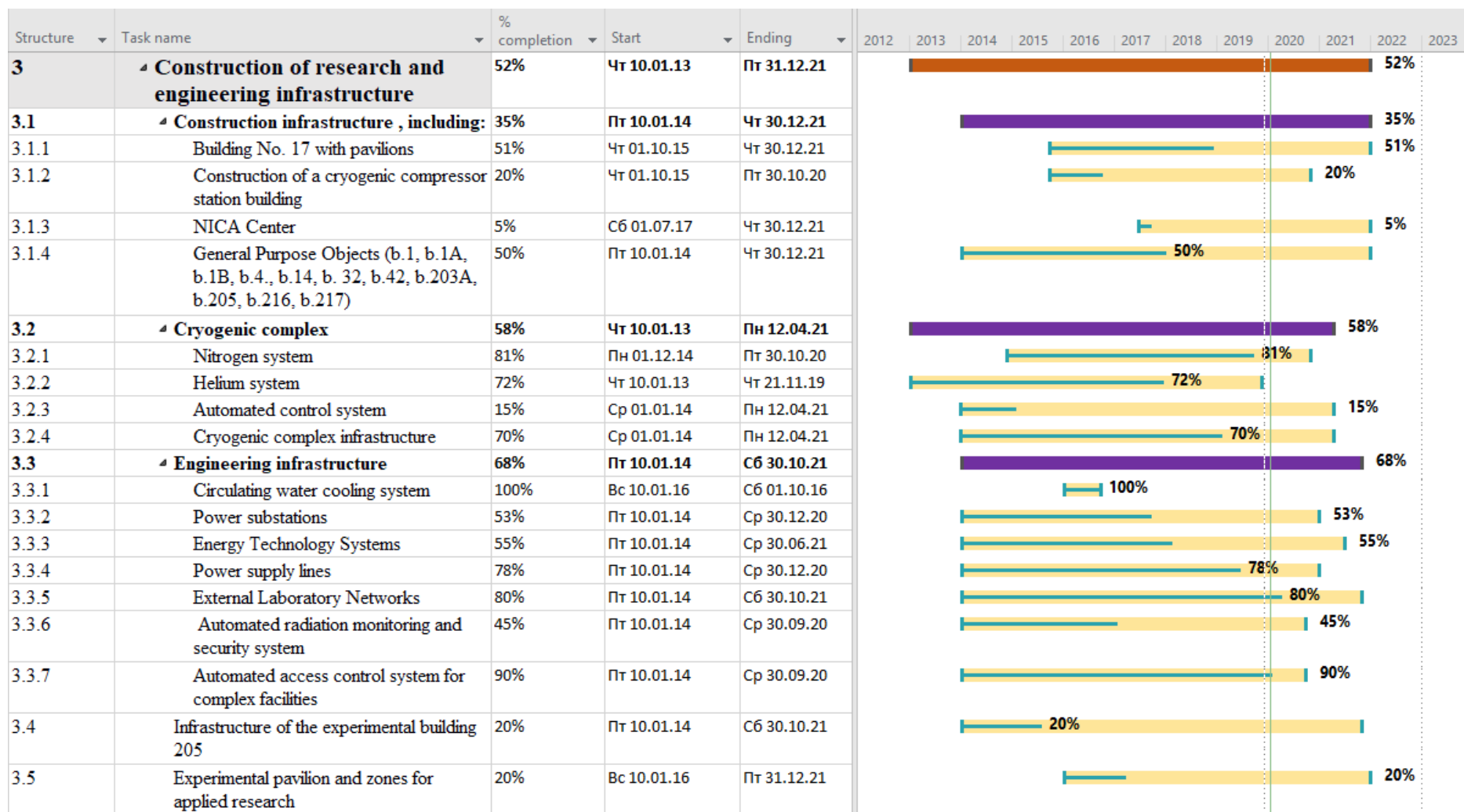


Fig. 2. A diagram of the implementation of the basic configuration of the NICA Complex